

CYTOMEGALOVIRUS INFECTION INDUCES COGNITIVE DEFICITS AND  
ALTERS NEUROBIOLOGICAL METABOLISM IN A MOUSE MODEL OF AGING

AN ABSTRACT

SUBMITTED ON THE NINETEENTH DAY OF DECEMBER 2022

TO THE NEUROSCIENCE PROGRAM

IN PARTIAL FULFILLMENT OF THE REQUIREMENTS

OF THE SCHOOL OF SCIENCE AND ENGINEERING

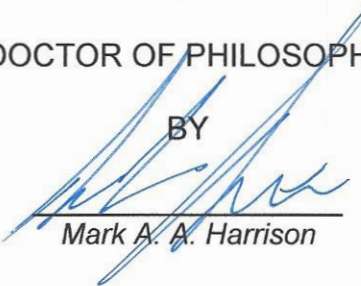
OF TULANE UNIVERSITY

FOR THE DEGREE

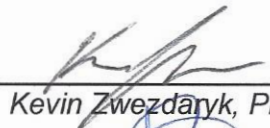
OF

DOCTOR OF PHILOSOPHY

BY

  
Mark A. A. Harrison

APPROVED:

  
Kevin Zvezdaryk, Ph.D.

  
Ricardo Mostany, Ph.D.

Andrew MacLean

Andrew MacLean, Ph.D.

  
Sean Lawler

Sean Lawler, Ph.D.

  
Tarun Mandal

Tarun Mandal, Ph.D.

## ABSTRACT

Cytomegalovirus (CMV) is a ubiquitous  $\beta$ -herpes virus with seroprevalence rates upwards of 80% in some populations. An obligate parasite, CMV alters the host cell's metabolic pathways to produce the biomaterials and energy necessary for successful viral replication. While congenital infections and those occurring in immunocompromised populations can have serious consequences, for the majority of the population, the virus is regarded as benign. However, accumulating evidence has implicated CMV in the progression of unhealthy aging and the development of age-associated diseases such as cancer (including glioblastoma (GBM)) and dementia.

We hypothesized that CMV may function in an oncomodulatory capacity providing some survival or proliferative benefit to the cancer. Following infection of GB cells with CMV we determined that infection enhanced both the glycolytic and oxidative phosphorylation pathways resulting in an increased production of lactate and reactive oxygen species. We also demonstrated that, independent of viral transmission, infected cells were able to alter the metabolism and epigenetic landscape of neighboring cells. These findings suggest that CMV infected cells possess a remarkable ability to manipulate the tumor microenvironment in a manner which likely provides the tumor with metabolic flexibility.

Following these *in vitro* results we examined the effect of periodic CMV reactivation in a murine model of aging. We discovered that CMV infection

produces an immediate systemic inflammation with a delayed neuroinflammation. Moreover, there was significant metabolic reprogramming and oxidative stress indicative of mitochondrial dysfunction in brain microvascular endothelial cells (BMECs). To understand the physical manifestations of the collective metabolic and functional changes observed in our mouse model, we completed a series of cognitive assays and identified clear cognitive impairment in spatial working memory at 12 months post infection. Taken together, our data indicates that periodic CMV exposure alters metabolic pathways in the BBB and accelerates cognitive decline. These results were observed at “middle age” in mice, a time in which human correlates would still be in the symptomless phase of cognitive decline. Our work demonstrates a mechanistic relation between pathogen exposure and cognitive decline or dementia related pathologies.

This research highlights metabolic dysfunction and oxidative stress as potential therapeutic targets to mitigate the impact of pathogen exposure on unhealthy aging. Findings from this research may enable future generations to experience enhanced quality of life at advanced age.

CYTOMEGALOVIRUS INFECTION INDUCES COGNITIVE DEFICITS AND  
ALTERS NEUROBIOLOGICAL METABOLISM IN A MOUSE MODEL OF AGING

A DISSERTATION

SUBMITTED ON THE NINETEENTH DAY OF DECEMBER 2022

TO THE NEUROSCIENCE PROGRAM

IN PARTIAL FULFILLMENT OF THE REQUIREMENTS

OF THE SCHOOL OF SCIENCE AND ENGINEERING

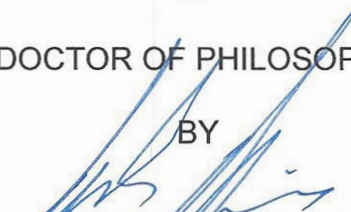
OF TULANE UNIVERSITY

FOR THE DEGREE

OF

DOCTOR OF PHILOSOPHY

BY



---

Mark A. A. Harrison

APPROVED:



---

Kevin Zvezdaryk, Ph.D.



---

Ricardo Mostany, Ph.D.

*Andrew MacLean*

---

Andrew MacLean, Ph.D.

*Sean Lawler*

---

Sean Lawler, Ph.D.

*Tarun Mandal*

---

Tarun Mandal, Ph.D.

© Copyright by Mark Alexander Awtrey Harrison, 2022  
All Rights Reserved

## TABLE OF CONTENTS

AKNOWLEDGEMENTS.....	ii
FORWARD.....	vii
LIST OF TABLES.....	viii
LIST OF FIGURES.....	ix
CHAPTERS	
<b>1. BACKGROUND.....</b>	<b>1</b>
1.1. Cytomegalovirus.....	2
1.2. Cytomegalovirus and glycolysis.....	3
1.3. Cytomegalovirus and mitochondria.....	5
1.4. Cytomegalovirus and cancer.....	7
1.5. Cytomegalovirus and the blood brain barrier.....	9
1.6. Cytomegalovirus and dementia.....	11
1.7. Research plan.....	13
<b>2. METABOLIC REPROGRAMMING OF GLIOBLASTOMA CELLS DURING HCMV INFECTION INDUCES SECRETOME-MEDIATED PARACRINE EFFECTS IN THE MICROENVIRONMENT.....</b>	<b>15</b>
2.1. Abstract.....	15
2.2. Introduction.....	16
2.3. Methods.....	19
2.4. Results.....	26
2.4.1. HCMV infects and replicates in a human glioblastoma cell line LN- 18.....	26
2.4.2. HCMV infection metabolically reprograms LN-18 cells.....	29
2.4.3. HCMV infection increases oxidative phosphorylation of host cells.....	31

2.4.4. HCMV infection increases mitochondrial membrane potential and production of reactive oxygen species.....	34
2.4.5. HCMV infection increases glycolytic rate and capacity.....	36
2.4.6. Elevated aerobic glycolysis following HCMV infection alters lactate production and flux.....	39
2.4.7. Co-culture of HCMV-infected LN-18 with HFFs alters expression of key metabolic proteins and epigenetic markers in both cell lines.....	42
2.5. Discussion.....	49
2.6. Limitations.....	54
2.7. Conclusions.....	55
<b>3. CYTOMEGALOVIRUS INFECTION INDUCES COGNITIVE DEFICITS AND ALTERS NEUROBIOLOGICAL METABOLISM IN A MOUSE MODEL.....</b>	<b>56</b>
3.1. Abstract.....	56
3.2. Introduction.....	57
3.3. Methods.....	59
3.4. Results.....	69
3.4.1. Intermittent MCMV infection exhibits delayed inflammatory cytokine expression in the brain.....	69
3.4.2. Intermittent MCMV infection alters the transcriptional profile of brain cells.....	73
3.4.3. Blood brain barrier metabolic pathways are rewired with increased MCMV exposure.....	77
3.4.4. Hallmarks of mitochondrial dysfunction and oxidative stress are elevated in BMECs intermittently exposed to MCMV.....	80
3.4.5. MCMV infection metabolically rewires astrocytes as a function of age.....	84
3.4.6. Cognition is impaired with intermittent MCMV infection.....	87
3.5. Discussion.....	91
3.6. Limitations.....	98
3.7. Conclusions.....	99
<b>4. CONCLUSIONS AND FUTURE DIRECTIONS.....</b>	<b>100</b>

4.1. Conclusions.....	100
4.2. Future Direction 1: CMV-mediated changes in metabolite secretion following infection.....	105
4.3. Future Direction 2: CMV-mediated changes in intracellular communication following infection.....	106
4.4. Future Direction 3: Investigating targeted areas within the murine brain.....	107
4.5. Future Direction 4: Examination of the impact of mitochondria-derived reactive oxygen species on aging and/or cognitive decline and development of therapeutics.....	108
4.6. Final Thoughts.....	109
<b>5. APPENDIX A: Supplemental information for Chapter 2.....</b>	<b>111</b>
<b>6. APPENDIX B: Supplemental information for Chapter 3.....</b>	<b>117</b>
<b>7. APPENDIX C: ESTABLISHING THE ADIPOSE STEM CELL IDENTITY: CHARACTERIZATION ASSAYS AND FUNCTIONAL PROPERTIES.....</b>	<b>130</b>
7.1. Introduction.....	130
7.2. Physical Characterization.....	131
7.3. Multipotent Differentiation.....	140
7.4. Characterization of <i>In Vitro</i> Immunomodulatory Abilities.....	161
7.5. Conclusions and Future Directions.....	181
<b>8. APPENDIX D: ADIPOSE-DERIVED STEM CELLS FROM OBESE DONORS POLARIZE MACROPHAGES AND MICROGLIA TOWARD A PRO-INFLAMMATORY PHENOTYPE.....</b>	<b>183</b>
8.1. Abstract.....	183
8.2. Introduction.....	184
8.3. Materials and Methods.....	187
8.4. Results.....	196
8.4.1. ObASCs Exhibit Reduced Stemness Characteristics when Compared with LnASCs.....	196

8.4.2. Indirect Co-Culture with ObASCs, but not LnASCs, Induces Polarization Towards M1 Phenotype in RAW264.7 Macrophages.....	199
8.4.3. LnASCs and ObASCs Differentially Affect the Migration and Phagocytic Abilities of RAW264.7 Macrophages.....	202
8.4.4. Indirect Co-Culture with ObASCs, but not LnASCs, Induces Polarization Towards M1 Phenotype in SIM-A9 Microglia.....	205
8.4.5. LnASCs and ObASCs Differentially Affect the Migration and Phagocytic Abilities of SIM-A9 Microglia.....	209
8.5. Discussion.....	212
8.6. Conclusions.....	216
LIST OF REFERENCES.....	217
BIOGRAPHY.....	263

## **AKNOWLEDGEMENTS**

It's been a long, weird road to this point and there are quite frankly too many people to thank for believing in me far more than they had any reason to. It's rare that the opportunity comes to "officially" thank them so I'll take these pages to give it my best. Chronologically seems like the best way to address them (as memory permits).

First and foremost, massive thanks to my parents Dr. Colin and Lynn Harrison both for mutually agreeing to raise me and for their unflagging support despite periods of "adversity". Dad, for pushing me to excel, for being a model of hard work, and for your/our odd sense of humor. Mom, for your love, compassion, understanding, and intelligence. You are both exceptional role models and I couldn't have asked for better parents.

Rachel Kaplan, you haven't always made my life the easiest, but you have always made it more interesting. Thank you for your constant support, your belief in me, and your continuing friendship. You've left an indelible impression on my life and I truly wouldn't have made it this far without you.

For all of the teachers, professors, and mentors who have supported me throughout the years prior to grad school. My high school English teacher, Mrs. Bennett, who showed exceptional kindness to a student in desperate need of it. Dr. Benjamin Miller, professor of psychology at Salem State University, for your

guidance, passion for teaching, and good humor. Dr. Randy Wetzel, director of antibody applications, and Gregory Innocenti, group leader of immunofluorescence, for encouraging me to pursue a PhD and being excellent non-academic mentors throughout this endeavor. Despite all the years, the marks you all have left on my life remain, resilient as ever.

Grad school came with its own unique set of challenges and there has been no better support than my lab mates. Members of the Bunnell lab, my time with y'all was a blast. I'm sorry things ended the way they did but you will always be part of my life. Dr. Omair Mohiuddin, thank you for your guidance, your friendship, and sharing your wonderful family with me. Dr. Rachel Wise, where do I begin? The human Weeble Wobble, nothing can keep you down. You're an incredible scientist, an exceptional colleague, and the dearest of friends. I cannot understate the impact you made on my career and life. I'll always think of you as the big sister who will never let me quit. Thank you for all of the memories. I'm blessed to have you in my life. To Dr. Brianne Sullivan, my mutually co-dependent grad sister and bestie. We've been through so much in these past 5 years, think how we've grown! I'm forever thankful that, no matter what, you were right there by my side. Eternal thanks for forcing me to be your friend and constantly pushing me out of my comfort zone. You and Dr. Sam Bliesner have been the best of friends and I'll always treasure our Thursday movie nights and vacations at the lake. Your friendship and support are an impossible debt to repay, but I'll spend my life trying.

To the burgeoning Zwezdaryk lab. When I started working with Kevin I was all alone, something I, an introvert, cherished. Despite my trepidation at having to

share my space, you have all brought such positivity and light to the lab that now I cannot imagine it any other way. First of all, while I was still alone, members of the Norton lab made me feel at home. Ivy Trinh, Addison Stone, and Amelie Murrell you are all such amazing, intelligent scientists and humans I am blessed to have known you these past several years. Special thanks to Ivy Trinh for your good humor, hard work, and persistence. Your friendship has brought so much happiness into my life and brightened many bleak days in lab. You and Kenny are the best support network and officially my favorite people in Tennessee. Juniper Rosen, you are a constant source of inspiration. We made a scrappy little team for a while. I'll never forget our "vacation" to Montgomery, AL with all the animals. Your patience and positivity is infectious. I'm so excited to see you grow as a scientist and a human. Dan Rittenhouse, the most consistent member of the lab, thank you for all of the work you took over from me. It was a pleasure working with you day in and day out. Chandler Monk, the original Zwezy, thank you for welcoming me into the lab with such enthusiasm. I only wish we had had more time to work together. You are an excellent scientist and I can't wait to see your career take off. Sara Morris, you strange, wonderful girl. Your spirit lights up the lab, never lose that enthusiasm. Enormous thanks for bravely taking on such a weighty project. I leave knowing that it is in good hands. Your intelligence and drive will make quick work of a PhD I'm sure!

To the undergraduate students that worked so hard and put up with my terrible jokes. Y'all never cease to amaze me with your intelligence, persistence, and drive. Thank you all for your contributions to my work and life. A very special

thank you to my long term undergrads Emily Hochreiner and Brooke P. Benjamin. I hope that someday I can repay you for all the hard work, good humor, and Gen Z lingo you provided while working with me. It was my greatest pleasure being your grad student mentor and I'm so proud of the work you're doing in med school. Additional thanks to my most recent undergrad Grace Rudman, the embodiment of a Leo. Your passion for learning, impeccable organization skills, and warmth made working with you a joy.

Thank you to my committee members Dr. Ricardo Mostany, Dr. Manus MacLean, Dr. Tarun Mandal, and Dr. Sean Lawler. I am lucky to have had such an intelligent and supportive team to guide me through my PhD. Drs. Mostany and MacLean, immense thanks for allowing me to rotate through your labs mid-pandemic when circumstances demanded it. Dr. Mandal, thank you for sticking with me through this whole process even though we never did get the exosome project off the ground. Dr. Lawler, thank you for collaborating with me and introducing me to a new field of study.

Finally, immense thanks to Dr. Kevin Zwezdaryk, the type of mentor I never knew existed. You took me in when I was "homeless" and miraculously agreed to a two year dissertation research commitment. Think how much we could have accomplished given 4 full years! Endless thanks for your enthusiasm, your unflappable optimism, and your patience through this whole process. I can honestly say that I have thoroughly enjoyed working for you these past few years. I am proud to call you my mentor, my colleague, and my friend.

Thank you ALL for your contributions to my life and career. This never would have been possible without your guidance, support, and love. You have made me the man I am today and I can never thank you enough for that.

## FOREWARD

“There's nothing more exciting than science. You get all the fun of sitting still, being quiet, writing down numbers, paying attention. Science has it all.”

Seymour Skinner, *The Simpsons*

## LIST OF TABLES

<b>Table B1</b> Antibodies and Assays.....	117
<b>Table B2</b> Virus and Chemicals.....	118
<b>Table B3</b> Organisms, Software, Other.....	119
<b>Table C1</b> Positive and Negative Selection Markers Used for the Characterization of ASCs.....	139
<b>Table D1</b> Primer Sequences.....	193

## LIST OF FIGURES

<b>Figure 2.1</b> HCMV can productively infect the glioblastoma cell line LN-18.....	28
<b>Figure 2.2</b> HCMV infection of LN-18 cells increases host ATP production using glycolysis and oxidative phosphorylation metabolic pathways.....	30
<b>Figure 2.3</b> HCMV infection increases oxidative phosphorylation in LN-18 cells.....	33
<b>Figure 2.4</b> HCMV infection increases electron transport chain function.....	35
<b>Figure 2.5</b> HCMV infection increases glycolysis and glycolytic capacity.....	38
<b>Figure 2.6</b> HCMV-associated alterations to lactate dynamics.....	41
<b>Figure 2.7</b> HCMV infected cells alter metabolic pathways of uninfected cells in a paracrine manner.....	44
<b>Figure 2.8</b> Metabolic reprogramming and paracrine effects of HCMV infection in glioblastoma.....	48
<b>Figure 3.1.1</b> Intermittent MCMV infection exhibits delayed inflammatory cytokine expression in the brain.....	68
<b>Figure 3.1.2</b> Intermittent MCMV infection exhibits delayed inflammatory cytokine expression in the brain.....	71
<b>Figure 3.2</b> Intermittent MCMV infection alters the transcriptional profile of brain cells.....	75
<b>Figure 3.3</b> Blood brain barrier metabolic pathways are rewired with increased MCMV exposure.....	79

<b>Figure 3.4</b> Hallmarks of mitochondrial dysfunction and oxidative stress are elevated in BMECs intermittently exposed to MCMV.....	82
<b>Figure 3.5</b> MCMV infection metabolically rewires astrocytes as a function of age.....	86
<b>Figure 3.6</b> Cognition is impaired with intermittent MCMV infection.....	89
<b>Figure A1</b> HCMV infection of LN-18 cells increases glycolysis and oxidative phosphorylation ATP production .....	111
<b>Figure A2</b> HCMV infection increases oxidative phosphorylation. OCR was measured at 72 and 120 hours post infection using the Seahorse XFe24 MitoStress Kit.....	112
<b>Figure A3</b> Gating strategy for flow cytometric analysis of HCMV infected cells.....	113
<b>Figure A4</b> The ECAR was measured at 72 and 120 hours post infection using the Seahorse XFe24 Glycolysis Stress Kit.....	114
<b>Figure A5</b> HCMV infection downregulates expression of key lactate regulatory genes.....	115
<b>Figure B1.1</b> Intermittent MCMV infection exhibits delayed inflammatory cytokine expression in the brain.....	120
<b>Figure B1.2</b> Intermittent MCMV infection exhibits delayed inflammatory cytokine expression in the brain.....	122
<b>Figure B1.3</b> Intermittent MCMV infection exhibits delayed inflammatory cytokine expression in the brain.....	124
<b>Figure B2</b> Flow cytometry panel.....	125

<b>Figure B3</b> Blood brain barrier metabolic pathways are rewired with increased MCMV exposure.....	126
<b>Figure B4</b> Hallmarks of mitochondrial dysfunction and oxidative stress are elevated in BMECs intermittently exposed to MCMV.....	127
<b>Figure B5</b> MCMV infection metabolically rewires astrocytes as a function of age.....	128
<b>Figure B6</b> Cognition is impaired with intermittent MCMV infection.....	129
<b>Figure C1</b> ASC morphologic analysis and colony formation assay.....	133
<b>Figure C2</b> Overview of differentiation of ASCs to Adipocytes, Osteoblasts, and Chondrocytes and methods of differentiation confirmation.....	159
<b>Figure C3</b> <i>In vitro</i> effects of ASCs on cell of the innate immune system.....	163
<b>Figure C4</b> <i>In vitro</i> effects of ASCs on cells of the adaptive immune system.....	175
<b>Figure D1</b> Pooled ObASCs exhibit reduced stemness characteristics.....	197
<b>Figure D2</b> RAW264.7 cells following indirect co-culture with ASCs in a Transwell system.....	200
<b>Figure D3</b> LnASCs and ObASCs differentially alter the migration and phagocytotic abilities of RAW264.7 cells.....	203
<b>Figure D4</b> SIM-A9 cells following indirect co-culture with ASCs in a Transwell system.....	207
<b>Figure D5</b> LnASCs and ObASCs differentially alter the migration and phagocytic abilities of SIM-A9 cells.....	210

## **CHAPTER 1**

### **BACKGROUND**

As obligate parasites, viruses rely on their host's metabolic machinery to generate the energy and building blocks necessary for viral replication. Viral manipulation of a large number of cellular processes such as regulation of the cell cycle, prevention of apoptosis, and evasion of the immune system are all necessary for successful viral replication. The ability of viruses to so completely manipulate the cellular and metabolic environment of their hosts is far from accidental. Certain viruses, such as the herpesviruses, have co-evolved with their hosts over the last several million years [1]. Such extensive co-evolution has molded these viruses so that they are well adapted to their hosts.

What remains unclear is how these lifelong infections mold their hosts and what effects their presence have on the organism as a whole. Classical and modern medicine have focused largely on treatment of acute infections which may threaten the life or wellbeing of the patient. However, this fails to address the long term consequences of latency and periodic reactivation. Additionally, while pathogen exposure has been linked to the development of numerous age-related pathologies such as cancer and dementia, the mechanistic drivers of these interactions remains unclear. In an effort to elucidate these mechanisms and

explain the findings of a great deal of correlative research, we undertook *in vitro* and *in vivo* studies using cytomegalovirus (CMV) as a model pathogen.

### **1.1 Cytomegalovirus**

Human herpesvirus-5, commonly referred to as cytomegalovirus (CMV), is ubiquitous with seroprevalence rates upwards of 80% in many populations [2-4]. In congenital infection, CMV is the leading cause of virus-associated hearing loss and developmental delay. Due to broad tropism, the effects of congenital CMV are varied and can involve hepatosplenomegaly, microcephaly, encephalitis, retinitis leading to vision loss, and, in severe cases, death [5]. In immunocompromised adults, such as those related to AIDS, cancer therapy, or organ transplant, infection or reactivation of the virus can occur in any number of organs and can be life threatening if not treated aggressively with anti-viral medication. Immunocompetent infection commonly produces mild flu-like symptoms followed by a lifelong period of latency punctuated by periodic reactivations. During these periods of reactivation, virus is transmitted to others via bodily fluids, including saliva and urine. In recent years, correlative and longitudinal research has begun to investigate the long-term effects of cytomegalovirus infection. Thus far, it has been associated with increased risk of age-related diseases such as type 2 diabetes, cancer, heart disease among others [6].

CMV has a large genome that is composed of linear double stranded DNA of about 240 kilobase pairs encoding roughly 165 genes [7, 8]. The genome is divided into two main regions the unique long (UL) and the unique short (US) which

are bounded by terminal and internal repeat sequences. The genome encodes protein coding transcripts, long non-coding RNA, and microRNAs many of which have unknown function. It is tightly packed and pressurized within an icosahedral nucleocapsid [9]. The nucleocapsid is surrounded by a tegument containing proteins which aid in viral genome replication and modulation of the host's immune system. Finally, these are enclosed by a viral envelope, a phospholipid bilayer adorned with glycoproteins that aid in cell surface interaction and infection of host cells [10]. Following viral entry, the virus replicates its genome and its nucleocapsid is assembled within the nucleus. Viral replication culminates in destruction of the host cell and release of mature virions into the environment.

In order to successfully replicate itself, CMV must control numerous host cell pathways. Extensive co-evolution has provided CMV with an ability to manipulate the metabolic functions of host cells, altering fatty acid oxidation [11], glycolysis [12], and oxidative phosphorylation [13, 14]. These pathways provide the energy and raw materials needed for the production of new infectious virions. In addition to metabolically reprogramming host cells, CMV has also been shown to disrupt anti-viral signaling pathways [15], induce chromosomal aberrations by inhibiting DNA repair mechanisms [16], and inhibit the function of various immune cell populations [17].

## ***1.2 Cytomegalovirus and glycolysis***

Cellular metabolism is an incredibly intricate process involving, at the most basic level, the catabolism of materials to release energy and/or smaller materials

which can then be used in anabolic processes to create materials necessary for a cell to perform whatever function is needed. In CMV replication, the virus requires purines and pyrimidines in order to replicate its genome, amino acids to produce its proteins, lipids to create its viral envelope, and a significant amount of energy to perform all of these tasks. In order to accomplish this, CMV metabolically reprograms the host cell.

Glycolysis is the process in which glucose is taken up from the extracellular environment by glucose transporters, such as GLUT1, and then modified by a series of enzymes to finally produce pyruvate. Previous research in fibroblasts has shown that CMV infection enhances the expression of glucose transporters, specifically GLUT4 [18]. Following import, a key kinase in the pathway, hexokinase II, prevents the diffusion of glucose out of the cell along its concentration gradient by phosphorylating it and producing glucose-6-phosphate. Following phosphorylation, a series of enzymes are responsible for the conversion of glucose-6-phosphate to pyruvate which enters the mitochondria and joins the tricarboxylic acid cycle (TCA) to fuel oxidative phosphorylation (OXPHOS). Metabolic analysis has demonstrated increases in metabolites and enzymes involved in glycolysis, such as phosphofructokinase and pyruvate dehydrogenase [19]. These findings emphasize the increased demand for energy as OXPHOS is the most efficient cellular metabolic pathway for large amounts of energy production.

### **1.3 Cytomegalovirus and mitochondria**

In the most simplistic sense, the mitochondria is the powerhouse of the cell. During cellular respiration, pyruvate from glycolysis is converted to Acetyl-CoA and enters the TCA cycle. This cycle produces reducing equivalents, NADH and FADH<sub>2</sub>, which are used in the electron transport chain (ETC) to establish a proton gradient between the inner and outer mitochondrial membrane. This gradient produces the proton motive force which powers complex V of the ETC, adenine triphosphate (ATP) synthase, to produce ATP from adenine diphosphate (ADP).

One product of the ETC function is the free radical superoxide (SO<sub>2</sub>). Reactive oxygen species (ROS), such as SO<sub>2</sub>, are neutralized by enzymes and co-enzymes of the endogenous antioxidant response system. While certain levels of ROS production are essential for proper cellular signaling pathway function, elevated levels of ROS which outstrip the neutralization abilities of the cell can result in oxidative stress and damage to proteins, nucleotides, and lipids [20]. Prolonged exposure to elevated levels of oxidative stress can lead to various pathologies associated with aging such as cancer, cardiovascular disease, and neurodegeneration.

ROS production resulting from uncontrolled OXPHOS would result in significant mitochondrial damage and dysfunction. As such, mitochondria are in constant communication with the extra-mitochondrial environment to assess and respond to the metabolic needs of the cell. This metabolic cross-talk is at least partly mediated by voltage gated ion channel (VDAC1). VDAC1 resides in the outer mitochondrial membrane and regulates the passage of molecules and ions into

and out of the mitochondria. Importantly, VDAC1 is responsible for the exchange of ADP for ATP and the release of ROS into the cytoplasm [21]. Another protein in mitochondrial cytoplasmic dynamics is the translocase of outer mitochondrial membrane 20 (TOMM20). TOMM20 is responsible for binding mitochondria targeting sequences of proteins from the cytoplasm and facilitating their entry into the mitochondria [22].

CMV has evolved numerous ways to manipulate the host cell's mitochondria. They provide CMV with both a source of energy and the ability to further manipulate numerous functions of cells. Research in human fibroblasts has demonstrated significant increases in mitochondrial function following cytomegalovirus infection [14]. The increase in respiration led to increased SO production and induced mitochondrial fission presumably to accommodate the increasing metabolic demands. By targeting different complexes of the ETC they were able to reduce viral replication [23]. This suggests that CMV replication is dependent on mitochondrial function.

In addition to their metabolic functions, mitochondria play a critical role in apoptosis. Cellular detection of viral proteins or genetic material will initiate innate viral response pathways promoting pro-inflammatory signaling such as mitochondrial anti-viral signaling (MAVS) or stimulator of interferon genes (STING). In order to evade these innate immune responses CMV produces mitochondria-localized inhibitor of apoptosis (vMIA) and inhibitor of caspase-8 induced apoptosis (vICA) [24, 25]. vMIA functions by binding and sequestering, pro-apoptotic protein, Bax at mitochondria inhibiting the release of cytochrome c.

vICA associates with caspase-8 and prevents its activation by the death-inducing signaling complex. Finally, the CMV glycoprotein US9 is able to target and inhibit both MAVS and STING signaling pathways. Inhibition of these apoptotic pathways is essential for the virus to produce and eventually release fully infectious virions.

#### **1.4 Cytomegalovirus and cancer**

Cancer represents one of the leading causes of mortality and morbidity worldwide, accounting for roughly 1 in 6 total deaths. Significant effort has, and is, being made to understand cancer and create effective treatments. As proposed by Hanahan and Weinberg, the Hallmarks of Cancer (HoC) include a set of 10 cellular changes which are characteristic of cancers and allow a cell to successfully evade replicative control and become cancerous [26, 27]. The majority of these changes are not random, they are the result of exposure to toxins, radiation, or pathogens such as viruses. Some viruses have become such potent manipulators of their host cells that they are able to induce many of these HoC. Thus far, seven viruses are classified as oncogenic. Of these seven, two are herpesviruses, Epstein-Barr Virus (HHV-4) and Kaposi sarcoma-associated herpesvirus (HHV-8) [28, 29]. Successful viral replication often requires reprogramming of energy metabolism, evasion of immune destruction, and resistance of cell death, three of the HoC [26].

This is true of CMV, which is known for metabolic reprogramming, inhibition of apoptotic mechanisms, and immune evasion. CMV has regularly been found in >90% of early breast cancers and breast cancer metastases [30-33]. While the role of CMV in various cancers is still being hotly debated, many have suggested

that CMV may behave in an oncomodulatory capacity, altering the tumor microenvironment to promote tumor survival, expansion, and metastasis.

Gliomas are glia-derived tumors of the central nervous system with the most aggressive, grade IV, representing the most common primary malignant nervous system neoplasia known as glioblastoma (GBM). Patients with GBM have poor prognosis. Following diagnosis, patients have a median survival of 13 months [34], with 5-year survival rates hovering around 5% [35]. The present standard of care is tumor resection, irradiation, and treatment with the chemotherapy drug temozolomide [36]. However, despite significant research and numerous clinical trials, patient 5-year survival has failed to improve over the past decade [35]. Because of this, development of improved therapeutic approaches is of paramount importance.

The presence of CMV in glioma tumor and surrounding tissue was first reported by Cobbs and Britt in 2002 [37]. Since then numerous groups have reported CMV proteins and/or transcripts in glioblastoma patients [38-45]. However, there is much debate within the field as to the validity of these findings because many groups have found no evidence of CMV [46, 47]. Seropositivity for CMV has been associated with poorer prognosis in GBM patients [48]. The lack of effective treatment options inspired researchers to initiate limited clinical trials adding valganciclovir (an anti-viral agent used to treat CMV infection) to the current standard of care. The results were impressive, with increased median overall survival (24.1 vs 13.3 months) and 2-year survival rate (49.8% vs 17.3%) [49, 50]. Similar results were seen in both primary and secondary glioblastoma during these

trials. More recently, targeted CMV-pp65 vaccination of patients with GBM was found to prolong progression free survival and overall survival [51]. These findings support the hypothesis that CMV plays a role in cancer progression but fail to elucidate the mechanism of action.

### ***1.5 Cytomegalovirus and the blood brain barrier***

Owing largely to its critical importance for organismal survival, the brain is maintained as a privileged environment. Components of the peripheral immune system have very limited access to the brain parenchyma. Consequently, the brain is largely surveilled by yolk sac-derived resident macrophages, termed microglia [52]. As the most metabolically demanding organ in the body, a significant amount of nutrients, especially glucose, are required to maintain normal function. The passage of these nutrients while limiting non-essential entry is mediated by the blood brain barrier (BBB). As the primary interface between systemic circulation and the central nervous system, the BBB is a critical structure which tightly regulates vascular permeability, nutrient diffusion, and immune extravasation.

The BBB is a cellular structure [53] formed by four primary components: (1) tightly apposed brain microvascular endothelial cells (BMECs) making up the walls of the blood vessels that feed the CNS; (2) a basement membrane providing structural integrity; (3) a non-continuous layer of pericytes; and (4) astrocytic end-feet which tightly enclose the blood vessel [54]. This structure employs tight junctions and transport proteins to restrict access to, and actively shuttle unwanted foreign substances out of the brain. During a systemic inflammatory response,

activated immune cells express pro-inflammatory cytokines such as TNF $\alpha$  and IL-6 which leads to increased BMEC permeability [55]. This permeability allows immune cells to extravasate from the bloodstream and enter the CNS as mediated by vascular cell adhesion molecules and selectin expression. Activated T cell entry produces classical activation of microglia which express pro-inflammatory cytokines [56]. This activity causes activation of astrocytes, which retract their end-feet from the endothelial cells. Activated astrocytes secrete VEGF-A which downregulates expression of proteins essential for tight junction (TJ) maintenance culminating in regional disruption of the BBB [57]. This disruption allows for enhanced entry of undesirable cells and molecules which can produce significant damage.

Viruses have several methods by which they negotiate entry into the brain. Paracellular entry involves matrix metalloprotease mediated degradation of the tight junction proteins claudin and occludin [58] allowing viruses to enter between BMECs. Some viruses such as human immunodeficiency virus are able to cross the BBB by passing through the endothelial cells, and often infecting them, in a process termed transcellular migration [59]. Finally, the “trojan-horse” strategy allows viruses which infect immune cells to pass through the BBB undetected. Regardless of the mechanism of entry, active viral infection of the CNS can produce a wide range of symptoms both cognitive and physiological. Brain entry can result in viral encephalitis as observed with herpesviruses, retroviruses, and coronaviruses [59] [60] [61]. However CMV, in non-congenital infections, has great difficulty crossing the BBB. Research in a murine model has demonstrated that

immune deficiency is necessary for CMV to enter the brain parenchyma [62]. Thus, the most severe effects of CMV infection occur in congenital infections where the virus is easily able to cross the BBB.

### ***1.6 Cytomegalovirus and dementia***

Dementia is an umbrella term for the loss of memory and other cognitive abilities which become severe enough to interfere with daily life. This impairment is produced by brain damage caused by injury or disease. Many different subtypes of dementia exist as classified by the underlying pathology. Some less common types of dementia are vascular, Lewy body, frontotemporal, and those associated with neurodegenerative diseases such as Huntington's. However, the vast majority, over 60%, of dementias worldwide are caused by Alzheimer's disease [63]. In the United States alone there are over 6 million individuals with AD [64]. Functionally, AD is typified by memory loss, changes to mood, disorientation, and language problems. As a degenerative disease, these symptoms progressively get worse until the final stages. Patients often die of pneumonia resulting from swallowing difficulties and aspiration of food or drink. AD is a strongly age-associated disease with a prevalence of roughly 1 out of 3 in adults over the age of 85 [65]. Medical advances have resulted in greatly increased longevity suggesting that the number of individuals with AD will increase with time [66]. Though links have been made to specific risks such as genetics, successful therapeutic development remains elusive. Numerous drugs have been created but

none have been able to demonstrate improved cognition or significantly decreased cognitive decline in clinical trials [67].

This lack of effective therapeutics is almost certainly due to a paucity of understanding regarding the factors and mechanisms driving AD progression. AD has historically been characterized based on the accumulation of intracellular hyperphosphorylated tau tangles and extracellular amyloid plaques. The accumulation of these results in neurotoxicity leading to cell death and an overall decrease in white matter. Thus far, therapies have focused on reduction of plaque and tangle burdens of AD brains. Though several have been successful at reducing plaque burden, they all have failed to produce any functional improvements in cognition [67]. The most recent trials show promise but they have resulted in brain bleeding and swelling in about 40% of the participants.

At its core, AD is a disease of aging and age-related dysfunction. Mild cognitive impairment is rarely seen until the disease has been developing for many decades. In fact, plaques and tangles can be detected long before there is any measurable cognitive decline [64]. These findings indicate a long prodromal period during which numerous factors may accelerate AD progression. Studies of aged individuals has linked increased exposure to HSV-1 and other pathogens with decreased cognitive function and accelerated cognitive decline [68, 69]. In fact, elevated cytomegalovirus-specific antibody levels have been associated with decreased cognitive function in non-elderly adults [70]. These associations suggest a role for pathogens and the body's reaction to pathogens as potential

drivers of AD. However, the mechanism behind such a role is unclear and remains an ideal candidate for future research.

### **1.7 Research plan**

Metabolic reprogramming is one of the hallmarks of cancer with tumors upregulating aerobic glycolysis despite adequate oxygen in a process known as the Warburg Effect [71, 72]. It was initially speculated that upregulation of glycolysis rapidly produced the energy necessary to maintain tumor proliferation and progression despite mitochondrial dysfunction. However, more recently, another hypothesis posits that some cancers cells have elevated OXPHOS which is able to maintain the health of the cell despite being exposed to stress (i.e. chemotherapy). In this model, the transfer of metabolites between cells accommodates the proliferation and survival of neighboring cells in a process termed the Reverse Warburg Effect [73]. CMV has been shown to induce significant metabolic reprogramming in cells causing increases in both glycolysis and oxidative phosphorylation (OXPHOS) [12-14].

We hypothesize that CMV infection of cancer cells may provide some benefit to their metabolic flexibility. To test this hypothesis we will employ an *in vitro* approach in which we infect GBM cells and examine the metabolic changes that occur. These changes will aid our understanding of the potential CMV has to further alter the metabolic landscape of an already metabolically aberrant cell. Findings from this study may allow us to identify whether CMV produces functional changes in GBM cells that may enhance their ability to survive and/or proliferate.

The knowledge gained from these experiments may lead to novel therapeutic targets for treatment of GBM.

CMV has the ability to exert significant control over many different cell types. This control often manifests as enhanced OXPHOS function and the production of elevated levels of ROS. Considering the effects that oxidative stress has on a cellular level we plan to examine the effects of infection and reactivation on an organismal level. As a critical and also extremely sensitive organ, we will focus our attention on the brain. We hypothesize that CMV infection will accelerate cognitive aging in a synergistic manner with normal aging. Knowledge gained from this vein of research may prove invaluable for the development of therapeutics or prophylactics to address the inexorable process of cognitive decline.

## CHAPTER 2

### METABOLIC REPROGRAMMING OF GLIOBLASTOMA CELLS DURING HCMV INFECTION INDUCES SECRETOME-MEDIATED PARACRINE EFFECTS IN THE MICROENVIRONMENT<sup>1</sup>

#### **2.1 ABSTRACT**

Glioblastoma (GBM) is an aggressive primary central nervous system neoplasia with limited therapeutic options and poor prognosis. Following initial reports of cytomegalovirus (HCMV) transcripts and proteins in GBM tumors, the anti-viral drug Valganciclovir was added to the current standard of care and was found to significantly increase longevity of GBM patients. However, the underlying mechanism behind the effects of CMV on GBM progression has yet to be elucidated. We hypothesized that HCMV infection would metabolically reprogram GBM cells and that these changes would allow for accelerated tumor progression. We infected LN-18 GBM cells with HCMV and employed a Seahorse Bioanalyzer to characterize cellular metabolism. Increased mitochondrial respiration, glycolytic rate, and production of both reactive oxygen species and lactate were observed

---

<sup>1</sup> As published: Harrison MAA et al. Metabolic Reprogramming of Glioblastoma Cells during HCMV Infection Induces Secretome-Mediated Paracrine Effects in the Microenvironment. *Viruses*. 2022; 14(1):103. <https://doi.org/10.3390/v14010103>

following infection. Examination of paracrine signaling between HCMV-infected GBM cells and uninfected stromal cells, indicated that, independent of viral transmission, HCMV-infected GBM cells were able to alter the expression of key metabolic proteins and epigenetic markers of stroma cells. These results suggest an oncomodulatory role linked to tumor metabolism for HCMV in the context of GBM.

## **2.2 INTRODUCTION**

Glioblastoma (GBM) is the most common primary malignant central nervous system neoplasia. Patients have a poor prognosis, with 5-year survival rates around 5% [35]. The current standard of care is tumor resection, irradiation, and treatment with the chemotherapy drug temozolomide [36]. Notably, patient survival has failed to improve significantly over the past decade emphasizing the urgent need for improved or novel therapies [35]. One field currently under investigation is the role of viruses in oncogenesis or oncomodulation. Several viruses have been closely associated with cancers and are identified as oncogenic accounting for approximately 15% of human cancer [28, 29, 74]. In the context of GBM, numerous neurotropic viruses have been investigated mainly in the polyomavirus and herpesvirus families due to prevalence and persistence but no direct association has been identified [75, 76].

The presence of human herpesvirus-5 (cytomegalovirus (HCMV)) in GBM tumor and surrounding tissue was first reported by Cobbs and Britt in 2002 [37]. Since then numerous groups have reported HCMV proteins and/or transcripts in

GBM specimens [38-45]. However, there is much debate within the field as to the validity of these findings as other groups have found no evidence of HCMV in GBM tumors [46, 47]. Despite the absence of a clearly defined role for HCMV in GBM progression, Phase 2 clinical trials were initiated adding valganciclovir (an antiviral agent used to treat HCMV infection) to the current standard of care. Inclusion of valganciclovir increased median overall survival (24.1 vs 13.3 months) and 2-year survival rate (49.8% vs 17.3%) [49, 50]. These findings support the hypothesis that HCMV plays a role in GBM but fail to elucidate a mechanism of action. The role of HCMV in cancer remains a polarizing topic. A current hypothesis suggests that HCMV may behave in an oncomodulatory capacity, altering the tumor microenvironment to promote tumor survival, expansion, and metastasis. These properties have been linked to multiple mechanisms including increased cell division, cell migration and angiogenesis. However, the effects of HCMV on tumor metabolism have not been examined. We hypothesize that metabolic reprogramming of host cells following HCMV infection may play a significant role in tumor progression.

HCMV is a ubiquitous herpesvirus with seroprevalence rates upwards of 80% in many populations [2-4]. Most primary infections are asymptomatic or result in flu-like symptoms followed by lifelong episodes of latency and reactivation. HCMV infection has been demonstrated to disrupt anti-viral signaling pathways [15], induce chromosomal aberrations by inhibiting DNA repair mechanisms [16], and inhibit the function of various immune cell populations [17] resulting in immune evasion. HCMV has also been reported to manipulate the metabolic functions of

host cells, affecting, fatty acid oxidation [11], glycolysis [18, 19], and oxidative phosphorylation (OXPHOS) [13, 14, 77]. Intriguingly these consequences of HCMV infection, reprogramming of energy metabolism and evading immune destruction, represent the two “Emerging Hallmarks” of cancer as described by Hanahan and Weinberg [26]. Many cancer cells, despite the presence of adequate oxygen, upregulate aerobic glycolysis, commonly referred to as the Warburg Effect [71, 72]. Interestingly, upregulation of aerobic glycolysis has been observed in fibroblasts following HCMV infection [18, 19]. More recently, another related hypothesis posits that cancerous cells alter the surrounding stromal cells’ metabolism resulting in the Warburg Effect [73]. These cells produce metabolic products which are then transported to the cancer cells to accommodate their proliferation and survival in a process termed the Reverse Warburg Effect.

In this manuscript we characterize the metabolic reprogramming that occurs following acute infection of GBM with HCMV *in vitro*. We provide evidence that infection produces a significant increase in the rate of host cell glycolysis and OXPHOS. Additionally, we demonstrate that these alterations lead to the production of metabolites which may significantly alter the tumor microenvironment. Finally, we demonstrate the ability of HCMV infected GBM cells to alter the levels of key metabolic proteins and induce epigenetic changes in uninfected neighboring cells. These data lay the foundation of a mechanism of HCMV-mediated tumor progression in the context of both GBM and cancers in general.

## **2.3 METHODS**

### **CELL AND VIRUS CULTURE**

Glioblastoma (LN-18), and human foreskin fibroblast (HFF) cell lines were purchased from American Type Culture Collection (ATCC #CRL-2610, #SCRC-1041; Manassas, VA, USA) and cultured in Dulbecco's Modified Eagle Medium (DMEM; #11965-084; Thermo Fisher Scientific, Waltham, MA, USA) containing 4.5 g/L glucose and 4mM L-glutamine supplemented with 5% or 10% fetal bovine serum (FBS; #S11550; Atlanta Biologicals, Flowery Branch, GA, USA) respectively. Cells were maintained at 37°C with 5% CO<sub>2</sub> and routinely tested for mycoplasma using the MycoAlert PLUS kit (#LT07-701; Lonza, Morristown, NJ, USA).

Viral stocks of HCMV Towne-GFP were propagated in HFF cells using a multiplicity of infection (MOI) of 0.1 as previously described [78]. Briefly, cells were cultured with virus until ~90% cytopathic effect was observed. Remaining adherent cells were scraped from plates. Cellular debris and supernatant were pelleted by centrifugation. Clarified supernatant was added to thin-wall, ultra-clear 25x89mm tubes (#344058; Beckman Coulter, Brea, CA, USA), a 20% sucrose solution was underlaid, and cells were centrifuged for 40 minutes at 104,000 xg at 16°C. Viral pellet was resuspended in tris sodium chloride (TN) buffer.

Viral titers were determined by serial titration of viral stocks on HFF cells in triplicate. Following 48 hours of culture, media was removed, cells were washed with 1x PBS, and fixed with 95% ethanol. Cells were incubated with anti-HCMV IE1 mouse polyclonal antibody (1:200; Generously gifted by Bill Britt) for one hour

at 37°C followed by Alexa Fluor 594 goat anti-mouse polyclonal secondary antibody (1:1000; #A11005; Invitrogen Corp., Carlsbad, CA, USA) for 1 hour at room temperature. Stained cells were counted manually using a Nikon Eclipse Ti2 microscope (Nikon Inc., Tokyo, JP).

Viral infection was performed on confluent LN-18 cells using a MOI of 3 for 90 minutes. Mock-infected and infected cells were then washed with 1xPBS, fresh complete culture media was added, and cells were maintained for the indicated infection period.

#### xCELLigence REAL-TIME CELL ANALYSIS

An Agilent xCELLigence platform (Agilent Technologies Inc., Santa Clara, CA, USA) was used to examine cytopathic effect following infection with HCMV. Cells were seeded into a 96-well E-plate at 80% confluence and Cell index (impedance) was measured at 15-minute intervals. When Cell Index stabilized (~48 hours post seeding) cells were infected with HCMV at a MOI of 3. Cell index was measured every 15 minutes for the duration of the experiment. Reads were normalized to the timepoint immediately prior to infection.

#### RNA ISOLATION AND qRT-PCR

RNA was isolated using the RNeasy Minikit (#74106; Qiagen, Hilden, DE) and converted to cDNA using the iScript cDNA synthesis kit (#1708891; Bio-Rad, Hercules, CA, USA) according to manufacturer's instructions. qRT-PCR was conducted on cDNA using Sso Advanced SYBR Green Supermix (#1725271; Bio-Rad) and gene-specific primers.

Primers: SCL16A1 (MCT1; qHsaCID0008777; Bio-Rad); SLC16A3 (MCT4; qHsaCID0014322; Bio-Rad); LDHA (qHsaCED0001212; Bio-Rad) LDHB (qHsaCID0012068; Bio-Rad); HCMV IE1 (F: 5'-CAAGTGACCGAGGATTGCAA-3', R: 5'-CACCATGTCCACTCGAACCTT-3'; IDT DNA Technologies, Coralville, IA, USA); RPL13A (F: 5'-CTCAAGGTCGTGCGTCTGAA-3', R: 5'-TGGCTGTCACTGCCTGGTACT-3'; IDT DNA).

Cycle values were normalized to ribosomal protein L13a (RPL13A), and relative gene expression was determined using the  $2^{-\Delta\Delta C_t}$  method and reported as fold change relative to untreated controls.

### RNA-Seq

RNA isolation and sequencing were performed as previously described [79]. Briefly, G44 glioblastoma stem cells were mock- or HCMV-infected in triplicate and maintained for 72 HPI. RNA was isolated, assessed for degradation and contamination, and sequencing libraries were prepared using the Illumina paired-indexing protocol. STAR software was used to map raw reads to the reference organism. Data was cleaned and deposited in EMBL-EBI's ArrayExpress database (E-MTAB-7613).

### SEAHORSE BIOANALYZER

Metabolic profiling was conducted with XFe24 Seahorse Bioanalyzer (Agilent) according to manufacturer's instructions. Briefly, XFe24 cell plates were coated with Cell-Tak cell and tissue adhesive (#354240; Corning Inc., Corning, NY, USA) at a concentration of 3.5  $\mu\text{g}/\text{cm}^2$ . Cells were seeded at a concentration of  $1.2 \times 10^5$  cells per well and centrifuged at 450 rpm to permit adherence to the tissue

adhesive. Oxygen consumption rate (OCR) and extracellular acidification rate (ECAR) were measured for at least three independent experiments and used to characterize the metabolic phenotype of the cells. *XF Real-Time ATP Rate Test* (#103592-100; Agilent) was used to determine total ATP production and ATP production derived from either glycolysis or oxidative phosphorylation (OXPHOS) following treatments with oligomycin (1.5  $\mu$ M) and rotenone/antimycin A (0.5  $\mu$ M). *XF Mito Stress Test* (#103015-100, Agilent) was used to examine mitochondrial metabolic function by injecting oligomycin (1  $\mu$ M), FCCP (1  $\mu$ M), and rotenone (0.5  $\mu$ M) according to the manufacturer's protocol. *XF Glycolysis Stress Test* (#103020-100, Agilent) was used to measure glycolysis by injecting glucose (10 mM), oligomycin (1  $\mu$ M), and 2-deoxyglucose (100 mM) according to the protocol. At the completion of the Seahorse assay cells were stained with Hoechst 33258 (#H21491; Thermo Fisher) and imaged using a Nikon Eclipse Ti2 to quantify cell number. Normalization was completed using these cell counts.

### WESTERN BLOTTING

Following infection, cells were washed with cold 1xPBS and lysed with RIPA buffer supplemented with phosphatase and protease inhibitors (#88662, #88661; Thermo Fisher). Cells were sonicated and protein concentration of the soluble fraction was determined using a BCA assay (#23235; Thermo Fisher). Proteins were separated on a 4-12% Bis-Tris gel (#NP0322-BOX; Thermo Fisher) and transferred to nitrocellulose using the iBlot system (#IB301002; Thermo Fisher). Membranes were blocked with 5% nonfat dry milk (wt/vol) in 1xTBS with 1% Tween-20. Membranes were then incubated with primary antibodies overnight at

4°C, washed, and incubated at room temperature for 1 hour with anti-mouse (1:2,000; #7076; Cell Signaling Technology, Danvers, MA, USA) or anti-rabbit (1:10,000, #7074, Cell Signaling Technology) HRP-conjugated secondary antibodies. Membranes were imaged on an Amersham Imager 600 (General Electric, Boston, MA, USA).

Primary antibodies: anti-GAPDH Rabbit polyclonal antibody (1:1000; #G9545; Sigma Aldrich, St. Louis, MO, USA), anti-HCMV-IE1 mouse polyclonal antibody (1:200; Bill Britt), anti-HCMV-pp28 mouse monoclonal antibody (1:100; #sc-56975; Santa Cruz Biotechnology, Dallas, TX, USA), anti-HCMV-pp52 mouse monoclonal antibody (1:200; #sc-56971; Santa Cruz), anti-HCMV pp65 mouse monoclonal antibody (1:200; #sc-52401; Santa Cruz), anti-MCT1 mouse monoclonal antibody (1:100; #sc-365501; Santa Cruz), anti-MCT4 mouse monoclonal antibody (1:100; #sc-376140; Santa Cruz), anti-LDHA (1:1,000; #PA5-27406; Thermo Fisher), anti-LDHB (1:1,000; #PA5-96736; Thermo Fisher).

### FLOW CYTOMETRY

LN-18 cells were mock- or HCMV-infected for the desired timepoints and analyzed by flow cytometry as previously described [14]. Briefly, mitochondrial membrane potential was measured using MitoTracker Deep Red (200 nM; #M22426, Thermo Fisher) or MitoTracker Orange CMTMRos (250 nM; #M7510, Thermo Fisher). Reactive oxygen species production was assessed using CellROX Deep Red (750 nM; #C10491, Thermo Fisher) or CellROX Orange (750 nM; #C10493, Thermo Fisher). Superoxide production was examined using MitoSOX Red (5 µM; #M36008, Thermo Fisher). Representative gating strategy

used for these experiments is described in Supplementary Figure A.3A. Briefly, singlets were identified and selected for; live cells were gated using Sytox Blue Dead Cell Stain (1:1,000; #C10491, Thermo Fisher); GFP expression was used to gate on HCMV infected cells (Towne-GFP); finally the dye of interest was examined.

For metabolic flow panels, cells were mock- or HCMV-infected for the desired timepoints, incubated with LIVE/DEAD Fixable Dead Cell Stain (1:1,000; #L34957; Thermo Fisher) for 30 minutes at room temperature before fixation and permeabilization using eBioscience Foxp3 / Transcription Factor Staining Buffer Set (#00-5523-00; Thermo Fisher) for 20 minutes at room temperature. Cells were washed with 1x Perm Buffer and incubated with conjugated primary antibodies for 1 hour at room temperature. Cells were washed 2x with Perm Buffer and resuspended in flow buffer for analysis. Data was acquired using a LSRFortessa (BD Biosciences; San Jose, CA, USA) and quantified using FlowJo software (BD Biosciences).

Primary antibodies: anti-MCT1-AF647 (1:100; #sc-365501 AF647; Santa Cruz), anti-MCT4-PE (1:100; #sc-376140 PE; Santa Cruz), anti-Tomm20-AF405 (1:1,000; #ab210047; Abcam, Cambridge, UK), anti-H3K27me3-PE (1:1,000; #40724; Cell Signaling Technology), anti-GLUT1-AF647 (1:1,000; #ab195020; Abcam) anti-VDAC1 (1:1,000; #ab14734; Abcam). The VDAC1 antibody was conjugated to PE-Cy5 using the Lightning-Link Kit (#ab1023893; Abcam) according to the manufacturer's instructions.

### LACTATE ASSAY

LN-18 cells were mock- or HCMV-infected for the desired timepoints. Supernatant was collected and clarified by simple centrifugation. Cells were lysed with RIPA buffer as described above. Supernatant and cell lysates were deproteinized with TCA following manufacturer's instructions (#ab204708; Abcam). Lactate concentration was determined by comparison with standards using a L-lactate assay kit (#ab65331; Abcam).

### CO-CULTURE ASSAY

HFF cells were seeded into 6-well plates. LN-18 cells were seeded into the upper portion of a 6-well Transwell with 0.4  $\mu\text{m}$  pores (#3470; Corning) and cultured separately from the HFFs. Once confluent, the LN-18s were infected with HCMV Towne-GFP at a MOI of 3 and incubated for 90 minutes at 37°C. Cells were washed twice with 1xPBS, fresh complete culture media was added, then Transwells were placed in the 6-well plates with the HFFs for the desired infection period. At the final timepoint, HFFs were examined for signs of CPE and the cell culture medium was titered as described above to determine the presence of any virus. Cells were isolated and assayed by flow cytometry.

### STATISTICAL ANALYSIS

All data are expressed as mean standard error of the mean (SEM) from at least three independent experiments. All data were analyzed using Prism 9 software (GraphPad; San Diego, CA, USA). Comparisons between mock and HCMV groups were assessed using unpaired *t* tests. Ordinary one-way analysis of variance followed by Dunnett's multiple-comparison test were used to compare

samples across time points. For all comparisons, a  $p < 0.05$  was considered significant.

## **2.4 RESULTS**

### HCMV infects and replicates in a human glioblastoma cell line LN-18

We examined the infection kinetics of HCMV Towne-GFP (IE1-GFP) in the glioblastoma cell line LN-18 to confirm tropism and to characterize its replication cycle. Following infection, RNA, cell lysate, and supernatant were collected daily. Transcriptional expression of HCMV immediate early gene 1 (IE1) was evident at 24 hours post infection (HPI) and remained present throughout the time course (Figure 2.1A). Protein expression of IE1, early gene HCMV-pp65, leaky-late gene HCMV-pp52, and true late gene HCMV-pp28 matched published data defining HCMV gene expression products (Figure 2.1B) [18]. Consistent with our translational expression data, LN-18 cells exhibited a replication cycle of ~120 HPI as determined by initial cellular lysis and infectious virus release (Figure 2.1D).

An Agilent xCELLigence platform was used to dynamically monitor longitudinal viral infection of LN-18 cells following infection (Figure 2.1C). xCELLigence records the Cell Index, a unitless proxy for cellular impedance of electron flow produced by a confluent cell layer. As infection progresses, cytopathic effect (CPE) increases as the cells round, decreasing impedance and therefore Cell Index. As evidenced by the Cell Index plot, HCMV infection reduced Cell Index relative to mock infected cells at 48 HPI. Taken together, the transcriptional and translational detection of HCMV genes, induction of CPE, and

release of infectious virus by 120 HPI indicate that HCMV is able to productively infect LN-18 cells.

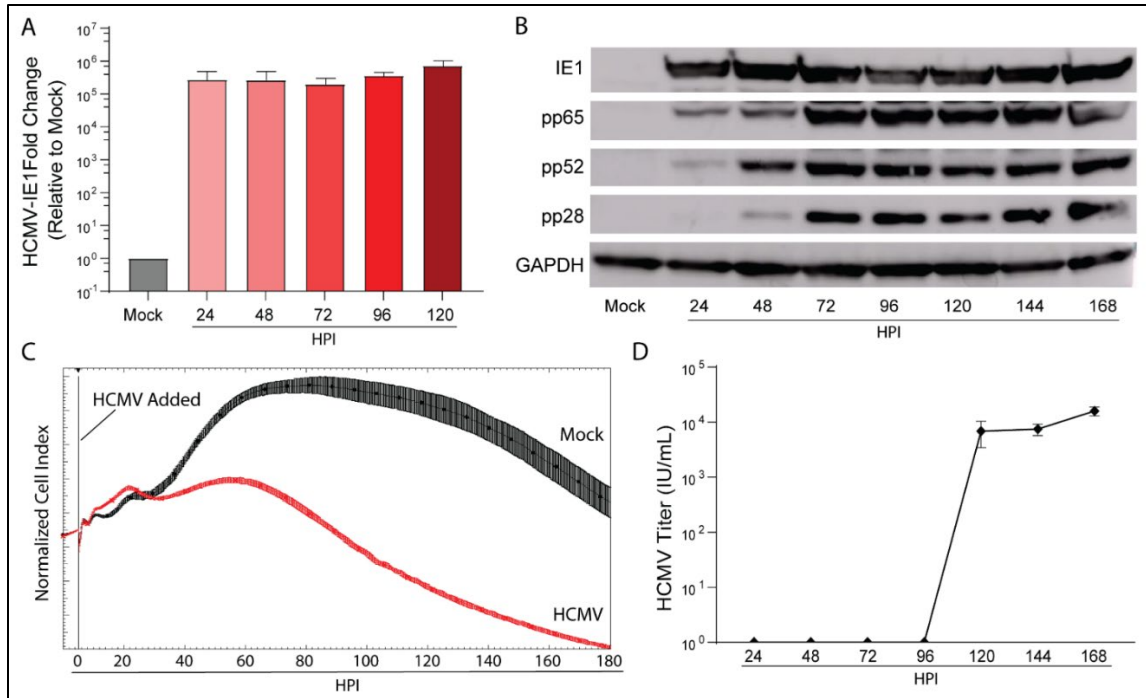


**Figure 2.1 HCMV can productively infect the glioblastoma cell line LN-18.**

LN-18 cells were infected with HCMV Towne strain and (A) transcriptional and (B) translational profiles of key HCMV proteins were examined by qPCR and WB. Mock infected cells served as controls. (C) Dynamic monitoring of LN-18 Cell Index (impedance) during HCMV infection using xCELLigence. (D) Viral titers of cell culture supernatant were quantified using an immunofluorescent based assay. Graphs represent pooled data from three independent experiments. Mean  $\pm$  the SEM of at least 3 triplicates.

### HCMV infection metabolically reprograms LN-18 cells

Previous research in HFFs has indicated that HCMV is a potent regulator of host cell metabolism and causes upregulation of aerobic glycolysis [18, 19]. To understand the metabolic profile of HCMV infected glioblastoma cells, we employed the Seahorse XFe24 Bioanalyzer and examined ATP production rate and source. The Seahorse Bioanalyzer measures cellular oxygen consumption rate (OCR) and extracellular acidification rate (ECAR) to assess mitochondrial oxidative phosphorylation (OXPHOS) and glycolysis respectively. Briefly, baseline readings were obtained followed by injection of oligomycin to inhibit ATP production by ATP synthase (Complex V) of the electron transport chain (ETC). This allowed for calculation of the mitochondrial ATP production rate. Next a mixture of rotenone and antimycin A, inhibitors of ETC Complex I and III, was added to cells to abolish any extracellular acidification related to ETC function. ATP production rate exclusively derived from glycolysis was determined by ECAR measurements. Total ATP production rate was then subdivided into mitochondrial (mitoATP) and glycolysis (glycoATP) derived ATP. All measurements were normalized to cell number.

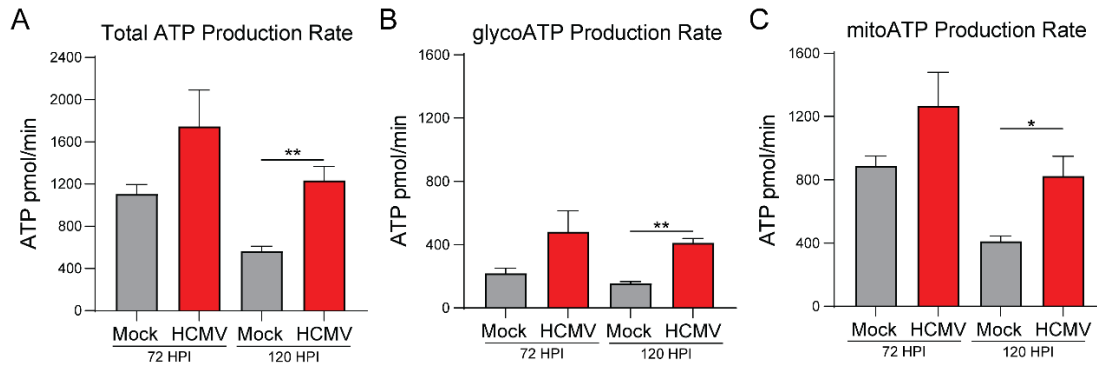


**Figure 2.2 HCMV infection of LN-18 cells increases host ATP production using glycolysis and oxidative phosphorylation metabolic pathways.**

(A) Total ATP, (B) glycoATP, and (C) mitoATP production rates were quantified at 72 and 120 hours post infection using the Seahorse XFe24 Real-Time ATP Rate kit. All samples were normalized to cell number. Graphs represent pooled data from three independent experiments. Mean  $\pm$  the SEM of at least 3 triplicates. \*,  $P < 0.05$ ; \*\*,  $P < 0.01$ .

At 120 HPI, we witnessed a significant increase in total ATP production rate in HCMV infected cells (Figure 2.2A). Significant increases in both glycoATP (Figure 2.2B) and mitoATP (Figure 2.2C) production rates were also observed.

Interestingly, there was a significant increase in the percentage of glycoATP and a corresponding decrease in the percentage of mitoATP at 72 HPI (Figure A1B, A1C). Overall, the mitoATP:glycoATP ratio, termed XF ATP Rate Index, favored ATP production by OXPHOS in mock- and HCMV-infected cells (Figure A1A). We conclude that HCMV infection induces significant metabolic reprogramming to increase ATP production largely irrespective of pathway (aerobic glycolysis versus OXPHOS). Presumably this reprogramming is necessary to meet the increased metabolic and bioenergetic demands of viral replication.

#### HCMV infection increases oxidative phosphorylation of host cells

To further examine the increased mitoATP production rate, we evaluated mitochondrial function using the Seahorse Bioanalyzer. Briefly, basal respiration rate was assessed via baseline OCR measurement of mock- or HCMV-infected cells (Figure 2.3A). The cells were treated with oligomycin to inhibit ATP synthase which indicates the respiration linked to ATP production. Next carbonyl cyanide-4 phenylhydrazone (FCCP) was used to disrupt the proton gradient and mitochondrial membrane potential. With maximal ETC complex I-IV function, OCR was used to determine the maximal respiration rate of the mitochondria and the spare respiratory capacity. Finally, rotenone and antimycin A, inhibitors of ETC

complexes I and III, were added to determine oxygen consumption unrelated to mitochondria function.

HCMV infection produced an increase in mitochondrial respiration in all treatment conditions (Figure 2.3B). We saw increases in basal respiration relative to mock-infected cells and maximal respiration capacity (Figure 2.3C and 2.3D). This increase in maximal respiration also indicates a significant increase in spare respiratory capacity of HCMV infected cells (Figure 2.3E; Figure A2C). These results suggest that HCMV infection has increased host cell mitochondrial function permitting increased energetic production as observed in Figure 2.

In agreement with the previous ATP Rate Assay, HCMV-infected cells exhibit significantly increased ATP production (Figure A2B). Additionally, host cells had elevated basal respiration accounting for a greater percentage of their maximal respiratory capacity. This suggests that host cells are increasing mitochondrial respiration to produce the biosynthetic materials and bioenergy necessary for viral replication.

Proton leak, a measure of mitochondrial damage or alternatively a means of regulating mitochondrial membrane potential, was significantly increased in HCMV infected cells relative to controls (Figure 2.3E). Finally, there were no significant changes in non-mitochondrial oxygen consumption or coupling efficiency with HCMV infection at either timepoint (Figure A2A and 2.2D).

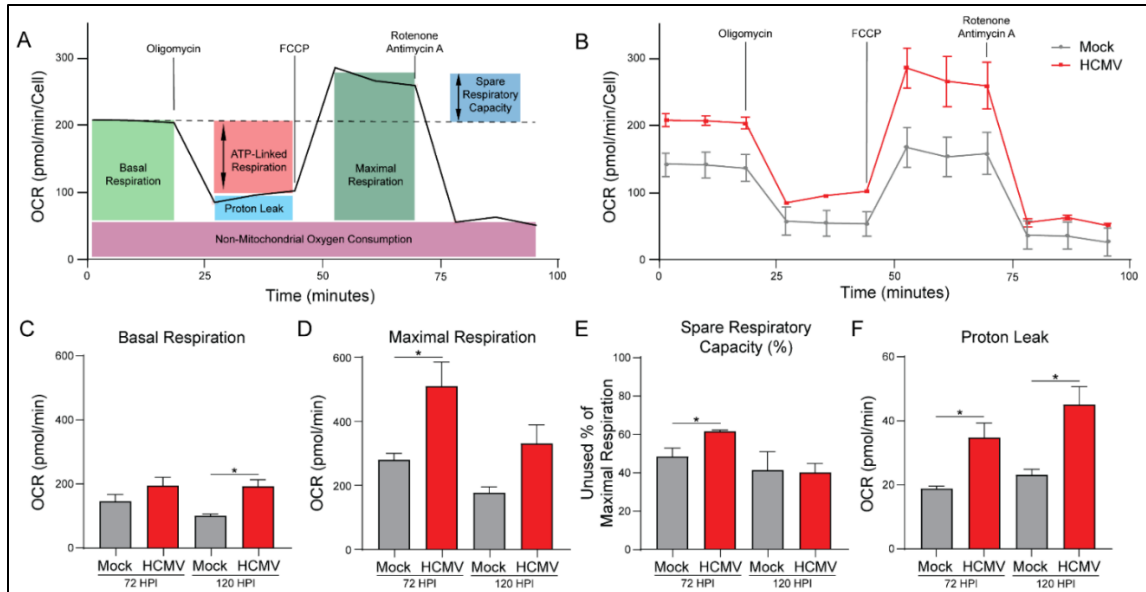


**Figure 2.3 HCMV infection increases oxidative phosphorylation in LN-18 cells.** (A) A cartoon illustrating how mitochondrial function was measured at 72 and 120 hours post infection (HPI) using the Seahorse XFe24 MitoStress Kit. (B) Representative data output of LN-18 cells mock- or HCMV-infected at 72 HPI. (C) Basal Respiration, (D) Maximal Respiration, (E) Spare Respiratory Capacity, and (F) Proton Leak were derived from these measurements. All samples were normalized to cell number. Graphs represent pooled data from three independent experiments. Mean  $\pm$  the SEM of at least 3 triplicates. \*,  $P < 0.05$ .

HCMV infection increases mitochondrial membrane potential and production of reactive oxygen species

Upregulation of OXPHOS can result in increased mitochondrial membrane potential as the mitochondria attempt to meet energetic demands. To investigate HCMV-mediated alterations in membrane potential we labeled cells with MitoTracker Orange CMTMRos, a reduced rosamine-based dye which, when oxidized by oxygen in respiring cells, becomes fluorescent. At all timepoints following infection, HCMV-infected cells exhibited increased membrane potential relative to their mock-infected counterparts with a peak at 96 HPI (Figure 2.4A). To confirm these findings, we used another membrane-potential dependent dye, MitoTracker Deep Red. MitoTracker Deep Red is an inherently fluorescent carbocyanine-based dye that has a high affinity for mitochondria. Following infection with HCMV, cells stained with MitoTracker Deep Red exhibited increased mitochondrial membrane potential relative to their mock-infected controls which became statistically significant at 96 and 120 HPI. Despite the differences in mechanism of action, both dyes produced similar results indicating increased membrane potential in HCMV-infected cells (Figure A3B).

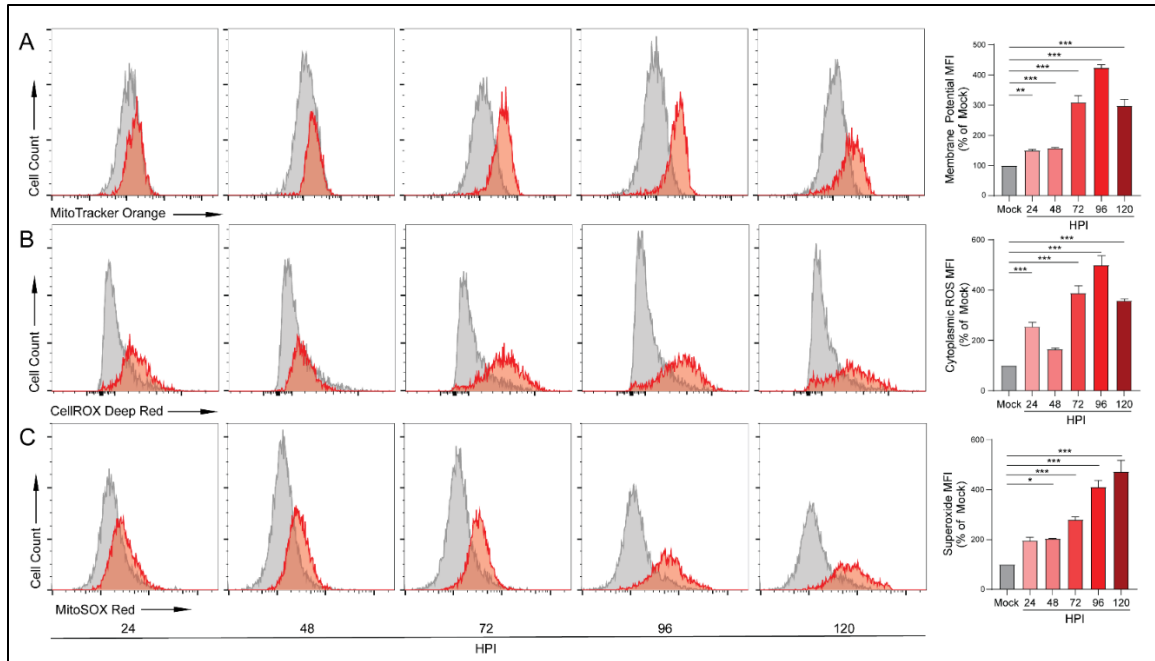


**Figure 2.4 HCMV infection increases electron transport chain function.**

Flow cytometry was used to quantify functional aspects of the electron transport chain. (A) Mitochondrial membrane potential was analyzed in mock- or HCMV-infected LN-18 cells using the reduced rosamine-dye, MitoTracker Orange which is dependent on mitochondrial oxidation to become fluorescent (B) cytoplasmic ROS production was detected by CellROX Deep Red, and (C) mitochondrial superoxide levels were measured using MitoSOX Red. All samples were gated on singlets and live cells only. Graphs represent pooled data from three independent experiments. Mean  $\pm$  the SEM of at least 3 triplicates. \*,  $P < 0.05$ ; \*\*,  $P < 0.01$ ; \*\*\*,  $P < 0.001$ .

Upregulation of OXPHOS can result in the production of reactive oxygen species (ROS) that exceeds the neutralization ability of the antioxidant systems including nicotinamide adenine dinucleotide (NAD/NADH). At low levels, ROS acts in a variety of intra- and inter-cellular signaling cascades. However, excessive ROS can cause significant cellular oxidative stress resulting in DNA, protein, and lipid damage and potentially cell death[80]. We examined ROS production using CellROX Deep Red, a dye which becomes fluorescent following oxidation by ROS. We detected increases in ROS species which peaked at 96 HPI (Figure 2.4B). These findings were confirmed using another oxidation dependent dye, CellROX Orange (Figure A3C).

During respiration, superoxide can be produced from specific mitochondrial sites. We employed MitoSOX Red, a dye that becomes fluorescent following oxidation by superoxide but is resistant to oxidation by other ROS. Similar to the CellROX results, we witnessed significant increases in superoxide production at 48 HPI and at all subsequent timepoints (Figure 2.4C). These increases in superoxide were not observed in the mock infected cells. These findings suggest that, following infection, the ETC is running at an elevated rate and producing superoxide at a rate that surpasses the neutralization ability of antioxidant pathways.

#### HCMV infection increases glycolytic rate and capacity

The ATP Rate Assay indicated increased glycoATP and percentage of ATP derived from glycolysis. To further investigate this, we again employed the Seahorse Bioanalyzer. Briefly, ECAR measurements were taken for both mock-

and HCMV-infected cells prior to the introduction of glucose (Figure 2.5A). Measurements obtained in the presence of glucose established the baseline rate of glycolysis. Next, oligomycin was added to inhibit ATP synthase and eliminate all mitochondrial ATP production, forcing the cells to depend on glycolysis for energy production. This provided the maximal glycolytic capacity as well as the glycolytic reserve available. Finally 2-deoxy-D-glucose, a glucose analog and inhibitor of hexokinase-2, was added to inhibit glycolysis and identify ECAR unrelated to glycolysis.

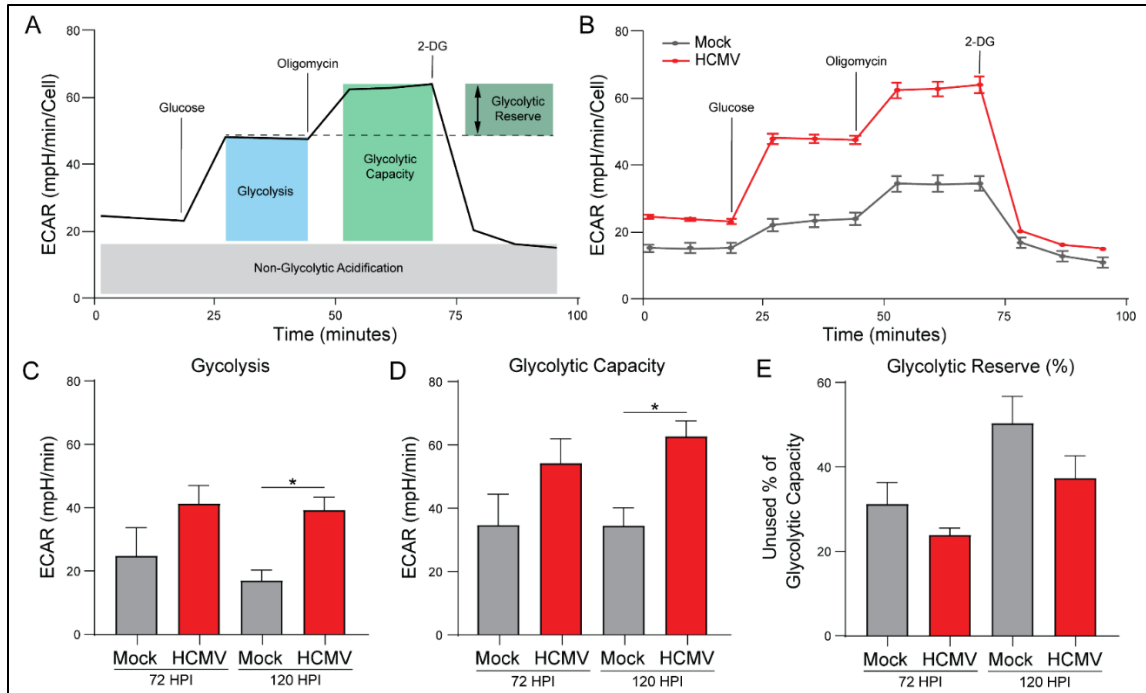


**Figure 2.5 HCMV infection increases glycolysis and glycolytic capacity.**

(A) Measurements of the extracellular acidification rate (ECAR) determined using a Seahorse XFe24 Glycolysis Stress Kit are illustrated. (B) Representative data output of LN-18 cells mock- or HCMV-infected. (C) Glycolysis, (D) Glycolytic Capacity, and (E) Glycolytic Reserve were derived from these measurements. All samples were normalized to cell number. Graphs represent pooled data from three independent experiments. Mean  $\pm$  the SEM of at least 3 triplicates. \*,  $P < 0.05$ .

HCMV infection resulted in increased glycolysis in all treatment conditions (Figure 2.5B). HCMV-infected cells exhibited increased basal and maximal glycolytic rate relative to mock-infected cells (Figure 2.5C and 2.5D). These results suggest that HCMV has started to alter the glycolytic behavior of the cells and is consistent with previous studies of HCMV infection indicating increases in glycolysis due to upregulation of GLUT4 [18].

There was a trend for HCMV-infected cells to use more of their maximal glycolytic capacity relative to mock-infected cells as evidenced by decreased percentage of glycolytic reserve (Figure 2.5E). Finally, there were no significant differences in non-glycolytic acidification or glycolytic reserve between mock- and HCMV-infected cells, although both trended toward an increase with HCMV infection. Taken together, these findings suggest that HCMV reprograms host cells to respond to increased energetic needs by increasing basal- and the potential for maximal-glycolysis relative to mock-infected cells. Thus, we decided to examine the effects of increased aerobic glycolysis on lactate production.

#### Elevated aerobic glycolysis following HCMV infection alters lactate production and flux

Our Seahorse Bioanalyzer data indicated significant increases of glycolysis following infection with HCMV. One product of aerobic glycolysis is lactate; thus, we employed a L-lactate assay kit to examine both the intracellular (Figure 2.6A) and extracellular (Figure 2.6B) concentrations of lactate. Intracellular lactate was increased in HCMV-infected cells from 48 HPI through 168 HPI relative to mock-infected cells. This correlates well with the enhanced glycolysis and glycoATP

production previously discussed at 72 and 120 HPI. We also observed significantly increased extracellular lactate at 144 HPI and 168 HPI in the supernatant of HCMV-infected cells relative to mock-infected cells. These findings suggest that lactate production and homeostasis were significantly altered following HCMV infection. Increased lactate concentrations also agree with previously published work in MRC5 cells following HCMV infection [81].

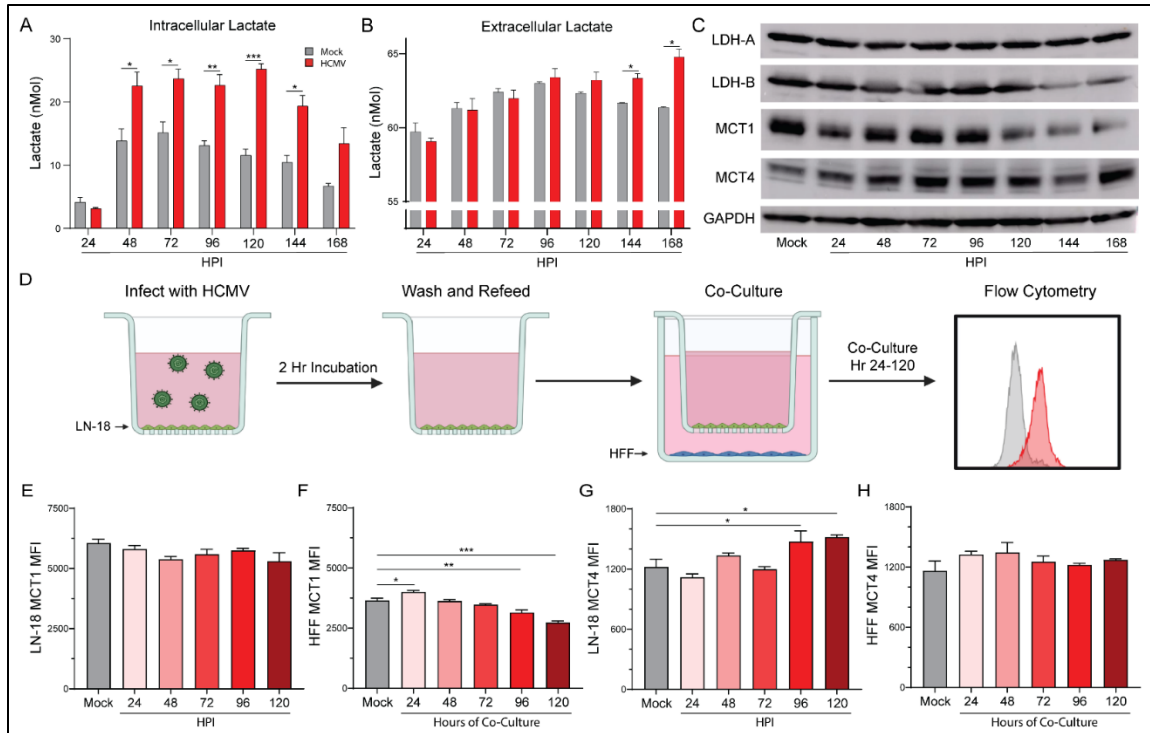


**Figure 2.6 HCMV-associated alterations to lactate dynamics.**

Lactate concentration was determined in the (A) extracellular and the (B) intracellular compartment of mock- or HCMV-infected LN-18 cells using a colorimetric L-lactate assay kit with a standard. (C) Protein expression of prominent lactate regulators LDH-A, LDH-B, MCT1, and MCT4 were examined following infection using western blot assays. (D) Schematic of co-culture experiment in which HCMV-infected LN-18 cells were co-cultured, but physically separated from, HFF cells using Transwells with 0.4  $\mu\text{m}$  pores in 6-well culture dishes. At indicated points post infection, cells were collected separately and processed by flow cytometry for expression of MCT1 (E, F) and MCT4 (G, H) in infected LN-18 and non-infected HFF cells respectively. Graphs represent pooled data from three independent experiments. Mean  $\pm$  the SEM of at least 3 triplicates.

\*,  $P < 0.05$ ; \*\*,  $P < 0.01$ ; \*\*\*,  $P < 0.001$ . Created with Biorender.com.

Lactate, in addition to being an end product of glycolysis, is a potent signaling molecule that can function in both a paracrine and an autocrine manner. As a result, lactate homeostasis is an important mechanism within cells. Initially we investigated the transcriptional changes of key lactate genes following infection with HCMV. Surprisingly, we observed a downregulation of gene expression for several lactate enzymes and transporters relative to mock infected controls (Figure A5). These results were reiterated by RNA-seq data from mock- or HCMV-infected G44 GBM cells at 72 HPI. However, when we examined the protein expression following HCMV infection we found surprising changes (Figure 2.6C). Lactate dehydrogenase (LDH)-A, responsible for the conversion of pyruvate to lactate, expression remained stable throughout infection. However, LDH-B, responsible for the conversion of lactate to pyruvate, decreased at later timepoints. Two monocarboxylate transporters, MCT1 and MCT4, responsible for lactate-influx and -efflux respectively were examined. HCMV-infected cells demonstrated decreases in MCT1, but MCT4 increased relative to mock-infected cells. The protein expression changes cumulatively suggest a lactate management phenotype that favors the production of lactate from pyruvate. It also suggests that elevated intracellular lactate concentration increases MCT4 expression which provide a mechanism for export and may allow for improved lactate homeostasis.

#### Co-culture of HCMV-infected LN-18 with HFFs alters expression of key metabolic proteins and epigenetic markers in both cell lines

In an effort to examine the effects of HCMV-infected LN-18 cells on neighboring non-cancerous cells, we established physically separated co-cultures

with HFFs using 0.4  $\mu\text{m}$  pore Transwells (Figure 2.6D). LN-18s were seeded in Transwells and infected with HCMV for two hours followed by washing and refeeding. At this point the LN-18 Transwells were placed in a 6-well plate containing confluent HFFs. This allowed for paracrine communication between cell lines while keeping them physically separated. Flow cytometry demonstrated HCMV-GFP positivity in the LN-18s and an absence of HCMV-GFP positivity at the longest co-cultured timepoint, 120 HPI, in HFFs (Figure 2.7A). Additionally, HFFs were confirmed negative for CPE and their supernatant was titered and found free of virus at the longest co-culture timepoint, 120 HPI (Figure 2.7B).

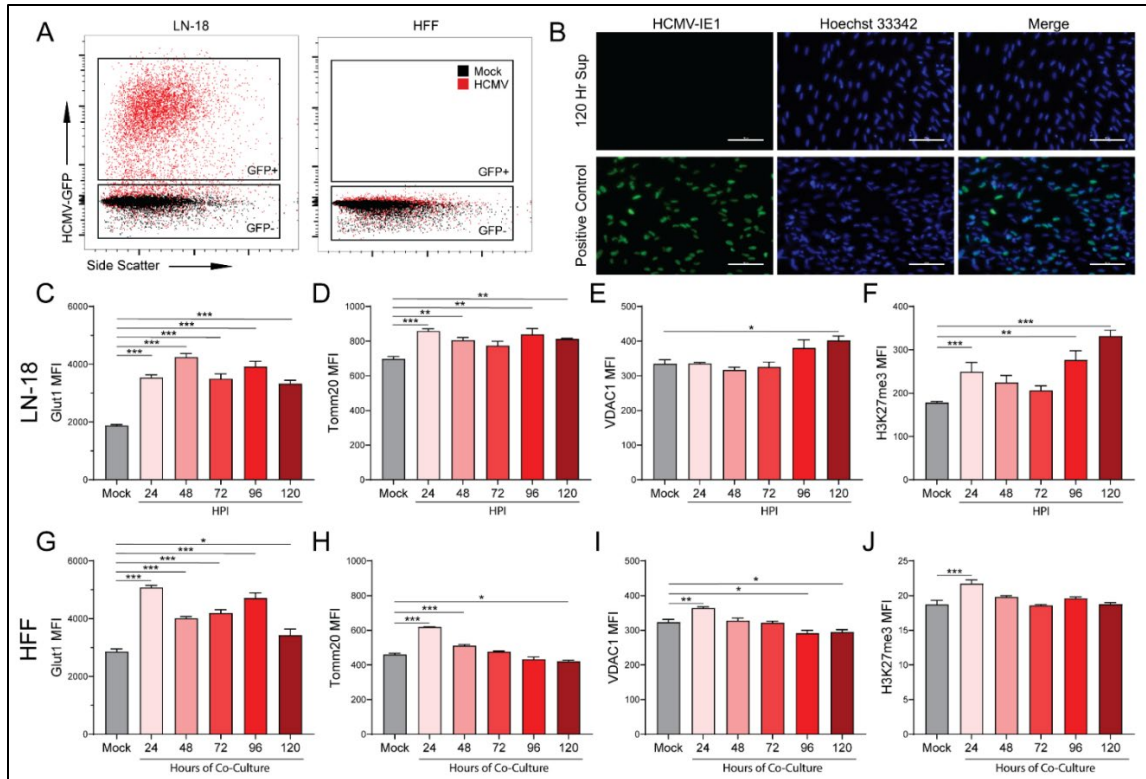


**Figure 2.7 HCMV infected cells alter metabolic pathways of uninfected cells in a paracrine manner.**

Mock- and HCMV-infected LN-18 cells were co-cultured with HFFs as described in Figure 2.6D and then the separate populations were subjected to flow cytometry. Infection of LN-18 cells and absence of infection of HFFs was established following 120 Hr co-culture by (A) HCMV-GFP expression. A titer was performed on fresh HFFs using supernatant from the 120 Hr co-culture HFF compartment, to ensure an absence of viral infection, and cells which had been infected with HCMV as a positive control for the immunocytochemistry staining. (B) HCMV-IE1 staining was performed at 20x magnification. HCMV-IE1 is shown in green and Hoechst 33342 stained nuclei are shown in blue. Scale bar: 100  $\mu$ M. (*Figure legend continues on next page*)

Flow cytometry was used to quantify changes in glycolytic marker (C, G) Glut1, oxidative phosphorylation markers (D, H) Tomm20 and (E, I) VDAC1, and an epigenetic marker (F, J) H3K27me3 in infected LN-18 and non-infected HFF cells respectively. Graphs represent pooled data from three independent experiments. Mean  $\pm$  the SEM of at least 3 triplicates. \*,  $P < 0.05$ ; \*\*,  $P < 0.01$ ; \*\*\*,  $P < 0.001$ .

Based on the MCT expression changes following co-culture, we used the same experimental method to examine several metabolic and transcriptional targets. Glucose transporter 1 (Glut1), the primary glucose importer of cells, was found to be upregulated at all timepoints in both LN-18 (Figure 2.7C) and HFF (Figure 2.7G) cells. Mitochondrial import receptor subunit TOM20 homolog (TOMM20), a key mitochondrial import receptor, was found to be increased in HCMV-infected LN-18 cells (Figure 2.7D). In HFFs there was a similar increase at early timepoints followed by decreased expression at the latest timepoint (Figure 2.7H). Voltage gated mitochondrial membrane ion channel (VDAC1) is responsible for the transport of ions, nucleotides, and metabolites through the mitochondrial membrane and was upregulated in LN-18 cells at the last timepoint (Figure 2.7E). However, in HFFs, VDAC1 was upregulated at the earliest timepoint and subsequently downregulated at the final two timepoints (Figure 2.7I). Taken together, these expression changes provide support for the hypothesis that HCMV infected cells can alter the metabolic function of neighboring cells in a paracrine manner akin to the Reverse Warburg Effect described in the cancer field [71].

Evidence of paracrine signaling-mediated effects on neighboring uninfected cells suggests that HCMV infection may also be able to alter the transcriptional landscape of both host and neighboring cells. We examined tri-methylation of histone H3 lysine 27 (H3K27me3) as an indicator of epigenetic regulation following infection with HCMV. Hypermethylation is a potent repressor of gene expression. Histone 3 lysine 27, transcriptional repression has been linked to regulation of cell differentiation and proliferation [82]. Numerous studies have linked alterations in

H3K27me3 to development and progression of cancer [83-85]. In the HCMV-infected LN-18 cells there was a significant increase in methylation at the first and two final timepoints (Figure 2.7F). Additionally, there was significant upregulation of H3K27 tri-methylation of the HFF cells at the first timepoint. These findings suggest that HCMV infection produces epigenetic changes in the host cells that may favor tumor progression. Additionally, it indicates that neighboring cells are also susceptible to epigenetic modifications as a result of an unidentified paracrine messenger.

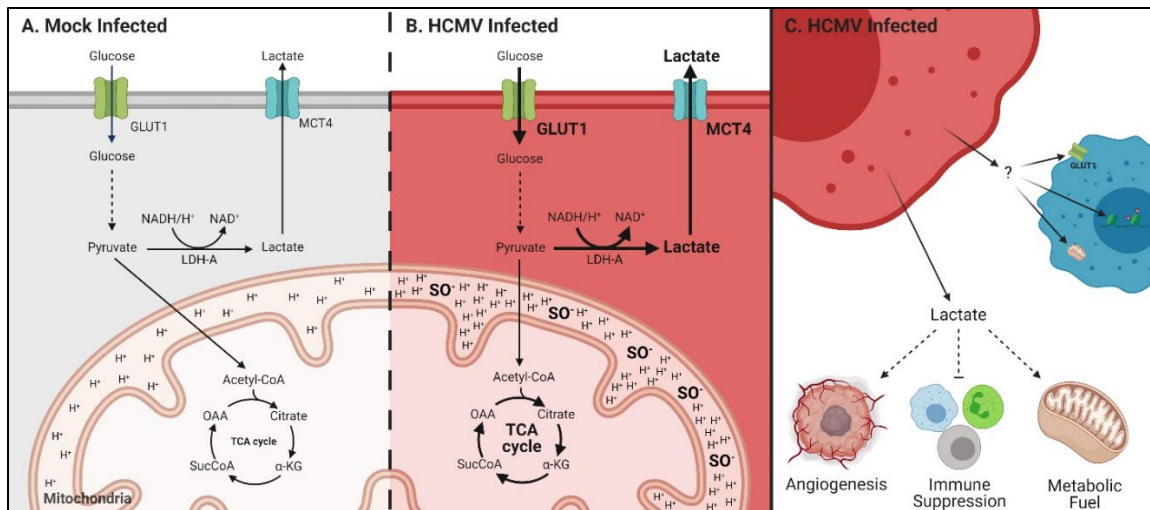


**Figure 2.8 Metabolic reprogramming and paracrine effects of HCMV infection in glioblastoma.**

Schematic of glycolysis and respiration in (A) mock- and (B) HCMV-infected cells highlighting upregulation of GLUT1 and MCT4 expression; increased lactate production and export; enhanced respiration and resultant increases in mitochondrial membrane potential and superoxide production. (C) HCMV infected cells export lactate which has been reported to increase angiogenesis, suppress the immune response, and can be used as a metabolic fuel by neighboring cells. The secretome from HCMV-infected cells can influence transporter expression, mitochondrial function and induce epigenetic changes in surrounding stromal cells. Created with BioRender.com.

## 2.5 DISCUSSION

HCMV has been implicated as a potential oncomodulatory virus in GBM and some other tumor types [32, 38, 79]. Defining a role for HCMV in human cancers has been hindered by numerous factors. In GBM specifically, conflicting results on the presence of HCMV in primary GBM samples has created justified questioning of significance (reviewed in [86]). Lack of reproducibility between laboratories employing similar techniques suggests that current experimental approaches are inadequate. Identifying a relationship is further complicated by the long period between initial HCMV infection and the initiation or manifestation of cancer. Yet, under *in vitro* conditions HCMV can alter or influence all the hallmarks of cancer. *In vivo* murine GBM studies displayed reactivation of MCMV in the tumor and promotion of tumor growth [79]. Preliminary clinical studies using herpesvirus antivirals in addition to the standard of care demonstrated increased life expectancy in patients with GBM [49, 87]. These observations collectively suggest a role for HCMV in GBM. Our work and others have shown that HCMV infection rewires host metabolic pathways to meet biosynthetic and bioenergetic requirements of viral replication [14, 18, 81, 88, 89]. Dysregulated cellular energetics is an emerging hallmark of cancer [26]. Thus, viral manipulation of host metabolism represents a potential mechanism underlying the influence of HCMV on tumor progression in GBM.

Our work presented here shows that HCMV alters the metabolic phenotype of an infected GBM cell line. This does not require transformation of the cells. We observed upregulation of glycolysis and mitochondrial respiration following

infection with HCMV. These results are similar to the metabolic reprogramming previously demonstrated in HFF cells [14, 18, 77]. They also resulted in the production of metabolic byproducts, such as ROS and secreted metabolites such as lactate, which have been shown to play roles in cancer progression. Further, infected cells exhibited alterations in epigenetic markers associated with cancer initiation. Finally, we demonstrated that HCMV infected cells were able to manipulate key metabolic pathways of neighboring cells in a paracrine manner independent of viral transmission. These findings suggest a role for HCMV-mediated metabolic reprogramming in manipulation of the tumor microenvironment (TME) potentially leading to cancer progression.

Upregulation of oxidative phosphorylation (Figure 2.3) during HCMV infection of GBM cells suggests that HCMV may be metabolically synergistic, driving metabolic rates above what is possible following oncogenesis alone. GBM have been shown to display high OXPHOS levels *in vivo* [90]. Glioblastoma stem-like cells (GSCs) and surgically resected tumors from GBM patients use oxidative and non-oxidative pathways to generate energy and biomass [90, 91]. It is possible that HCMV infection enhances metabolic potential allowing for the maintenance of high proliferation rates seen in GBM. Increases in spare respiratory capacity (Figure 2.3, Supplementary Figure A.2) observed following HCMV infection suggest that there are significant bioenergetic reserves soon after HCMV infection. GSCs are reliant on OXPHOS for proliferation and has been proposed as a potential therapeutic target [92]. Increases in both OXPHOS and bioenergetic

reserves highlight the potential for HCMV infection to allow for increased growth rate, metabolic flexibility, and potential for drug resistance in GBM cells.

Alternatively, as a consequence of upregulated OXPHOS, we observed increased production of ROS (Figure 2.4), specifically superoxide, following infection of GBM cells. High levels of oxidative stress can damage proteins, lipids, and DNA further contributing to conditions conducive for cancer initiation or progression (reviewed in [93, 94]). Specifically, ROS mediated oxidation of phosphatase and tensin homolog (PTEN) causes a loss of function and activates the phosphoinositide 3-kinase (PI3K), protein kinase B (Akt), mammalian target of rapamycin (mTOR) signaling cascade, leading to protein synthesis and proliferation [95]. Sustained proliferative signaling is one of the hallmarks of cancer and genomic instability and mutation is described as an enabling characteristic of cancer [26]. An examination of HCMV-associated alterations to PI3K/Akt/mTOR signaling following infection could yield intriguing insights in relation to cancer. Additionally, this mechanism could point towards the use of an ETC inhibitor such as metformin to control the production of ROS and subsequent activation of the PI3K/Akt/mTOR signaling cascade. We recently reported that ETC inhibitors, specifically metformin, can negatively impact HCMV replication [23].

Many of the metabolic changes closely resemble metabolic alterations reported in cancer such as the upregulation of aerobic glycolysis (Figure 2.5). GBM is dependent on a functioning glycolytic cycle with targeted knockdown of glycolytic enzymes producing increased longevity in a murine model of GBM [96]. The HCMV protein US28 has been demonstrated to increase hypoxia inducible factor-

1 (HIF-1)-dependent proliferation of GBM cell line U251 through upregulation of glycolysis [97]. Therefore, the increased glycolytic capacity and rate that we see following infection with HCMV may support enhanced tumor growth rates. In the context of GBM, increased Glut1 expression may allow for enhanced glucose uptake which may help compensate for poor vascularization and nutrient dispersal in the tumor microenvironment. This may allow GBM cells to maintain their characteristic growth and proliferation rates despite environmental stress.

Following glycolytic conversion of glucose to pyruvate, enzymes can convert pyruvate to lactate. Previous studies have shown that HCMV infection increased the concentration of L-lactate in supernatant of cultured U251 GBM cells [97]. We observed changes to lactate levels (Figure 2.6) in both intracellular and extracellular compartments relative to mock infected cells. Lactate secretion into, and acidification of, the TME has been shown to promote GSC phenotypes, induce angiogenesis, and inhibiting immune responses [98]. Notably, significant increases to lactate exporter MCT4 expression were seen (Figure 2.6, Figure A5) and may account for the increased extracellular concentrations of lactate. MCT4 expression is elevated in GBM, has been positively correlated with the pathological grades of glioma, and was found to promote GBM migration [99]. Therefore, the HCMV-mediated increases in MCT4 levels we witnessed may prove beneficial to tumor progression and metastasis.

The reverse Warburg Effect has been proposed as a mechanism that exploits the metabolic potential of cells in the TME for the benefit of cancer stem cells [73]. In addition to its role acidifying the TME, extracellular lactate can also

act as a fuel source for oxidative cancer cells and cells with stem-like phenotypes [100, 101]. Reciprocal metabolic associated interactions involving catabolism of glucose, lactate, fatty acids and other metabolites impact cancer aggressiveness. This suggests that HCMV infection of GBM cells could alter the surrounding TME via the secretion of metabolites or proteins in a mechanism similar to that employed by tumors to promote growth and invasion. Our co-culture experiments (Figure 2.7) show that this is possible and that the infected secretome can alter metabolism-associated and epigenetic targets. Notably, hypermethylation of H3K27 has been linked to the development and progression of cancer [82]. Epigenetic modifications have the potential to alter transcription of large groups of genes and can produce potent phenotypic changes in cells. HCMV-mediated epigenetic alterations in both infected and neighboring cells suggest the potential for a small number of cells to have exponential effects within the TME. It is unknown, at this time, if these epigenetic alterations promote a tumor-like phenotype, can prime surrounding cells for infection, or rewire metabolism in infected and uninfected cells. It will be interesting to explore what mechanistic effect the secretome is having and how this affects the long-term state of the tumor cells. Targeted experiments identifying secreted metabolites, signaling proteins, or extracellular vesicles are currently underway in the laboratory. GSCs have been shown to communicate to the tumor microenvironment through extracellular vesicles (reviewed in [102]). It will be intriguing to understand how HCMV infected cells and GSCs communicate and if this communication drives synergistic effects that promote tumor growth and metastasis.

## **2.6 LIMITATIONS**

There are several limitations to our study. We used a GBM cell line that is immortalized and grown as a monolayer using high glucose media in supraphysiological oxygen. As we compared changes with and without HCMV infection, with all other variables controlled for, we believe that this caveat is negligible. Regardless, ongoing work in the laboratory is employing primary GSCs grown under serum-free conditions. Also, we did not explore all major metabolic pathways known to be affected by HCMV infection. HCMV infection has been shown to block beta-oxidation of fatty acids in order to promote the lipogenesis necessary to produce the viral envelope [103]. Human glioma cells have been reported to be dependent on fatty acid oxidation under tissue culture conditions [104]. We also have not explored the role of glutamine as cultured astrocytes have been shown to support the growth of glutamine deprived GBM cells [105]. Our model ignores any contributions of oxygen tension which are prevalent in the context of the TME. There is ample literature describing metabolic interplay between hypoxic and normoxic tumor microenvironments and how this dictates catabolic versus anabolic behavior. Hypoxic conditions also increase the expression of MCT4 [106]. Finally, we do not account for the relationship between increasing HCMV seroprevalence and GBM incidence with advancing chronologic age. Integrating this correlation into our experimental approach would be intriguing.

## **2.7 CONCLUSIONS**

Our results provide several potential mechanisms by which HCMV could contribute to GBM and possibly other cancers. It also offers insight into the difficulty detecting HCMV in GBM samples. First, HCMV would only need to infect a small number of cells to exert a significant effect on the tumor microenvironment. Second, our data suggests that HCMV infected cells can employ paracrine signaling to modify neighboring cells independent of infection, thus not requiring direct infection of GBM cells to produce significant changes. The ability of HCMV infected cells to transiently alter epigenetic signatures in neighboring cells hints at the possibility of a role in cancer initiation. At this point, it is unknown if this mechanism has the potential to be cancer initiating or merely promote the progression of established GBMs. The metabolic reprogramming we demonstrated following infection, compliments a study by Liu *et al.* that showed HCMV infected primary GBM cells exhibit a stem cell like phenotype which enhance their ability to resist chemotherapy [107]. Our work establishes a framework for future studies defining how HCMV can contribute to GBM through an oncomodulatory mechanism. The manipulation of host metabolic pathways may prove to be a common mechanism linking only by HCMV, but other pathogens, to numerous cancers. These insights could be used to develop therapies that incorporate metabolic targets in combination with the current standard of care.

## CHAPTER 3

### INTERMITTENT CYTOMEGALOVIRUS INFECTION ALTERS NEUROBIOLOGICAL METABOLISM AND INDUCES COGNITIVE DEFICITS IN MICE<sup>2</sup>

#### **3.1 Abstract**

Risk factors contributing to dementia are multifactorial. Pathogens as risk factors for dementia is largely correlative with few causal relationships. Here, we demonstrate that intermittent cytomegalovirus (CMV) infection in mice, alters blood brain barrier (BBB) metabolic pathways. An increase in basal mitochondrial function is observed in brain microvasculature endothelial cells (BMEC) at 12 months post infection but not at earlier time points and is accompanied by elevated levels of superoxide, indicative of oxidative stress. Further, these mice score lower in cognitive assays as compared to age-matched controls. Our data show that repeated systemic infection with CMV, alters BBB metabolic function and impacts cognition. These observations provide mechanistic insights through which pathogens contribute to the progression of pathologies associated with dementia.

---

<sup>2</sup> To be submitted to Cell Host and Microbe in December 2022.

### **3.2 Introduction**

Aging is a primary risk factor associated with cognitive decline and the development of dementia, such as Alzheimer's disease (AD) [63, 108]. Therapeutic strategies have focused on extracellular amyloid-beta (A $\beta$ ) oligomers and soluble fragments, or intracellular hyperphosphorylated-tau tangles. However, these hallmarks of AD are not evident until the disease has been developing for years and, even at that point, patients are often in a pre-clinical phase of the disease with little to no cognitive symptoms [109, 110]. These findings suggest that other initiating or contributing factors exist which may be addressed decades prior to the development of any cognitive symptoms.

Pathogens are increasingly recognized as risk factors in the etiology of age-associated neurodegeneration [63, 111]. A single viral or bacterial infection in adult rodents has been shown to promote sickness behavior, induce systemic and central nervous system (CNS) inflammatory cascades, alter memory performance, and disrupted synaptic communication via neuronal loss [112-117]. Humans do not experience a single infection during their lifetimes, but rather intermittent infections throughout life. The long-term consequences of intermittent infection are inadequately studied. Emerging preclinical evidence suggests that a higher lifetime infection burden impairs cognition, especially among transgenic mice carrying AD risk factors [111, 118]. Finally, studies in adult and aged humans show that higher cumulative exposure to HSV-1, cytomegalovirus (CMV), and bacterial infections was associated with impaired cognitive performance or an accelerated rate of cognitive decline [68-70, 119]. Converging evidence indicates that pathogen

exposure can promote features of dementia but the mechanisms for these effects have yet to be elucidated.

In this study, CMV was used as a model pathogen. CMV is a ubiquitous herpesvirus exhibiting 40-80% seropositivity in the human population [120]. Common to all herpesviruses, following acute infection, CMV becomes latent and reactivates sporadically throughout the lifetime of the host resulting in intermittent infection. Further, different CMV strains are thought to infect individuals throughout life. CMV's ability to evade immune clearance enables a persistent phenotype that is associated with immunosenescence, inflammaging, and memory T cell inflation [121]. Most individuals seroconvert before the age of 40 suggesting that the cycle of latency/reactivation or reinfection continues for decades [122].

The role of CMV in unhealthy aging, including dementias, remains largely correlative. Data suggesting individuals positive for CMV have an increased risk for AD and accelerated cognitive decline [123, 124] are contrasted with data suggesting a weak association [125]. Ultimately, a lack of mechanisms linking pathogens and the origins of dementia impede progress. Intriguingly, CMV pathogenesis mirrors many of the features of AD pathology including calcium dysregulation [24], amyloid deposition [119], iron dysfunction [126], autophagic [127], and mitochondrial dysfunction [14, 77, 128].

The ability of CMV to alter the metabolic profile of host cells to produce the biomaterials and energy needed for viral replication is well described [14, 128-130]. This metabolic reprogramming often results in impaired bioenergetics and subsequent increases in reactive oxygen species (ROS) production. Interestingly,

ROS production and impaired metabolism have been implicated in numerous neurodegenerative diseases [131-134]. Additionally, the Mitochondrial Cascade Hypothesis posits that AD pathogenesis is driven by progressive mitochondrial dysfunction [135]. Further, it has been shown that mitochondrial function directly alters the secretion or storage of A $\beta$  [136]. Finally, studies have demonstrated that metabolic and mitochondrial changes alter cellular proteostasis and precede the onset of clinical symptoms of AD [137]. Therefore, CMV, with its potent capacity to reprogram cellular metabolism is an ideal candidate for assessing the impact of pathogens on aging-associated pathology such as AD.

In this study, we demonstrate that intermittent CMV infection induces metabolic alterations in the blood brain barrier (BBB) that correlate with decreases in cognitive function. We observe that endothelial cells isolated from the BBB display enhanced oxidative phosphorylation (OXPHOS) and consequently produce elevated levels of superoxide (SO) following the pro-inflammatory immune response. These findings suggest that infection frequency and burden may accelerate cognitive decline by modulating BBB metabolism and increasing oxidative stress.

### **3.3 Methods**

\*For list of reagents, see (Table B1, B2, & B3)

#### VIRUS PROPAGATION AND QUANTIFICATION

Murine cytomegalovirus Smith strain was passaged through mice via and quantified via plaque assay as previously described [138, 139]. Briefly, mice were

i.p. injected with MCMV and sacrificed at 14 days post infection. Salivary glands were homogenized in PBS, aliquoted, and stored at  $-80^{\circ}\text{C}$ . Virus was quantified by plaque assay using M2-10B4 cells and a viscous overlay followed by fixation with formaldehyde and staining with 0.02% methylene blue.

### ANIMALS, INFECTIONS, AND SAMPLE COLLECTIONS

Female BALB/cJ mice aged 6 weeks were obtained from Jackson Laboratory and housed in disposable, sterile cages in groups of 5 with food and water provided *ad libitum*. All animal experiments were approved by the Tulane University Institutional Animal Care and Use Committee. Murine cytomegalovirus infections were conducted via i.p. injection with  $5 \times 10^4$  plaque forming units in 100 $\mu\text{L}$  sterile PBS. They were maintained on a diurnal light cycle (8-6) and all behavioral testing was performed in the first half of the light period. Mice were euthanized via i.p. injection with a lethal dose of ketamine and xylazine followed by exsanguination. Blood collected via cardiac puncture was processed for plasma. Mice were then perfused with ice-cold PBS and tissues were collected and processed as needed.

### BEHAVIORAL TESTING

Behavior in mice was evaluated using the Y-maze, Passive Avoidance, and Hot Plate tasks for “Cohort 2” at 1 month post initial infection and “Cohort 3” at 12 months post initial infection. The behavior tests described below were performed in the order they are listed. All animals underwent testing by a pair of treatment blinded researchers. Peroxiguard was used to disinfect and deodorize the apparatuses between each mouse trial.

Y-Maze: The Y-Maze was employed as a measurement of spatial working and reference memory [140]. Mice were placed in the three-armed maze with arm length of 38 cm, width of 8.25 cm, and height of 13.25 cm facing the end of arm designated “A”. Mice were allowed to explore the maze for 8 minutes. Movement around the maze was recorded by an overhead camera and tracked using ANY-Maze software. Mice were provided with large black geometric spatial clues on white backgrounds to help them navigate and discriminate between arms. Spontaneous alternation was calculated as percentage of correct alternations between the three arms without revisiting the previous arm. Total alternation was also recorded.

Passive Avoidance: As a measure of single-trial fear based aversive learning, mice were subjected to the step-through inhibitory (passive) avoidance task [141]. In this assay mice are placed in a two chamber device with a guillotine door between them. One chamber is brightly lit while the other is dark. The floor of the both chambers contains metal rungs on the floor connected to a shock delivery apparatus (Maze Engineers). For the training portion of the test, mice were placed in the illuminated side and allowed to explore until they entered the dark chamber. Once the mouse entered the dark chamber the door was closed and the mouse was administered a 3 second foot shock (0.3 mA). Mice that did not enter the dark chamber within 120 seconds were gently pushed to the dark chamber and a foot shock was administered. After all training trials were completed, animals were tested for learning ability (10 minutes after training trial) and memory retention (24 hours later) by placing the mice in the bright chamber and recording latency to

enter dark chamber. These retention trials were limited to 300 seconds and no foot shocks were administered.

Hot Plate: To examine nociceptive ability, mice were exposed to the hot plate test [142]. The hot plate (Maze Engineers) was set to 55.0°C and the mouse was placed onto the plate surface. Latency to first nociceptive behavior as well as total number of nociceptive behaviors was recorded for the 30 second duration of the experiment. Nociceptive behaviors were defined as shaking or flicking of hindlimbs and jumping.

#### SINGLE CELL MULTIOME ATAC AND GENE EXPRESSION SEQUENCING

Nuclei Isolation: Nuclei isolation for multiome sequencing was performed largely following the protocol from 10X Genomics protocol revision D. Following euthanasia and perfusion the brain was extracted and flash frozen in liquid nitrogen. The brain is lysed with 0.1x lysis buffer and homogenized with scissors and then a pellet pestle. The homogenate is incubated for 3 minutes on ice and then lysis is stopped via the addition of wash buffer. The suspension is filtered through a 70 µm filter and then subjected to a 30% Percoll Plus centrifugation to remove myelin. Nuclei were washed and resuspended in nuclei buffer. Finally, nuclei were visualized on a cell counter for nuclear membrane integrity (lack of blebbing) and counting.

Library Prep and Sequencing: The Chromium Next GEM Single Cell Multiome ATAC and GEX protocol (CG000338) and 10x reagent kit were used to prepare ~10,000 nuclei/sample for the Multiome sequencing. Briefly, nuclei suspensions were incubated with a Transposon Mix and DNA fragments were

transposed and barcoded. The transposed nuclei were partitioned into nanoliter-scale Gel Bead-In Emulsion (GEMs). The barcoded transposed DNA and barcoded full length cDNA from poly-adenylated mRNA were generated and amplified by PCR. P7 and a sample index were added to transposed DNA during ATAC library construction via PCR. Barcoded cDNA enzymatic fragmentation, end-repair, A-tailing, and adaptor ligation were followed by PCR amplification. Both final ATAC libraries and 3' Gene Expression libraries generated contained standard Illumina P5 and P7 paired-end constructs. Library quality controls were performed by using an Agilent High Sensitivity DNA kit with Agilent 2100 Bioanalyzer and quantified by Qubit 2.0 fluorometer. Libraries were sequenced separately with individual parameter settings. Pooled libraries at 650 pM were sequenced with paired end dual index configuration on an Illumina NextSeq 2000 using Illumina P3 100 cycle kit. Cell Ranger arc version 2.0.0 (10X Genomics) was used to process raw sequencing data and mapped to mouse genome mm10-2020-A to generate differentially expressed genes between specified cell clusters represented by Loupe Cell Browser (10X Genomics).

Multiome Data Analysis: Cell Ranger ARC v2.0 (10x Genomics) was used to process raw sequencing data for further downstream analyses. After filtering, we used 27,798 cells with high quality transcriptome and epigenome profiles. We followed the algorithms Seurat (v4.0) R package (v4.0.2) to generate the uniform manifold approximation and projection (UMAP) embeddings and differentially expressed (DE) gene. Fragment files were used as input for Seurat analysis. The input fragment file was processed as chunks per chromosome and stored in HDF5

format (hierarchical data format version 5), allowing rapid access and efficient read and write functions during analysis. The quality control steps involved the removal of all low-quality cells and predicted heterotypic doublets from our analysis. We used Morpheus (<https://software.broadinstitute.org/morpheus/>) software to generate the top 30 DE genes heatmap. A relative color scheme uses the minimum 0 and maximum 0.1 values in each row to convert values to colors.

### RNA ISOLATION AND qRT-PCR

Salivary glands were flash frozen in liquid nitrogen and stored at -80°C. RNA was isolated from 30 mg of salivary gland using the RNeasy minikit from Qiagen. iScript cDNA synthesis kit was used to create cDNA from 1 µg of RNA. qRT-PCR was conducted on 50 ng of each sample using Sso Advanced SYBR Green supermix and primers for MCMV immediate early gene 1 (mUL123) and murine 36B4 which was used as a housekeeping gene. qPCR products were run on a 2% agarose gel to confirm product size.

### FLOW CYTOMETRY

Brains were processed for flow cytometry as previously described [143]. Briefly, they were incubated with 5mg collagenase II and homogenized in MACS C-tubes with 5 mg collagenase II and 100U DNase I in HBSS with 3mM calcium chloride. Myelin debris was removed via a 30% Percoll Plus gradient. Cells were washed and resuspended in PBS with 0.4% BSA.

Neuro Flow Panel: Cells were incubated with fixable live dead stain and Fc block for 15 minutes at RT. Following washes with 20% BD Horizon Brilliant Stain Buffer, cells were incubated in an extracellular antibody cocktail for 20 minutes at

RT. Cells were washed, fixed and permeabilized with eBioscience FoxP3 Transcription Factor staining kit for 45 minutes. Fixed cells were washed and incubated with intracellular antibodies for 45 minutes at room temperature. Following washes, cells were resuspended in PBS with 0.5% BSA and flow cytometry was conducted on a Cytex Aurora. Data was analyzed using FCS Express 7.14.

Live Cell Mitochondrial Panel: Cells were incubated in a cocktail of, anti-CD31 BV605 antibody at 1:100, 1  $\mu$ M nonyl acridine orange (mitochondrial mass), 2.5  $\mu$ M MitoSOX Red (superoxide production), and 250 nM MitoTracker Red FM (mitochondrial membrane potential) for 45 minutes at 37°C. Following washes in PBS, cells were resuspended in PBS with Sytox Blue dead cell stain, incubated for 15 minutes, and flow cytometry was performed on a BD LSRFortessa. Data was analyzed using FCS Express 7.14.

### CYTOKINE ANALYSIS

Mouse brains were minced briefly in BioRad Cell Lysis Buffer followed by homogenization in MACS S-tubes and freezing at -80°C. Following thaw, lysate was sonicated briefly and then centrifuged to pellet debris before being quantified by BCA. Brain lysate was diluted to 4mg/mL in Bio-Plex diluent.

Both plasma and brain lysate cytokine levels were assessed using a Bio-Plex murine cytokine 23-plex assay kit at a dilution of 1:2 according to manufacturer recommendations. Briefly, samples were added to a 96-well plate with magnetic beads and incubated for 30 minutes while shaking. Well were washed three times and followed by addition of detection antibodies for 30 minutes

at room temperature. Three more washes were conducted and then streptavidin-PE was added and incubated for 10 minutes. After another three washes samples were read on the Bio-Plex 200 system with HTF. Standard curves were created for each cytokine from 1-32,000 pg/mL, a five-parameter logistic regression was fit, and sample cytokine concentrations were interpolated.

### ELISA

Antigen-specific quantitative ELISAs were performed using similar methods as described in ref. [144]. Briefly, 96-well plates were coated with 0.25 µg/well of UV-inactivated MCMV. Serial dilutions of plasma from animals was incubated for an hour at room temperature followed by detection using AP-conjugated rabbit anti-mouse IgG or IgM. ELISAs were quantified using dilutions of purified mouse standards IgG1-κ or IgM-κ and the results were expressed as ELISA units/mL (EU/mL).

### BRAIN MICROVESSEL ISOLATION

Excised brains were stored in ice-cold PBS. Brain microvessel endothelial cells (BMECs) were isolated as previously described [145]. Briefly, hemispheres were rolled on filter paper to remove surface vessels. Brains were homogenized in PBS, centrifuged, and the pellet was resuspended in 17.5% dextran solution. This process was repeated and each time floating white matter was removed from the pellet prior to resuspension. The resuspended cells were serially filtered through a 300 µm and 40 µm filters and then resuspended in Seahorse XF DMEM media.

### SEAHORSE

BMECs were loaded into Seahorse XFe24 cell plates with one animal used for each well. Plates were centrifuged and incubated for an hour at 37°C in a non-CO<sub>2</sub> incubator. Mitochondrial function was assessed using the Mito Stress Test Kit. Basal media contained 25 mM glucose, 10 mM sodium pyruvate, and 2 mM glutamate. The assay was completed using the manufacturers recommended protocols with following injections: Oligomycin (5 µM), FCCP (5 µM), and finally Rotenone/Antimycin A (2 µM/10 µM). Total protein per well was determined via BCA and oxygen consumption rates were normalized to total protein for each well. Normalized OCR was used to determine basal and maximal respiration, ATP coupled respiration, proton leak, and spare respiratory capacity.

#### STATISTICAL ANALYSIS

Statistical analyses were performed using Graphpad Prism v9. All data are expressed as the mean plus standard error of the mean (SEM) from at least three independent experiments or animals. Comparisons between groups were assessed using unpaired *t*-tests or Ordinary one-way followed by Dunnett's multiple comparisons test where appropriate. Outliers were identified and excluded where necessary using the ROUT method with a maximum desired false discovery rate (Q) of 2%. For all comparisons, a  $p < 0.05$  was considered significant.

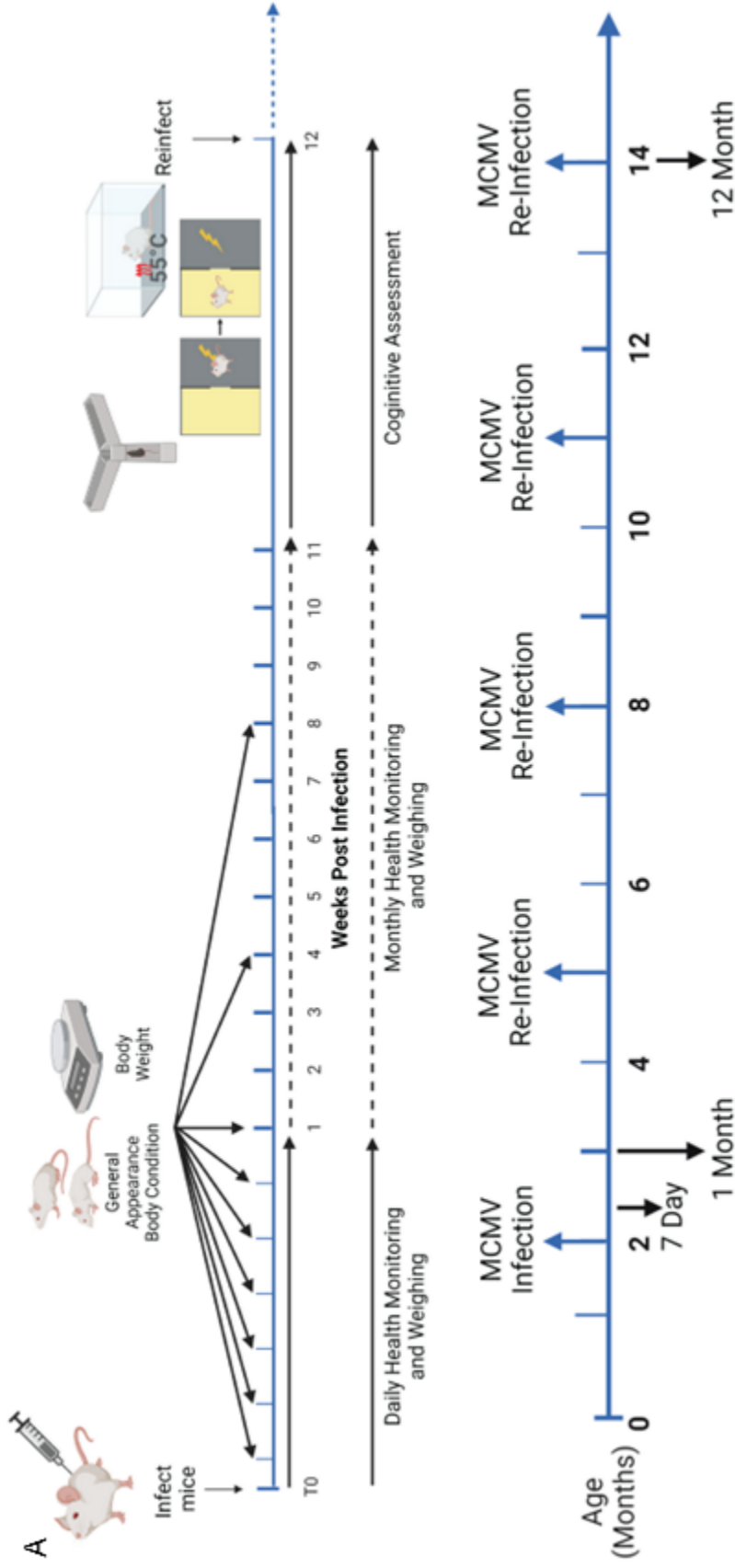


**Figure 3.1.1 Intermittent MCMV infection exhibits delayed inflammatory cytokine expression in the brain.** (A) Cartoon outlining the experimental design and re-infection timeline.

### **3.4 Results**

#### Intermittent MCMV infection exhibits delayed inflammatory cytokine expression in the brain

Pathogen exposure and burden increase with age [146]. Using a reductionist model, we examined how a single herpesvirus (CMV) can contribute to accelerated hallmarks of aging and dementia. As CMV exhibits species tropism, we used the well described Smith strain of murine CMV (MCMV) in our studies. We employed a murine model that integrates intermittent infection and natural aging (Figure 3.1.1A). In immunocompetent individuals, human CMV infection is asymptomatic, or results in mild flu-like symptoms and general malaise. Our murine model behaves similarly, exhibiting slight but significant changes in body weight 2-3 days post infection (DPI), but rapid recovery equaling mock-infected mice around 5 DPI (Figure 3.1.2B). Repeat MCMV exposures at 3-, 6-, and 9-months post infection (MPI) do not result in significant changes in body weight (Figure B1.1A). Additionally, there were no significant changes in weight at 1-MPI (Figure 3.1.2C) and mice exposed to intermittent infection did not exhibit significant changes in weight loss over 12 months (Figure B1.1B). Plasma IgM specific to MCMV exhibited high concentrations immediately after initial infection at 7 DPI (Figure 3.1.2D), but were reduced by 1-MPI. Subsequently, IgM concentrations increased at 6 and 12 MPI. IgG concentrations correlated strongly with IgM plasma concentration and significantly increased as a function of challenge number and remained quantitatively similar from 6-12 MPI (Figure 3.1.2E). All mock-infected mice failed to elicit an antibody response against MCMV, confirming the infection

status remained negative throughout our experimental timeline. To validate our measured results were not the result of active infection, PCR analysis was completed using salivary glands. MCMV can be detected at high viral loads in the salivary gland [147]. At 7 DPI we observed high levels of UL123, a viral gene expressed early during replication. Expression of UL123 decreases by 1-month post infection (Figure B1.1C). There was no replicating MCMV detected in salivary glands at 6- or 12-month timepoints suggesting a functional immune response and establishment of MCMV latency.

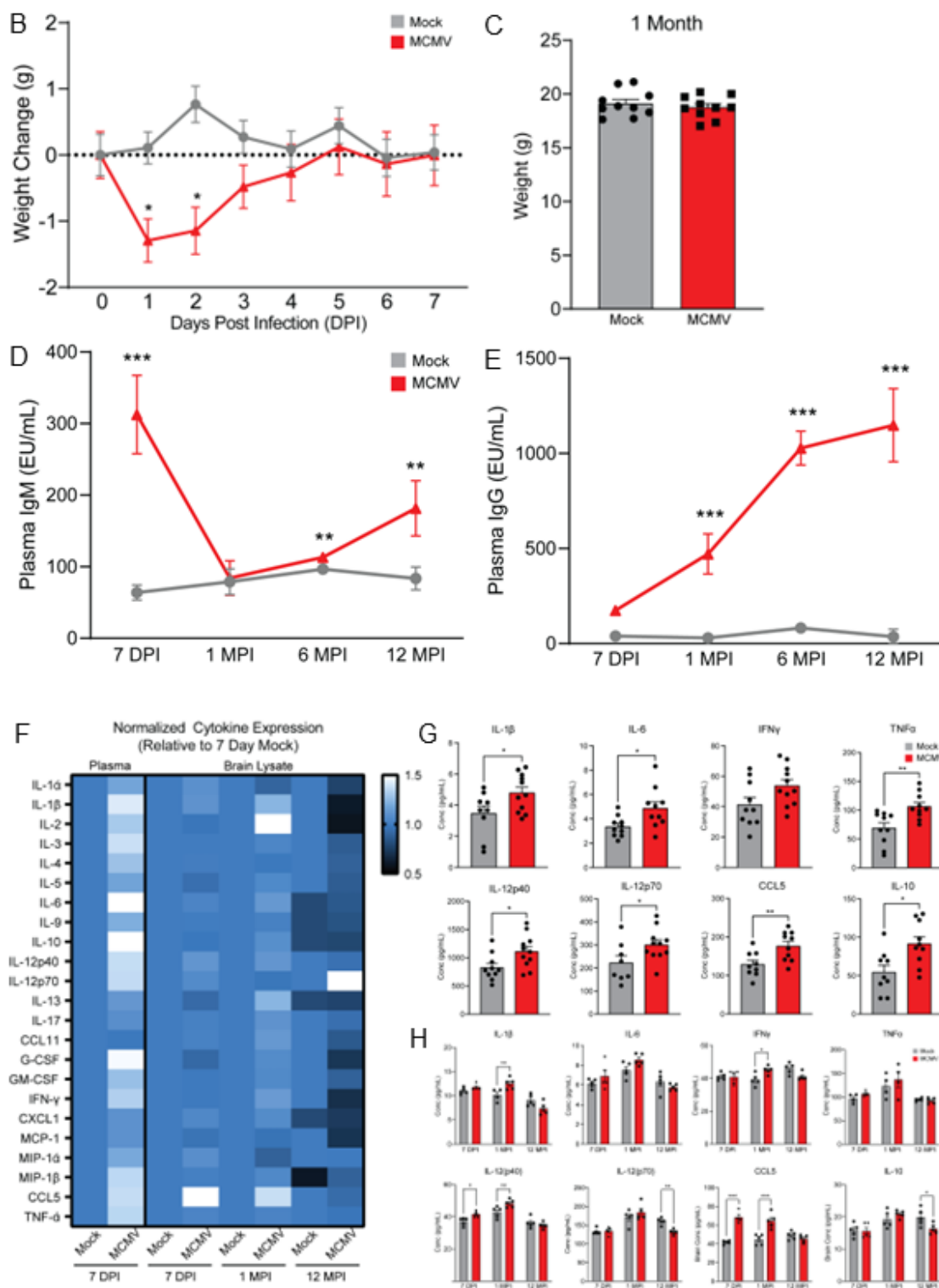


(Figure legend on next page)

**Figure 3.1.2 Intermittent MCMV infection exhibits delayed inflammatory cytokine expression in the brain.** (B) Weight change in mice over 1 week following initial infection. (C) Weight of mock- (grey) and MCMV-infected (red) mice at 1 month post infection. ELISA-derived concentration of MCMV-specific (D) IgM and (E) IgG from plasma across time. (F) Heatmap of cytokine expression in plasma and brain homogenate at 7 DPI, 1 MPI, and 12 MPI normalized to 7 DPI mock infected measurements. Levels of IL-1 $\beta$ , IL-6, interferon IFN $\gamma$ , TNF $\alpha$ , IL-12p40, IL12-p70, CCL5, and IL-10 from (G) plasma at 7 DPI (H) and brain homogenate at 7 DPI, 1 MPI, and 12 MPI as measured by Bio-Plex. Graphs represent pooled data from at least three individual animals. Mean  $\pm$  the SEM. \*,  $p < 0.05$ ; \*\*,  $p < 0.01$ ; \*\*\*,  $p < 0.001$ . Created with Biorender.com

Previous reports have suggested that in MCMV models, pro-inflammatory cytokine responses may inhibit the innate immune responses contributing to viral pathogenesis [148, 149]. We observe differential expression of cytokines in relation to infection frequency, time and the origin of the sample (Figure 3.1.2F). In blood at 7 DPI, we observed significant upregulation of pro-and anti-inflammatory cytokines including IL-1 $\beta$ , IL-6, TNF $\alpha$ , IL-12p40, IL-12p70, CCL5 and IL-10. (Figure 3.1.2G, Figure B1.1D). CCL5 has previously been identified as a commonly increased chemokine following CMV infection [150, 151]. In contrast, we did not observe increased inflammatory cytokine expression from brain homogenates at the 7 DPI timepoint (Figure 3.1.2H, Figure B.1.2E). IL-12(p40) and CCL-5 were the only differentially expressed brain cytokines at this timepoint. Interestingly, both have been linked to Alzheimer's disease [152, 153]. Unexpectedly, at 1 MPI, we observed an elevated expression of inflammatory cytokines similar to that measured in the periphery at 7 DPI (Figure 3.1.2H, Figure B1.2E). At this timepoint, the inflammation in the periphery was resolved (Figure B1.2F) However, at 12 MPI, after 4 MCMV challenges, inflammatory cytokine levels in the brain are consistently lower in expression (Figure 3.1.2H, Figure B1.2E). This pattern of cytokine expression is not observed in mock-infected mice (Figure B1.3G). Based on these findings, we conclude that peripheral inflammation results in a delayed inflammatory response in the CNS.

#### Intermittent MCMV infection alters the transcriptional profile of brain cells

To understand the impact of fluctuating cytokine levels in the brain as a function of age, single cell transcriptional analysis was completed on whole brain

lysates at 12 MPI. We observed similar cell population distributions as expressed by UMAP (Figure 3.2A). Additionally, we saw differential expression of genes related to calcium signaling (Figure 3.2B), focal adhesion (Figure 3.2C), and cellular processes related to intercellular signaling (Figure 3.2D). To confirm observations from single cell transcriptional data we phenotypically and metabolically assessed brain cells using spectral flow cytometry (Figure B2A, B2B). At all timepoints examined, there were minor changes in brain cell populations (Figure 3.2E, 3.2F, 3.2G). Significant increases in T-cell populations in infected mice occurred, indicating enhanced extravasation from the bloodstream into the neural parenchyma. Of the other cell types assayed there were no significant changes between Mock and MCMV infected animals. However, at 7-DPI, we discovered increased proliferation rates in activated microglia/macrophages and T cells (Figure 3.2H). These were accompanied by decreased proliferation in BMECs. Taken together, these findings suggest expanding immune populations in response to initial infection or resulting inflammation. At 1- and 12-MPI, only T-cell populations exhibit changes in proliferation rate with a decrease at 1 MPI and an increase at 12 MPI (Figure 3.2I, 3.2J).

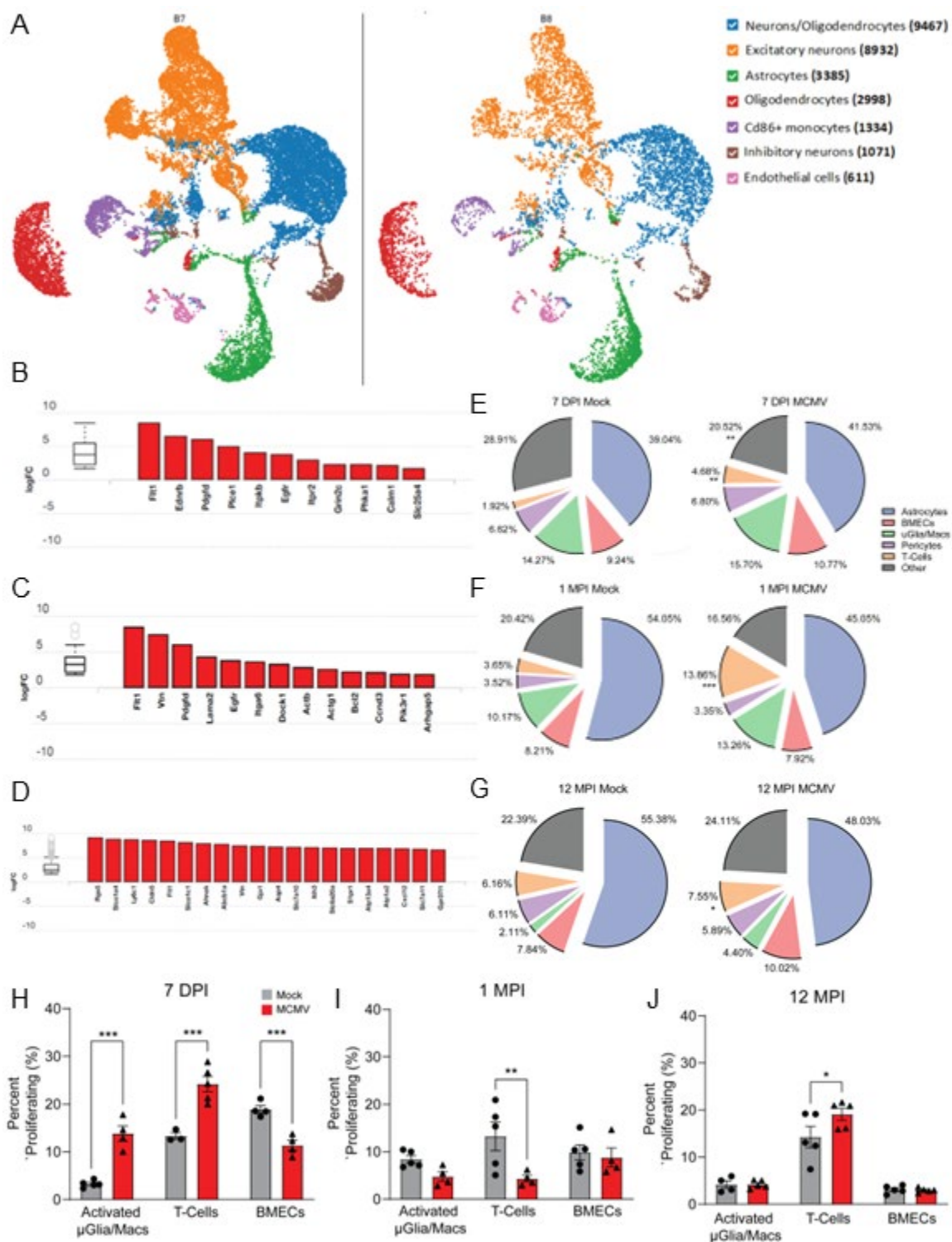


**Figure 3.2: Intermittent MCMV infection alters the transcriptional profile of brain cells.** (A) scRNA sequencing UMAP clustered neural cell populations. (Figure legend continues on next page)

Differential expression of genes in the endothelial cell populations following KEGG analysis of (B) calcium signaling and (C) focal adhesion pathways or Gene Ontology analysis of (D) cellular processes. Population distributions as a percentage of live cells isolated in mock- and MCMV-infected mice at (E) 7 DPI, (F) 1 MPI, (G) 12 MPI as assessed by flow cytometry. Percentage of proliferating cells in different cell populations as measured by Ki-67 positivity at (H) 7DPI, (I) 1 MPI, and (J) 12 MPI. Graphs represent pooled data from at least three individual animals. Mean  $\pm$  the SEM. \*,  $p < 0.05$ ; \*\*,  $p < 0.01$ ; \*\*\*,  $p < 0.001$ .

Blood brain barrier metabolic pathways are rewired with increased MCMV exposure

Our current data does not suggest that MCMV infection in our model directly infects the brain. Others have reported similar findings [62]. If peripheral MCMV infection can influence changes in the brain, the initial site of interaction is the BBB. Our Multiome data suggest that there is significant dysregulation of mitochondrial pathways. These findings are consistent with literature associating mitochondrial dysfunction and dementia [154, 155]. CMV has been reported to upregulate glycolysis pathways during infection [14, 18, 128] and similar findings are reported in AD brains [156]. Our group previously published that CMV infection induces mitochondrial dysfunction in fibroblasts and glioblastoma cell lines [128]. Our analysis of BMECs was split into two populations based on eNOS expression. We identified a large population of BMECs that had high expression while a minority exhibited low eNOS expression. We used glucose transporter 1 (GLUT1), hexokinase 2 (HKII), translocase of the outer mitochondrial membrane 20 (TOMM20) and voltage dependent anion channel 1 (VDAC1) as proxies for glycolytic and OXPHOS pathways (Figure 3.3A). Interestingly, at 7 DPI total and eNOS low BMECs had elevated expression of GLUT1 (Figure 3.3B) contrasted with a downregulation of GLUT1 at 1 MPI in total BMECs (Figure 3.3C) and downregulation at 12 MPI in the eNOS high group (Figure 3.3D). Hexokinase expression at 7 DPI was unchanged (Figure B3A), decreased at 1 MPI (Figure B3B), and only increased at 12 MPI in the eNOS low group (Figure B3C). Taken together, initial infection appears to enhance glycolytic function, but that change is

transient and trends towards decreased glycolytic function. In contrast, mitochondrial pathways appear to favor enhancement at 7 DPI in VDAC1 (Figure 3.3E) and TOMM20 (Figure B3D) expression. At 1MPI VDAC1 (Figure 3.3F) expression is decreased and TOMM20 (Figure B3E) is unchanged. By 12 MPI, total BMECs and the eNOS high group have significantly upregulated VDAC1 expression which suggests increased OXPHOS function as VDAC1 is the primary channel for ATP/ADP exchange in mitochondria (Figure 3.3G). Expression of the protein transporter TOMM20 was upregulated in eNOS high groups at 7 DPI (Figure B3D), unchanged at 1 MPI (Figure B3E), and downregulated at 12 MPI (Figure B3F). Previous research has demonstrated that, despite having access to sufficient oxygen, BMECs are highly glycolytic [157]. The 7 DPI timepoint suggests that MCMV enhances this characteristic. However, by 12 MPI, these cells have been reprogrammed to enhance OXPHOS as indicated by related protein expression. The impact of these changes is unknown but they suggest altered BMEC function and possibly BBB integrity.

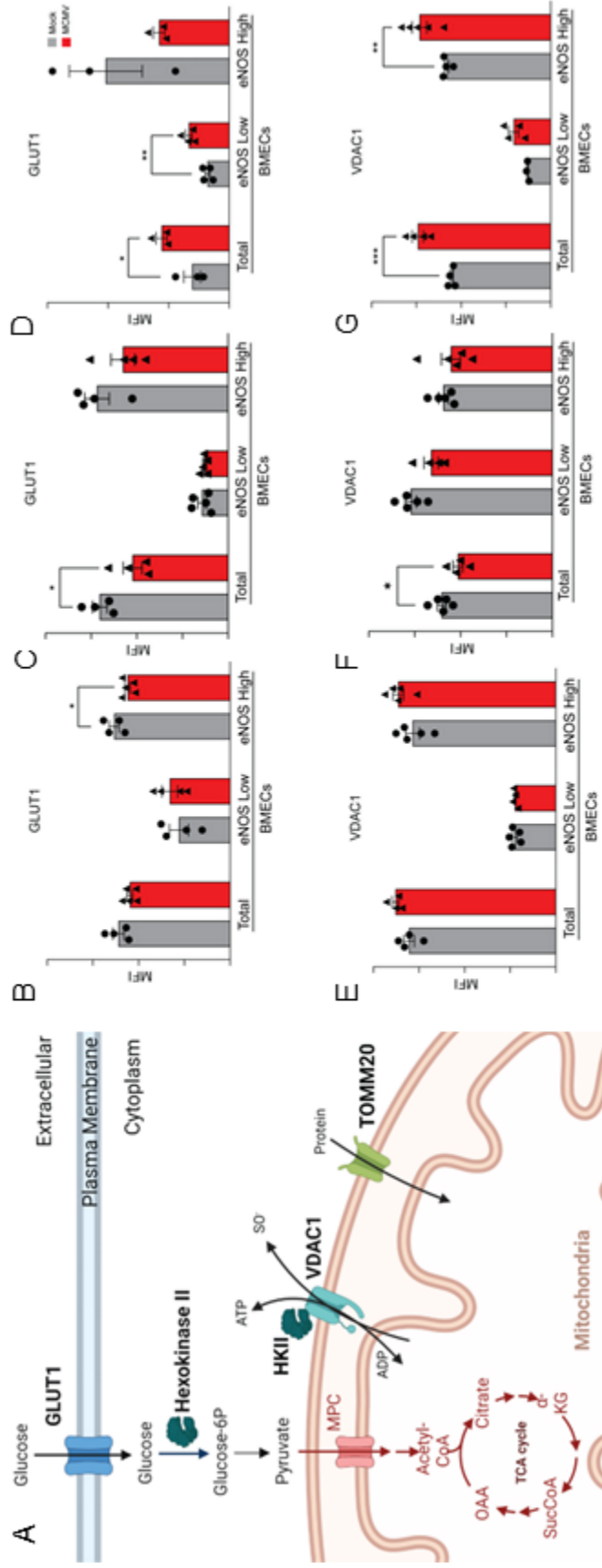


**Figure 3.3 Blood brain barrier metabolic pathways are rewired with increased MCMV exposure.** (A) Cartoon identifying key

proteins in glycolysis and mitochondrial function. Flow cytometry was used to examine expression of GLUT1 in populations of

BMECs at (B) 7 DPI, (C) 12 DPI, and (D) 12 DPI. Expression of VDAC1 in populations of BMECs at (E) 7 DPI, (F) 12 DPI, and (G)

12 DPI. Graphs represent pooled data from at least three individual animals. Mean  $\pm$  the SEM. \*,  $p < 0.05$ ; \*\*,  $p < 0.01$ ; \*\*\*,  $p <$

0.001. Created with Biorender.com.

Hallmarks of mitochondrial dysfunction and oxidative stress are elevated in BMECs intermittently exposed to MCMV

To better understand the impact of altered expression of metabolic markers, we isolated BMECs from the BBB and completed Seahorse bioanalyzer analysis (Figure 3.4A). At 1 MPI there were no significant changes to the OXPHOS markers including mitochondrial basal respiration, proton leak, non-mitochondrial respiration or mitochondrial ATP production rate (Figure 3.4B, 3.4C). Similarly, there were no changes in maximal respiration, spare respiratory capacity or total ATP production rate between mock and infected mice (Figure B4A). Intriguingly, at 12 MPI, the basal respiration rate, the minimal work required by the mitochondria to meet metabolic demand, was significantly increased in MCMV-infected mice (Figure 3.4D, 3.4E). This suggests that BMEC mitochondria from infected mice work harder to attain the same level of metabolic homeostasis as BMECs from mock-infected mice. No changes in maximal respiration or spare capacity (Figure B4B) were measured. Critically, we measured significant increases in proton leak and non-mitochondrial respiration (Figure 3.4E) in BMEC from MCMV infected mice, suggesting the presence of oxidative and mitochondrial stress. Mitochondrial ATP production rate was not found to be increased (Figure 3.4E). Live cell examination of mitochondria was performed by flow cytometry on CD31+ cells isolated from the brain. No changes in mitochondrial mass were detected at 1 MPI (Figure 3.4F) but increases were observed at 12 MPI (Figure 3.4G) suggesting mitochondrial fission. Critically, mitochondria-specific superoxide was upregulated at 12 MPI but not at 1 MPI (Figure 3.4H, Figure 3.4I). Together this data suggests

intermittent MCMV infection decreases BMEC mitochondrial efficiency and increases oxidative stress.

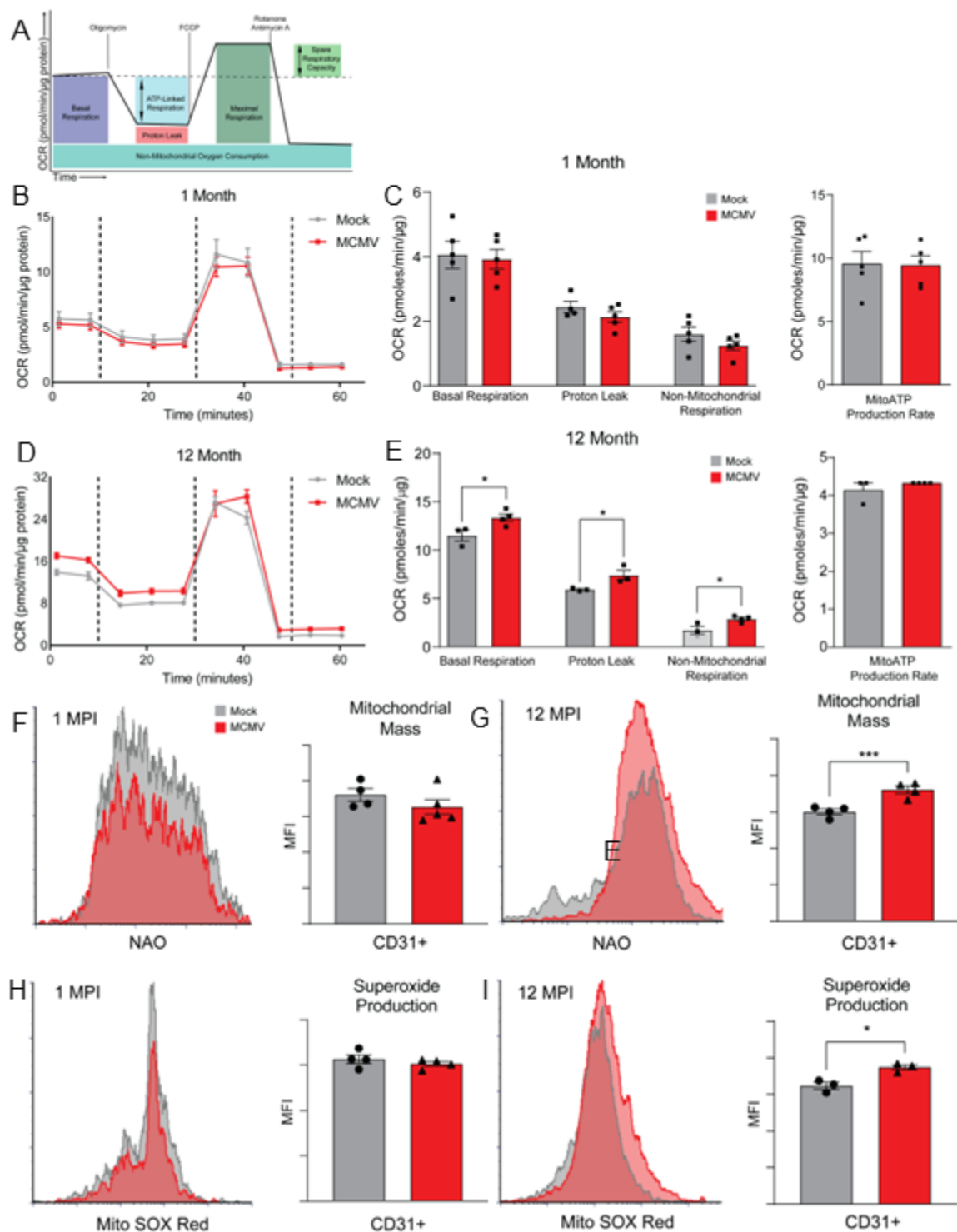


**Figure 3.4** Hallmarks of mitochondrial dysfunction and oxidative stress are elevated in BMECs intermittently exposed to MCMV. (Figure legend continues on next page)

(A) Cartoon illustrating how mitochondrial function was measured in BMECs using the Seahorse XFe24 MitoStress Kit. All samples were normalized to protein concentration. Representative data output of BMECs from the (B) 1 MPI and (D) 12 MPI timepoints. Basal Respiration, Proton Leak, Non-Mitochondrial Oxygen Consumption and mito ATP production rate were derived from the (C) 1 MPI and (E) 12 MPI measurements. Mitochondrial mass was determined by flow cytometry at (F) 1 MPI and (G) 12 MPI using nonyl acridine orange. Superoxide production was assessed using mitoSOX Red at (H) 1 MPI and (I) 12 MPI. Graphs represent pooled data from at least three individual animals. Mean  $\pm$  the SEM. \*,  $p < 0.05$ ; \*\*,  $p < 0.01$ ; \*\*\*,  $p < 0.001$ .

### MCMV infection metabolically rewires astrocytes as a function of age

We next asked if metabolic changes were restricted to the BBB or if changes were occurring in the brain. Due to their close interactions and functional cooperation with the BBB, astrocytes were further examined. Astrocytes uptake metabolites and proteins from the BBB to supply nutrients to neurons (Figure 3.5A). GLUT1 in astrocytes is responsible for uptake of glucose from the bloodstream [158] and AD patients have lower glucose levels in the brain [159-161]. At 7 DPI and 1 MPI GLUT1 expression in astrocytes is unchanged between mock and MCMV-infected mice but decreases at 12 MPI (Figure 3.5B). HKII levels are significantly decreased at 1 MPI but are unchanged at 12 MPI (Figure B5A).

OXPHOS function, as indicated by the protein import channel subunit TOMM20, demonstrated a significant decrease in expression at 12 MPI in the MCMV-infected mice. TOMM20 expression is unchanged in A1 astrocytes at 7 DPI but increases in A2 astrocytes (Figure B5B). However, by 12 MPI total astrocytes showed decreased TOMM20 expression (Figure 3.5C), findings which were echoed in both A1 and A2 populations (Figure B5C). These findings suggest that mitochondrial function is altered due to infection burden. No changes in VDAC1 were observed (Figure B5D). An examination of mitochondrial mass and superoxide production in ACSA-2 positive cells at 7 DPI found similar mass but significantly less superoxide production in MCMV-infected animals (Figure 3.5D). At 1 MPI both mass and superoxide production were similar in both groups of animals (Figure 3.5E). By 12 MPI the mitochondrial mass of astrocytes in the MCMV-infected mice was significantly decreased, however they were producing

similar levels of superoxide (Figure 3.5F). These findings correlate nicely with the decreases in TOMM20 however the similar levels of superoxide suggest that there may be mitochondrial dysfunction. Global decreases in astrocytic metabolic function, both glycolysis and OXPHOS, have been associated with AD and result in insufficient metabolic support for neighboring neurons [162].

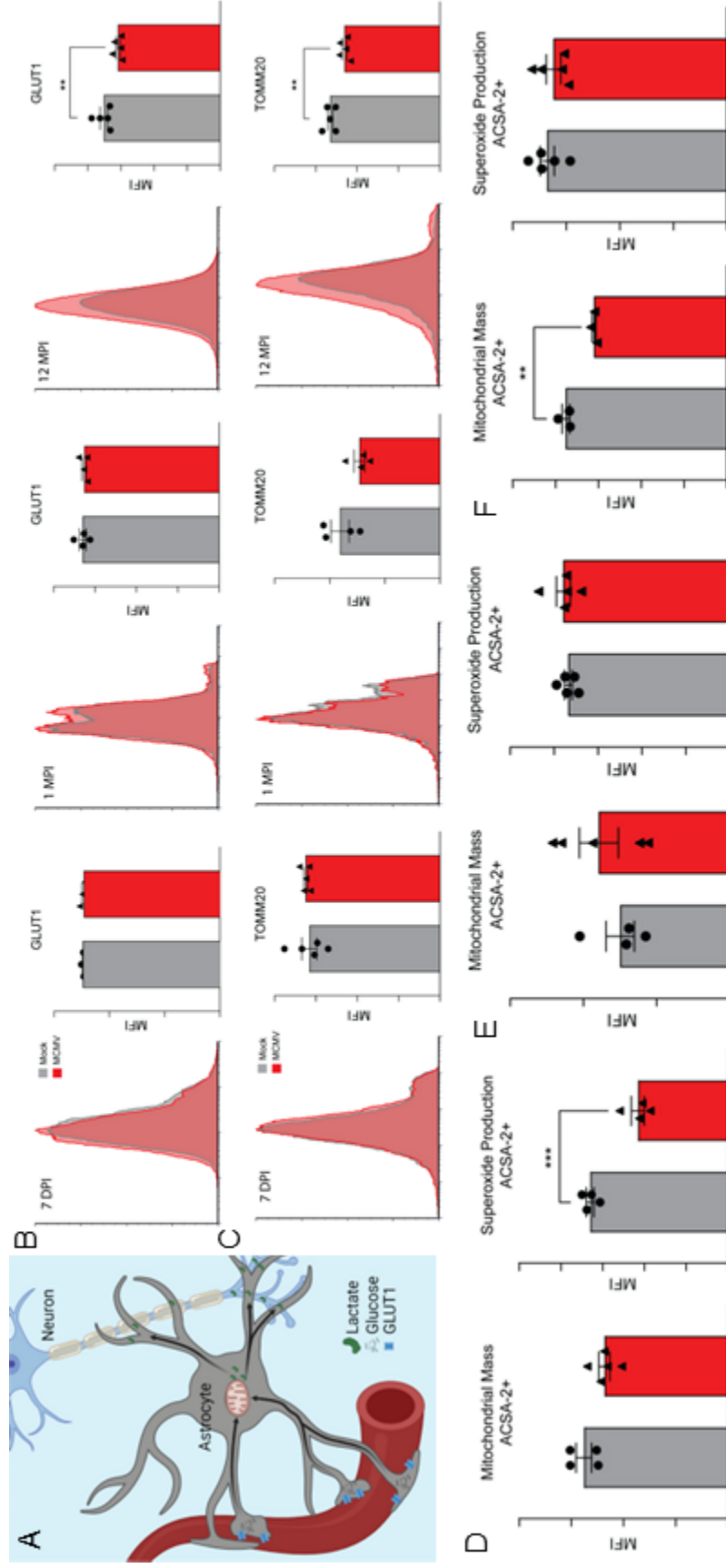


**Figure 3.5: MCMV infection rewires astrocytes as a function of age.** (A) Cartoon demonstrating the flow of metabolites from the bloodstream through astrocytes to neurons. Flow cytometry expression of (B) GLUT1 and (C) TOMM20 in astrocytes at 7 DPI, 1 MPI and 12 MPI. Mitochondrial mass and superoxide production were determined using nonyl acridine orange and mitoSOX red staining respectively and are quantified at (D) 7 DPI, (E) 1 MPI, and (F) 12 MPI. Graphs represent pooled data from at least three individual animals. Mean  $\pm$  the SEM. \*,  $p < 0.05$ ; \*\*,  $p < 0.01$ ; \*\*\*,  $p < 0.001$ .

### Cognition is impaired with intermittent MCMV infection

An increased percent of live T cells was detected at 7 DPI, 1 MPI, and 12 MPI indicating increased extravasation from the vasculature (Figure 3.6A, 3.6B). Further, phenotypical differences in T-cell populations isolated from the brain in MCMV-infected mice as a function of time was recorded. In the 1 MPI cohort, the T cells had decreased expression of OXPHOS and glycolysis metabolic markers relative to mock infected animals (Figure 3.6A). In the 12 MPI cohort, T cells had higher expression of OXPHOS and glycolysis metabolic markers relative to mock infected animals (Figure 3.6B). Additionally, these cells had significantly decreased H3K27me3 expression suggesting a more transcriptionally active population. The highly metabolic nature of these cells and retention in the parenchyma despite the absence of active infection or inflammation suggest that they represent a population of tissue resident T memory cells. Previous literature using a similar MCMV model has described brain resident memory CD8 T cells acting as inhibitors of MCMV reactivation [163]. The presence of resident memory T cells in the CNS may contribute to disease progression as the CNS has conventionally been perceived as an immune privileged environment.

To understand the physical manifestations of our collective molecular results, we completed cognitive assays on all mice used in the above experiments. Hot plate (Figure B6A) and passive avoidance (Figure B6B) assays were completed to identify innate differences in nociceptive ability and fear-aggravated learning. At 1 MPI (Figure B6C) and 12 MPI (Figure B6D), both groups exhibit similar latency to behavior and number of behaviors demonstrating that their

nociceptive capabilities are intact and similar between groups [142]. At both 1 (Figure B6E) and 12 MPI (Figure B6F), both groups exhibit near perfect retention of learning after 24 hours. Indicative that fear-based learning events (shock) with high salience are still able to be learned regardless of infection status. At 7 DPI, Y-maze assessment of spatial working memory (Figure 3.6C) demonstrated very similar number of alternations and spontaneous, correct alternations (Figure 3.6D). At 1 MPI, MCMV-infected mice exhibited a significantly lower number of total alternations, but no significant changes to spontaneous alternations (Figure 3.6E). Interestingly, at 12 MPI (3 months after last infection), no difference in total alternations was measured but there was a significant decrease in spontaneous alternations, indicative of impaired spatial working memory (Figure 3.6F).

Additionally, we see a significant decrease with age when comparing 1 MPI and 12 MPI mock infected mice (Figure 3.6G). These findings are in agreement with previous studies of cognitive impairment in BALB/cJ mice in which cognitive decline was first witnessed at 12 months of age [164]. We see an even more significant decrease in cognition with infection status and age when comparing 1 MPI mock and 12 MPI MCMV infected cohorts. This suggests a synergy between viral burden and age as they relate to cognitive decline.

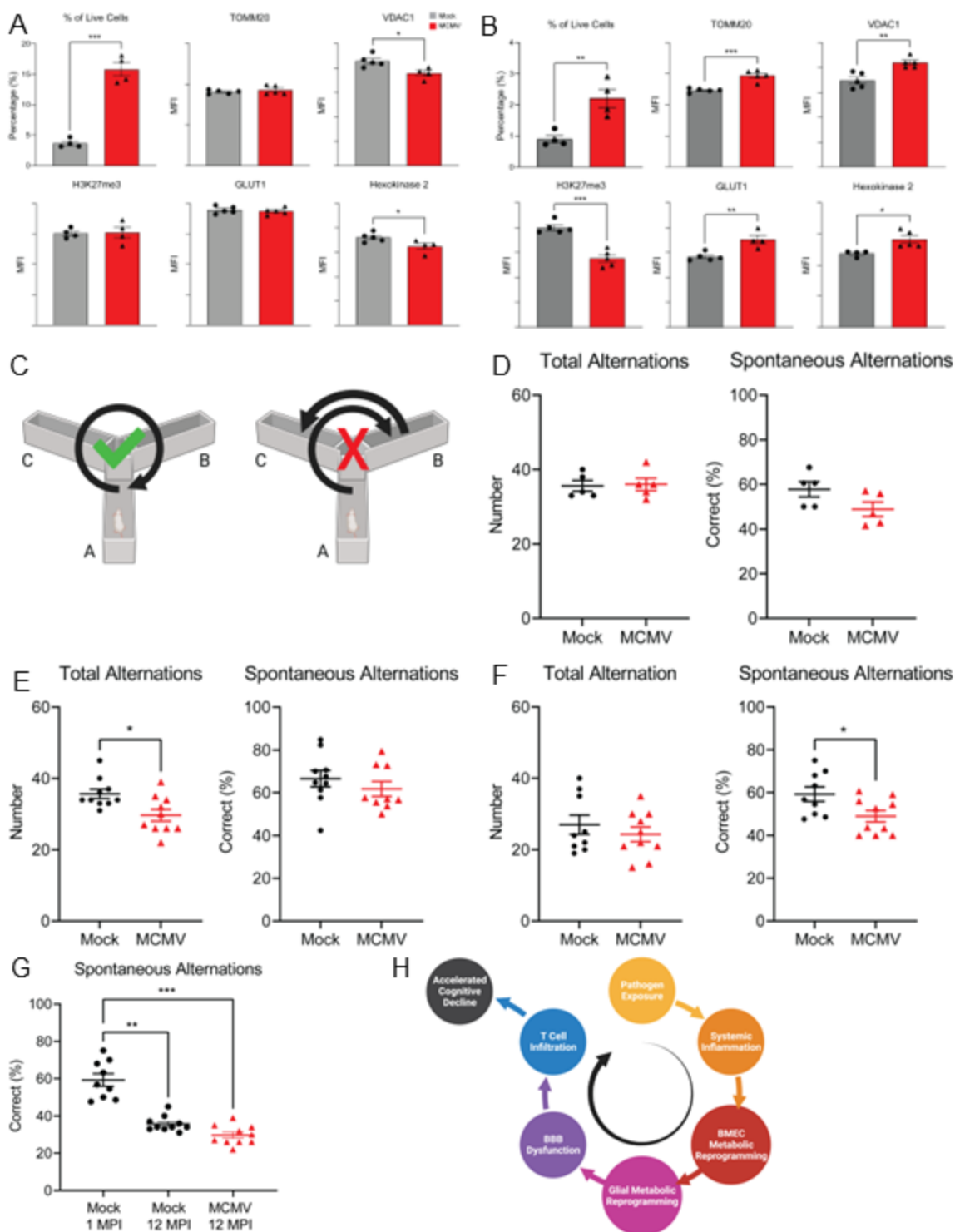


(Figure legend on next page)

**Figure 3.6: Cognition is impaired with intermittent MCMV infection.**

Proliferation, epigenetic, and metabolic markers of CNS resident T cells were examined using flow cytometry at the (A) 1 MPI and (B) 12 MPI animals (C) Cartoon illustrating correct versus incorrect alternations in the Y-maze. Quantification of number of alternations and percentage of spontaneous correct alternations at (D) 7 DPI, (E) 1 MPI, and (F) 12 MPI animals. (G) Comparison of spontaneous alternations examining the interactions between age and infection status. (H) Diagram presenting the model of pathogen associated accelerated cognitive aging. Graphs represent pooled data from at least three individual animals. Mean  $\pm$  the SEM. \*,  $p < 0.05$ ; \*\*,  $p < 0.01$ ; \*\*\*,  $p < 0.001$ . Created with Biorender.com.

### **3.5 Discussion**

Dementia, including Alzheimer's Disease, are identified clinically, years to decades after initiation and progression of disease. Pathogens and the resulting immune response have been correlated to AD, but mechanistic evidence integrating an infection model and aging is lacking. Here, we addressed the impact of viral infection on hallmarks of AD pathology as a function of age. The data demonstrate that intermittent CMV infection accelerates mitochondrial dysfunction and increases oxidative stress as a function of age. First, infection increased basal mitochondrial function over time. Second, mitochondrial specific ROS was elevated in aged CMV infected mice. Third, intermittent infection resulted in enhanced cognitive decline.

We report that repeated CMV challenge impacts metabolic function of endothelial cells in the BBB. The degree of functional change increases with viral burden and age. How these changes are mediated continue to be investigated. Metabolic pathways in BMECs are not altered during primary acute infection. Instead, rewiring occurs incrementally with subsequent reinfections. Inflammatory cytokines have been strongly associated with changes to BBB permeability [165]. We observed increased inflammatory markers in the blood at 7 DPI, but only minor changes in the brain (Figure 1). In brain lysate, IL-12p40 was significantly increased correlating with published data showing siRNA knock-down of IL-12p40 in SAMP8 mice ameliorated AD neuropathology [166]. IL-12(p40) antagonizes IL-12 function and upregulation is needed for efficient MCMV clearance [167]. CCL5 was also significantly increased and aids in migration of MCMV-specific CD8+ T

cells [151]. CMV encodes a highly specific RANTES decoy receptor [150] illustrating the importance of this cytokine during CMV infection. Both cytokines continue to be significantly upregulated 1 MPI, possibly due to paracrine effects of low-level viral persistence or residual viral products. At 1 MPI, we detect low levels of MCMV replication in the salivary gland (Figure B1). IL-1 $\beta$  and TNF $\alpha$  have been implicated in MCMV reactivation in vivo [168, 169] possibly establishing a cycle of intermittent reactivation. We did not include assays to quantify MCMV reactivation in this study design, but the significant increase in IgM levels at the 6 and 12 MPI timepoints suggest that MCMV has recently reactivated in these cohorts. It has been reported that CMV reactivates more frequently as a function of increased age [170]. Inefficient control of MCMV reactivation by the immune system may explain the emergence of subtle but significant changes at 12 MPI. Surprisingly, cytokine concentrations are significantly decreased in MCMV infected mice at 12 MPI. Mice were last exposed to MCMV 3 months prior to testing of cytokines so we expected concentrations similar to mock conditions, but not lower concentrations. It is possible that hypoactivation is driving low levels, suggesting dysfunction in one or more glial populations. Alternatively, this may be a response to the delayed expression of inflammatory cytokines seen at 1 MPI. It is also possible that anti-inflammatory mechanisms are over stimulated. Collectively, all scenarios suggest dysregulation of cytokine-associated mechanisms in the brain.

The BBB is the interface between the brain and the periphery and includes BMECs, astrocytes, and pericytes that actively regulate the movement of proteins, nutrients, ions, and small molecules. Systemic inflammation could exert effects on

the BBB by affecting the BMECs. Our omics approach at the 12 MPI timepoint indicated that the most significantly upregulated genes in BMECs were those related to calcium signaling, focal adhesion, and cellular processes (Figure 2A-D). Of note, MCMV treated animals significantly upregulated expression of claudin-5 (Cldn5). Claudin-5 is the dominant tight junction protein in the BBB. Upregulation of transcription may indicate impairment of tight junction formation or maintenance in endothelial cells. Our metabolic profiling of BMECs indicated a significant decrease in GLUT1 expression at 12 MPI. This is an area of active exploration in our lab. Glut1 is the main mediator of glucose uptake for the brain and alterations have been shown to initiate BBB changes, altering tight junction integrity [171]. Reduced GLUT1 may be indicative of reprogrammed BMEC metabolism, shifting dependency to OXPHOS which explains increased basal respiration in 12 MPI mice. This would be similar to a recent report showing CRISPR-Cas9 GLUT1 truncation decreased BMEC bioenergetics and negatively impacted neuro angiogenesis [172]. Expression of claudin-5 has been shown to decrease in parallel with GLUT1 following suppression of the Wnt/ $\beta$ -catenin pathway [173]. Our previous research has demonstrated that CMV infection dysregulates this pathway [174, 175], providing a possible mechanism for these changes.

In addition to the glycolytic changes discussed above, mitochondrial function is significantly altered in MCMV infected BMECs at 12 MPI. VDAC1, the primary channel for the exchange of ADP for ATP through the mitochondrial membrane is intrinsically linked to both the metabolic and the apoptotic functions of mitochondria. The increases in VDAC1 expression and mitochondrial mass with

age and infection suggests increased dependence on OXPHOS, however our Seahorse data demonstrate minimal change to mitochondrial ATP production. Intriguingly, VDAC1 has been reported to be elevated in the brains of AD patients and in APP transgenic mice [176, 177]. In the context of AD, VDAC1 is required for A $\beta$  uptake and apoptosis [178]. Our VDAC1 observations may coincide with hexokinase-influenced glycolytic changes mediating BBB activity [179]. Our model correlates strongly with these studies and demonstrate that further studies exploring VDAC1 function in our model are warranted. Decreased TOMM20 expression was also observed. TOMM20 is responsible for the import of proteins targeted to the mitochondria. A Parkinson's Disease model provided evidence that overexpression of TOMM20 protected against  $\alpha$ -synuclein-induced mitochondrial dysfunction and subsequent neurodegeneration [180]. Based on these observations, decreased TOMM20 levels in our model may suggest impaired A $\beta$  clearance due to dysfunctional mitochondrial transport functions.

Diminished glycolysis and increased OXPHOS has previously been reported using a senescence BMEC model related to aging [181]. Uncoupling of the ETC may explain the increased proton leak and play a protective role by mitigating ROS production and therefore oxidative damage [182]. Elevated endothelial cell activation driven by increased ROS production in the absence of increased ATP production has been reported [183]. Most intriguing is the detection of increased mitochondrial specific superoxide (Figure 4). ROS has been well documented to contribute to neurodegenerative disorders [184] specifically neuronal death due to A $\beta$  accumulation [185]. The increased total mitochondria

measurement suggest mitochondrial fission has occurred. This is likely due to metabolic stress and can be induced by CMV infection [186]. It would be interesting to define the impact on mitophagy to understand if damaged mitochondria remaining in the BBB further contribute to BBB functional changes and progression of AD related pathologies.

Astrocytes, the abundant glial cells whose endfeet reinforce the BMEC tight junctions in the BBB, act as the primary nutrient uptake agents for the brain. Similar to BMECs, astrocytes expressed significantly decreased levels of GLUT1 at 12 MPI. Astrocytic glycolysis is essential for neuron health as glycolysis-derived lactate is taken up by neurons and used as OXPHOS fuel in their axon terminals. Studies have demonstrated that astrocytic glycolysis decreases with age and is thought to contribute to AD-related impairments [187]. Additionally, astrocytic lactate is critical for providing neurons with the energy needed to form memories [188]. The impact of reduced glucose supply across the BBB into the cerebral parenchyma was not investigated in our model but may play a critical role linking metabolic rewiring to cognitive changes via reduced nutrient availability to neurons. Measuring glucose and lactate concentrations in memory centers of the brain may provide key insights linking intermittent infection with accelerated cognitive decline in our aging model.

The increased presence of T cells in the brain with intermittent infection and age is largely unexplained with our approach. We do not detect chronic inflammation in the periphery or the brain. A leaky BBB would provide increased and easier access for T cells to cross the BBB, but the reason for their recruitment

and persistence is unknown. These changes correlate with infection, but this alone does not fully explain our results. The highly metabolic nature of these T cells (Figure 6) suggest that they may be tissue resident T cells. Murine polyomavirus infection has been reported to produce a set of brain resident memory T cells [189]. Similar results were observed in Vesicular stomatitis virus (VSV) treated mice and it is thought that their persistence in the CNS may be problematic in an environment unaccustomed to immune surveillance [190]. However, these viruses are neurotropic and CMV has significant difficulty crossing the BBB in mature immunocompetent hosts [62].

The most compelling results linking our molecular results with a physical outcome are our cognitive function behavior tests. Foot-shock based passive avoidance test results were very similar between animals at all timepoints indicating the ability to learn fear-based, high salience stimuli effectively. An aging study in BALB/C mice only found significant differences in passive avoidance cognition beginning at 24 months of age [191], so our findings at 12 months were expected. We employed the Y-maze as a measure of spatial working and reference memory. Successful alternations between arms indicate an intact working memory and by extension suggest intact medial pre-frontal cortex and hippocampal functions. At 1 MPI MCMV-infected mice trend towards a decreased percent of correct alternations in the maze, possible due to lingering sickness behavior (Figure 6) or resulting from the impact of increased pro-inflammatory cytokines in brain (Figure 1). These events cannot explain the cognitive decline observed at 12 MPI as there is a decreased concentration of pro-inflammatory

cytokines (Figure 1). Similarly, the age-related motility can be disregarded as both mock and MCMV-infected animals exhibited similar number of alternations in the same timeframe. The significant decrease in cognitive function when merging the cofactors age and infection ( $p = <0.01$  when comparing 1 Mo Mock to 12 Mo MCMV) strongly points to a synergy between CMV infection and age. A study in BALB/c mice was first able to detect cognitive decline using the Y-maze when comparing 4 month old mice to 12 month old mice [164]. The fact that we detected impaired cognition with age matched controls at the 12 MPI timepoint strongly suggests that MCMV infection accelerates cognitive decline. CMV seropositivity has previously been associated with numerous pathologies including breast and brain cancers [32, 33, 37] suggesting it may play an oncomodulatory role in cancer development and/or progression. Anti-viral therapy targeting CMV has been used to treat patients with glioblastoma and has been shown to increase both overall and progression-free survival [49, 87]. We have demonstrated that systemic inflammation produces a delayed neuroinflammatory response which may be an initiation event for accelerated cognitive decline. We have linked these changes to altered metabolism in BMECs and enhanced production of ROS suggesting that oxidative stress may be a culprit for accelerated disease progression. MCMV is our model pathogen, however, any pathogen which produces transient systemic inflammation has the potential to contribute to cellular aging. It is the additive nature of these pathogen exposures over time which we suspect synergize with myriad other factors to accelerate aging and disease pathology.

### **3.6 Limitations**

Our experimental design does include limitations. We attempted a reductionist approach in which our animals were repeatedly exposed to a single pathogen, very dissimilar to the myriad pathogens experienced throughout life. We also employed a mouse model which is phenotypically “normal” with respect to many of the risk factors strongly correlated with the development of dementia or AD. Our goal was to determine if repeated infection, mimicking the intermittent reactivation of CMV that occurs throughout life, without any other complicating factors, could lead to markers of AD pathology. For this study we did not measure A $\beta$  plaques or accumulation of tau tangles, hallmarks of AD. Further, it is unknown, and likely variable, how frequently CMV reactivates in an immunocompetent individual. Our model assumes a single reactivation each decade. This study also used female mice only, future studies will include males to compare results from current models of dementia and aging [164]. Many of our assays used whole brain or a hemisphere. Despite the generation of exciting data, a region-specific analysis would be of great benefit to further understand how intermittent infection is impacting specific areas of the BBB. Applying this model to transgenic animals predisposed to AD development would provide additional insight into specific cell populations or molecular pathways that change over time. These are all approaches currently being considered by our team.

### **3.7 Conclusions**

In summary, our data demonstrate that intermittent CMV infection alters metabolic pathways in the BBB and accelerates cognitive decline. This model makes use of a genotypically and phenotypically normal mouse strain with no predisposition to cognitive deficits or dementia pathology. Importantly, the intermittently infected mice, even at the latest timepoint, appear and behave just like the mock infected animals. At 14 months of age, these animals are middle aged at which point the human development of dementias would still be in the prodromal, symptomless phase. Similar to the course of human disease, the MCMV mice are indistinguishable from their controls. Thus our model demonstrates a synergy between infection burden and age as contributing factors in AD progression. Our work strongly supports a role for pathogens as risk factors in dementia related pathologies.

## CHAPTER 4

### CONCLUSIONS AND FUTURE DIRECTIONS

#### **4.1 Conclusions**

Initially we focused on the impact of *in vitro* metabolic changes in a glioblastoma (GBM) cell line following infection with cytomegalovirus (CMV). We also wanted to determine the potential those changes had to alter the extracellular environment to the benefit of the tumor. We reported metabolic reprogramming which closely mirrored previous findings in other cell lines, notably enhanced rates of glycolysis and oxidative phosphorylation. These results compliment a study by Liu *et al.* which demonstrated that primary GBM cells exhibit a stem like phenotype which may enhance their ability to evade chemotherapy [107]. This metabolic reprogramming represents one way in which CMV infection may function in an oncomodulatory manner. Alterations to metabolic profile may allow tumor cells to make better use of the nutrients in the extracellular environment thus providing significant metabolic flexibility and enhancing their resilience to challenging environments.

We also found that infected cells were able to communicate with neighboring cells resulting in alterations to their metabolic and epigenetic landscape. These findings may seem banal, however, these changes occurred in

the *absence* of viral transmission. This research demonstrated that it would only require a small population of CMV infected cells to produce significant effects within the tumor microenvironment and on neighboring cells. In order to investigate the extent to which CMV infected cells could alter organism-wide metabolic pathways we employed a murine model of aging.

We hypothesized that repeated exposure to a pathogen, mimicking the reactivation seen with CMV and other herpesviruses throughout life, would result in minor changes in the animal in the short term. However, we anticipated that the repeated nature of these insults would compound over time, eventually leading to accelerated cellular aging. Our pathogen exposure model of aging represents a powerful tool for targeted discovery of pathogen mediated changes to the immune system as well as specific organ function. For the purpose of this dissertation we focused on results relating to the brain and cognitive function.

By examining three cohorts of animals (active infection, 1 month post infection, and 1 year post initial infection with re-infection every 3 months) we were able to characterize the immune and neuroimmune responses over time. We found that during active infection, there was an initial systemic inflammatory response which was absent in the CNS. However after 1 month, following resolution of the initial infection, there was a delayed inflammatory response in the CNS which was paired with enhanced leukocyte extravasation into the brain parenchyma. These findings suggest that MCMV induced peripheral inflammation is able to produce effects within the CNS.

As the interface between the periphery and the central nervous system, the blood brain barrier (BBB) actively controls the movement of cells, proteins, ions, and small molecules into and out of the brain. Extensive research has demonstrated that circulating pro-inflammatory cytokines have detrimental effects on BBB integrity. Thus, our focus moving forward relates specifically to cells of the BBB. To examine transcriptional changes in brain at the 12 MPI timepoint, we employed single-cell Multiome ATAC and gene expression sequencing. Our initial analysis of this data focused on the brain microvascular endothelial cells BMECs. In this population, we found significant upregulation of genes related to focal adhesion formation and BBB repair suggesting some degree of BBB dysfunction.

Next, we employed Seahorse Metabolic Analysis to examine the metabolic profile of live BMECs isolated from brains following sacrifice. BMECs from MCMV infected mice at 12 MPI demonstrated enhanced basal respiration, mitochondrial mass, and increased superoxide production. However, despite working harder, and having more mitochondria, there were no changes to mitoATP production rate, suggesting mitochondrial dysfunction. Additionally, though a certain level of ROS production is essential for proper cellular signaling, excess ROS production can cause oxidation of proteins, DNA, and lipids. Oxidation of these substrates can alter protein function, induce nucleoside base changes, and cause DNA strand breaks leading to significant cellular and mitochondrial damage.

As the most metabolically demanding organ, accounting for about 25% of the total glucose use, the brain is susceptible to damage caused by dysfunction of the BBB. The BBB represents the primary interface between the brain and the

body and proper function allows for the transport of glucose from the circulatory system to cells within the brain. Persistent dysfunction of the BBB as we have previously described in our BMECs could produce significant changes in cognition.

Astrocyte end feet surround and reinforce the endothelial tight junctions in the BBB. Through these end feet they regulate the uptake and dispersal of metabolites in the CNS. Astrocyte uptake of glucose and subsequent glycolysis produce large amounts of lactate which astrocytes release into the extracellular environment. This lactate is taken up by neighboring neurons and employed as an energy source by mitochondria in their axon terminals. Lactate is converted to pyruvate and funneled into the TCA cycle, powering oxidative phosphorylation in a metabolic transport paradigm known as the astrocyte-neuron lactate shuttle. It has been demonstrated that this lactate is critical for powering the neuro-energetic demands underlying learning [188]. Our findings demonstrate decreased GLUT1 expression in astrocytes following MCMV infection at the 12 month timepoint. This may result in a paucity of lactate production to fuel synapse formation and maintenance by neurons, providing an additional potential mechanism for accelerated cognitive impairment.

To examine cognitive function, we employed a bevy of behavioral assays. We were able to demonstrate that repeated MCMV infection produced significant cognitive deficits in short-term and spatial-working memory. This was observed at “middle age” in a mouse strain that is not predisposed to cognitive dysfunction. In fact, it was only at 12 months of age that researchers were able to identify cognitive deficits in BALB/c mice as compared to young (4 month old) mice [164]. We were

able to observe significant differences at the same age but in comparison to age-matched, uninfected mice further strengthening our findings. Esquivel et al. noted that elevated levels of oxidative damage to proteins of the brain were present in aged mice and likely accounts for their cognitive decline. Paired with the increased ROS production we saw in our BMECs, normal aging in conjunction with MCMV infection related oxidative stress may be directly related to accelerated cognitive decline in these animals.

Our long term pathogen exposure and aging paradigm produced some very interesting changes in both the blood brain barrier and in cognitive function of mice. Thus far, we have demonstrated that these persistent infection events have a cumulative, and possibly synergistic, effect on cognition even in middle aged mice. The presence of mitochondrial dysfunction and increased ROS production in BMECs suggest that BBB dysfunction may be a mechanism behind this accelerated cognitive decline. Therapeutics designed to enhance the antioxidant response of cells may provide protection against age- or pathogen-related cognitive decline. Our model provides a simple platform to test this hypothesis and others. Findings from these experiments and others may enable future generations to avoid or mitigate cognitive decline leading to enhanced quality of life at advanced age.

#### ***4.2 Future Direction 1: CMV-mediated changes in metabolite secretion following infection.***

Mechanistically we have we have already proposed that elevated lactate secretion from infected cells may result in metabolite transfer to neighboring OXPHOS dependent cells, in a mechanism akin to the astrocyte-neuron lactate shuttle. Changes to the metabolic milieu of microenvironment can easily result in alterations in the metabolic profile of cells. As one metabolite becomes abundant and another scarce, cells adjust their metabolic profile to suit the environment. In the case of increased extracellular lactate, cells are capable of taking up lactate via monocarboxylate transporter 1 (MCT1) and, employing a lactate dehydrogenase, to convert said lactate to pyruvate for use in the citric acid cycle. In cancer, lactate transfer from highly glycolytic to highly oxidative cancer cells allows the cells to mutually optimize tumor growth [192].

In addition to lactate uptake by MCT1, extracellular lactate acts as the ligand for a  $G_i$ -coupled g-coupled protein receptor, GPR81 (HCAR1). Activation of HCAR1 promotes a host of metabolism mediated signaling cascades including PKA, PI3K, and ERK1/2 activation ultimately leading to metabolic changes, proliferation, and survival induced by CREB phosphorylation [193, 194]. MCMV-mediated increases in extracellular lactate possess the ability to produce wide-ranging effects in both normal and cancerous cells. The viral benefit to these changes would make an interesting topic of research.

### ***4.3 Future Direction 2: CMV-mediated changes in intracellular communication following infection.***

As previously noted, metabolic and epigenetic alterations occurred in cells in close proximity to CMV-infected cells in the absence of viral infection. However, we are still unclear about the mechanisms that underly these changes. We heat inactivated CMV conditioned media and found that it was still able to produce similar metabolic and epigenetic effects on uninfected cells. These effects were blunted relative to non-heat denatured treatment groups but this indicates that at least a portion of the changes can be attributed to protein signaling.

Intercellular signaling is an incredibly complex process. Historically, it was thought that the vast majority of this communication was mediated by secreted proteins, cytokine and chemokines, and their receptors. However, since their discovery in 1983, the release of extraluminal vesicles, termed extracellular vesicles (EVs), was found to be a potent intracellular signaling mechanism [195, 196]. Unlike cytokines and chemokines which present a limited signal (activation of one RTK for instance), EVs can transfer proteins, micro-RNA, metabolites, and even mitochondria between cells allowing for activation of numerous signaling cascades and control of transcription and/or translation. While cytokines are subject to diffusion dilution (decreased concentration with increased distance from source) an EV can have the same impact on a cell immediately adjacent to- or a cell distant from- the source cell. This has been powerfully demonstrated by research showing exosome-mediated priming of the pre-metastatic niche and eventual metastasis of cancers [197].

With respect to CMV, could EV-mediated signaling be priming adjacent or distant cells for eventual infection? Could they represent a mechanism for CMV-infected cells to search out immune privileged niches more amenable to infection and replication? An understanding of the cargo present in EVs is critical to understanding the function of CMV-derived EVs. A full characterization of the protein, miRNA, and mRNA complement of these EVs in comparison to uninfected controls would provide valuable knowledge about the impact of CMV on the host as an organism, instead of just a cell. This may pave the way for new therapeutics and insights into the effect of CMV on aging, metabolism, and viral dissemination.

#### ***4.4 Future Direction 3: Investigating targeted areas within the murine brain.***

Perhaps the largest current failing of this current research model is the fact that all of our assays are focused on global changes in the mouse brain. The neural cytokine, flow cytometric, and even the BMEC seahorse assay make use of whole brain homogenates. As such, we are likely masking significant changes that are occurring in smaller compartments within the brain. For instance, we observe cognitive decline in spatial working memory with our aged, MCMV infected mice. Spatial working memory has largely been attributed to both the hippocampus and the medial prefrontal cortex [198].

A relatively simple method to address this failing would be to dissect out specific brain regions prior to Bio-Plex or flow cytometric processing. This would allow us to examine the function of glia and infiltrating cells in regions directly related to our behavioral assays. Alternatively, formalin fixed paraffin embedded

hemispheres can be examined histologically to reveal focal changes within the brain. This would additionally provide us with the ability to observe critical morphological and functional changes *in situ*. The added strength of this approach is that we would be able to follow changes as they accumulate over time and examine how they are affected by repeated pathogen exposure.

Another benefit of this approach would be the ability to identify which cells and cell types are actively or latently infected with MCMV at these timepoints. Previous studies have demonstrated infection of endothelial cells and the neighboring pericytes. This may account for the BBB changes we see at later timepoints. Confirmation of these findings would strengthen our understanding of the systemic effects of MCMV.

#### ***4.5 Future Direction 4: Examination of the impact of mitochondria-derived reactive oxygen species on aging and/or cognitive decline and development of therapeutics.***

Our findings largely implicate mitochondrial metabolic dysfunction and the production of excess superoxide for harmful effects on BMECs and other glial populations. Excessive ROS production can lead to numerous changes in cell function and survival. These changes may result in the accelerated cognitive decline we see with our MCMV mice at 12 MPI. To test this hypothesis, we would need to find a way to enhance the animal's antioxidant response or reduce the ability of their mitochondria to produce superoxide. A transgenic mouse line exists which expresses alternative oxidases (AOX) in the ETC while maintaining

essentially normal physiology [199]. In this model electrons are transferred from ubiquinol to oxygen without requiring proton transport across the mitochondrial membrane. Importantly, this allows for normal mitochondrial function while reducing reactive oxygen species production. Employing this transgenic strain would allow us to test the hypothesis that enhanced ROS production by MCMV-infected cells is responsible for the advanced cognitive decline witnessed in our mice.

Increased oxidative stress has long been described as a major component of cellular aging. This is largely the result of two age-related changes, increased ROS production and decreased expression of antioxidant enzymes [200]. Cumulatively, these changes have been correlated with numerous age-related pathologies such as neurodegenerative disease. As previously noted, Esquivel et al. demonstrated that cognitive decline in BALB/c mice was accompanied by enhanced oxidative damage to proteins in neural cells [164]. Our pathogen exposure-aging model provides us with a robust system in which to test potential therapeutics. By employing sensitive animal behavior assays to measure cognitive function, we can quantify and qualify cognitive decline as we manipulate oxidative stress in the organism.

#### ***4.6 Final Thoughts***

Overall, the research presented here provides evidence that repeated exposure to a pathogen, such as CMV, can produce significant long-term effects which are compounded by advancing age. Considering the innumerable

pathogens organisms experience throughout life it seems prudent to examine the effects that they have on aging. This aging pathogen model offers great flexibility to examine any number of pathogens. Findings from such research has great potential to improve the quality of life of an ever aging population.

It has been a great honor to optimize these assays and establish a model which has such potential to generate some truly amazing discoveries. I look forward to seeing the project evolve as bright new graduate students push this project further than I could ever imagine.

## APPENDIX A

### SUPPORTING INFORMATION FOR CHAPTER 2

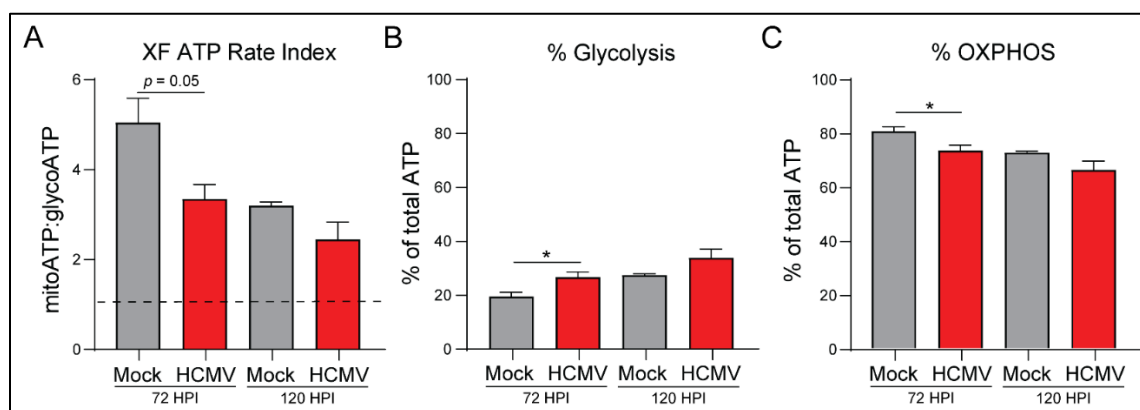


**Figure A1 HCMV infection of LN-18 cells increases glycolysis and oxidative phosphorylation ATP production.** OCR and PER were measured at 72 and 120 hours post infection using the Seahorse XFe24 Real-Time ATP Rate Kit. (A) XF ATP Rate Index, (B) % Glycolysis, and (C) % Oxidative Phosphorylation were derived from the measurements illustrated in Figure 2A. All samples were normalized to cell number. Graphs represent pooled data from three independent experiments. Mean  $\pm$  the SEM of at least 3 triplicates. \*,  $P < 0.05$ .

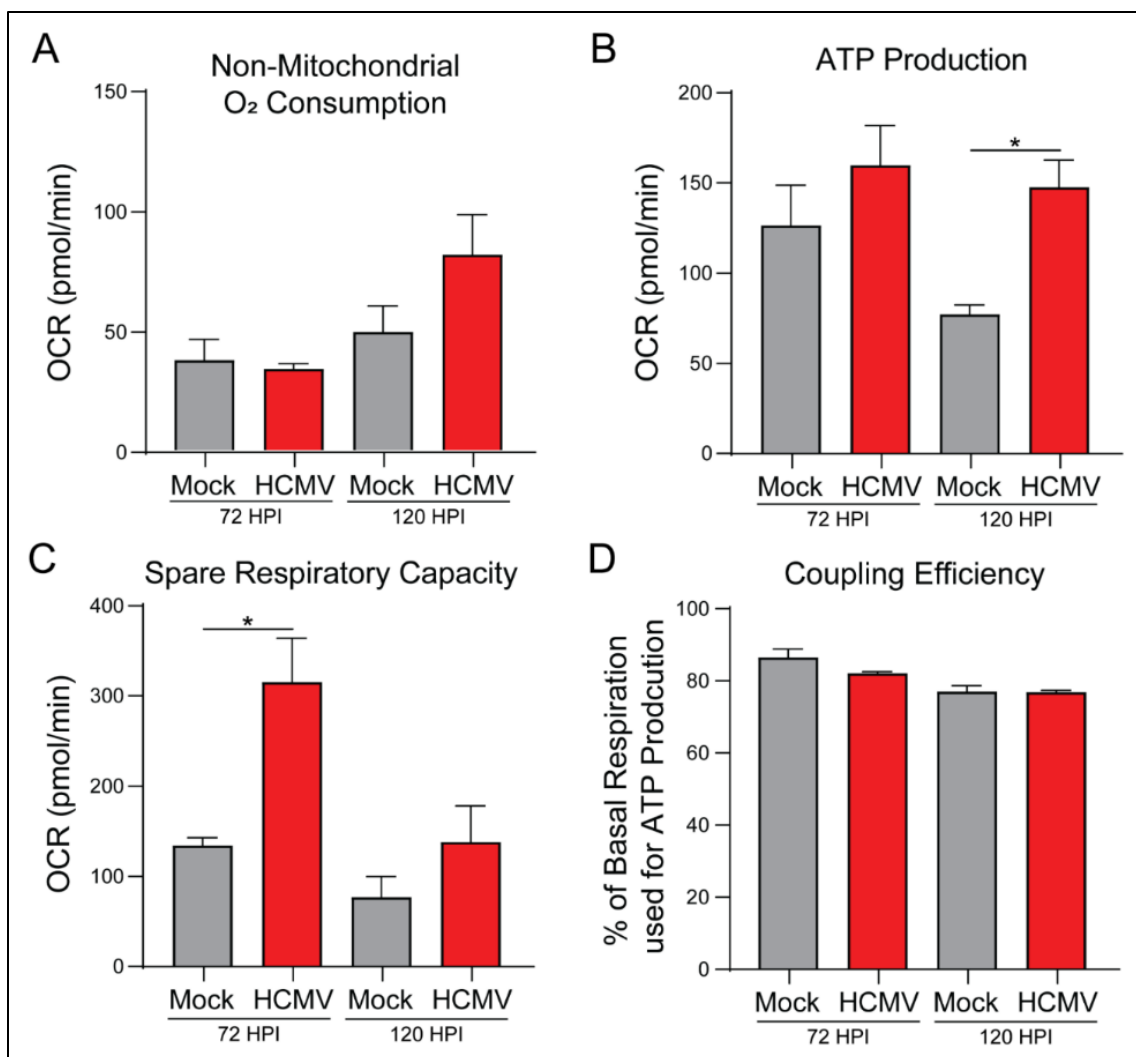


**Figure A2 HCMV infection increases oxidative phosphorylation. OCR was measured at 72 and 120 hours post infection using the Seahorse XFe24 MitoStress Kit. (A) Non-Mitochondrial Oxygen Consumption, (B) ATP Production, (C) Spare Respiratory Capacity, and (D) Coupling Efficiency were derived from these measurements. All samples were normalized to cell number. Graphs represent pooled data from three independent experiments. Mean  $\pm$  the SEM of at least 3 triplicates. \*,  $P < 0.05$ .**

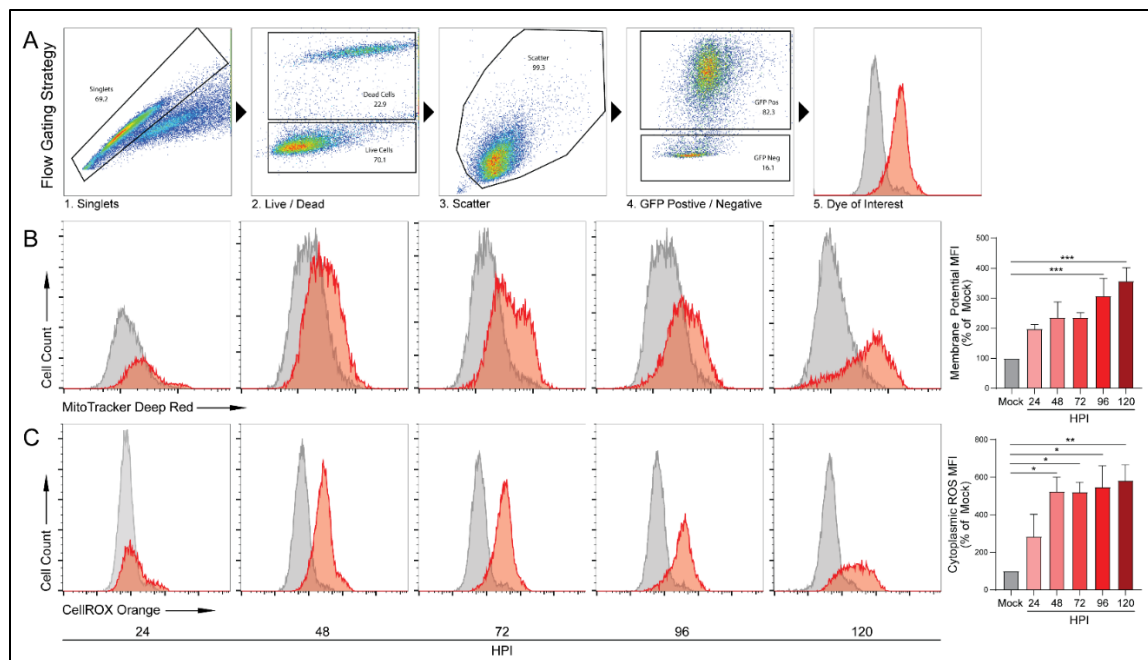


**Figure A3 Gating strategy for flow cytometric analysis of HCMV infected cells.** (A) Representative flow cytometry gating strategy. (B) Mitochondrial membrane potential was quantified using MitoTracker Deep Red, a carbocyanine dye that does not rely on oxidation to become fluorescent but is dependent on mitochondrial membrane potential for its sequestration. (C) Cytoplasmic ROS was labelled with CellROX Orange and analyzed by flow cytometric analysis. Graphs represent pooled data from three independent experiments. Mean  $\pm$  the SEM of at least 3 triplicates. \*,  $P < 0.05$ ; \*\*,  $P < 0.01$ .

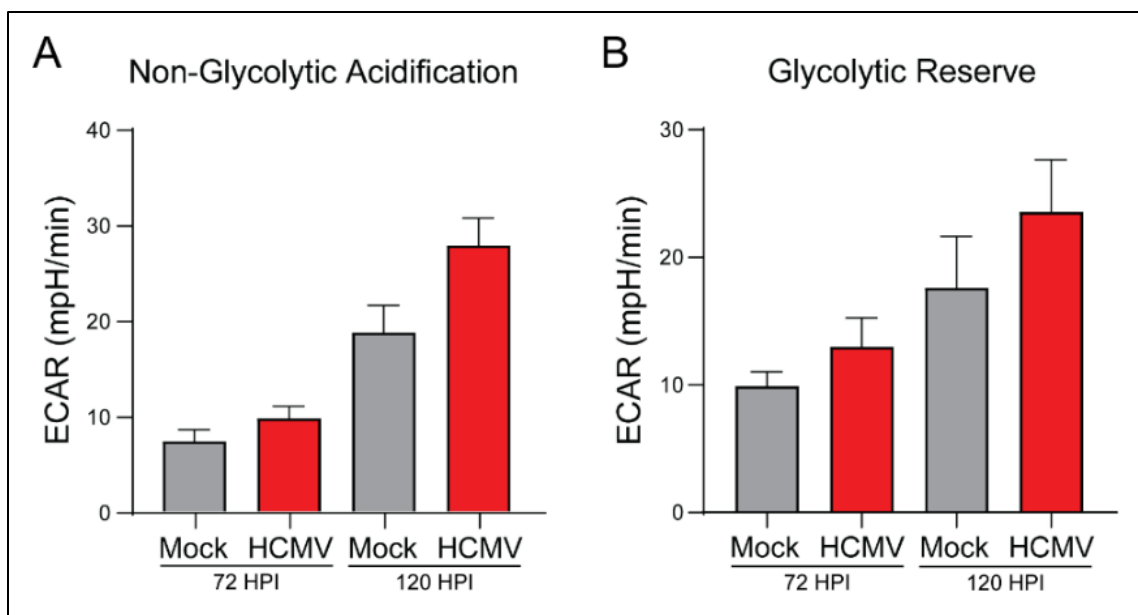


**Figure A4** The ECAR was measured at 72 and 120 hours post infection using the Seahorse XFe24 Glycolysis Stress Kit. (A) Non-glycolytic acidification and (B) Glycolytic Reserve were derived from these measurements. All samples were normalized to cell number. Graphs represent pooled data from three independent experiments. Mean  $\pm$  the SEM of at least 3 triplicates.

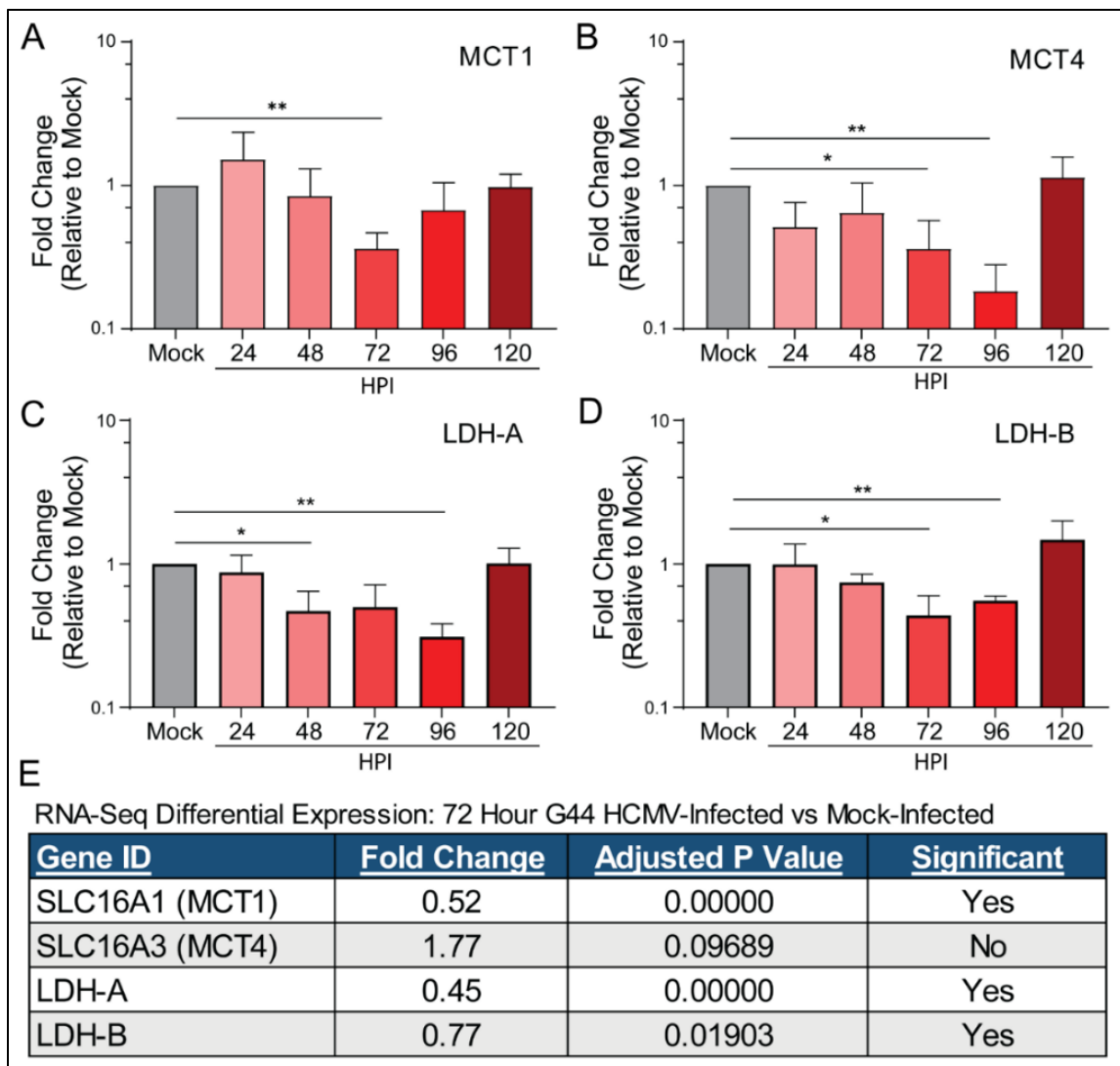


**Figure A5 HCMV infection downregulates expression of key lactate regulatory genes.** LN-18 cells were mock infected or HCMV infected and RNA was collected at the indicated timepoints following infection. RT-qPCR was conducted and fold changes relative to mock infected cells were calculated using the delta-delta Ct method. Following infection, cells displayed decreased gene expression for two key lactate transporters (A) MCT1 and (B) MCT4; and the two lactate dehydrogenase subunits (C) LDH-A (D) LDH-B. (*Figure legend continues on next page*)

(E) RNA-sequencing was conducted on G44 cells either mock-infected or 72 hours post HCMV infection. Graphs represent pooled data from three independent experiments. Mean  $\pm$  the SEM of at least 3 triplicates. \*,  $P < 0.05$ ; \*\*,  $P < 0.01$ .

## APPENDIX B

### SUPPORTING INFORMATION FOR CHAPTER 3

**Table B1:** Antibodies and Assays

REAGENT or RESOURCE	SOURCE	IDENTIFIER
<b>Antibodies</b>		
Rat monoclonal anti-Ki-67 (clone 11F6)	BioLegend	Cat# 151208; RRID:AB_2629748
Rabbit recombinant anti-TOMM20 (clone EPR15581-54)	abcam	Cat# ab186735; RRID:AB_2889972
Rabbit polyclonal anti-GBP2	Biorbyt	Cat# orb763167
Rat monoclonal anti-CD3 (clone 17a2)	BioLegend	Cat# 100234; RRID:AB_2562555
Rat monoclonal anti-CD31 (clone 390)	BioLegend	Cat# 102427; RRID:AB_2563982
Rat monoclonal anti-CD11b (clone M1/70)	BioLegend	Cat# 101259; RRID:AB_2566568
Rat monoclonal anti-CD206 (clone C068C2)	BioLegend	Cat# 141727; RRID:AB_2565822
Mouse monoclonal anti-CD45.2 (clone 104)	BioLegend	Cat# 109857; RRID:AB_2832376
Mouse monoclonal anti-NOS3	Santa Cruz Biotechnology	Cat# sc-376751; RRID:AB_2832203
Mouse monoclonal anti-GFAP (clone spm248)	Novus Biologicals	Cat# NBP2-34401AF532
Rabbit monoclonal anti-Tri-Methyl-Histone H3 (Lys27) (clone C36B11)	Cell Signaling Technology	Cat# 40724; RRID:AB_2799182
Mouse monoclonal anti-Claudin 5 (clone 4C3C2)	Thermo Fisher Scientific	Cat# 35-2500; RRID:AB_2533200
Rat monoclonal anti-Nos2 (clone W16030C)	BioLegend	Cat# 696802; RRID:AB_2687097
Rabbit recombinant anti-Hexokinase II (clone EPR20839)	Abcam	Cat# ab228819; RRID:AB_2868547
Rat monoclonal anti-CD86 (clone PO3.3)	Miltenyi Biotec	Cat# 130-105-135; RRID:AB_2660750
Rat monoclonal anti-ACSA-2 (clone IH3-18A3)	Miltenyi Biotec	Cat# 130-117-535; RRID:AB_2727978
Rabbit monoclonal anti-Glucose Transporter GLUT1 (clone EPR3915)	Abcam	Cat# ab195020; RRID:AB_2783877
Rabbit polyclonal anti-CD163/M130	Bioss	Cat# bs-2527R; RRID:AB_10856166
Mouse recombinant anti-S100A10	biotechne	Cat# FAB2377N
Mouse monoclonal anti-VDAC1/Porin (clone 20B12)	Abcam	Cat# ab14734; RRID:AB_443084
Mouse monoclonal anti-NG2 (clone G-9)	Santa Cruz Biotechnology	Cat# sc-166251; RRID:AB_2261269
Rabbit Anti-mouse IgG AP	Sigma	A1902
Goat Anti-mouse IgM AP	Southern Biotech	Cat# 1021-04
<b>Critical commercial assays</b>		
Micro BCA Protein Assay Kit	Thermo Fisher Scientific	Cat# 23235
Bio-Plex Pro Mouse Cytokine Grp I Panel 23-Plex	Bio-Rad	Cat #M60009RDPD
Bio-Plex Cell Lysis Kit	Bio-Rad	Cat #A1049201
Chromium Next GEM Single Cell Multiome ATAC + Gene Expression Reagent Bundle	10X Genomics	Cat #1000283
NextSeq 2000 P3 Reagents (100 Cycles)	Illumina	Cat #20040559
High Sensitivity DNA Kit	Agilent	Cat #5067-4626
Seahorse Mito Stress Test	Agilent	Cat #103015-100
RNeasy Mini Kit (250)	Qiagen	Cat# 74106

**Table B2:** Virus and Chemicals

<b>Virus strains</b>		
Murine Cytomegalovirus Smith Strain	ATCC	VR-1399
<b>Chemicals, peptides, and recombinant proteins</b>		
Collagenase II	Cell Signaling Technologies	CST #77336
Sodium Carbonate	Sigma	S2127
Sodium Bicarbonate	Sigma	S8875
Sodium Azide	Sigma	S2002
Magnesium chloride hexahydrate	Sigma	M2773
Diethanolamine	Sigma	D8885
IgG1, Kappa from murine myeloma	Sigma	M9269
IgM, Kappa from murine myeloma	Sigma	M3795
4-Nitrophenyl phosphate disodium salt hexahydrate	Sigma	N2765
Percoll PLUS	Cytiva	#17544502
DNase 1	Worthington Biochem	LS006333
Ketaset	Zoetis	
AnaSed LA	Vet One	13985-704-10
Bovine Serum Albumin	Sigma Aldrich	A9418-100G
iScript cDNA Synthesis Kit	Bio-Rad	Cat #1708891
SsoAdvanced Universal SYBR Green Supermix	Bio-Rad	Cat #1725271
Live/Dead Fixable Yellow dead cell stain	Thermo Fisher Scientific	L34959
Brilliant Stain Buffer Plus	BD Biosciences	Cat# 566385
eBioscience Fixation/Permeabilization Concentrate	Invitrogen	Cat# 00-5123-43
eBioscience Fixation/Permeabilization Diluent	Invitrogen	Cat# 00-5223-56
eBioscience Permeabilization Buffer (10X)	Invitrogen	Cat# 00-8333-56
Peroxiguard Disinfectant	Lighthouse Life Sciences	
UltraComp eBeads Plus Compensation Beads	Invitrogen	Cat# 01-3333-42
Seahorse XF DMEM medium, pH 7.4, 500 mL	Agilent	103575-100
DMEM, high glucose	Thermo	11965092
Fetal Bovine Serum Premium Select	R&D Systems	S11550
Tween-20	Fisher Scientific	BP337-500
Certified Molecular Biology Agarose	Bio-Rad	Cat #161-3100
5x DNA Loading Buffer Blue	Meridian Bioscience	Cat #BIO-37045
SYBR™ Safe DNA Gel Stain	Thermo Fisher Scientific	Cat# S33102
ACK Lysing Buffer	Thermo Fisher Scientific	Cat# A1049201
UltraPure™ 0.5M EDTA, pH 8.0	Thermo Fisher Scientific	Cat# 15575020
SYTOX™ Blue Nucleic Acid Stain - 5 mM Solution in DMSO	Thermo Fisher Scientific	S11348
MitoTracker™ Red FM Dye, for flow cytometry	Thermo Fisher Scientific	M46751
MitoSOX™ Mitochondrial Superoxide Indicators, for live-cell imaging	Thermo Fisher Scientific	M36008
Nonyl Acridine Orange (Acridine Orange 10-Nonyl Bromide)	Thermo Fisher Scientific	A1372
GlutaMAX Supplement	Thermo Fisher Scientific	35050061
16% Formaldehyde Solution Methanol-Free	Thermo Fisher Scientific	Cat# 28906
Methylene Blue (Certified Biological Stain), Fisher Chemical™	Fisher Scientific	M291-25

**Table B3:** Organisms, Software, Other

<b>Experimental models: Cell lines</b>		
M2-10B4	ATCC	CRL-1972
<b>Experimental models: Organisms/strains</b>		
Mouse: BALB/cAnNCrl	Charles River	Oder # 028
<b>Oligonucleotides</b>		
Primer: m36B4 Forward 5'-CGACCTGGAAGTCCAACACTAC-3'	Griessler et al. (2017)	
Primer: m36B4 Reverse 5'-ATCTGCTGCATCTGCTTG-3'	Griessler et al. (2017)	
Primer: mUL123 Forward 5'-TCAGCCATCAACTCTGCTACCAAC-3'	Tang-Feldman et al. (2006)	
Primer: mUL123 Reverse 5'-ATCTGAAACAGCCGTATATCATCTTG-3'	Tang-Feldman et al. (2006)	
<b>Software and algorithms</b>		
Gen5 v3.11	Agilent	
Wave v2.6.1.53	Agilent	
ANY-maze v7.0	ANY-maze	
CFX Maestro v4.1.2433.1219	Bio-Rad	
Bioplex Manager v6.1	Bio-Rad	
SpectroFlo v3.0	Cytek	
Prism 9.4.1	GraphPad	
Biorender	Biorender.com	
Cell Ranger ARC v2.0.0	10X Genomics	
Loupe Cell Browser	10X Genomics	
FCS Express 7 Research Edition v7.14.0020	De Novo Software	
FACSDiva v9.0	BD Biosciences	
<b>Other</b>		
gentleMACS C-tube	Miltenyi Biotec	130096334
gentleMACS Dissociator	Miltenyi Biotec	130-093-235
Passive Avoidance Chamber and Shock Control	Maze Engineers	
Hot Plate	Maze Engineers	
Control Company 3389 Variable Speed Peristaltic Pump	Mitchell Instrument Co	CNC-3389
Cytek Aurora	Cytek	
Illumina NextSeq 2000	Illumina	
2100 Bioanalyzer	Agilent	
Synergy HTX	Agilent	BTS1LF7A
Seahorse XFe24 Analyzer	Agilent	
405TS Microplate Washer	Agilent	Cat# 405TS
Bio-Plex 200 System with HTF	Bio-Rad	#171-000205
Bio-Plex Pro™ Wash Station	Bio-Rad	#30-034376
CFX Connect Real-Time PCR Detection System	Bio-Rad	Cat# 1855201
iMark Microplate reader	Bio-Rad	Cat #1681135
LSRFortessa Flow Cytometer	BD Biosciences	

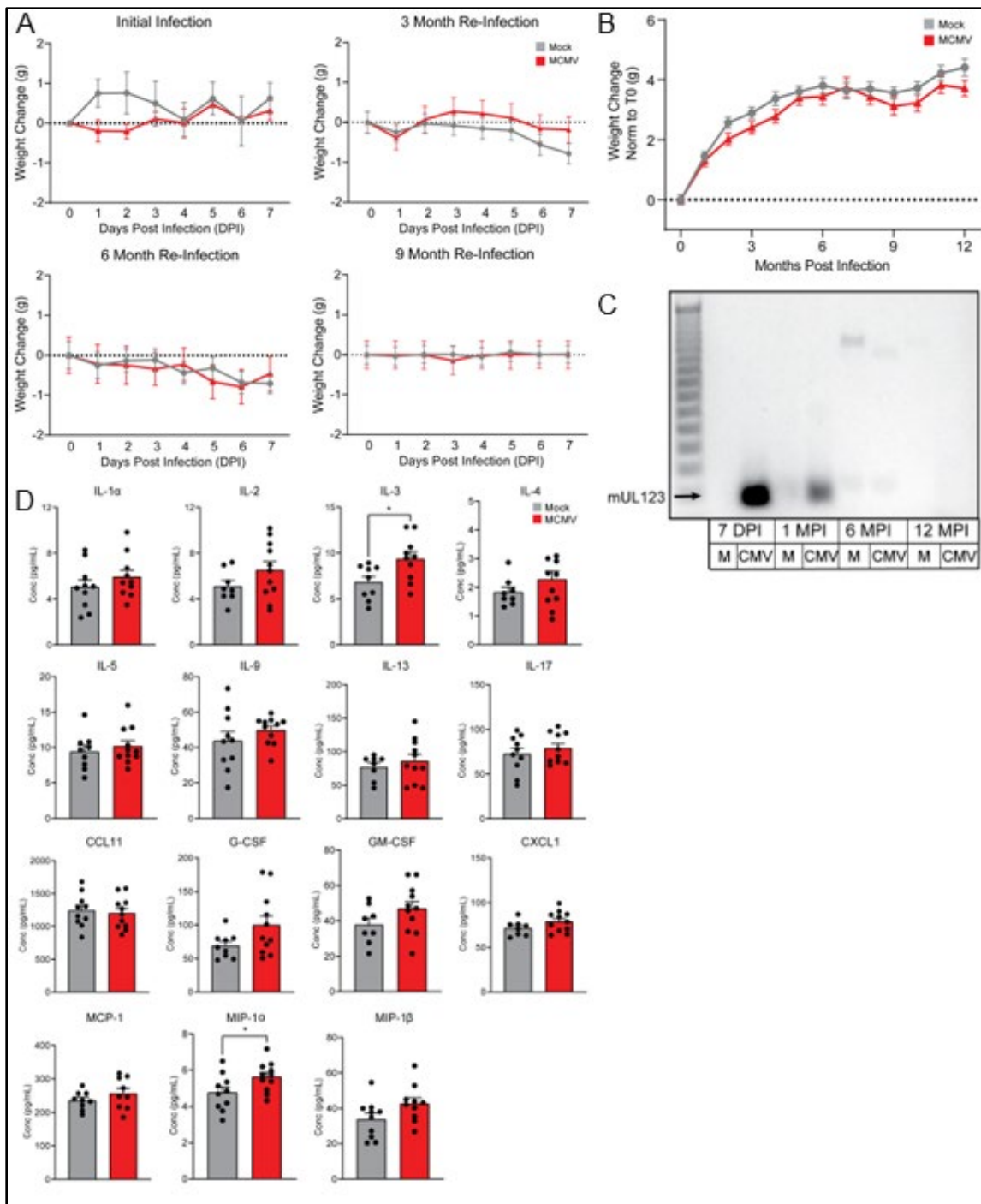


**Figure B1.1 Intermittent MCMV infection exhibits delayed inflammatory cytokine expression in the brain.** (A) Weight change in mock- (grey) and MCMV-infected (red) animals through 7 DPI from initial infection through the 9 month infection. (*Figure legend continues on next page*)

(B) Monthly weight of animals from initial infection through 12 MPI. (C) Agarose gel displaying UL123 qRT-PCR products from salivary glands at 7 DPI, 1 MPI, 6 MPI, and 12 MPI. Levels of IL-1 $\alpha$ , IL-2, IL-3, IL-4, IL-5, IL-9, IL-13, IL-17, CCL11, G-CSF, GM-CSF, CXCL1, MCP-1, MIP-1 $\alpha$ , and MIP-1 $\beta$  from (D) plasma at 7 DPI. Graphs represent pooled data from at least three individual animals. Mean  $\pm$  the SEM. \*,  $p < 0.05$ ; \*\*,  $p < 0.01$ ; \*\*\*,  $p < 0.001$ .

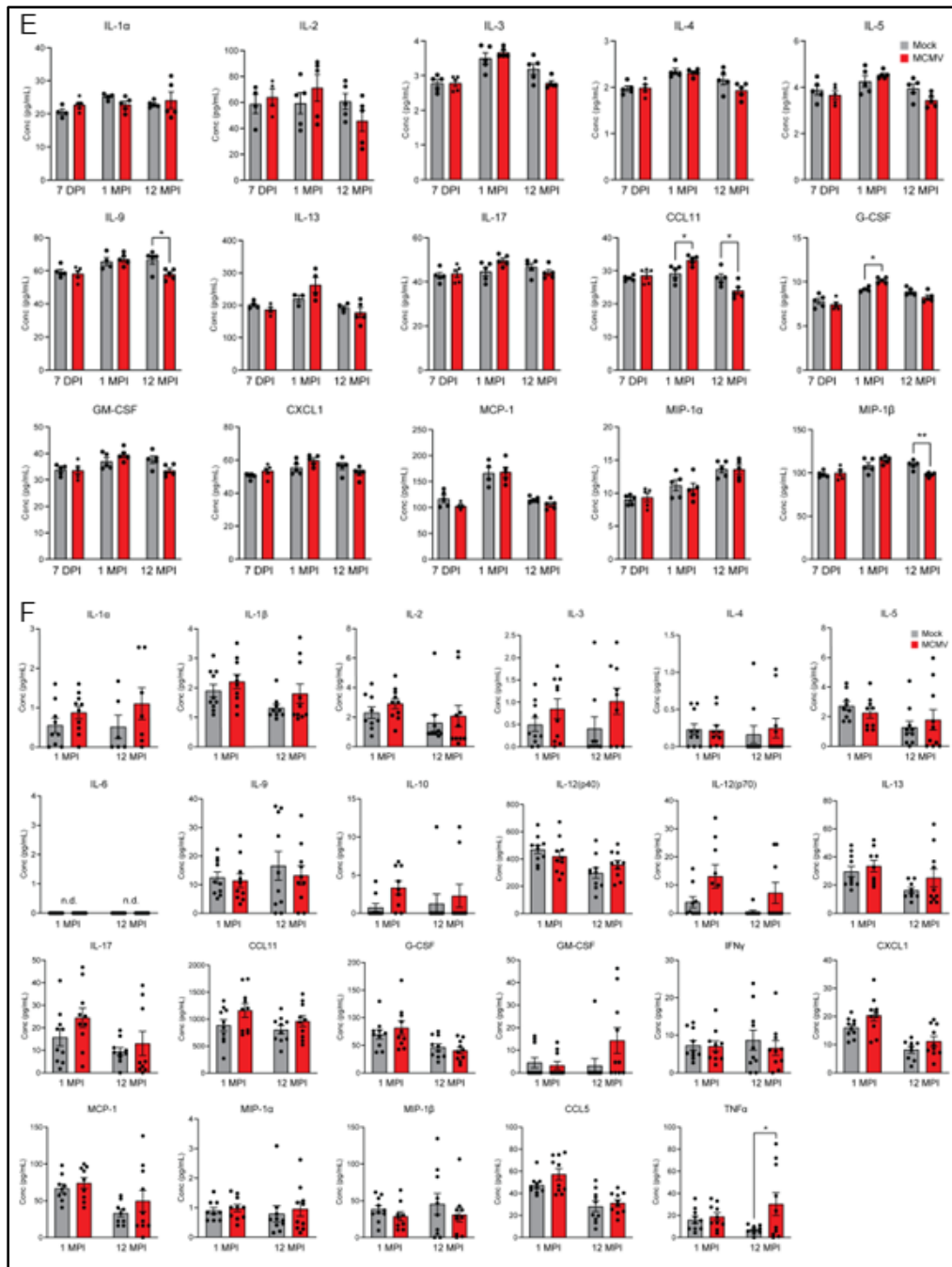


**Figure B1.2 Intermittent MCMV infection exhibits delayed inflammatory cytokine expression in the brain.** Levels of IL-1 $\alpha$ , IL-2, IL-3, IL-4, IL-5, IL-9, IL-13, IL-17, CCL11, G-CSF, GM-CSF, CXCL1, MCP-1, MIP-1 $\alpha$ , and MIP-1 $\beta$  from (E) brain homogenate at 7 DPI, 1 MPI, and 12 MPI as measured by Bio-Plex. (Figure legend continues on next page)

Levels of IL-1 $\alpha$ , IL-1 $\beta$ , IL-2, IL-3, IL-4, IL-5, IL-6, IL-9, IL-10, IL-12p40, IL-12p70, IL-13, IL-17, CCL11, G-CSF, GM-CSF, IFN $\gamma$ , CXCL1, MCP-1, MIP-1 $\alpha$ , MIP-1 $\beta$ , CCL5, and TNF $\alpha$  in (F) plasma at 1 and 12 MPI. Graphs represent pooled data from at least three individual animals. Mean  $\pm$  the SEM. \*,  $p < 0.05$ ; \*\*,  $p < 0.01$ ; \*\*\*,  $p < 0.001$ .

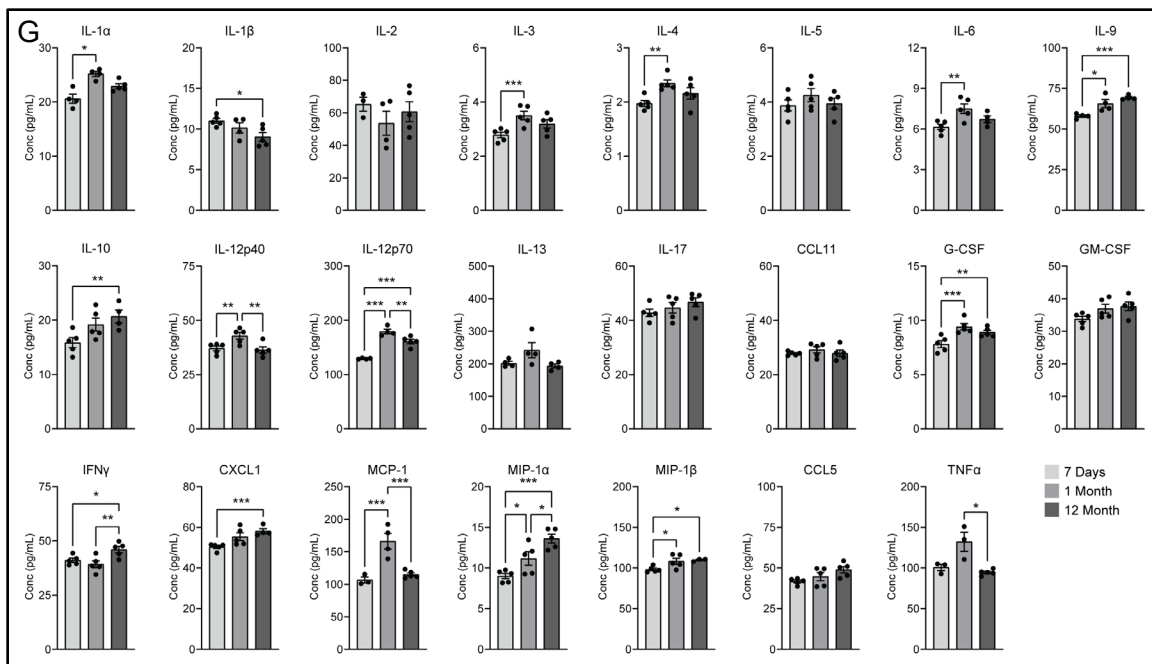


**Figure B1.3 Intermittent MCMV infection exhibits delayed inflammatory cytokine expression in the brain.** Levels of IL-1 $\alpha$ , IL-1 $\beta$ , IL-2, IL-3, IL-4, IL-5, IL-6, IL-9, IL-10, IL-12p40, IL-12p70, IL-13, IL-17, CCL11, G-CSF, GM-CSF, IFN $\gamma$ , CXCL1, MCP-1, MIP-1 $\alpha$ , MIP-1 $\beta$ , CCL5, and TNF $\alpha$  in (G) brain homogenate in mock infected animals at 7 DPI, 1 MPI, and 12 MPI. Graphs represent pooled data from at least three individual animals. Mean  $\pm$  the SEM. \*,  $p < 0.05$ ; \*\*,  $p < 0.01$ ; \*\*\*,  $p < 0.001$ .

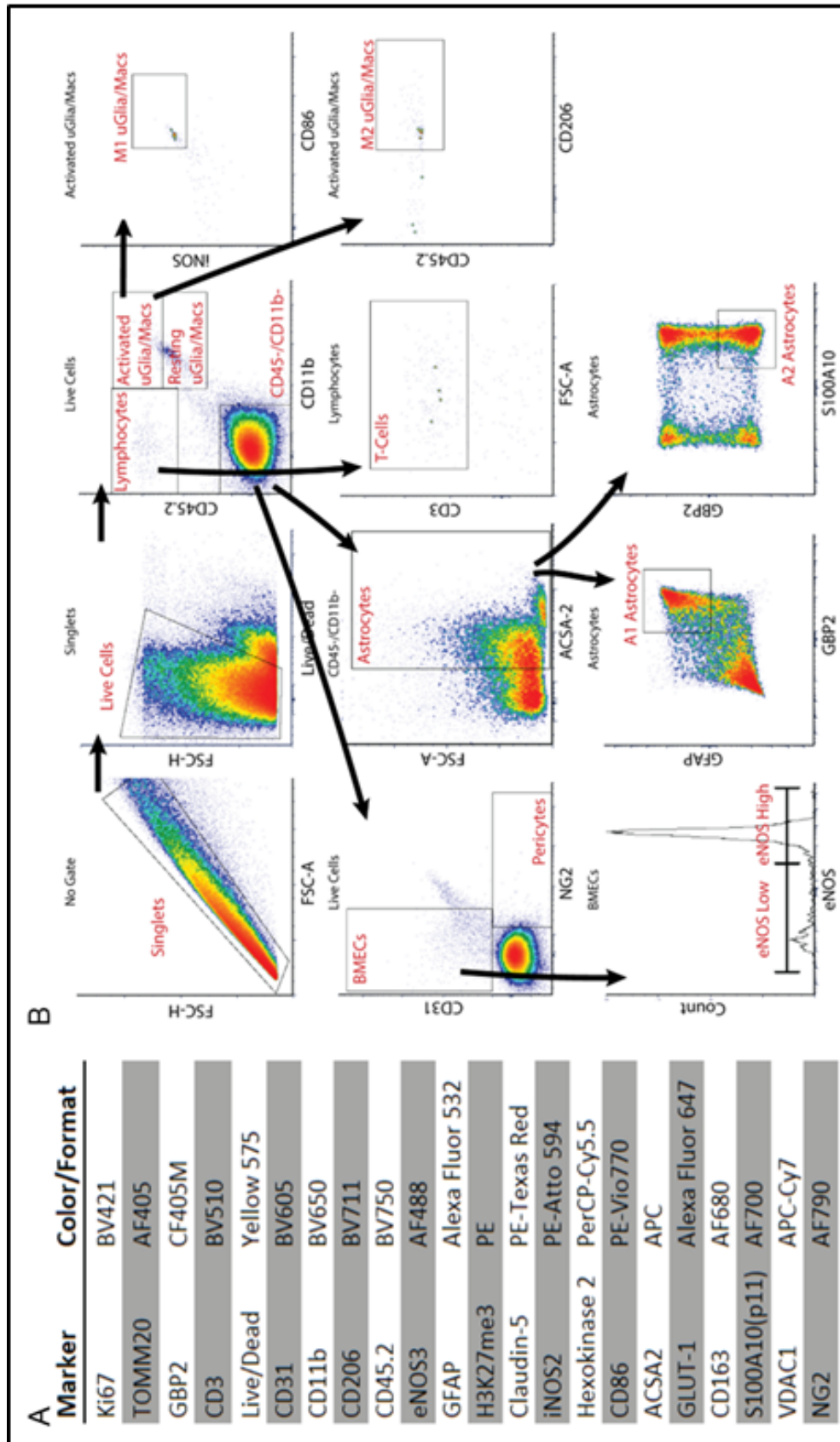


**Figure B2:** Neuro flow cytometry (A) panel and (B) gating strategy.

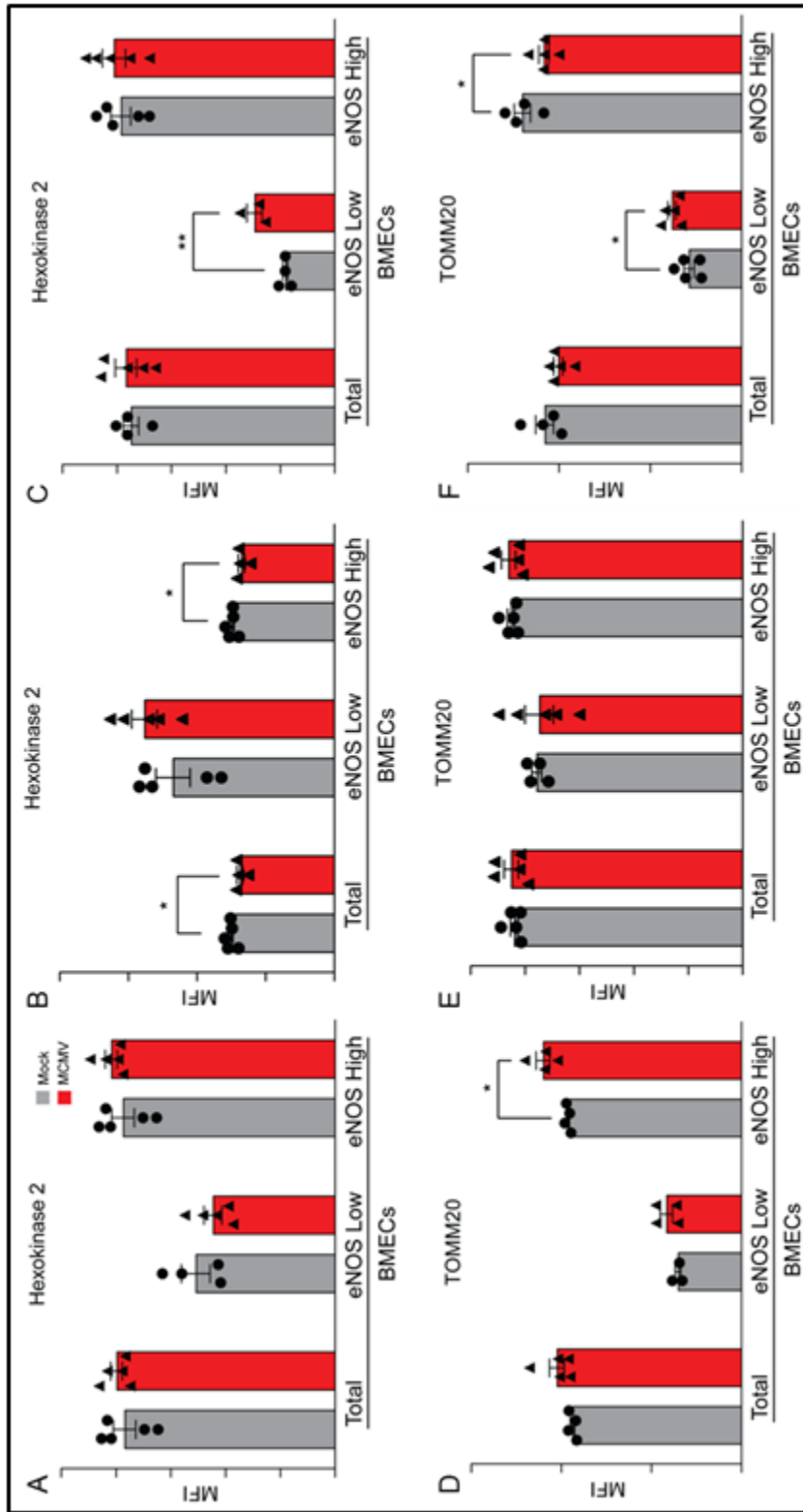


**Figure B3 Blood brain barrier metabolic pathways are rewired with increased MCMV exposure.** Flow cytometry was used to examine expression of Hexokinase 2 in populations of BMECs at (A) 7 DPI, (B) 1 MPI, and (C) 12 MPI. Expression of TOMM20 in populations of BMECs at (D) 7 DPI, (E) 1 MPI, and (F) 12 MPI. Graphs represent pooled data from at least three individual animals. Mean  $\pm$  the SEM. \*,  $p < 0.05$ ; \*\*,  $p < 0.01$ ; \*\*\*,  $p < 0.001$ .

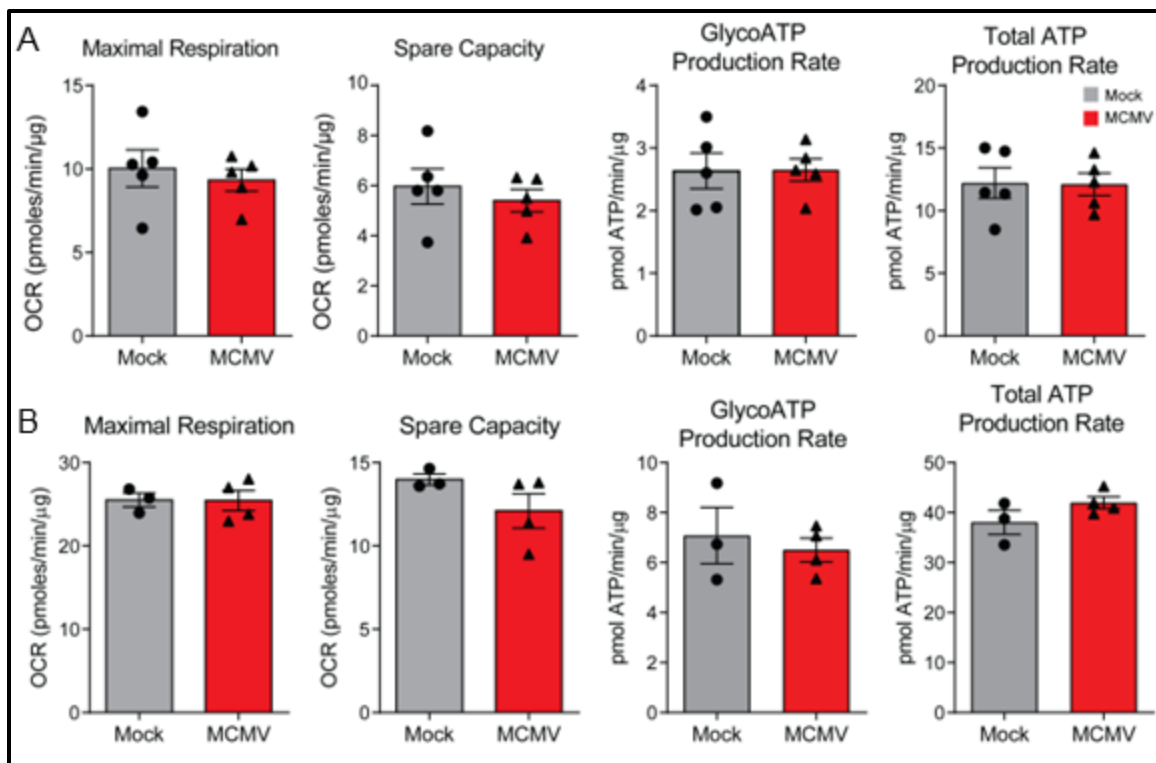


**Figure B4** Hallmarks of mitochondrial dysfunction and oxidative stress are elevated in BMECs intermittently exposed to MCMV. Maximal Respiration, Spare Respiratory Capacity, GlycoATP Production Rate, and Total ATP Production Rate were derived from the (A) 1 MPI and (B) 12 MPI measurements. Graphs represent pooled data from at least three individual animals. Mean  $\pm$  the SEM.

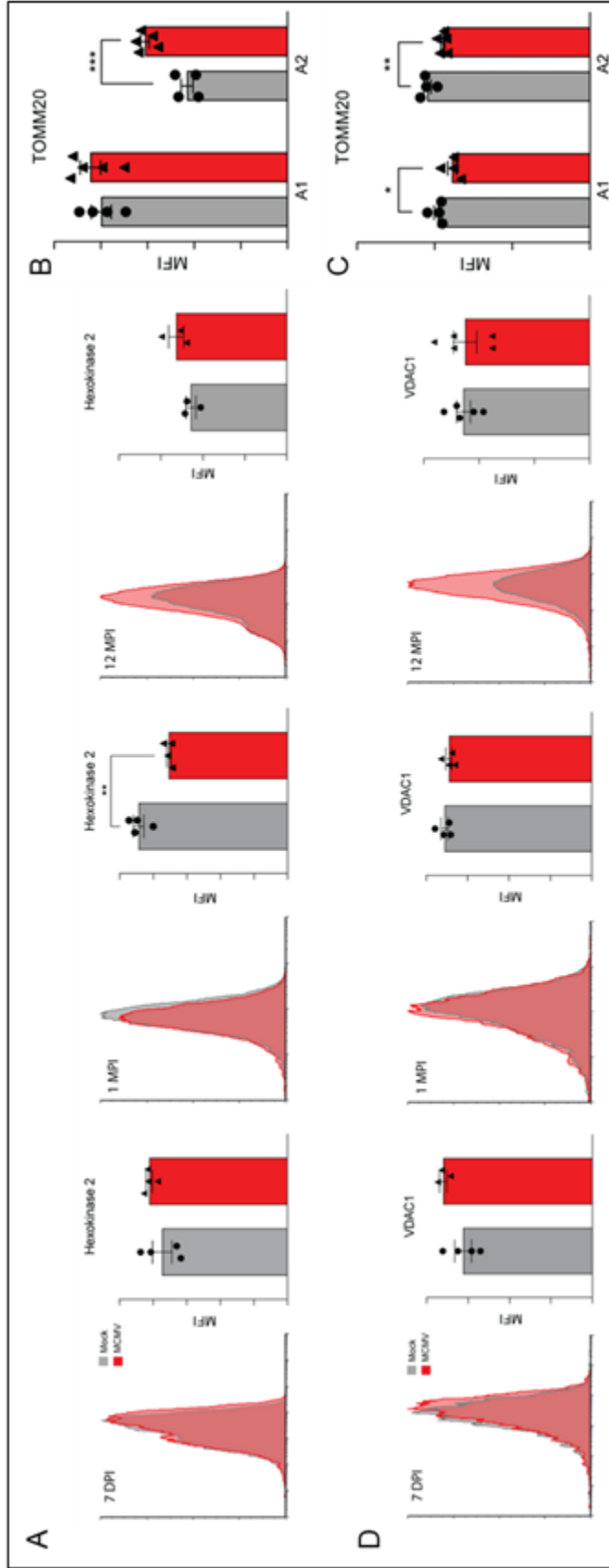


**Figure B5: MCMV infection metabolically rewires astrocytes as a function of age.** Flow cytometry expression of (A) Hexokinase 2 in astrocytes at 7 DPI, 1 MPI and 12 MPI. TOMM20 expression in A1 and A2 astrocytes at (B) 7 DPI and (C) 12 MPI. (D) VDAC1 expression in astrocytes at 7 DPI, 1 MPI, and 12 MPI. Graphs represent pooled data from at least three individual animals. Mean  $\pm$  the SEM. \*,  $p < 0.05$ ; \*\*,  $p < 0.01$ ; \*\*\*,  $p < 0.001$ .

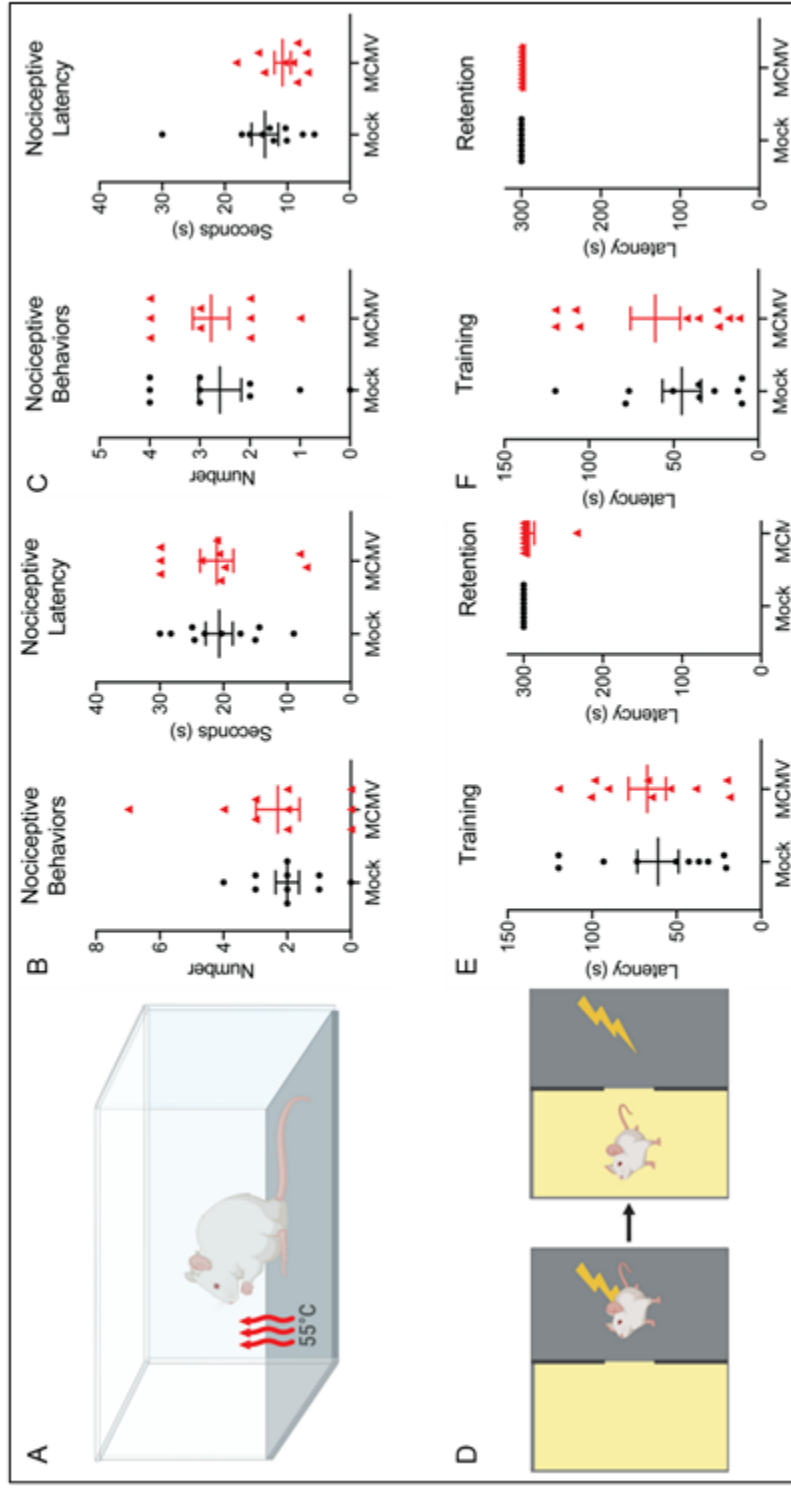


**Figure B6: Cognition is impaired with intermittent MCMV infection.** (A) Cartoon of the hot plate assay. Quantification of the number and latency to produce nociceptive behaviors in the hot plate assay at (B) 1 MPI and (C) 12 MPI. (D) Cartoon of the passive avoidance foot shock assay. Quantification of latency to enter the dark, foot-shock chamber during training and 24-hour retention testing in (E) 1 MPI (F) 12 MPI animals. Graphs represent pooled data from at least three individual animals. Mean  $\pm$  the SEM. \*,  $p < 0.05$ ; \*\*,  $p < 0.01$ ; \*\*\*,  $p < 0.001$ ; \*\*\*\*,  $p < 0.0001$ . Created with Biorender.com.

## APPENDIX C

### ESTABLISHING THE ADIPOSE STEM CELL IDENTITY: CHARACTERIZATION ASSAYS AND FUNCTIONAL PROPERTIES<sup>3</sup>

#### ***C1 Introduction***

Following their initial description by Zuk et al. in 2001, adipose stem cells (ASCs) rapidly gained interest as a potential therapeutic tool and became the topic of intense research [201]. In comparison to other mesenchymal stem cell (MSC) sources, the abundance, ease of both harvest and isolation, and proliferative abilities make ASCs ideal for research purposes. Adipose tissue, removed either by lipectomy or liposuction, can be subjected to enzymatic digestion and centrifugation to produce a cell pellet known as the stromal vascular fraction (SVF) [202]. This pellet contains numerous cell populations, including immune cells, endothelial cells, pericytes, and ASCs. Isolation of these ASCs can be accomplished by plating the SVF onto standard cell culture plastic and maintaining only the plastic adherent cells. Following this, the appropriate characterization of the isolated cells is essential. Both the International Federation for Adipose Therapeutics and Science (IFATS) and the International Society for Cellular

---

<sup>3</sup> As published: Harrison, M.A.A. et al. (2022) Chapter 3 - Establishing the adipose stem cell identity: Characterization assays and functional properties. L. Kokai, K. Marra, J.P. Rubin (Eds.) *Scientific Principles of Adipose Stem Cells* (pp. 23-56). Elsevier Academic Press. Doi: 10.1016/B978-0-12-819376-1.00002-0

Therapy (ISCT) have released positional statements regarding the minimum characterization requirements necessary for identifying multipotent mesenchymal stromal/stem cells [203, 204]. In addition to these characterization standards, assessment of the immunomodulatory abilities of isolated ASCs may provide valuable information prior to use in downstream applications. The aim of this chapter is to describe the characterization and functional assays needed to appropriately determine the identity of ASCs. Where possible, comparisons to other common sources of MSCs will be made. Finally, the impact of donor-to-donor variation, focused on factors such as age, body mass, and health status, in relation to ASC function will be discussed.

## ***C2 Physical Characterization***

### **Morphological Characterization**

ASCs are a heterogeneous population characterized by their ability to adhere to tissue culture plastic, readily proliferate in culture, form colonies, and differentiate into multiple lineages *in vitro* and *in vivo* [205, 206]. ASCs display a spindle-shaped morphology with a distinctly fibroblast-like appearance in passages lower than 10 (p10), very similar to the appearance of bone marrow-derived mesenchymal stem cells (BMSCs) (Figure C1). This morphology and the ability to adhere to plastic are both retained following cryopreservation [207, 208]. Following long-term culture, greater than p15, ASC morphology changes into large trident shaped senescent cells. Senescence can be verified by employing a staining assay in which a chromogenic substrate 5-bromo-4-chloro-3-indolyl-beta-

d-galactopyranoside (X-gal) is incubated with cells to determine the presence of  $\beta$ -galactosidase [209-211]. Dmitrieva *et al.* demonstrated that senescence in BMSCs could be detected as early as p3, whereas ASCs did not show any evidence of cellular senescence prior to p6 [212]. These results were further corroborated by numerous studies indicating that ASCs exhibit decreased senescent features in comparison to BMSCs [213-215]. However, it has been demonstrated that the percentage of senescent cells in ASC cultures does increase significantly following extended passaging [209]. Thus, although several studies have encouraged the use of long-term culture-expanded ASCs for clinical trials, a careful morphological assessment prior to their use is crucial.

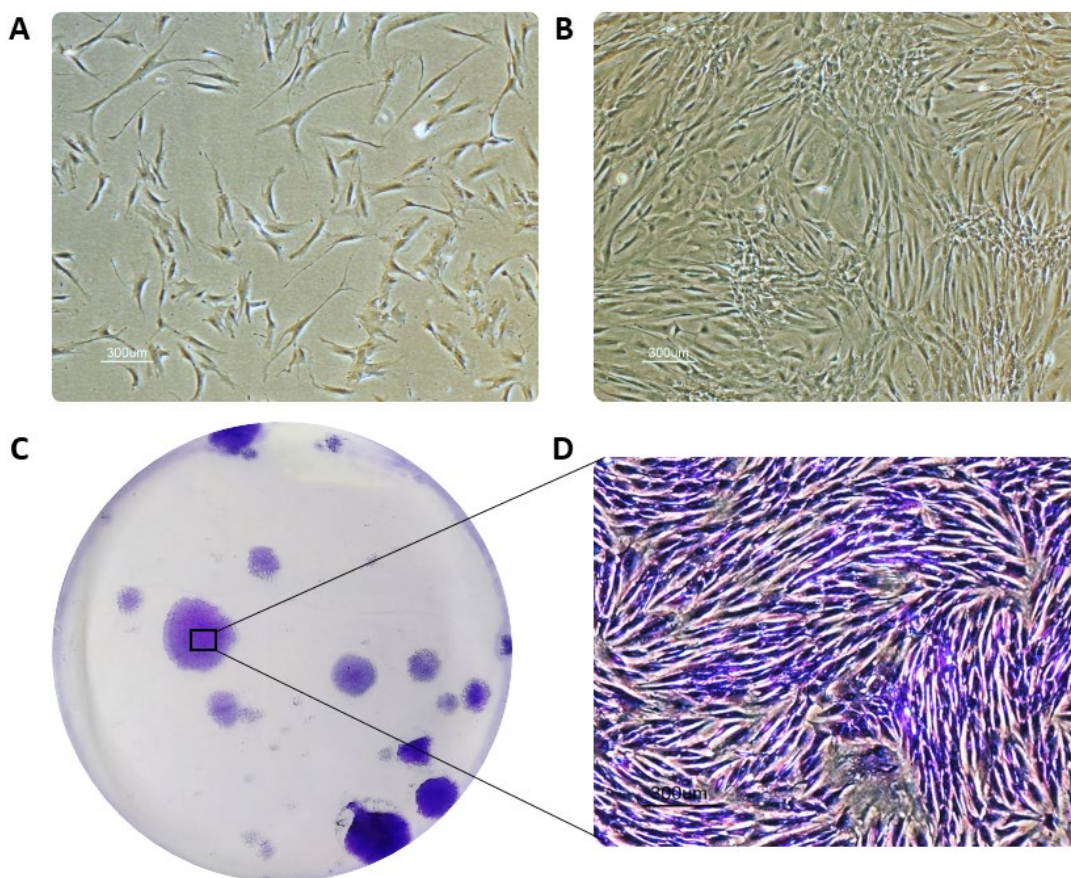


**Figure C1: ASC morphologic analysis and colony formation assay.** Bright field imaging of ASCs at low (A) and high (B) confluence using a 4x objective. Colony formation fibroblast assay plate following staining with crystal violet (C) and bright field image of the same staining using a 4x objective (D).

### Assessment of Proliferation

Human ASC proliferation is variable and primarily determined by passage number, donor characteristics such as age and body mass index (BMI), harvest site, surgical procedure, and culture conditions [216-218]. ASCs begin proliferating once they adhere to tissue culture plastic and can be assessed by Trypan Blue-assisted cell counting. In a study conducted by Di Battista *et al.*, the ability of ASCs to proliferate increases in early passages (p2-p3), decreases at p4 but then increases again at p6 [219]. Similar studies have demonstrated decreases in proliferation at p10 followed by significant decreases after p15 without any changes in the expression of tumor-related genes or the development of chromosomal abnormalities [220, 221]. Cryopreservation of ASCs has not been demonstrated to affect the rate of their proliferation nor their differentiation potential when compared with non-cryopreserved cells [222]. However, ASCs isolated from donors who are either older, have a high BMI, or both exhibit a decreased proliferation potential in comparison to young, lean donor-derived ASCs [223, 224].

A significant factor in the ability of ASCs to adhere and proliferate is the choice of culture medium. Studies have shown that the addition of growth factors (fibroblast growth factor (FGF), epidermal growth factor (EGF), platelet-derived growth factor (PDGF)), cytokines (interleukin-6, (IL-6)), and ascorbic acid to serum-supplemented media enhances their growth rate [225]. The source of serum is also a significant concern for the culture of ASCs. The risks involved in the use of fetal bovine serum (FBS), including the transmission of zoonotic microorganisms and induction of an immune response, which may result in the

rejection of transplanted cells [226]. Many translational studies are now considering the use of human platelet lysate (hPL) as a safe, effective substitute for FBS owing to its rich protein and growth factor complement and minimal risk of xenogenic immune reaction [225, 227, 228]. ASCs cultured in hPL-supplemented media have been shown to proliferate faster than those in FBS-supplemented media, thus making hPL ideal for large-scale expansion of ASCs [228].

ASC proliferation rate can also be significantly affected by the harvest site of adipose tissue and the surgical procedure used to collect it. ASCs isolated from the hip/thigh and abdomen using resection and tumescent liposuction displayed increased yield and proliferation rate in comparison to ASCs obtained by ultrasound-assisted liposuction [216]. Breast tissue-derived ASCs have exhibited very low cell yield, decreased proliferation, and impaired differentiation abilities in comparison to subcutaneous fat, which was likely due to the significant presence of glandular and connective tissue characteristic of the harvest site [216]. Finally, adipose tissue yields a greater number of stem cells and increased proliferation rate as compared to BMSCs [213].

#### Colony Forming Unit-Fibroblast Assay

Self-renewal is one of the primary characteristics of stem cells and can be readily assessed using the colony-forming unit-fibroblast assay (CFU-F). ASCs are plated on plastic cell culture dishes at a low density, and their clonal expansion is assessed following two weeks of culture. Crystal-violet staining can be used to identify and visualize colonies under a bright field microscope (Figure C1). The number of colonies of greater than 50 cells (2mm in diameter) is counted and

reported. Similar to the proliferation rate, the clonogenic potential of ASCs can be affected by donor characteristics as well as tissue harvest site. Frazier *et al.* have shown that ASCs isolated from lean donors (BMI <25) form significantly higher numbers of colonies than ASCs isolated from overweight (BMI 25-30) and obese donors (BMI >30) [217]. Likewise, ASCs isolated from subcutaneous abdominal adipose tissue have 50% higher clonogenic potential than those isolated from hip/thigh tissue [229, 230]. Compared with BMSCs, ASCs yield approximately four times more colonies per milliliter of harvested tissue sample, making them preferable for research purposes [218].

### Phenotypic Characterization

Phenotypic characterization is an essential part of defining the stem cell identity. It should be performed at different passages during *in vitro* expansion to ensure the maintenance of the stem cell identity. Flow cytometry is ideal for this characterization as most of the canonical markers for stem cells are cell surface cluster of differentiation (CD) proteins. Similar to BMSCs, ASCs express the classical mesenchymal stem cell markers and negative for endothelial and hematopoietic markers as well as the human leukocyte antigen (HLA)-DR. According to IFATS and ISCT, ASCs are distinct from BMSCs in their expression of fatty acid translocase marker CD36, and the absence of vascular cell adhesion molecule (VCAM-1/CD106) [204, 231, 232]. Generally, both positive and negative selection markers are employed to ensure that the isolated cells are stem cells and that they are not contaminated with other cell types (Table C1).

### Positive Selection Markers

Human ASCs express the traditional mesenchymal stem cell surface markers including: CD29, CD34, CD44, CD73, CD90, CD105, CD146, and CD166. Although ASCs retain the classic mesenchymal characteristics at least up to p10, the expression of certain markers such as CD105 and CD166 can be decreased at early passages, particularly when the cells are committed toward particular lineages [231, 233]. Phenotypic characterization of ASCs isolated from young and old donors have demonstrated no significant differences [223]. However, ASCs obtained from obese donors exhibit a decrease in typical stemness markers as compared to those isolated from non-obese donors [234]. Moreover, cryopreserved ASCs did not elicit changes in cell surface marker expression when compared to non-cryopreserved cells [207].

### Negative Selection Markers

Ensuring that isolated ASCs are not contaminated with another cell type is critical. The SVF, from which ASCs are isolated, is rich in hematopoietic cells, endothelial cells, and immune cells [235]. Thus, the use of a wide array of surface markers is required to ensure purity. ASCs lack the expression of hematopoietic lineage markers, including CD11b, CD13, CD14, CD19, and CD45. They are also negative for the endothelial markers CD31 and HLA-DR [204]. In addition to these classical negative selection markers identified by ISCT, studies have shown that ASCs do not express CD163, CD200, CD271, or CD274, allowing them to be distinguished from chondrocytes and osteoblasts [236]. The same study suggested that CD163, a marker of monocytes and macrophages, could be used

to differentiate ASCs from other MSCs. Finally, negative selection using CD54 permits ASCs to be distinguished from fibroblasts, and the CD54<sup>-</sup> ASC population demonstrated increased osteogenic and adipogenic differentiation abilities [237].

Donor-to-donor variability, culture media, and growth factors have also been shown to impact the growth of distinct ASC subpopulations. These different ASC subpopulations, as characterized by their phenotypic expression patterns, may also possess varied functional characteristics. For instance, positive selection for CD105<sup>+</sup> ASCs resulted in a population of ASCs that displayed significantly greater osteogenic and chondrogenic differentiation potential than CD105<sup>-</sup> ASCs [238]. Nevertheless, CD105<sup>-</sup> ASCs demonstrated stronger immunomodulatory abilities than the CD105<sup>+</sup> population [239]. Additionally, populations of CD34<sup>+</sup> ASCs were shown to proliferate faster than CD34<sup>-</sup> ASCs, although the latter exhibited an increased ability to differentiate along several mesenchymal lineages [240]. Results such as these represent the potential for significant future research to identify and characterize optimal ASC populations for various *in vitro* and *in vivo* applications.

CD Markers	Descriptive Names	Cell Expression
<b>Positive Markers</b>		
CD29	Integrin beta-1 (ITGB1)	MSCs, Including ASCs
CD34	Hematopoietic progenitor cell antigen CD34	MSCs, Including ASCs
CD44	Homing cell adhesion molecule (HCAM)	MSCs, Including ASCs
CD73	5'-nucleotidase	MSCs, Including ASCs
CD90	Thy-1 GPI-anchored glycoprotein	MSCs, Including ASCs
CD105	Endoglin	MSCs, Including ASCs
CD146	Melanoma cell adhesion molecule (MCAM)	MSCs, Including ASCs
CD166	Activated leukocyte cell adhesion molecule (ALCAM)	MSCs, Including ASCs
<b>Negative Markers</b>		
CD3	T cell receptor T3 complex	Hematopoietic cells, endothelial cells, T cells
CD11b	Integrin alpha M (ITGAM)	Monocytes
CD14	Monocyte differentiation antigen CD14	Macrophages
CD19	B lymphocyte surface Antigen B4	B cells
CD31	Platelet endothelial cell adhesion molecule (PECAM1)	Hematopoietic cells, endothelial cells, platelets
CD45	Protein tyrosine phosphatase receptor type C (PTPRC)	Leukocytes
CD163	Scavenger receptor cysteine-rich type 2 protein	Monocyte, macrophage
CD200	OX-2 membrane glycoprotein	B cells, activated T cells, endothelial cells, neuronal cells
CD271	Low-affinity nerve growth factor receptor	BMSCs
HLA-DR	Human leukocyte antigen DR-isotype	Activated T cells

**Table C1:** Positive and Negative Selection Markers Used for the Characterization of ASCs

### ***C3 Multipotent Differentiation***

The ability to differentiate into a variety of lineage-specific cell types is a defining characteristic of stem cells. Like all MSCs, ASCs maintain the ability to differentiate into adipocytes, osteoblasts, and chondrocytes when exposed to specific differentiation factors and conditions. The ability of isolated ASCs to differentiate into these lineages is essential for proper characterization and demonstration of their stemness. ASCs have also been differentiated into cells of non-mesodermal lineage such as cardiomyocytes [241], endothelial cells [242], neurons [243], and hepatocytes [244]. However, when it comes to the characterization of ASCs, differentiation into the three primary mesenchymal cell types is sufficient according to ISCT and IFATS [203, 204].

#### **Adipogenesis**

*In vitro*, ASCs act as a reservoir of cells that can efficiently differentiate into mature adipocytes. Due to their location, many believe that ASCs have an increased adipogenic potential as compared to MSCs from other depots. Multiple studies have demonstrated that ASCs have an increased adipogenic potential and a corresponding decrease in osteogenic and chondrogenic potential [245, 246]. However, other studies have found no difference in the differentiation abilities between ASCs and BMSCs [247, 248]. These conflicting findings are potentially due to donor variability in age, BMI, and health status, as well as which adipose depot from which the cells were isolated. These factors all have an impact on the ability of ASCs to differentiate into adipocytes [223, 249-253].

### Mechanism(s) of Differentiation

Due to the obesity epidemic, significant research has been performed to elucidate the differentiation pathway(s) from ASCs to mature adipocytes *in vivo*. Still, it is a complicated pathway involving myriad genetic and biologic factors that are being updated constantly. Evidence has suggested that Wnt/ $\beta$ -Catenin, Hedgehog, and transforming growth factor- $\beta$  (TGF- $\beta$ )/mothers against decapentaplegic homolog 3 (Smad3) signaling pathways all serve to inhibit adipogenesis while extracellular matrix (ECM) stiffness plays a significant role in adipogenesis [254-256]. However, *in vitro* differentiation strategies often skip the early differentiation stages and focus instead on increasing late-stage differentiation regulators such as CAAT/enhancer-binding proteins (C/EBPs) and peroxisome proliferator-activated receptor gamma (PPAR $\gamma$ ) (Figure C2).

The adipogenic differentiation is a multi-step process progressing from ASCs to preadipocytes and finally ends with mature adipocytes. Correspondingly, the genetic differentiation pathway is divided between early, mid, and late stage genes. Understanding of the transition from ASC to pre-adipocyte is still in its infancy, but recent work suggests that transcriptional factors PPAR $\gamma$  and zinc-finger protein 423 (ZNF423) may play roles in this process [257]. While preadipocyte commitment is not well understood, maturation from preadipocyte to adipocyte has been well characterized. The C/EBP family of transcription factors are potent regulators of adipogenesis. In particular, C/EBP $\beta$  and C/EBP $\delta$  are significantly upregulated in the early stages of adipogenesis, during preadipocyte commitment, and maturation of adipocytes [258, 259]. The upregulation of C/EBP $\beta$

is largely mediated by glucocorticoid signaling and cAMP induction [259]. Binding of these transcription factors to their targeted promoters induces transcription of C/EBP $\alpha$  and PPAR $\gamma$ , widely considered the master regulators of adipocyte commitment and maturation [259, 260]. The activation of these regulators leads to a positive feedback loop which results in maturation and lipid accumulation. Work by Wu *et al.* has demonstrated that inhibition of PPAR $\gamma$  results in the loss of preadipocyte commitment, while the inhibition of C/EBP $\alpha$  still allows for lipid accumulation but also results in a loss of insulin sensitivity [261-263]. The effect of this is critical, as insulin receptor activation results in phosphatidylinositol 3-kinase (PI3K)/Akt signaling which is the driving force behind lipid accumulation in maturing adipocytes [259]. Canonical Akt signaling has been shown to play a crucial role in adipocyte formation through PPAR $\gamma$  signaling [264, 265]. Akt knockout mouse models have demonstrated an inhibition of adipogenesis through the loss of PPAR $\gamma$  expression. This is mediated through the activation of mammalian target of rapamycin complex 1 (mTORC1) signaling, which directly regulates adipocyte protein synthesis and morphology [266]. Akt signaling also inhibits the expression of forkhead box O1 (FOXO1) which is an inhibitor of PPAR $\gamma$  [267, 268]. Late-stage adipogenic genes are those required for the healthy maintenance of the mature adipocyte. They include adipokines such as adiponectin (APN) and leptin (LEP). Additionally, the expression of lipoprotein lipase (LPL), perilipin (PL1N), and fatty acid binding protein 4 (FABP4) are all critical for the production and maintenance of the classic lipid-filled vacuoles.

#### Differentiation Methodology

Strategies for adipogenic differentiation often vary in the composition and concentration of their additives, but the overall strategy remains the same [269-273]. Cells are cultured in adipogenic media consisting of standard stromal media supplemented with several additives. Dexamethasone, a corticosteroid, is used to stimulate transcription of C/EBP $\beta$ . 3-isobutyl-1-methylxanthine (IBMX), an inhibitor of cyclic adenosine monophosphate (cAMP) phosphodiesterase, is used to increase the cytosolic concentration of cAMP, resulting in the transcription of C/EBP $\delta$ . The activity of C/EBP $\beta$  and C/EBP $\delta$  result in the expression of PPAR $\gamma$  and C/EBP $\alpha$ , the master regulators of adipogenesis, which initiate differentiation. Periodic exposure to high levels of PPAR $\gamma$  agonists such as indomethacin or rosiglitazone serves to maintain differentiation and push the cells towards a mature state by reinforcing the PPAR $\gamma$  C/EBP $\alpha$  positive feedback loop. Finally, insulin is used to activate PI3K/Akt signaling, which encourages the storage of lipids and increases the size of neutral lipid vacuoles in the cytosol [269-273].

#### Confirmation of Adipogenesis

In 2D cultures, adipogenesis can be confirmed by microscopy, as neutral lipid droplets are readily visible in the cytosol of differentiated ASCs. However, appropriate staining of lipid droplets or lipid droplet associated proteins as well as analysis of gene expression patterns of the differentiated cells, is preferred to ensure appropriate differentiation.

The staining of neutral lipid droplets can be achieved by several methods; however, it should be noted that use of any fixative containing significant amounts of alcohols can disrupt the lipid droplets. Sudan Red and Oil Red O are diazo dyes

that preferentially stains lipids and can be used to visualize adipogenesis on a bright field microscope. Quantification of Sudan Red and Oil Red O staining is possible since isopropanol can be used to extract the stain from the cells. The absorbance of the solution can be read at 507nm and 584 nm, respectively [270, 271]. In order to make comparisons between ASC populations, it is necessary to normalize the absorbance values to the total protein content of a sample.

Fluorescent microscopy is another method by which ASC adipogenesis can be examined. Of the lipid droplet specific fluorescent probes, the most well-known is BODIPY. However, a wide range of fluorescent probes exist for visualizing lipid droplets in all different excitation and emission spectra as expertly reviewed by Fam *et al.* [274]. The availability of these probes in varying spectra allows for the use of nuclear and cytoskeletal counterstains to visualize overall cell morphology. As ASCs differentiate, they gain a rounded morphology with spiky projections. The neutral lipid droplets will appear in a rough circle surrounding the nucleus before slowly gaining size. As differentiation progresses, these droplets will begin to push all of the other organelles to the edges of the cell as they combine and continue to grow [275-277].

Assessment of adipocyte differentiation of ASCs can also be performed by examination of essential differentiation genes via qPCR. Upregulation of C/EBP $\alpha$  and PPAR $\gamma$  in comparison to undifferentiated ASCs is considered sufficient to illustrate initiation of the positive feedback loop that leads to the commitment of ASCs to adipocyte lineages. While C/EBP $\beta$  and C/EBP $\delta$  upregulation precede induction of C/EBP $\alpha$  and PPAR $\gamma$ , evidence of this alone does not demonstrate

adipocyte commitment. Finally, upregulation of late-stage genes such as APN, LPL, PL1N, or FABP4 demonstrate the development of mature adipocytes (See Figure C2).

### ASC Adipocyte Secretome

Historically, adipose tissue was believed to be merely an energy depot in the form of triglyceride packed vacuoles. Recent advances, however, have demonstrated that adipose tissue is a highly active endocrine organ whose interactions extend to many tissues, including the liver, brain, and vasculature. Collectively, the endocrine and paracrine effects of adipocytes are mediated by adipokines. The most common adipokines are involved in appetite suppression (LEP), glucose storage mediated by insulin sensitivity (APN), and insulin resistance (resistin) [278]. ASCs differentiated into adipocytes will secrete similar proteins; however, discrepancies may exist possibly attributable to differentiation protocol employed [279]. Of increasing interest are the immunomodulatory adipokines that are thought to play a major role in the inflammatory state of obese and diabetic patients [280]. Undifferentiated ASCs produce anti-inflammatory adipokines such as APN and IL-10 [279, 281]. However, upon differentiation towards adipocytes, there is an increase in the expression of pro-inflammatory genes and concurrent decrease of anti-inflammatory genes [282]. Adipocyte differentiation and adipokine secretion will also vary by adipose depot and donor obesity status [253, 283, 284]. Additionally, the expression of adipocyte pro-inflammatory cytokines IL-1 $\beta$ , IL-6, and IL-8 are elevated in obese patients [285, 286]. Age and gender of donor also play a role in the ability of ASCs to differentiate.

It has been demonstrated that ASCs isolated from a more aged donor have a reduced ability to differentiate into adipocytes [223, 252].

### Osteogenesis

BMSCs are typically the cells of choice for bone regeneration, with some studies suggesting that they exhibit superior osteogenic capacity than ASCs [287-290]. Recently, however, there has been an increased focus on ASC-based bone regeneration due to ASCs' ease of harvest, availability, reduced need for *in vitro* expansion, and proven osteogenic abilities [291]. Further characterization of the osteogenic potential of ASCs has revealed that higher donor BMI results in reduced differentiation [217, 292]. On the other hand, donor age and cryopreservation status have not been found to affect the osteogenic differentiation abilities of ASCs [293-295].

### Mechanism(s) of Differentiation

The capacity of ASCs to undergo osteogenic differentiation is well established; however, the underlying molecular mechanism(s) is not thoroughly understood. Several different signaling pathways have been found to play a role in the osteogenic differentiation of ASCs. These signaling pathways include extracellular signal-related kinase (ERK), Notch, TGF- $\beta$ , Wnt/ $\beta$ -Catenin, and phosphoinositide 3-kinase/Akt (PI3K/Akt) signaling Figure C2) [296-298].

Osteogenic differentiation of ASCs results in a significant upregulation of ERK signaling. A study by Liu *et al.* demonstrated that ASCs cultured in osteogenic media display increased ERK levels by day 7, peak at day 10, and decreased levels at day 14 [299]. Additionally, pharmacologic inhibition of ERK activation by

PD98059 reduced the osteogenic differentiation capabilities of ASCs [299, 300]. When these same ERK-inhibited ASCs were exposed to dexamethasone, they proceeded to differentiate into adipocytes [299, 300]. Similarly, active ERK signaling results in phosphorylation of PPAR $\gamma$ , which decreases its activity and produces an anti-adipogenic effect on ASCs [297]. Thus, ERK represents a key regulatory pathway for the commitment of ASCs to either the osteogenic or adipogenic lineage.

The Notch signaling pathway also plays a significant role in the osteogenic differentiation of ASCs. Inhibition of Notch signaling results in reduced osteogenic differentiation, while transfection of the downstream Notch-1 intracellular domain (ICD) restored their osteogenic potential [301].

Bone morphogenic proteins (BMP) and TGF- $\beta$  regulate osteogenic differentiation via the TGF- $\beta$  signaling pathway and result in upregulation and activation of downstream transcription factors including Smads, runt-related transcription factor-2 (RUNX2), and osterix (Osx) all of which are key promoters of osteogenesis [296, 302-304].

Activation of PI3K/Akt signaling pathway and Wnt/ $\beta$ -Catenin pathway have also been shown to upregulate osteogenesis in ASCs [305-307]. Wnt5a specifically promotes osteogenesis by activating the Wnt/ $\beta$ -Catenin pathway and suppressing the activation of PPAR $\gamma$  [304].

Of particular interest is the contradictory role of nuclear factor kappa-light chain-enhancer of activated B cells (NF- $\kappa$ B). Wang *et al.* reported that the inhibition of prostaglandin G/H synthase 1 (PTGS1) caused suppression of NF- $\kappa$ B signaling,

resulting in enhanced differentiation [308]. However, Cho *et al.* demonstrated that TNF- $\alpha$  treatment of ASCs during the early stages of osteogenic differentiation enhanced osteogenic differentiation of ASCs via the upregulation of NF- $\kappa$ B. This effect was further validated by direct inhibition of NF- $\kappa$ B, which resulted in decreased osteogenesis [309]. In contrast, NF- $\kappa$ B activation has been shown to be an inhibitor of osteogenic differentiation in BMSCs [310-313].

The coordinated regulatory effects of the aforementioned signaling pathways lead to the activation of pro-osteogenic transcription factors RUNX2 and Osx that transform ASCs into osteoblasts. RUNX2 is one of the earlier markers of osteogenic differentiation and promotes the formation of osteoblast-specific ECM by regulating collagen I and osteopontin (OPN) expression [314, 315]. Collagen I represents the principle structural protein of bone ECM [299, 316]. Osx, a later marker of osteogenic differentiation, is a zinc finger transcription factor that regulates several other key osteogenic genes such as osteocalcin (OCN), osteonectin (ON), and bone sialoprotein (BSP) [292, 315]. OCN, ON, and BSP are involved in the regulation of osteoclast activity, binding of collagen, and the calcification of the ECM [299, 316].

#### Differentiation Method

Differentiation of ASCs begins with the formation of osteoblast precursor cells, which later mature to form osteoblasts capable of producing and depositing minerals in the ECM [314]. Thus far, ASCs have been encouraged to undergo osteogenic differentiation *in vitro* using differentiation media, electromagnetic stimulation [317], and mechanical stimulation [318]. While the mechanisms behind

electromagnetic and mechanical stimulation have not been fully elucidated, osteogenic differentiation media is well-established and is the method of choice for the characterization of ASCs.

Osteogenic differentiation media is primarily composed of standard stromal media supplemented with dexamethasone, ascorbic acid 2-phosphate, and  $\beta$ -glycerophosphate [304, 314, 315, 319-321]. Dexamethasone, a glucocorticoid, promotes osteogenic differentiation by increasing the transcription of four and a half LIM domains protein 2 (FHL2), which then binds to  $\beta$ -Catenin, translocates to the nucleus and initiates transcription of RUNX2 [322]. Ascorbic acid 2-phosphate serves as a co-factor for the hydroxylation of proline and lysine molecules in collagens and results in the upregulation of pro-collagen, alkaline phosphatase (ALP), and OCN [272, 323]. Finally,  $\beta$ -glycerophosphate aids in the synthesis of hydroxyapatite by providing inorganic phosphate molecules [324]. The activation of these signaling pathways and the synthesis of hydroxyapatite lead to the osteogenic differentiation of ASCs and the deposition of calcium in the ECM.

#### Confirmation of Osteogenesis

ASC osteogenic differentiation *in vitro* is typically confirmed by assessment of ALP activity and examination of calcium deposition. This evidence is then further reinforced by gene expression profiling of the cells and analysis of secreted factors.

ALP is an enzyme that is used to detect early stages of osteogenesis. ALP expression is upregulated in osteoblasts in comparison to ASCs [314]. Staining of ALP can be accomplished with nitro blue tetrazolium/5-bromo-4-chloro-3-indolyl

phosphate (NBT/BCIP) that can then be viewed on a bright-field microscope [299, 303, 306, 308, 317, 319]. For a quantifiable measurement of ALP, its activity can be examined following cell lysis. The lysate is mixed with p-nitrophenyl phosphate substrate solution and incubated. The reaction is stopped using a sodium hydroxide solution, and the absorbance of the solution can be measured at 405 nm for quantification of ALP [299, 317, 325, 326].

Extracellular calcium deposition is a defining characteristic of terminally differentiated osteoblasts and can be stained using alizarin red [292, 299, 317, 319, 327-329]. Calcium deposits are then visualized using a bright field microscope. For the purposes of quantification, alizarin red can be extracted via incubation with cetylpyridinium chloride or acetic acid, and its absorbance can be measured at 584 nm and 405 nm, respectively [292, 303, 306, 319, 327].

Gene expression changes can also be used to verify the osteogenic differentiation of ASCs using RT-qPCR (See Figure C2). Commonly upregulated genes include RUNX2, *Osx*, collagen 1 $\alpha$ 1 (COL1 $\alpha$ 1), ALP, OCN, ON, and BSP. The differentiation process can be broken down into early, middle, and late stages based on gene expression patterns. Typical early gene markers include RUNX2 and ALP, whereas BSP and OCN are intermediate and late-stage osteogenic differentiation markers, respectively [314, 315, 317].

#### ASC Osteoblast Secretome

A limited number of studies have focused on the quantification of cytokines such as interleukins and growth factors secreted by osteogenically differentiated ASCs. Mussano *et al.* used bio-plex analysis to compare the levels of IL-6, IL8, IL-

10, IL-12, monocyte chemoattractant protein-1 (MCP-1), vascular endothelial growth factor 1 (VEGF-1), and hepatocyte growth factor (HGF) between undifferentiated and osteogenically differentiated ASCs. Analysis of conditioned media revealed decreased levels of all the aforementioned cytokines except for IL-8 [326, 330]. Transcriptome profiling of osteogenically differentiated ASCs using RNA-sequencing resulted in the upregulation of several transcripts, including vascular cell adhesion molecule-1 (VCAM-1), vascular endothelial growth factor-B (VEGF-B), insulin-like growth factor-1 (IGF-1), TNF- $\alpha$ , BMP-4, platelet factor-4, IL-16, and angiopoietin-1 [298]. Of particular interest, this same group found that two major classes of ECM remodeling enzymes, the matrix metalloproteinases (MMPs) 2, 15, 28, and the a disintegrin and metalloproteinase with thrombospondin motifs (ADAMTs) 8, 13, 15, and 18 were upregulated in osteogenically differentiated ASCs. Further analysis of osteogenically differentiated ASC media based on the current transcriptomic findings would provide greater insight into the composition of the osteogenic ASC secretome and could provide valuable insight into their use for bone regeneration.

### Chondrogenesis

Due to the prevalence of joint injuries and diseases such as osteoarthritis where cartilage is degraded, there is great interest in the processes that control chondrogenesis. Comparisons have been made surrounding BMSCs and ASCs' ability to differentiate. A study by Mohammad-Ahmed *et al.* used donor-matched BMSC and ASCs and claimed that BMSCs possess superior chondrogenic differentiation potential [331]. These results were predicated on increased

aggrecan (ACAN) gene expression in BMSCs after 28 days of differentiation. However, Alcian Blue staining for the presence of glycosaminoglycans (GAGs) demonstrated few differences between the pellets at the same timepoint. Another study by Pagani *et al.* showed that ASCs produced superior chondrogenic differentiation abilities. However, when the same MSCs were differentiated in a pro-inflammatory environment, meant to mimic osteoarthritic conditions, the findings were reversed [332]. Research employing bisulfite sequence examination of the differences in methylation of CpG islands in important chondrogenic promotor regions found that there were no significant differences between BMSCs or ASCs [333]. Thus far, no studies have been conducted demonstrating differences in chondrogenic abilities of ASCs from high BMI donors; however, it has been shown that increased age in donor results in decreased chondrogenic ability [223]. Finally, cryopreservation of ASCs does not seem to affect the chondrogenic differentiation abilities of ASCs, though freezing media of 10% dimethyl-sulfoxide, 90% serum freezing media is preferred.

#### Mechanism(s) of Differentiation

The similarities between the osteogenic and chondrogenic differentiation often complicate the understanding of both, though there are a few notable exceptions (Figure C2). Canonical Wnt/ $\beta$ -catenin signaling, which is essential for osteogenesis, has been shown to repress chondrogenesis. Functional loss of  $\beta$ -catenin also rendered cells unable to differentiate into osteoblasts, instead the cells become chondrocytes [334]. The upregulation of ERK signaling is also important for osteogenesis. However, the pharmacologic inhibition of ERK signaling using

PD98059 was shown to promote chondrogenesis and also suppress hypertrophic chondrocytes as evidenced by decreased COL10A1 and RUNX2 expression [335].

*In vitro* chondrogenesis is mediated by both environmental factors and cellular signaling molecules. They act to upregulate the expression of the transcription factor SRY-related HMG-box-9 (Sox9). Sox9 is the primary transcription factor regulating chondrogenic differentiation and, in combination with Sox5 and Sox6, is a direct regulator of COL2A1 the primary collagen species in cartilage [336].

Sox9 expression has been shown to be enhanced in transcription factor ZFN145 overexpressing cells leading to chondrogenesis [337]. Signaling mediated by the TGF- $\beta$  family of growth factors, including the BMPs, results in phosphorylation of Smad1/5/8, leading to expression, and phosphorylation-mediated stabilization, of Sox9 [338]. Additionally, the upregulation of yes-associated protein-1 (YAP) decreased Smad1/5/8 phosphorylation and inhibited chondrogenic differentiation [339].

TGF- $\beta$  signaling also encourages chondrogenesis through inhibition of RUNX2 and COL10 transcription [340]. Many different combinations of TGF- $\beta$ s and BMPs have been examined to assess their contribution to chondrogenesis. It has been separately shown that TGF- $\beta$ 1 and BMP2 both promote chondrogenesis and that when combined, they produce a synergistic effect [341]. Similarly, TGF- $\beta$ 2 and BMP7 were shown to enhance chondrogenesis [342]. Finally, incorporation of FGF-18 and TGF- $\beta$ 3 also produced a synergistic pro-chondrogenic effect [343].

Micromass culture, the preferred mechanism for *in vitro* chondrogenesis, produces a dense ASC cell pellet that promotes a rounded cell morphology and mimics the initial cell condensation stage of *in vivo* chondrogenesis [344]. The culture of cells in this manner also induces hypoxic conditions reminiscent of the largely avascular end product of chondrogenesis, cartilage [345]. Hypoxia has been shown to preferentially promote chondrogenesis over osteogenesis by inducing p38 MAPK signaling, which results in transcription of COL2 and ACAN [346]. Hypoxic conditions also stimulate early commitment to chondrogenesis by inducing HIF-1 $\alpha$  signaling leading to a two-fold increase in Sox9 expression. The ablation of HIF-1 $\alpha$  was found to reverse this finding [347].

While several studies have reported transdifferentiation of hypertrophic chondrocytes into osteoblasts, inhibition of chondrocyte hypertrophy is essential to avoid unwanted mineralization of the ECM [348, 349]. This collagen to bone process is known as endochondral bone formation. In hypertrophic chondrocytes, this transition can be examined and is mediated by the expression and activity of COL10, ALP, and MMP-13 [349]. The continued expression of Sox9 has been shown to actively repress transcription of COL10A1 by inhibiting activity the of RUNX2 [350]. Hypoxia also results in the downregulation of COL10A1 and MMP13, thus inhibiting chondrocyte hypertrophy [351]. Parathyroid hormone-related peptide (PTHrP) supplementation has been shown to suppress chondrocyte hypertrophy [352].

#### Differentiation Method

Unlike adipogenic and osteogenic differentiation of ASCs, chondrogenic differentiation is often not performed in a cell monolayer. Monolayer differentiation of ASCs can be achieved, and evidence suggests that coating cell culture plastic with fibroblast-derived ECM may aid the process [353]. However, an environment more conducive to chondrogenesis can be achieved by pelleting the cells in a conical tube or v-bottomed plate [344, 354, 355]. It has also been shown that ASCs cultured in a variety of scaffolds can also improve their chondrogenic differentiation [355-359].

Media supplements and concentrations may vary between protocols, but the overall differentiation strategy remains the same. ASC stromal media is supplemented with dexamethasone, L-ascorbic acid 2-phosphate, and members of the TGF- $\beta$  family. Additionally, some labs include an insulin, transferrin, selenium mixture to help differentiation along [270-272, 341-343, 354, 360]. Similar to adipogenic and osteogenic differentiation, dexamethasone is used to initiate differentiation and in combination with other signaling molecules, has been shown to upregulate transcription of several collagens. L-ascorbic acid 2-phosphate, again, acts as a co-factor for the hydroxylation of prolines in collagens and induces transcription of COL2A1 [272, 342]. Importantly, the inclusion of different TGF- $\beta$ s, BMPs, and FGFs have been shown to increase the differentiation of ASCs into chondrocytes that secrete the appropriate extracellular matrix [341-343, 360].

#### Confirmation of Chondrogenesis

Confirmation of chondrogenesis is largely determined by the analysis of the extracellular matrix that was deposited around the cells in micromass culture. This

can be accomplished by embedding, sectioning, and staining the pellet or by proteolytic enzyme-mediated digestion followed by component analysis (See Figure C2).

The Bern scoring system, introduced by Grogan *et al.*, can be used for the qualification of *in vitro* engineered cartilaginous tissue. The Bern system uses a 0-9 score to describe cartilage quality [361]. It is assessed using a 0-3 scale along three axes: (1) Safranin O-fast green staining to examine GAG uniformity and intensity, (2) distance between cells as a measure of matrix deposition, and (3) assessment of typical rounded chondrocyte morphology.

Paraffin-embedded chondrogenic pellets can be sectioned and subjected to numerous histological stains to confirm chondrogenesis. The most common of these are Alcian Blue, Toluidine Blue, and Safranin O, all of which stain polysaccharides such as those found in GAGs [270, 355, 361]. The intensity and evenness of staining can be used to assess the degree of differentiation of ECM producing chondrocytes. Picrosirius red is a linear anionic dye that can be used to stain collagen networks [362]. Additionally, collagen subtype-specific antibodies can be used to determine which types of collagens are present in the chondrogenic pellets.

Following digestion with a proteolytic enzyme, assessment of GAG content can be made using dimethylmethylene blue (DMMB). DMMB is a cationic dye that preferentially stains sulfated GAGs in solution and can be quantified by measuring its absorbance at 525 nm [343]. The amount of DNA that can be isolated from each pellet should be used to normalize the DMMB measurements to control for cell

number. Similarly, a hydroxy-proline assay can be used to determine collagen content indirectly. Briefly, hydroxyprolines are hydrolyzed, oxidized into pyrroles, and reacted with p-dimethylaminobenzaldehyde (DMAB, Ehrlich's reagent) to form a chromophore whose absorbance can be read at 550 nm [343, 363]. The absorbance can be used to calculate initial collagen content. Alternatively, the hydroxyproline to collagen ratio of 1:7.69 has been used to determine collagen content [343]. Again, these results should be normalized to the DNA content of the pellet.

Finally, the digestion of the pellet allows for analysis of gene expression of the cells following RNA isolation. Gene expression analysis can be used to examine the chondrocyte stages of maturation. Immature and mature chondrocytes can be determined through the expression of Sox 5, Sox6, Sox9, COL2A1, and ACAN [364, 365]. Finally, hypertrophic chondrocytes can be assessed by the expression of COL10A1, ALP, and MMP13 [366, 367].

#### ASC Chondrocyte Secretome

Chondrocytes' secretome is predominantly related to the production and maintenance of the extracellular matrix. This consists of predominantly of GAGs and collagens supplemented by stabilizing proteins such as link protein, cartilage oligomeric protein, decorin, and fibromodulin [367]. Of importance, once chondrocytes become hypertrophic, they begin to secrete COL10, ALP, and various MMPs, which work in a concerted effort to initiate bone deposition. Thus, inhibition of chondrocyte hypertrophy is essential for the maintenance of clinically relevant chondrogenesis and cartilage formation. Future research optimizing

chondrogenic differentiation and maintenance of mature chondrocytes will provide valuable information for both treatment and prevention of disease.

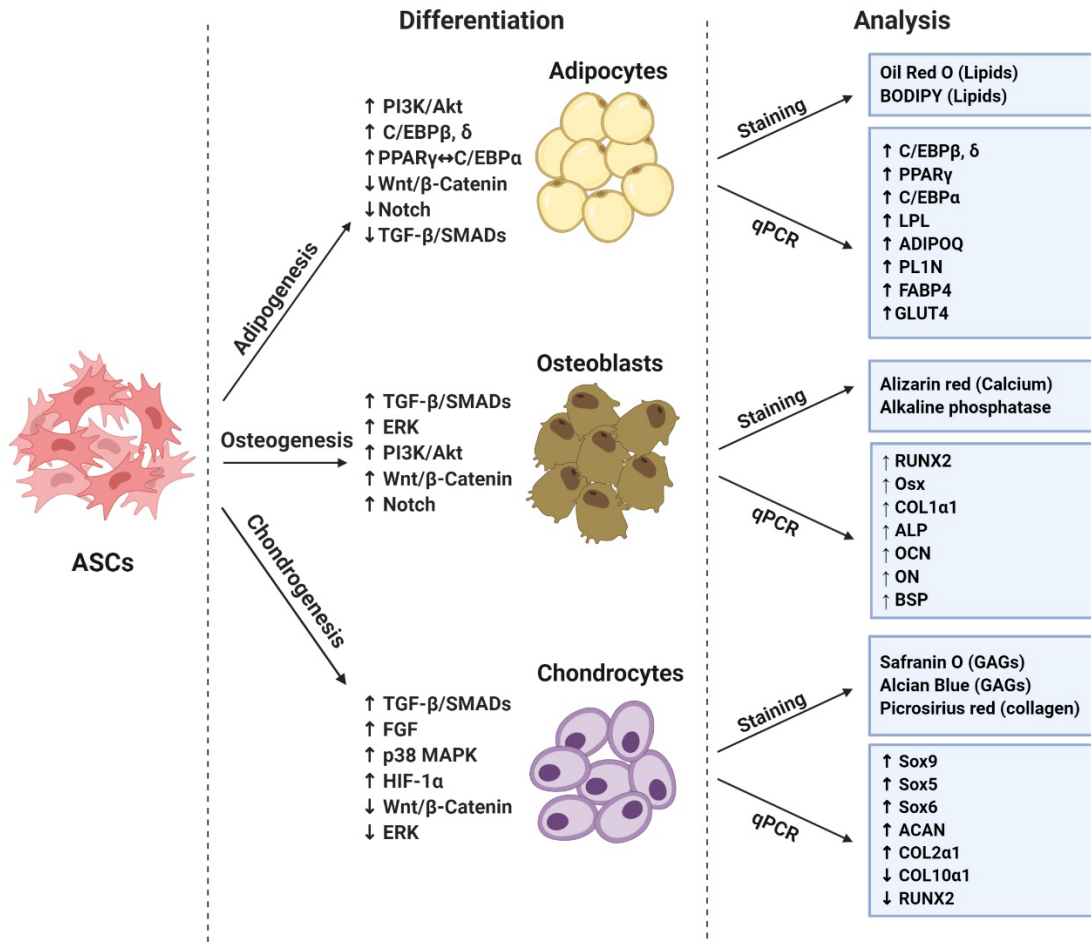


**Figure C2: Overview of differentiation of ASCs to Adipocytes, Osteoblasts, and Chondrocytes and methods of differentiation confirmation.** Overlapping signaling pathways work in concert to induce differentiation and establish tissue line commitment. Various cellular stains and gene expression analysis using qPCR are used to confirm differentiation (*Figure Legend continues on next page*).

**PI3K**, phosphatidylinositol 3-kinase; **TGF- $\beta$** , transforming growth factor beta; **Smad**, TGF $\beta$  mothers against decapentaplegic; **FGF**, fibroblast growth factor; **p38** **MAPK**, p38 mitogen-activated protein kinase; **HIF-1 $\alpha$** , Hypoxia-inducible factor 1-alpha; **ERK**, extracellular signal-regulated kinase **C/EPB**, CAAT/enhancer-binding protein; **PPAR $\gamma$** , peroxisome proliferator-activated receptor gamma; **LPL**, lipoprotein lipase; **ADIPOQ**, Adiponectin; **PL1N**, perilipin; **FABP4**, fatty acid binding protein 4; **GLUT4**, Glucose transporter type 4; **RUNX2**, runt-related transcription factor-2; **Osx**, Osterix; **COL1 $\alpha$ 1**, Collagen 1-alpha-1; **ALP**, Alkaline phosphatase; **OCN**, Osteocalcin; **ON**, Osteonectin; **BSP**, Bone sialoprotein; **GAGs**, Glycosaminoglycans **SOX**, SRY-related HMG-box; **ACAN**, Aggrecan; **COL2 $\alpha$ 1**, Collagen 2-alpha-1; **COL10 $\alpha$ 1**, Collagen 10-alpha-1. Created with BioRender.com.

#### ***C4 Characterization of In Vitro Immunomodulatory Abilities***

The immunomodulatory capabilities of MSCs were only recently reported by Bartholemew *et al.* in a landmark 2002 publication illustrating their suppressive effects on lymphocyte proliferation [368]. Since then, their potent immunomodulatory potential has made them the subject of intense research. Much of this research has focused on their secreted immunomodulatory molecules, such as cytokines and growth factors. However, recently researchers have started examining MSC-secreted extracellular vesicles carrying immunomodulatory proteins and RNA species. It has also been demonstrated that treatment of ASCs with pro-inflammatory factors such as lipopolysaccharide (LPS) [369, 370], and interferon-gamma (IFN- $\gamma$ ) [371] or exposure to hypoxic conditions [372] can enhance the secretion of immune-active compounds.

Regardless of the mechanism of action, the ability of MSCs, including ASCs, to modulate components of the immune environment *in vitro* and *in vivo* make them exciting potential therapeutics. For the purposes of this chapter only the *in vitro* activity of ASCs relative to specific immune populations is discussed. The immunomodulatory impact of ASCs can be assessed via direct co-culture, indirect co-culture, or treatment of immune cells with ASC conditioned media. Depending on the intended application of ASCs, the characterization of their immunomodulatory capacity may or may not be necessary. However, analysis of their activity *in vitro*, as well as examination of their secreted immuno-active compounds may serve as a helpful tool to evaluate their immunomodulatory potential prior to use.

### ASCs and the Innate Immune System

Innate immunity is one of two interconnected systems, along with adaptive immunity, used by most vertebrates to mount a response against foreign insults such as viruses, bacteria, and parasites. The innate immune system serves as the first line of defense, providing both physical barriers and specialized immune cells. Physical barriers like the skin, gastrointestinal tract, and their respective acellular defense mechanisms help prevent the invasion of pathogens, while the specialized immune cells are responsible for rapidly and indiscriminately killing any pathogens that breach these barriers. The primary subsets of innate immune cells are macrophages, dendritic cells (DCs), and natural killer (NK) cells.

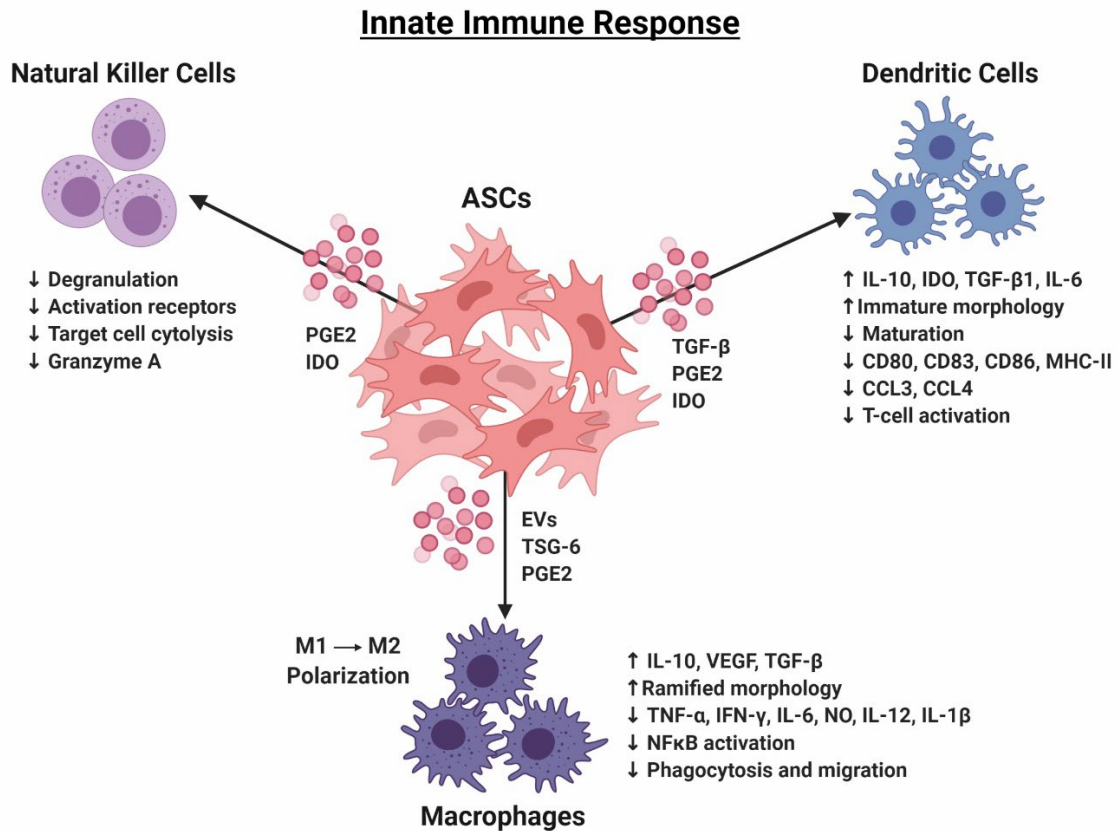


**Figure C3:** *In vitro* effects of ASCs on cell of the innate immune system. ASCs display robust contact-dependent and paracrine-mediated immunomodulatory effects on dendritic cells, macrophages and NK cells *in vitro*.

**ASCs**, Adipose-derived stem cells; **IDO**, Indoleamine 2,3-dioxygenase; **PEG2**, prostaglandin E2; **TGF- $\beta$** , Transformation growth factor-beta; **IFN- $\gamma$** , Interferon-gamma; **IL-10**, Interleukin 10; **IL-6**, Interleukin 6; **TNF- $\alpha$**  Tumor necrosis factor alpha; **TSG-6**, TNF- $\alpha$ -stimulated gene-6; **VEGF**, Vascular endothelial growth factor; **EVs**, extracellular vesicles; **NF $\kappa$ B**, Nuclear factor kappa-light-chain-enhancer of activated B cells; **NO**, Nitric oxide; **IL-12**, Interleukin 12; **IL-1 $\beta$** , Interleukin 1 beta; **CCL3**, C-C motif chemokine ligand 3; **CCL4**, C-C motif chemokine ligand 4. Created with Biorender.com.

## Macrophages

Macrophages are highly plastic phagocytic cells derived from either the embryonic yolk sac or circulating monocytes [373]. They are present in specialized forms in nearly every tissue of the body and exert their critical immune function by engulfing and phagocytosing pathogens and apoptotic cells, acting as professional antigen-presenting cells (APCs), and secreting effector molecules like chemokines and cytokines to direct the recruitment and activation of other immune cells. Primary monocytes and macrophages can be isolated from peripheral blood mononuclear cells (PBMCs), bone marrow, or peritoneal lavage for *in vitro* studies, and are typically selected or validated by their expression of CD14. Furthermore, immortalized cell lines like U-937, THP-1 (human), and RAW264.7 (mouse) can be used to examine macrophages *in vitro*.

Activated macrophages are classified into two primary categories: classically activated, or “M1” macrophages, which elicit pro-inflammatory activity, and alternatively activated, or “M2” macrophages which are anti-inflammatory and pro-angiogenic. Polarization of macrophages into M1 phagocytes requires the use of any combination of activation compounds such as LPS, IFN- $\gamma$ , TNF- $\alpha$ , and phorbol-12-myristate-13-acetate (PMA). M2 phagocyte polarization can be achieved through exposure to IL-4 and/or IL-13. Macrophage dynamics are characterized *in vitro* through a comprehensive examination of cell surface phenotype, secretome, morphology, and phagocytic capacity [374, 375].

Macrophage polarization state can be determined by measuring gene transcript and protein expression of cell surface markers like the co-stimulatory

molecules CD80 and CD86 (M1) and the pattern recognition receptors CD206 and CD163 (M2). Interestingly, exposure of both primary CD14<sup>+</sup> monocyte and M1-activated macrophages to ASCs consistently downregulates surface expression of M1 markers and upregulates M2 markers, and this is most likely due to soluble factors from ASCs as conditioned medium, Boyden chamber systems and isolated extracellular vesicles all produce equally robust effects when compared to direct co-culture [376-380].

Canonical M1 secreted factors include TNF- $\alpha$ , IFN- $\gamma$ , IL-6, nitric oxide (NO), IL-12, and IL-1 $\beta$ , which cumulatively promote a T-helper cell 1 (Th1) and Th17-driven immune response. In contrast, M2 macrophages commonly secrete IL-10, VEGF, and TGF- $\beta$  which promote a shift towards a Th2 and regulatory T-cell (Treg)-driven immune response [381, 382]. ASCs' paracrine activity has profound effects on the monocyte, and macrophage secretome, as conditioned medium or Boyden chamber co-cultures induce powerful downregulation of M1-secreted cytokines and chemokines and concomitant upregulation of M2 factors [377-379, 383-387]. The ASC-derived soluble factors suggested to be responsible for this influence include microRNA-packed extracellular vesicles [380], TNF- $\alpha$ -stimulated gene-6 (TSG-6) [388], or prostaglandin E2 (PGE2) [378, 379, 389]. Regardless, several groups have demonstrated robust suppression of NF- $\kappa$ B activation in macrophages following exposure to ASCs, which may explain these phenotypic shifts [380, 383, 384].

In addition to the modulation of their secretory profile, ASCs can also alter the morphology, migration ability, and phagocytic rate of macrophages. Following

the exposure to ASCs or their secretome, macrophages decrease their phagocytic and migratory abilities and adopt a ramified morphology [377, 380, 384]. The ASC secretome is powerful enough to induce these functional and phenotypic shifts even in macrophages from septic or colitic mice [386]. Overall, evidence suggests that ASCs are superior to BMSCs in their ability to shift the balance of macrophages in favor of the anti-inflammatory M2 phenotype [383, 389, 390]. This effect is enhanced when ASCs are stimulated with either TNF- $\alpha$  or IFN- $\gamma$ , or cultured in low serum medium or hypoxic conditions to enhance their immunomodulation [376, 380, 388, 389].

Certain disease conditions may alter this ability of ASCs to influence macrophage activation and polarization. Interestingly, when ASCs isolated from equine metabolic syndrome animals were co-cultured with a mouse macrophage cell line, they exhibited increased gene expression and secretion of pro-inflammatory cytokines [391]. Alternatively, ASCs isolated from patients with coronary heart disease were still able to suppress activation and lipid droplet accumulation in oxidized low-density lipoprotein (ox-LDL)-treated foamy macrophages. They also outperformed BMSCs in the ability to induce secretion of anti-inflammatory mediators and protect against ox-LDL-mediated apoptosis [392]. When comparing lipoma-derived ASCs to control, both cells similarly suppressed the secretion of pro-inflammatory mediators by mouse macrophage cell line, RAW264.7. However, lipoma-derived ASCs did result in a downregulation of IL-10 after co-culture, suggesting they may be less immunosuppressive than controls [387].

Finally, the interaction between ASCs and macrophages is bi-directional, and crosstalk between these two cell types has been reported by several groups. As a result of co-culture with monocytes and macrophages, ASCs upregulate expression of M2-priming cytokines IL-4, IL-13, and PGE2, and exhibit enhanced migration abilities [377, 378, 389].

These data point to the ability of ASCs to outperform BMSCs and regulate the activation, polarization, and immune function of macrophages. This results from their potent paracrine activity, and while this may be impaired in some disease states, it can also be restored and even enhanced with exogenous pre-conditioning strategies. Thus, ASCs are able to dynamically respond to macrophage signals to adapt their immunosuppressive vigor to meet the needs of a changing environment (Figure C3).

### Dendritic Cells

Dendritic cells are phagocytes that primarily differentiate from circulating, bone marrow-derived hematopoietic progenitors. They are the most potent APC in the innate immune system and also perform a variety of functions, including surveillance for pathogens or danger signals, phagocytosis, and processing of antigens for major histocompatibility complex (MHC)-II presentation, and trafficking to lymphoid organs to convey activation signals to adaptive immune cells. They form a crucial bridge between the innate and adaptive immune systems by communicating directly with B and T lymphocytes to initiate antigen-specific immune responses. After encountering an antigen, the immature DC (iDC) engulfs and processes the antigen and initiates maturation. They upregulate expression of

chemokine receptors that direct their migration to draining lymph nodes, co-stimulatory and MHC molecules that allow for antigen presentation and priming of naïve T cells, and cytokines that direct recruitment and activation of adaptive immune cells [393, 394]. DCs are grouped into two main subsets based on their developmental pathways, surface marker expression, and molecular signature. The myeloid DCs (mDC) are derived from the common myeloid progenitor (CMP) that also gives rise to macrophages, while the plasmacytoid DCs (pDC) are derived from the common lymphoid progenitor (CLP) that also gives rise to B cells, T cells and NK cells. Functionally, mDCs respond to immune stimulation by inducing either Th1 or Th2 cell activation, while pDCs produce the bulk of type I interferons and induce either Th2 or Tregs [395].

Generation of DCs for *in vitro* assays is typically accomplished by CD14<sup>+</sup> positive selection from PBMCs or bone marrow. This is followed by the differentiation of immature CD14<sup>+</sup> monocytes into either immature mDCs using a combination of IL-4, granulocyte-macrophage colony-stimulating factor (GM-CSF), and/or TNF- $\alpha$ ; or immature pDCs using IL-3 [396]. This is then followed by maturation of iDCs using LPS or other pro-inflammatory stimuli [397].

Due to the heterogeneity of DC subsets, several *in vitro* assays have been developed to examine specialized cell functions. Some of the most commonly employed include characterization of maturation state, secretory activity, and the ability to induce activation and proliferation of CD4<sup>+</sup> T lymphocytes. Flow cytometric phenotyping is used to determine the maturation state of DCs based on surface expression of CD14 (immature only) and the mature DC markers CD83,

CD80, CD86, and HLA-DR or MHC-II. Additionally, morphology can be used to discern maturation state, as iDCs have a smooth and round appearance while mDCs display the dendritic morphology that lends these cells their name [398]. Activated DCs exhibit a unique secretory signature that produces both paracrine and autocrine effects on naïve T cells and other iDCs, respectively [399]. Finally, T cell proliferation and activation phenotype are used as indirect measures of mDC function in mixed lymphocyte reaction (MLR) assays.

The effect of MSCs on DC maturation and function has been well characterized. Comparisons between the effects of BMSCs and ASCs have repeatedly shown the latter to be more potent inhibitors of DC maturation in both direct and indirect co-culture [396, 400-403]. These results are evidenced by elevated numbers of CD14<sup>+</sup> cells exhibiting smooth immature morphology and dampened expression of the mature DC markers CD83, CD80, CD86, and MHC-II. The secretory activity of DCs plays a role in how they recruit and activate adaptive immune cells and has thus been a major focus of investigation. In response to direct co-culture with ASCs, levels of the secreted chemokine ligands CCL3 (macrophage inflammatory protein 1 alpha , or MIP1 $\alpha$ ) and CCL4 (macrophage inflammatory protein 1 beta , or MIP1 $\beta$ ), both of which act as chemoattractants for CD8<sup>+</sup> T effector cells, is nearly abolished in DCs [400]. ASCs also significantly upregulate secretion of the anti-inflammatory cytokine IL-10 when co-cultured with CD14<sup>+</sup> monocytes. This cytokine inhibits not only the maturation of iDCs but also the subsequent production of the Th1-priming cytokines, IL-12, TNF- $\alpha$ , and IFN- $\gamma$  [396, 400, 402, 403].

An essential immune function of DCs is the ability to prime naïve CD4<sup>+</sup> and CD8<sup>+</sup> T cells against a particular antigen and promote their proliferation. Some groups purport that PGE2 plays an indispensable role in the ability of DCs to suppress activated T cell proliferation. In co-culture with MSCs, particularly ASCs, the ability of iDCs to induce T cell proliferation in mixed lymphocyte assays is significantly suppressed [396]. This suppression is likely to be a result of the robust increase in the secretion of PGE2 by ASCs, as blockade of PGE2 but no other upregulated cytokines negates this outcome. In comparison to DCs alone, those that are directly co-cultured with ASCs produce higher levels of the anti-inflammatory and pleiotropic cytokines TGF- $\beta$ 1, IL-10, IL-6, and indoleamine 2,3-dioxygenase (IDO) [396, 402, 403]. When these DCs are subsequently cultured with CD4<sup>+</sup> T cells, those that were treated with ASCs suppress T cell proliferation and induce significantly more Tregs than those cultured alone. This effect was attributed to TGF- $\beta$ -induced elevations in IDO, as ASCs pre-treated with TGF- $\beta$ 1 siRNAs or the IDO inhibitor, indomethacin, did not produce this effect [396, 402, 403].

Overall, ASC paracrine activity demonstrates robust and reliable suppression of dendritic cell maturation and T cell-activating function, making them promising agents for combating inflammation and autoimmune conditions (Figure C3).

### Natural Killer Cells

NK cells are cytolytic effector cells of lymphoid origin that derive their name from their ability to “naturally” kill defective or foreign cells without initial priming or antigen presentation. NK cytolytic activity is determined by the balance of

activating or inhibiting ligands on the surface of target cells. Healthy cells expressing high levels of the “self” MHC-I molecules evade NK cytotoxicity, while those experiencing viral infection or malignant transformation downregulate MHC-I and shift the balance toward NK cell activation [404]. Once activated, NK cells perform their cell-killing function by either inducing Fas/FasL-dependent apoptosis or releasing lysosomal granules filled with perforin and granzymes to digest the target cell [405].

NK cells can be isolated from PBMCs using either positive selection for the canonical NK marker CD56 or negative selection to eliminate monocytes, other lymphocytes, granulocytes, and erythrocytes [406]. *In vitro* analysis of NK cell phenotype and function is performed using surface marker expression of the pathogen recognition receptor (PRR) CD56, degranulation assays measuring the expression of lysosomal-associated membrane proteins CD107a/b (LAMP1/2), and intracellular staining for cytokines like IFN- $\gamma$  in the presence of protein transport inhibitors [407].

Comparative studies examining the effects of different MSC sources on NK cell characteristics have yielded somewhat contradictory findings. Some reports detail an enhanced immunosuppressive effect of ASCs over other MSC sources on NK cell activation, proliferation, and cytotoxic capacity [408-410]. Others, however, argue that ASCs perform similarly to BMSCs when it comes to suppressing activation, proliferation or cytokine secretion and that BMSCs are more potent inhibitors of NK cytotoxicity than ASCs (See Figure C3) [401, 411].

These discrepancies may derive from different NK purification methods, culture conditions, and activation stimuli.

The enhanced potency of ASC-mediated suppression of NK cytolytic function in comparison to BMSCs has been demonstrated in both direct and indirect co-cultures. Results have shown evidence of significantly less degranulation of IL-2 activated, allogeneic NK cells [408]. Incubation of NK cells with both ASCs and BMSCs significantly downregulated NK cell surface expression of the activation receptor DNAX accessory molecule-1 (DNAM-1), reduced degranulation capacity when subsequently cultured with K562 target cells, and downregulated levels of granzyme A suggesting less NK cell activation [408]. However, both MSC types elicited a similar IFN- $\gamma$  response as measured by intracellular staining. The ability of ASCs to suppress activation and proliferation of NK cells has been attributed to the downregulation of NK activation receptors like NKp30, NKp44, and NKG2D through the activity of PGE2 and IDO, both of which are upregulated by co-culture with ASCs [409, 410]. Other groups have demonstrated no significant differences between BMSCs and ASCs in immunosuppression of NK cells or susceptibility to their cytotoxic function [401, 411].

MSCs are proven immunomodulators capable of soothing inflammation and promoting an environment of repair and homeostasis. NK cells are primarily responsible for the rapid clearance of transplanted MSCs, and resilience to NK-mediated cytotoxicity is, therefore, a valuable measure of how long MSCs will survive in the post-transplant environment to exert their therapeutic benefit. Here, again,

results appear contradictory, with some arguing that ASCs are equally vulnerable to NK cell-induced apoptosis as BMSCs. Others purport reduced susceptibility of ASCs to the cytolytic activity of NK cells due to lower surface expression of HLA class I molecules and negligible expression of activating ligands for NK cells [408]. This enhanced resilience is further confirmed when ASCs are used as target cells for activated NK cells, as they induce significantly less degranulation compared to BMSCs [408].

Evidence suggests that ASCs are at least comparable to BMSCs in their ability to suppress NK cell activation and evade cytolytic destruction and may even be superior to BMSCs in these respects. These abilities indicate that ASCs may be able to persist longer after transplantation and exert enhanced immunomodulatory effects by suppressing NK cell activation.

#### ASCs and the Adaptive Immune System

While the innate immune system is critical for the rapid identification and elimination of pathogens, the adaptive immune system provides a selective and specific mechanism for recognizing self- and non-self-antigens [412]. There are two main types of cells in the adaptive immune system: the T-lymphocytes which derive from bone marrow, mature in the thymus, and are the primary effectors of cellular immune response; and the B-lymphocytes which arise in the bone marrow and are the antibody-producing cells of the body [412, 413]. Following their development, lymphocytes will migrate to secondary lymphoid organs such as the lymph nodes and spleen, which serve to capture circulating antigens. After

exposure to these antigens, lymphocytes migrate to antigen rich target sites throughout the body and employ their effector functions [412].

MSCs, including ASCs, have been shown to exhibit significant immunomodulatory effects on lymphocytes *in vitro*, via both contact-dependent and paracrine signaling. Several studies have compared the ability of ASCs, BMSCs, and AMSCs to inhibit PBMC-derived lymphocyte proliferation [414, 415]. In lymphocytes, proliferation is most often assessed through the addition of carboxyfluorescein diacetate succinimidyl ester (CFSE) to the culture. CFSE is membrane permeable and is readily incorporated into cells. With each cell division, its signal is diluted two-fold, allowing for generational tracking of populations via flow cytometry [416]. MSC-mediated anti-proliferative effects were shown to be more robust when cells were directly co-cultured as opposed to indirect co-culture, illustrating the importance of cell-cell contact [414, 415]. These results highlight the ability of ASCs to modulate general lymphocyte populations and the potential to actively modulate the adaptive immune response (Figure C4).

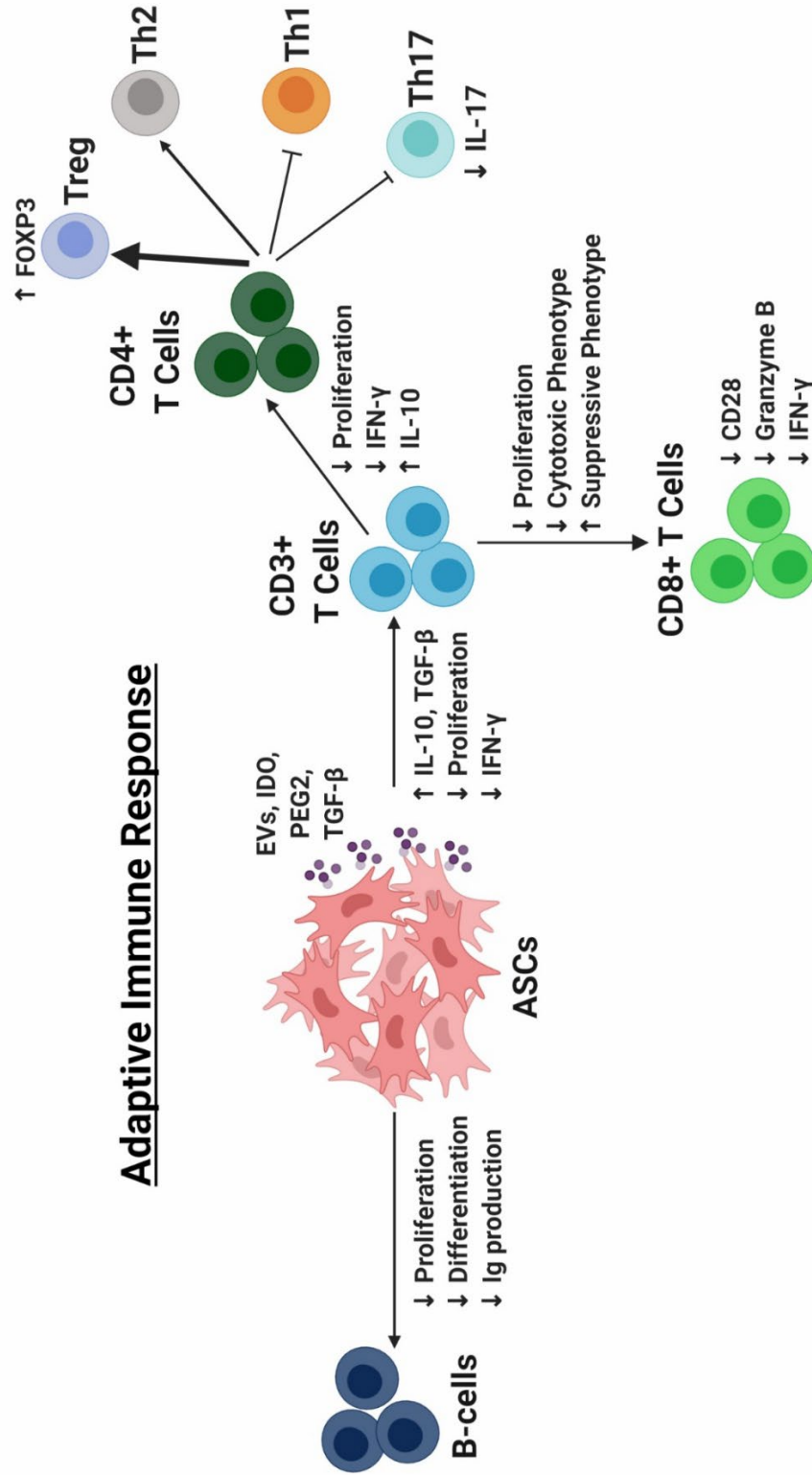


(Figure legend on next page)

**Figure C4: *In vitro* effects of ASCs on cells of the adaptive immune system.**

ASCs exhibit significant immunomodulatory effects on both B and T lymphocytes *in vitro*. This effect is mediated by both contact-dependent and paracrine signaling mechanisms.

**ASCs**, Adipose-derived stem cells; **IDO**, Indoleamine 2,3-dioxygenase; **PEG2**, Prostaglandin E2; **TGF- $\beta$** , Transforming growth factor-beta; **IFN- $\gamma$** , Interferon- $\gamma$ ; **IL-10**, Interleukin 10; **CD28**, Cluster of differentiation 28; **Treg**, Regulatory T-cells; **Th2**, T-helper 2; **Th1**, T-helper 1; **Th17**, T-helper 17; **FOXP3**, Forkhead box P3; **IL-17**, Interleukin 17. Created with Biorender.com.

## T-Cells

T-cells are responsible for mediating cellular immunity. When T-cells encounter activated APCs, such as dendritic cells, macrophages, or B-cells, they proliferate and differentiate into subtypes that coordinate to mediate the removal of the antigen [417, 418]. Depending on cytokines present in the environment, T-cells are capable of differentiating into several different subtypes, the effects of which are defined by their cytokine expression profiles. T-cells are also able to maintain a sort of cellular memory for antigens, which allows them to respond more rapidly to a previously encountered antigen [419].

A defining feature of the T-cell lineage is the expression of CD3, which serves as a co-receptor in conjunction with the T-cell receptor (TCR). Isolation of T-cells from PBMCs, spleen, or other lymphatic tissue can be accomplished via positive or negative selection. Selection for CD3<sup>+</sup> T-cells selects for all subtypes and allows for whole population interrogation. Following indirect co-culture with ASCs, CD3<sup>+</sup> T-cells exhibited significantly decreased proliferation rates [420-422]. Additionally, this anti-proliferative effect could be enhanced by directly co-culture [421, 422]. Pre-stimulation of ASCs with pro-inflammatory cytokines such as IFN- $\gamma$  or TNF- $\alpha$  can also significantly enhance these anti-proliferative effects [421]. ASC effects on T-cell proliferation are mediated by the secretion of IDO. Co-cultured cells produced more IL-10 and PGE2 than isolated T-cell or ASC cultures, indicating communication-related alterations in their secretomes [420-422]. Another study by Chein *et al.* demonstrated an increase in the concentrations of the central anti-inflammatory cytokines IL-10 and TGF- $\beta$  following indirect co-

culture of activated T-cells and ASCs [423]. Importantly, the protein concentration of pro-inflammatory cytokine IFN- $\gamma$  was significantly reduced when ASCs were indirectly cocultured with activated CD3<sup>+</sup> T-cells, in comparison to activated T-cells alone [423]. The results of these studies demonstrate the ability of the ASCs to modulate general T-cell differentiation and proliferation *in vitro*.

CD4<sup>+</sup> T-cells: Also known as helper T-cells, CD4<sup>+</sup> T-cells carry TCRs that recognize antigens presented by MHC II molecules [413, 417, 418]. ASCs have been shown to be more robust in their suppression of helper T-cell proliferation than BMSCs and Wharton's Jelly mesenchymal stem cells (WJMSCs) [422]. Though these results have been demonstrated to be dose-dependent, advanced age and chronic inflammatory disease states both have been shown to negatively impact ASCs ability to suppress T-cell proliferation [424, 425].

CD4<sup>+</sup> T-cells can be further divided into subtypes defined by their cytokine expression and immune function. These include the pro-inflammatory, anti-tumorigenic Th1 and Th17 cells; the anti-inflammatory, pro-tumorigenic Th2 cells; and the anti-inflammatory Treg cells [426]. Culturing CD4<sup>+</sup> T-cells in ASC conditioned media elicits a shift towards to Treg subtype as evidenced by a significant increase in forkhead box P3 (FoxP3) expression, the master regulator of Treg cell development [427]. This shift towards Tregs as well as the reported increase in IL-10 secretion suggests that ASCs can promote robust anti-inflammatory responses in mixed T-cell populations.

CD8<sup>+</sup> T-Cells: CD8<sup>+</sup> T-cells, known as cytotoxic T-cells, recognize antigens presented by MHC I molecules, which in combination with CD80 or CD86

interaction will result in activation and killing of infected or malignant cells [417, 418]. Similar to NK cells, CD8<sup>+</sup> T-cells can secrete cytotoxic granules containing perforin and granzymes or employ Fas/Fas-L binding to induce caspase-mediated apoptosis in target cells [428, 429]. As previously seen with CD4<sup>+</sup> T-cells, ASCs cultured directly with CD8<sup>+</sup> T-cells suppress their proliferation in a dose-dependent manner [422]. These effects were found to be stronger than those of BMSCs or WJMSCs. Additionally, direct co-culture of ASCs with CD8<sup>+</sup> T-cells resulted in decreased CD8 expression [430]. Thus, ASCs push cytotoxic T-cells towards a more suppressive, less cytotoxic phenotype. In these same cells, expression of CD28 was also significantly decreased, indicating a CD8<sup>+</sup> T-cell suppressor state [430]. Further, the shift towards a regulatory phenotype in CD8<sup>+</sup> T-cells following ASC co-culture was found to be functional as ASCs were able to significantly reduce the production of Granzyme B and IFN- $\gamma$  [430]. Interestingly, unlike the effects observed with CD4<sup>+</sup> T-cells, the immunosuppressive capabilities of ASCs on CD8<sup>+</sup> T-cells were found to be unaffected by donor age [425].

### B-Cells

B-lymphocytes are responsible for mediating humoral immunity. Their primary function is to produce and secrete antibodies that recognize foreign antigens. Following antigen recognition via B-cell receptor (BCR), the B-cells become activated, proliferate, and differentiate into antibody-secreting cells that may later become memory cells [431]. B-cells are primarily identified by the expression of CD19 and can be isolated from PBMCs via negative selection for other cell types.

To date, the number of *in vitro* studies evaluating the immunomodulatory properties of ASCs on B-cells has been minimal, but the overall consensus has been that ASCs are immunosuppressive. ASCs secrete factors that promote B-cell migration and chemoattraction to a greater extent than other mesenchymal cell types [432]. Although ASCs secrete distinct chemokines and produce other factors involved in cell motility and chemotaxis, the specific factor that promotes B-cell migration and chemoattraction is unknown at this point [432]. In comparison to BMSCs, direct co-culture resulted in enhanced CD19<sup>+</sup> B-cell proliferation. This finding was enhanced when the cells were co-cultured with ASCs [421]. Stimulation of ASCs with pro-inflammatory cytokines, which has previously been shown to increase their immunomodulatory capabilities, reversed the effect, and inhibited B-cell proliferation to the same level as BMSC co-culture [421].

Antibody production is one of the primary functions of B-cells; thus, analysis of immunoglobulin (Ig) production following co-culture is a simple heuristic used to assess the impact of MSCs on B-cell function [433, 434]. A study by Bochev *et al.* demonstrated that co-culture of ASCs with stimulated PBMCs resulted in potent suppression of B-cell Ig production. The suppression was due to the ability of ASCs to inhibit the differentiation of B-cells to Ig-producing cells and was found to be more robust than co-culture with BMSCs [434]. Overall, these results suggest that ASCs are able to modulate the B-cell population *in vitro* and thus may possess significant immunomodulatory capacity in more complex systems.

### Summary

While donor variability has not been thoroughly examined in the context of ASC-mediated immunomodulation of the innate or adaptive immune system, the ASC secretome is crucial to their influence over immune cells. It may, therefore, be hypothesized that impaired secretion of key factors like PGE<sub>2</sub>, IDO, TGF- $\beta$ , and IL-10 from donors with advanced age, elevated BMI, or underlying comorbidities would result in diminished immunomodulatory control over each of these specialized cells. Further studies need to be conducted to fully elucidate the impact of donor characteristics on immunomodulatory capabilities.

### ***C5 Conclusion and Future Directions***

Minimal characterization of ASCs by their adherence to plastic, expression of well-defined surface markers, and the ability to differentiate into mesenchymal lineages ensures that scientists are examining related populations of cells. Further assessment of their secretome and immunomodulatory profiles may allow for the identification of ASC subpopulations, which can be tailored to specific translational applications. Already, researchers have identified several surface-marker expression patterns that are indicative of ASCs with unique characteristics. Future investigations into surface marker-defined subpopulations may lead to exciting new therapeutic approaches. Donor variation has also been shown to significantly affect the ability of ASCs to differentiate, grow, and produce immunomodulatory effects. Further research into the impact of donor characteristics such as age, BMI, and health status on therapeutic potential will allow for the selection of adipose tissue with optimal characteristics.

Adipose stem cells represent a valuable resource for use in regenerative medicine due to their ease of acquisition, high cell yield, and potent immunomodulatory abilities. Thorough characterization of these cells is not only essential for defining them as adipose-derived mesenchymal stem cells but also necessary for collaborative efforts between labs. By fully characterizing ASCs, scientists will be able to share discoveries and reproduce results more effectively, leading to an accelerated rate of scientific breakthroughs.

## APPENDIX D

### ADIPOSE-DERIVED STEM CELLS FROM OBESE DONORS POLARIZE MACROPHAGES AND MICROGLIA TOWARD A PRO-INFLAMMATORY PHENOTYPE<sup>4</sup>

#### ***D1 Abstract***

Macrophages and microglia represent the primary phagocytes and first line of defense in the peripheral and central immune systems. They activate and polarize into a spectrum of pro- and anti-inflammatory phenotypes in response to various stimuli. This activation is tightly regulated to balance the appropriate immune response with tissue repair and homeostasis. Disruption of this balance results in inflammatory disease states and tissue damage. Adipose stem cells (ASCs) have great therapeutic potential due to potent immunomodulatory capabilities which induce the polarization of microglia and macrophages to the anti-inflammatory, M2, phenotype. In this study, we examined the effects of donor heterogeneity on ASC function. Specifically, we investigated the impact of donor obesity on ASC stemness and immunomodulatory abilities. Our findings revealed that ASCs from obese donors (ObASCs) exhibited reduced stem cell

---

<sup>4</sup> As published: Harrison, M.A.A. et al. (2020). Adipose-Derived Stem Cells from Obese Donors Polarize Macrophages and Microglia Toward a Pro-Inflammatory Phenotype. *Cells*, 10(1), 26. <https://doi.org/10.3390/cells10010026>

characteristics when compared to ASCs from lean donors (LnASCs). We also found that ObASCs promote a pro-inflammatory phenotype in murine macrophage and microglial cells, as indicated by upregulated expression of pro-inflammatory genes, increased nitric oxide pathway activity, and impaired phagocytosis and migration. These findings highlight the importance of considering individual donor characteristics such as obesity when selecting donors and cells for use in ASC therapeutic applications and regenerative medicine.

## ***D2 Introduction***

Adipose tissue-derived stem cells (ASCs), a type of mesenchymal stem cell (MSC), possess significant anti-inflammatory and immunomodulatory properties that make them an attractive therapeutic option for numerous inflammatory diseases. ASCs exert their effects on the adaptive and innate immune system via the secretion of soluble molecules and extracellular vesicles (EVs), which alter the inflammatory microenvironment [378, 380, 388, 435]. This is partially accomplished by transitioning activated macrophages from pro-inflammatory towards anti-inflammatory, pro-repair phenotypes [378, 435]. Additionally, pre-treatment of ASCs with pro-inflammatory factors or hypoxic conditions strengthens their immunomodulatory abilities [370-372, 380, 436]. These stressful conditions mimic the post-transplant tissue niche and provide some evidence for their behavior *in vivo*. Due to these properties, ASCs have been investigated as therapeutic agents in animal models of various diseases such as multiple sclerosis (MS) [235, 437], uveitis [438, 439], kidney injury [155, 440], inflammatory bowel

disease [441-443], and cutaneous wound healing [444, 445]. Results from these studies suggest that ASCs possess robust immunosuppressive potential in numerous disease states; however, the application of ASC-based therapies to the clinic has met with limited success.

One hindrance to clinical translation may be the heterogeneity of ASC function amongst different donors. It is known that individual donor characteristics such as age and comorbidities can alter the physiology and function of ASCs [446-453]. Research has shown that generating pools of donor ASCs can mitigate some donor-to-donor variation and may help combat these effects [454]. However, the examination of donor characteristics and their impact on ASC function represents a valuable area of research that will inform donor selection and prove important for future clinical trials. Specifically, the aim of this study is to examine the impact of exposure to ASCs from either lean or obese donor pools have on circulating or tissue resident phagocytes. An investigation of phenotypic and functional changes in these phagocytes will provide valuable insight into the differential effects of ASCs dependent on obesity status.

Obesity is characterized by increased deposition of white adipose tissue in both the subcutaneous and visceral fat depots. This increase in adipose tissue is a result of both hypertrophy, an increase in adipocyte size, and hyperplasia, an increase in adipocyte proliferation [455]. Obesity-related adipose tissue hypoxia also causes the activation of signaling cascades that lead hypertrophic adipocytes to express pro-inflammatory cytokines [456, 457]. These cytokines activate tissue-resident macrophages and circulating lymphocytes, leading to a chronic state of

tissue inflammation [458]. In response to the chronic inflammation and hypoxia in obese adipose tissue, ASCs exhibit distinct physiological changes. Studies have demonstrated that ASCs from obese individuals (ObASCs) produced elevated levels of pro-inflammatory mediators [282, 459, 460], exhibit reduced stem cell characteristics [217, 234, 459-461], and display reduced immunomodulatory abilities [462]. Our laboratory has previously shown that ObASCs do not possess the same therapeutic efficacy as lean ASCs (LnASCs) in a mouse model of MS [452]. We also showed that ObASCs produce an exaggerated immune response following exposure to an inflammatory environment, which we suspect resulted in increased CD4<sup>+</sup> and CD8<sup>+</sup> T cell proliferation and the increased lesion area seen in the mouse model of MS [452]. These findings are intriguing; however, the effects of ObASCs on phagocytes of the innate immune system have not yet been elucidated.

Macrophages and microglia, brain-resident macrophages, are primary components of the innate immune system and represent the first line of defense against foreign pathogens and tissue damage. In response to an array of extracellular signals, they activate and adopt phenotypically and functionally distinct profiles. Initially, these were described as either classically activated (M1), pro-inflammatory, or alternatively activated (M2), anti-inflammatory phenotypes [463, 464]. More recently, however, the spectrum of macrophages has been expanded from this binary system to one which more accurately encompasses the diverse phenotypic and functional behavior of macrophages [374]. Appropriate pro-inflammatory macrophage and microglial response is essential for defense

against pathogens however, if left unchecked it can result in significant tissue damage. Therefore, induction of anti-inflammatory, pro-repair and regulatory macrophages are essential for orchestration of the adaptive immune response, resolution of inflammation, and initiation of tissue repair [464, 465].

Considering the importance of macrophage polarization and function following tissue damage or infection, this study aimed to determine whether obesity status of ASC donors alters the phenotypic and functional characteristics of these highly mutable cells. We hypothesized that ObASCs have been fundamentally altered by their chronically inflamed tissue niche and that this results in an impaired ability to promote an anti-inflammatory phenotype in murine macrophages and microglia. To investigate this, we compared standard stem cell characteristics of LnASCs and ObASCs. Next, we determined the effects of indirect co-culture of LnASCs and ObASCs on both macrophages and microglia. Our results provide additional evidence for the impact of obesity on ASC stemness, relate these changes to the immunomodulatory capabilities of ASCs, and provide mechanistic insight into previous findings that indicate a loss of therapeutic efficacy in an animal model of inflammatory disease [452].

### ***D3 Materials and Methods***

#### **Cell culture**

Human female, subcutaneous, abdominal ASCs were obtained from LaCell LLC/Obatala Sciences Inc. (New Orleans, LA). Individual ASC cell lines were previously fully characterized by our laboratory prior to being pooled [292, 451,

452, 466, 467]. Following pooling an abbreviated characterization was completed to ensure expression of basic stemness characteristics. Lean donors were considered those with a BMI less than 25 kg/m<sup>2</sup> while obese donors were considered those with BMI greater than 30 kg/m<sup>2</sup> as previously described by Sabol et al. 2019 [466]. Donor pools were created using lean donors (LnASCs; n=6; BMI = 22.45 ± 1.51; age = 36.33 ± 5.62) and obese donors (ObASCs; n=6; BMI = 33.97 ± 3.11; age = 40.50 ± 7.46). Cells were maintained in stromal media consisting of Dulbecco's Modified Eagle's Media and Nutrient Mixture F12 (DMEM:F12; ThermoFisher; Waltham, MA, USA) supplemented with 10% heat-inactivated fetal bovine serum (FBS; Hyclone; Logan, UT, USA) and 1% anti-mycotic, anti-biotic (ThermoFisher). Cells were harvested at passage four (p4) with 0.25% trypsin, 1mM EDTA (ThermoFisher) and all experiments were conducted with p5 ASCs. As in previous studies, immortalized macrophage and microglial cell lines were used in order to control for passage number and to avoid the impact of accidentally co-isolated cell populations common in primary culture [468-471]. The murine microglial cell line SIM-A9 was purchased from ATCC (Manassas, VA, USA) and maintained in DMEM:F12 culture medium supplemented with 10% heat-inactivated FBS (ThermoFisher), 5% heat inactivated horse serum (HS; ThermoFisher), and 1% anti-mycotic, anti-biotic. SIM-A9 cells were lifted for passage by incubating with 1xPBS supplemented with 1mM EGTA (Sigma, St. Louis, MO, USA), 1 mM EDTA (Sigma), and 1mg/mL glucose (Sigma). The murine monocyte/macrophage cell line RAW264.7 was also purchased from ATCC and was cultured in high-glucose DMEM (ThermoFisher) supplemented with 10% FBS

and 1% anti-mycotic, anti-biotic. RAW264.7 cells were lifted for passage by manual scraping when cells reached 80% confluence. All murine lines were used between passage 5 and 10.

#### Characterization of ASCs

Flow Cytometry: Phenotypic characterization of pooled human ASCs was completed using flow cytometric analysis of positive and negative surface markers as previously described [203, 204]. Briefly, cells were harvested, washed with 1xPBS, and incubated with fluorochrome-conjugated primary antibodies at room temperature (RT) for 15 minutes. Cells were then fixed in 1% paraformaldehyde (PFA) (Santa Cruz Biotechnology; Dallas, TX, USA) for 5 minutes at RT and analyzed with a Gallios Flow Cytometer and Kaluza software (Beckman Coulter; Brea, CA, USA). The following antibodies were purchased from BD Biosciences (San Jose, CA, USA): anti-CD3-PE-Texas Red, anti-CD31 PE-Cy7, and anti-CD73-PE. Anti-CD90-FITC and anti-CD105-APC were purchased from Invitrogen (Waltham, MA, USA). Finally, anti-CD14-PECy5 and anti-CD45-AF700 were purchased from Beckman Coulter.

Adipogenic Differentiation and Quantification: ASCs were seeded at  $1 \times 10^5$  cells per well in a 12-well plate (Corning Inc.; Corning, NY, USA) and cultured in stromal media until confluent. Cells were then switched into adipocyte differentiation media (ADM) consisting of stromal media supplemented with dexamethasone (1  $\mu$ M; Sigma), isobutylmethylxanthine (IBMX) (250  $\mu$ M; Sigma), rosiglitazone (5  $\mu$ M; Sigma), biotin (66  $\mu$ M, Cayman Chemical; Ann Arbor, MI, USA), calcium d-pantothenate (34  $\mu$ M, Sigma), and human insulin (200 nM,

Sigma). ASCs were maintained in ADM for 21 days, with fresh ADM or adipose maintenance media (ADM without IBMX and rosiglitazone) added every 3 days on an alternating cycle. After 21 days cells were fixed for 30 minutes with 4% PFA (Santa Cruz) followed by incubation in a 0.5% solution of Oil-Red-O (Sigma) for 10 minutes at RT. Neutral lipid droplets were imaged with a 10x objective on a Nikon Eclipse TE-200 (Nikon; Melville, NY, USA) using Nikon's ACT-1 software. Quantification of Oil-Red-O staining was accomplished by destaining with 100% isopropanol and absorbance at 584 nm was determined using a Synergy HTX plate reader (BioTek; Winooski, VT, USA). Differentiation was reported as a percentage of control well staining.

Colony Forming Unit Fibroblast (CFU-F) Assay: ASCs were seeded at  $5 \times 10^2$  cells per 10 cm plate (Corning Inc.) and cultured for 14 days. On day 14, cells were fixed and stained with 3% crystal violet (Sigma) in methanol (Sigma) for 30 minutes at RT. Plates were then washed with DI water until clear and the number of colonies with a diameter greater than 2 mm was manually recorded.

Population Doubling Time: ASCs were seeded at  $1 \times 10^4$  cells per well in a 6 well plate and cultured in stromal media. Every 24 hours for a total of 8 days cells were harvested with 0.25% trypsin and 1mM EDTA (ThermoFisher), and viable cells were manually counted using trypan blue exclusion (ThermoFisher). Population doubling times (DT) were calculated using the previously described equation [472]:

$$DT = \frac{CT \times \ln 2}{\ln (Nf/Ni)}$$

where CT is culture time in hours, Ni is the initial cell number as counted on day 1, and Nf is the final cell number. Doubling time was reported as the mean  $\pm$  standard deviation.

#### Indirect Co-Culture Experiments

Co-Culture Conditions: Indirect co-culture of RAW264.7 or SIM-A9 cells with ASCs was accomplished using polyethylene terephthalate (PET) Transwells with a diameter of 24 mm and a pore size of 0.4  $\mu\text{m}$  (Corning Inc.). ASCs were seeded at  $5 \times 10^4$  cells per Transwell in stromal media. ASCs were treated with human interferon gamma (hIFN $\gamma$ ; 20 ng/mL; EMD Millipore; Billerica, MA, USA) for 48 hours to activate them and enhance their immunomodulatory activity as previously described [371, 380]. Concurrently, RAW264.7 or SIM-A9 were seeded into 6-well plates at  $5 \times 10^4$  or  $2 \times 10^4$  cells per well, respectively. After 48 hours, all cells were rinsed with 1xPBS, fresh media was replaced, and ASC seeded Transwell inserts were moved into the 6-well plate for a 48-hour co-culture. After 48 hours, inserts containing ASCs were removed and RAW264.7 or SIM-A9 cells were imaged for morphology, lysed for RNA isolation, or maintained for a further 48 hours in culture to generate conditioned medium. Control wells with no ASCs were run in parallel. All experiments were performed in triplicate.

RNA Isolation and qRT-PCR: RNA was isolated from RAW264.7 and SIM-A9 cells using a RNeasy Mini Kit (Qiagen). Following RNA isolation, 1  $\mu\text{g}$  of total mRNA was used to synthesize cDNA using the Applied Biosystems High-Capacity cDNA Reverse Transcription Kit (ThermoFisher). Quantitative reverse transcription PCR (qRT-PCR) was performed using SsoAdvanced Universal

SYBR Green SuperMix (Bio-Rad; Hercules, CA, USA) according to the manufacturer's instructions. Oligonucleotide primer sets were designed using PrimerBLAST software and manufactured by Integrated DNA Technologies (IDT; Coralville, IA, USA) and sequences are listed in Table E1. Relative gene expression was determined using the  $2^{-\Delta\Delta Ct}$  method and reported as fold change relative to untreated controls following normalization to the housekeeping gene, 40S ribosomal protein S29 (RPS29).

**Table D1: Primer Sequences**

**Table 1: Primer Sequences**

Target Gene	Forward	Reverse
iNOS	5'-GCCACCAACAATGGCAACA-3'	5'-CGTACCGGATGAGCTGTGAATT-3'
IL-1 $\beta$	5'-CCTGCAGCTGGAGAGTGTGGAT-3'	5'-TGTGCTCTGCTTGTGAGGTGCT-3'
TNF $\alpha$	5'-ATGGCCTCCCTCTCATCAGTTC-3'	5'-TTGGTGGTTTGCTACGACGTG-3'
Arg1	5'-GTGAAGAACCCACGGTCTGT-3'	5'-CCAGCACCACACTGACTCTT-3'
Mrc1	5'-GTGGAGTGATGGAACCCAG-3'	5'-CTGTCCGCCAGTATCCATC-3'
IL-10	5'-GCTCTTGCACTACCAAAGCC-3'	5'-CTGCTGATCCTCATGCCAGT-3'
RPS29	5'-TTCCTTTCTCCTCGTTGGGC-3'	5'-TTCAGCCCGIATTTGCCGAT-3'

Migration Assay: Migration efficiency of the RAW264.7 macrophages and SIM-A9 microglia in the presence or absence of LnASCs or ObASCs was determined using Transwells with a diameter of 6.5 mm and a pore size of 5.0  $\mu\text{m}$  (Corning Inc.). Transwells were coated with rat tail collagen type 1 (Corning) at a concentration of 50  $\mu\text{g}/\text{mL}$  for 2 hours at 37°C, then dried and stored at 4°C until use. Meanwhile, LnASCs and ObASCs were seeded into 24-well plates at  $1 \times 10^4$  cells per well and pre-stimulated for 24 hours with hIFN $\gamma$  as described above. ASCs were then washed with 1xPBS and stromal media was replaced with serum-free media. Transwell inserts were rehydrated with serum-free media for 30 minutes and RAW264.7 or SIM-A9 cells were seeded at  $1 \times 10^5$  or  $5 \times 10^4$  cells per Transwell, respectively, in serum-free media. RAW264.7 macrophages were allowed to migrate for 72 hours, and SIM-A9 microglia were allowed to migrate for 24 hours. After migration, Transwells were removed and stained with 3% crystal violet (Sigma) in methanol for 30 minutes at RT. Transwells were washed with DI water and the upper surface of the Transwell was brushed with a cotton swab to remove non-migrated cells. As previously reported by Yin et al. 2017 and Yu et al 2018, three random fields were chosen and imaged using a 10x objective for each Transwell [473, 474]. The number of migrated cells was manually counted for each image by a group-blinded researcher and reported as the average cells migrated per field.

Phagocytosis Assay: RAW264.7 and SIM-A9 cells were seeded separately into 96-well plates at  $2.5 \times 10^3$  cells per well in either control growth media or media supplemented with 50% LnASC or ObASC conditioned media and cultured

for 48 hours. The CytoSelect Phagocytosis Assay *E. coli* Substrate Kit (Cell Biolabs; San Diego, CA, USA) was employed to assess phagocytic ability according to the manufacturer's instructions. Briefly, cells were incubated with *E. coli* for 4 hours at 37°C, followed by fixation, permeabilization, and incubation with substrate to visualize phagocytosis. Absorbance was read at 450nm on a Synergy HTX plate reader (BioTek).

Nitric Oxide Production: After co-culture, RAW264.7 or SIM-A9 cells were cultured for a further 48 hours and conditioned media (CM) was collected and immediately frozen at -80°C. When thawed, CM was diluted 1:2 and a Griess assay was used to determine levels of NO metabolites according to the manufacturer's instructions (Cell Signaling Technology; Danvers, MA, USA). Briefly, samples were run in triplicate, incubated in sulfanilamide solution for 10 minutes at RT, and absorbance was measured at 540 nm with a wavelength correction at 690 nm using a BioTek Synergy HTX plate reader. Nitrite concentrations in CM were extrapolated from a standard curve.

#### Statistical Analysis

All data are expressed as mean  $\pm$  standard deviation from at least three independent experiments. The statistical differences between two groups was determined by a Mann-Whitney test. Differences between three or more groups was determined by one-way ANOVA followed by Dunnett's multiple comparisons test. For all comparisons, a  $p < 0.05$  was considered to indicate a significant difference. GraphPad Prism 8 software was used for all statistical analysis (GraphPad; San Diego, CA, USA).

## **D4 Results**

### ObASCs Exhibit Reduced Stemness Characteristics when Compared with LnASCs

Human adipose stem cells (ASCs) were pooled from six lean (BMI < 25) or six obese (BMI > 30) donors. No statistical differences were found in the age of donors between groups ( $p = 0.513$ ). Similar cell morphology was seen in both LnASCs and ObASCs (data not shown). Following a 21-day adipogenic differentiation, both LnASCs and ObASCs differentiated into adipocytes, which produced lipid droplets (Figure D1A). However, the degree of adipogenic differentiation observed in ObASCs was significantly lower than that of LnASCs (Figure D1B). Colony-forming unit fibroblast (CFU-F) assay indicated that ObASCs had an impaired ability to form colonies relative to LnASCs (Figure D1C). Flow cytometric analysis of the ASC phenotype based on positive (CD73, CD90, CD105) and negative (CD4, CD14, CD31, CD45) markers was conducted for both groups (Figure D1D). The data indicated that the ObASCs exhibited significantly decreased expression of CD90 and CD105 relative to LnASCs. Interestingly, ObASCs exhibited a slightly elevated level of CD73 relative to LnASCs ( $p < 0.01$ ). Finally, the average population doubling time was determined for each pool over an 8-day period and revealed no significant differences between groups (Figure D1E).

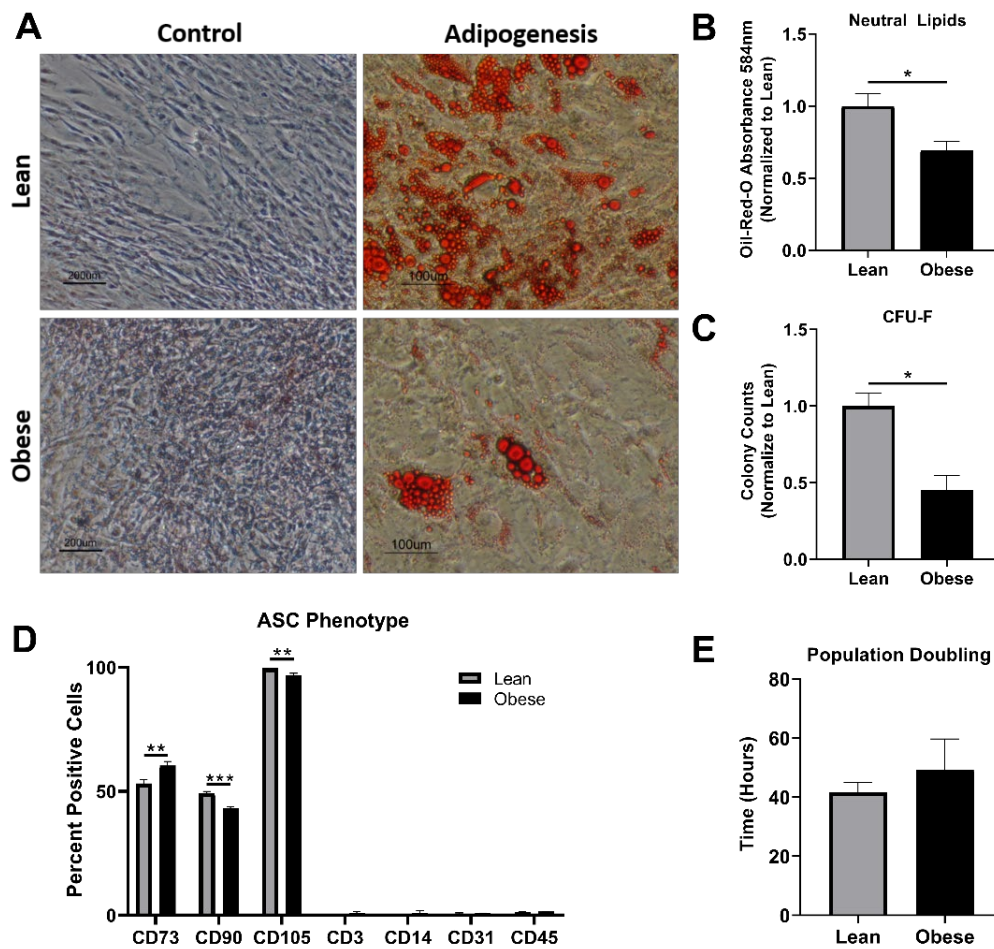


**Figure D1. Pooled ObASCs exhibit reduced stemness characteristics.** (A) LnASCs and ObASCs were differentiated with adipogenic media for 21 days and stained with Oil-Red-O and imaged at 10x (scale bar is 200  $\mu\text{m}$  for controls and 100  $\mu\text{m}$  for adipogenesis). (B) Oil-Red-O destain absorbance was measured at 584nm and normalized to the LnASCs. (C) CFU-F assay was completed with both LnASCs and ObASCs and the results were normalized to the LnASC colony counts. (D) Flow cytometry analysis of LnASCs and ObASCs using both positive and negative MSC markers. (E) Average population doubling time of LnASCs and ObASCs expressed in hours. (Figure legend continues on next page)

Values are presented as means (N=3)  $\pm$  SD of three independent experiments using Mann-Whitney tests. Statistical differences between the means are marked with \* $p < 0.05$ , \*\* $p < 0.01$ , \*\*\* $p < 0.001$ . Abbreviations: LnASCs, lean ASCs; ObASCs obese ASCs; CD, cluster of differentiation.

### Indirect Co-Culture with ObASCs, but not LnASCs, Induces Polarization Towards M1 Phenotype in RAW264.7 Macrophages

To determine the effect of LnASCs' and ObASCs' secretome on macrophage gene expression and function, indirect co-culture with RAW264.7 cells for 48 hours was performed. The morphology of RAW264.7 cells following co-culture was examined and no significant alterations were noted between groups (Figure D2A). The gene expression analysis of key anti-inflammatory (Figure D2B) factors revealed no significant changes in anti-inflammatory gene expression following either LnASC or ObASC co-culture relative to untreated macrophages. However, co-culture with ObASCs resulted in a roughly 50-fold increase in expression of inducible nitric oxide synthase (iNOS) and a 26-fold increase in interleukine-1 beta (IL-1 $\beta$ ) expression (Figure D2C). Similarly, in comparison to LnASCs, ObASCs induced a 10-fold and a 16-fold increase in iNOS and IL-1 $\beta$  expression respectively. Consistent with the upregulation of iNOS transcripts, RAW264.7 cells co-cultured with ObASCs demonstrated a 47-fold increase in iNOS metabolite production relative to untreated control cells as measured by a Griess assay (Figure D2D). These findings were echoed in the 90-fold increase in iNOS metabolites in ObASC exposed cells relative to LnASC exposed cells.

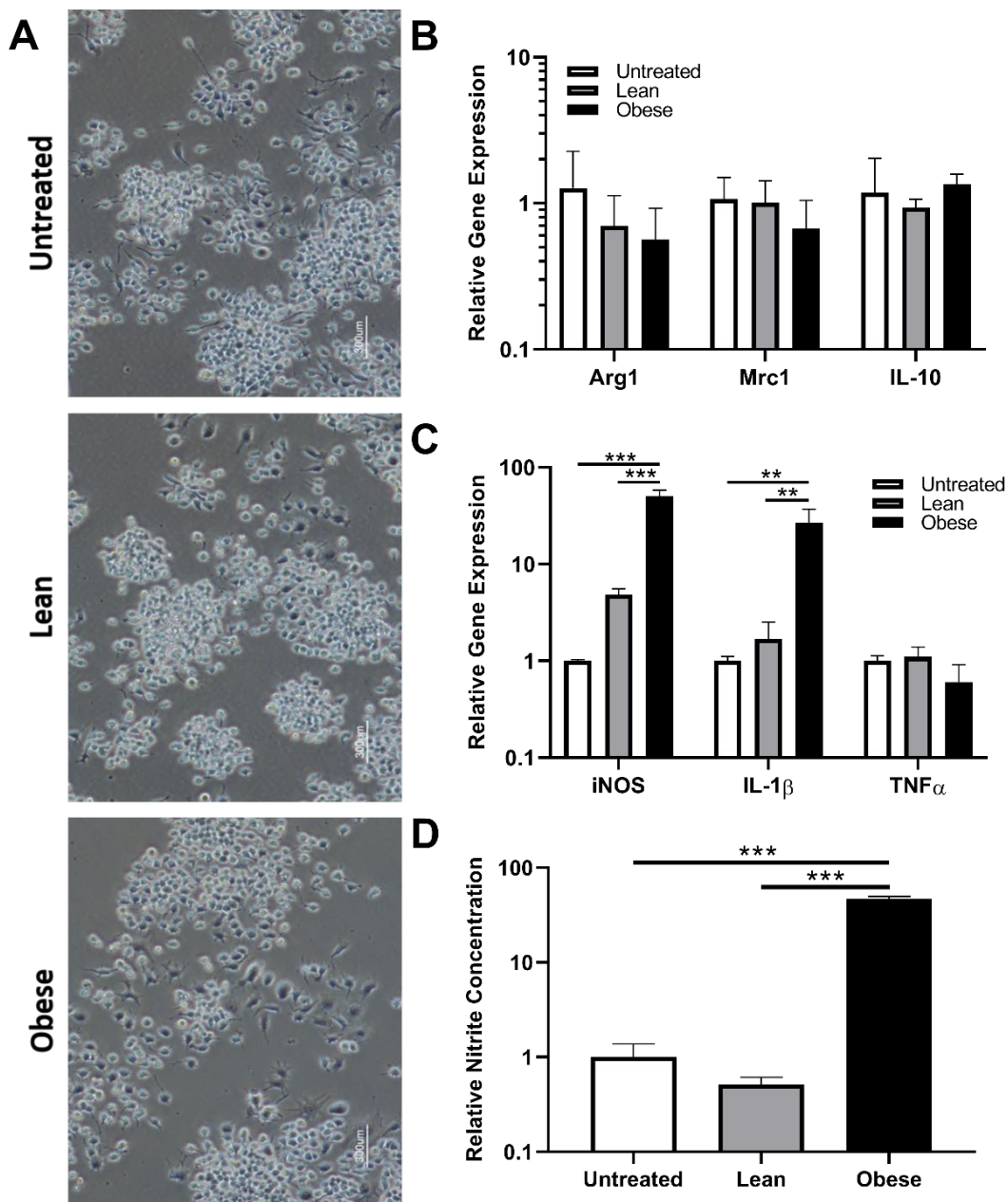


**Figure D2. RAW264.7 cells following indirect co-culture with ASCs in a Transwell system.** (A) Representative images of RAW264.7 morphology following either LnASC or ObASC co-culture for 48-hours. (B) Changes in anti-inflammatory gene expression of RAW264.7 cells following 48-hour co-culture relative to untreated controls. (Figure legend continues on next page)

(C) Changes in pro-inflammatory gene expression of RAW264.7 cells following 48-hour co-culture relative to untreated controls. (D) Griess assay determination of nitrite concentration of 48-hour conditioned media following 48-hour co-culture relative to untreated controls. Values are presented as means (N=3)  $\pm$  SD of three independent experiments using one-way ANOVA followed by Dunnett's multiple comparisons test. Statistical differences between the means are marked with \*\* $p < 0.01$ , \*\*\* $p < 0.001$ . Abbreviations: Arg1, arginase 1; Mrc1, mannose receptor C-type 1; IL-10, interleukin 10; iNOS, inducible nitric oxide synthase; IL-1 $\beta$ , interleukin 1 beta; TNF $\alpha$ , tumor necrosis factor alpha.

### LnASCs and ObASCs Differentially Affect the Migration and Phagocytic Abilities of RAW264.7 Macrophages

Following the changes in gene expression observed in RAW264.7 cells, we sought to determine what impact LnASCs and ObASCs have on the functional properties of macrophages, namely migration and phagocytosis. The number of macrophages able to digest the collagen-coating and migrate through a 0.4 $\mu$ m-pore Transwell towards the ASCs was used to determine their migratory abilities. Following 72-hour co-culture, more than three times as many RAW264.7 cells migrated through the collagen-coated Transwell when cultured with LnASCs than untreated controls ( $p < 0.001$ ) (Figure D3C). Likewise, a comparison between LnASC and ObASC exposed groups resulted in more than four times as many RAW264.7 cells migrated. There was no statistical difference between ObASC co-cultured RAW264.7 cell migration and untreated control cells. The ability of RAW264.7 macrophages to phagocytose when cultured with LnASC or ObASC conditioned media (CM) was assessed with colorimetric quantitative analysis of engulfed *E. coli* particles. When cultured with ObASC CM, but not LnASC CM, macrophages exhibited a 24% decrease in phagocytic ability when compared to untreated control macrophages (Figure D3D). The decrease in phagocytic ability between LnASC and ObASC groups was less extreme at a 20% decrease, but still statistically significant.

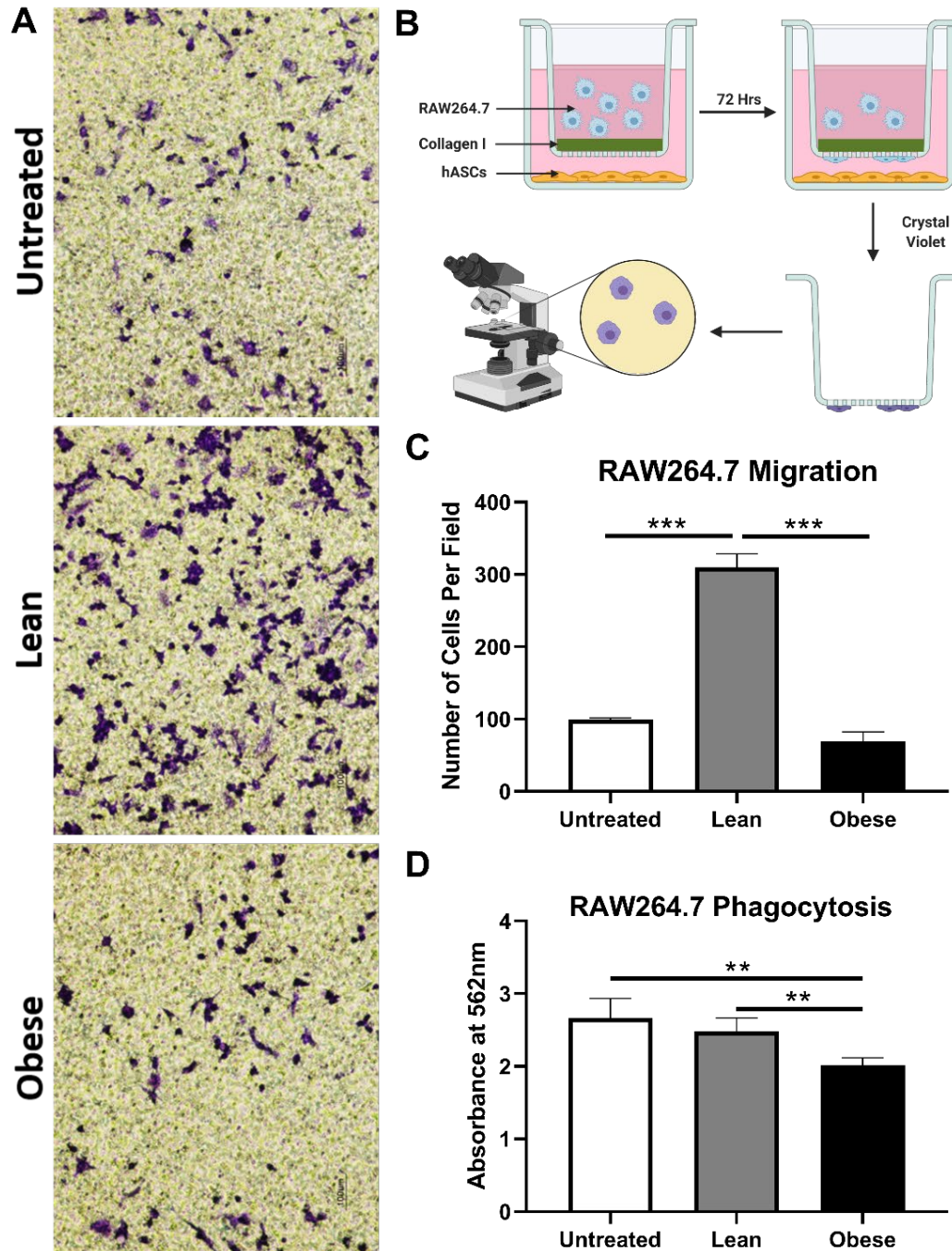


(Figure legend on next page)

**Figure D3. LnASCs and ObASCs differentially alter the migration and phagocytotic abilities of RAW264.7 cells.** (A) Representative images of crystal violet stained RAW264.7 cells following migration through a collagen-coated Transwell in the presence of LnASCs or ObASCs. (B) Diagram of migration assay process including staining and imaging. (C) Quantification of the cells migrated per field based on three randomly chosen fields for each Transwell migration performed. (C) Phagocytosis of *E. coli*-substrate by RAW264.7 cells following 48-hour treatment with LnASC or ObASC conditioned media. Values are presented as means (N=3)  $\pm$  SD of three independent experiments using one-way ANOVA followed by Dunnett's multiple comparison test. Statistical differences between the means are marked with \*\* $p < 0.01$ , \*\*\* $p < 0.001$ .

### Indirect Co-Culture with ObASCs, but not LnASCs, Induces Polarization Towards M1 Phenotype in SIM-A9 Microglia

Microglia are the primary brain-resident macrophages and represent the second line of CNS defense following the blood-brain barrier. Since we observed significant changes in macrophage physiology and function, the impacts of LnASC and ObASCs on microglia were assessed to determine how consistent these effects are on cells of similar functionality but differing origin. The morphology of SIM-A9 cells was consistent across all co-cultures (Figure D4A). Following 48-hour co-culture, alterations in gene expression of anti-inflammatory (Figure D4B) and pro-inflammatory (Figure D4C) factors were examined in LnASC and ObASC co-culture samples relative to untreated controls. Interestingly, both LnASC and ObASC co-culture enhanced the expression of arginase-1 (*Arg1*) but lacked differences of expression when compared with each other. However, another anti-inflammatory marker, mannose receptor 1 (*Mrc1*; CD206) was downregulated to 0.7-fold following LnASC co-culture. This effect was further decreased to 0.26-fold expression following ObASC co-culture and exhibited a statistically significant decrease when compared with the LnASC group. Importantly, expression of the anti-inflammatory cytokine interleukin-10 (IL-10) was upregulated 2.4-fold by SIM-A9s following LnASC co-culture. This increase was not evident in the ObASC group and was significantly less than the expression of the LnASC group.

Examination of pro-inflammatory genes yielded a significant increase in expression of iNOS (52-fold), IL-1 $\beta$  (8.5-fold), and tumor necrosis factor alpha (TNF $\alpha$ ) (2.8-fold) in ObASC co-cultures, and a non-significant decrease in

expression of these genes in LnASC co-cultures. In all three pro-inflammatory genes examined, there was also a significant difference in expression level between the LnASC and ObASC groups. A Griess assay was employed to examine the nitrite concentration of SIM-A9 conditioned media following co-culture (Figure D4D). In agreement with the RAW264.7 data, the ObASC co-cultured SIM-A9 microglia produced 2.7-fold higher levels of nitrite species than untreated controls. This was increased to a 4.6-fold difference when comparing LnASC to ObASC co-cultured SIM-A9 cells.

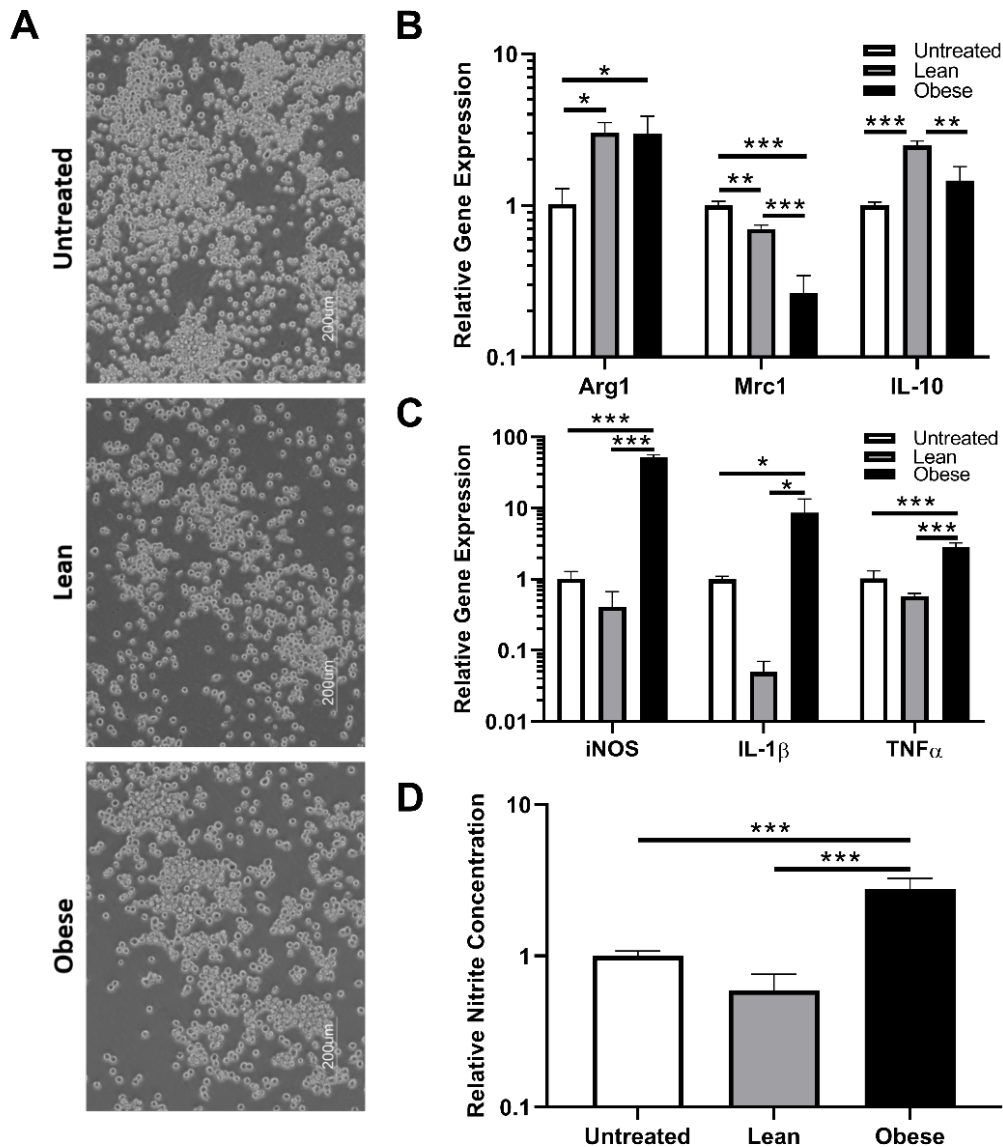


**Figure D4. SIM-A9 cells following indirect co-culture with ASCs in a Transwell system.** (A) Representative images of SIM-A9 morphology following either LnASC or ObASC co-culture. (B) Changes in anti-inflammatory gene expression of SIM-A9 cells following 48-hour co-culture relative to untreated controls. (C) Changes in pro-inflammatory gene expression of SIM-A9 cells following 48-hour co-culture relative to untreated controls. (*Figure legend continues on next page*)

(D) Griess assay determination of nitrite concentration of 48-hour conditioned media following 48-hour co-culture relative to untreated cells. Values are presented as means (N=3)  $\pm$  SD of three independent experiments using one-way ANOVA followed by Dunnett's multiple comparison test. Statistical differences between the means are marked with \* $p < 0.05$ , \*\* $p < 0.01$ , \*\*\* $p < 0.001$ . Abbreviations: Arg1, arginase 1; Mrc1, mannose receptor C-type 1; IL-10, interleukin 10; iNOS, inducible nitric oxide synthase; IL-1 $\beta$ , interleukin 1 beta; TNF $\alpha$ , tumor necrosis factor alpha.

### LnASCs and ObASCs Differentially Affect the Migration and Phagocytic Abilities of SIM-A9 Microglia

Changes in the functional properties of microglia following ASC co-culture were determined. The migration efficiency of SIM-A9 cells was examined using the aforementioned collagen-coated 5  $\mu\text{m}$  pore Transwells. After 24 hours, 37% more microglia had migrated in the LnASC co-culture than the untreated controls. ObASC co-cultured SIM-A9s demonstrated an increased trend in migration but failed to reach significance (Figure D5C). Comparisons between the LnASC and ObASC groups also failed to reach significance. The ability of SIM-A9 cells to phagocytose *E. coli* following exposure to LnASC or ObASC conditioned media was also examined (Figure D5D). Exposure to ObASC CM resulted in a 48% decrease in the phagocytic abilities of SIM-A9 cells relative to untreated controls and a 65% decrease relative to LnASC CM exposure.

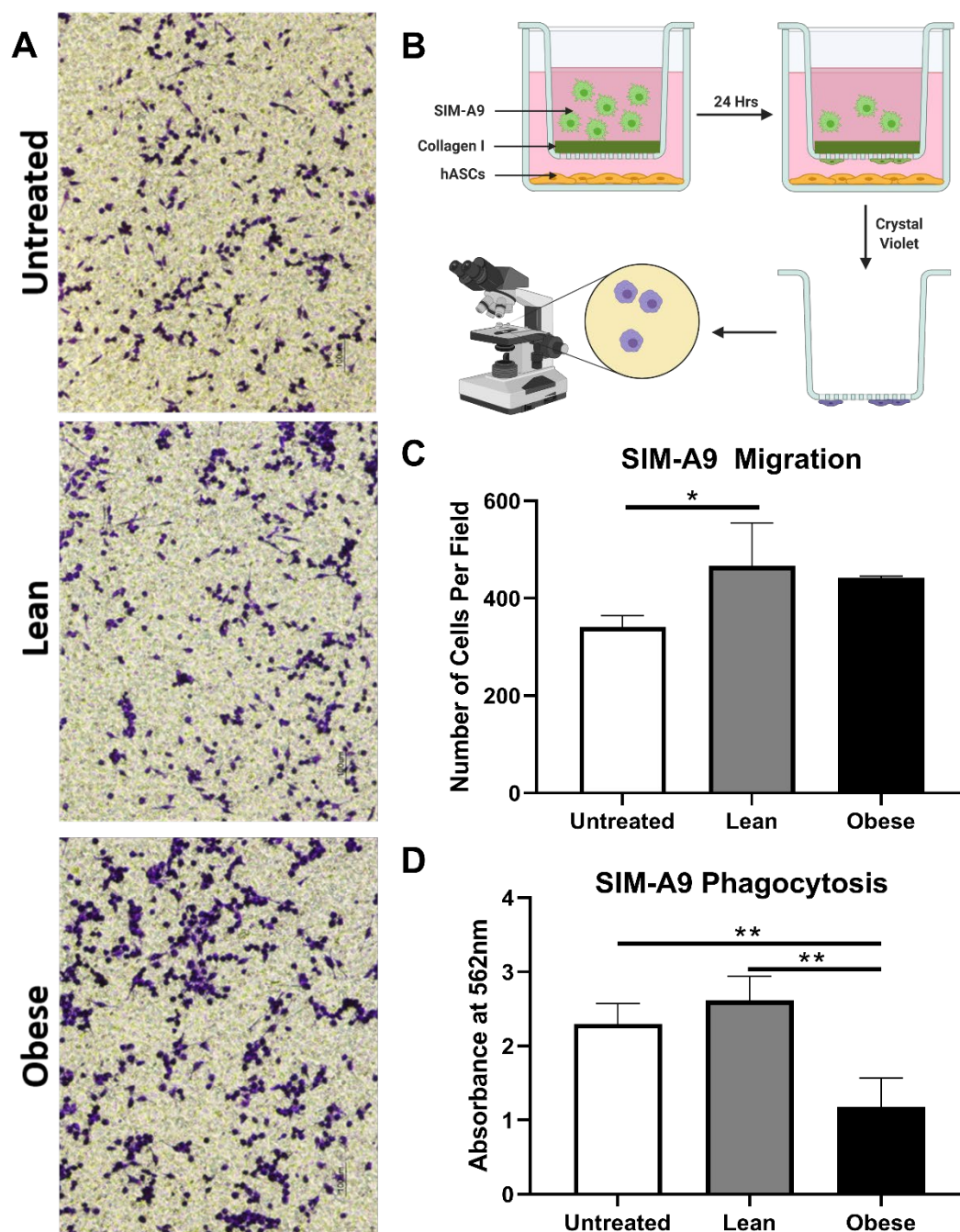


**Figure D5. LnASCs and ObASCs differentially alter the migration and phagocytic abilities of SIM-A9 cells.** (A) Representative images of crystal violet stained SIM-A9 cells following migration through a collagen-coated Transwell in the presence of LnASCs or ObASCs. (Figure legend continues on next page)

(B) Diagram of migration assay process including staining and imaging. (C) Quantification of the cells migrated per field based on three randomly chosen fields for each Transwell migration performed. (C) Phagocytosis of *E. coli*-substrate by SIM-A9 cells following 48-hour treatment with LnASC or ObASC conditioned media. Values are presented as means (N=3) of three independent experiments  $\pm$  SD using one-way ANOVA followed by Dunnett's multiple comparison test. Statistical differences between the means are marked with \* $p < 0.05$ , \*\* $p < 0.01$ .

## **D5 Discussion**

Adipose stem cells have tremendous therapeutic potential due to their ability to migrate to sites of inflammation where they recruit immune cells and orchestrate tissue repair [475-477]. Adipose stem cells are isolated from donor tissue following liposuction or lipectomy and, as such, are often from obese adipose tissue. Obese adipose tissue is chronically inflamed and hypoxic; therefore, the resident ASCs may be fundamentally altered relative to ASCs from lean donor tissue. Our initial characterization of stemness traits of ObASCs relative to LnASCs yielded results in agreement with numerous previous studies including: reduced adipogenic differentiation capacity [459, 478-480]; impaired self-renewal ability [217, 234]; and diminished expression of standard stem cell phenotypic markers [234, 479]. Additionally, our group's previous work demonstrated an exaggerated immune response of ObASCs to inflammatory stimuli [452], suggesting that the chronic inflammatory environment of obese adipose tissue may alter not only ASC phenotype but also their immunosuppressive function. In support of this theory, an *in vivo* study conducted by our lab demonstrated a loss of therapeutic efficacy of ObASCs in a mouse model of MS as demonstrated by lack of symptomatic improvement, lack of lesion reduction, and increased in pro-inflammatory cytokine expression [452]. Therefore, we hypothesized that the ability of ObASCs to induce an anti-inflammatory, pro-repair phenotype in macrophages and microglia would be impaired relative to LnASCs. In the present study, we examined, *in vitro*, the gene expression profiles, migration, and phagocytic abilities of both macrophages and microglia in the presence of ASCs.

We concluded that exposure to ObASCs, but not LnASCs, resulted in pro-inflammatory phenotypes in both macrophages and microglia.

Pro-inflammatory macrophages and microglia exhibit unique gene expression profiles, in part characterized by high levels of iNOS and the production of several cytokines, including IL-1 $\beta$ , IL-6, and TNF $\alpha$  [481]. The secretion of these cytokines results in a pro-inflammatory microenvironment that initiates the polarization of other macrophages and the recruitment and differentiation of naïve T cells towards pro-inflammatory phenotypes. In the present study, we demonstrated that, following co-culture with ObASCs, macrophages significantly upregulated iNOS and IL-1 $\beta$  gene expression when compared with LnASCs and untreated controls. Similarly, microglia exhibited significant upregulation of iNOS, IL-1 $\beta$ , and TNF $\alpha$  transcripts. In contrast, the co-culture of microglia and macrophages with LnASCs demonstrated no significant changes in the expression of pro-inflammatory cytokines in comparison to untreated controls. Direct comparisons made between LnASC and ObASC-exposed cells demonstrated similar significant upregulation of pro-inflammatory genes in the ObASC group. Nitric oxide (NO), the product of iNOS enzymatic activity on L-arginine, is one of the effector molecules of pro-inflammatory phagocytes. It produces metabolites which can be examined as an indirect measure of NO activity. In both cell lines, there were significantly more nitrite species produced following incubation with ObASCs indicating enhanced activity of NO in ObASC exposed cells. No change in NO activity was observed in cells co-cultured with LnASCs. These data suggest that ObASCs, but not LnASCs, promote gene expression resembling the pro-

inflammatory polarization of macrophages and microglia *in vitro*. Interestingly, although the ObASC-exposed SIM-A9 cells significantly downregulated their expression of the anti-inflammatory gene *Mrc1*, they maintained an elevated expression of *Arg1* and similar levels of IL-10 expression as control cells. In addition to being a traditional anti-inflammatory cytokine, IL-10 also has significant effects on the adaptive immune response by promoting the development of regulatory T cell populations [374]. This combined pro-inflammatory, regulatory microglial phenotype is an illustration of the diversity of potential responses to a complex extracellular signaling milieu. Further, it illustrates the inability of an oversimplified characterization system to appropriately describe these responses.

Gene expression analysis tells an incomplete story and does not demonstrate the effect that ASCs have on the function of macrophages and microglia. As immune surveillance and effector cells, macrophages and microglia must be able to migrate to areas of damage and phagocytose invading pathogens and cell debris. Anti-inflammatory, pro-repair phenotypes express an array of anti-inflammatory cytokines and are responsible for the phagocytosis of cellular debris and orchestration of tissue repair. Our migration assay demonstrated a significant increase in migration of both macrophages and microglia in the presence of LnASCs, which was absent in the presence of ObASCs. These findings are in agreement with several *in vitro* studies that demonstrated increased speed and distance of migration in a synthetic extracellular matrix by both M2 macrophages and microglia relative to M1 macrophages and microglia [482, 483]. Similar results were also found in a rat microglial migration study, which noted significant M2

microglial migration through a matrix relative to M1 [484]. Phagocytosis is another function of macrophages and microglia and is essential for pathogen defense and tissue regeneration. Previous studies have demonstrated a decrease in the ability of macrophages to phagocytose *E. coli* following polarization to M1 [485, 486]. Similarly, our results demonstrated decreased phagocytosis in the macrophages and microglia exposed to ObASCs. The cells which were exposed to LnASCs exhibited phagocytic abilities very similar to untreated control cells. Taken together, the decrease in mobility and phagocytic abilities of both macrophages and microglia are suggestive of polarization to an M1 phenotype as a result of exposure to ObASCs. Persistent M1 polarization results in a pro-inflammatory extracellular milieu which is essential for fighting infection and recruitment of additional immune cell populations, but it can also result in extensive tissue damage. M2 polarization is important for reduction of inflammation, degradation of cellular debris, and initiation of tissue repair mechanisms. Thus, ObASCs may possess limited therapeutic potential due to their promotion of pro-inflammatory phenotypes.

## ***D6 CONCLUSIONS***

The data from these studies suggest that ObASCs are fundamentally altered by their environment. This alteration manifests as a phenotype that preferentially induces a pro-inflammatory polarization in both macrophages and microglia, as evidenced by elevation of pro-inflammatory transcripts, decreased mobility, and diminished phagocytosis. The results of this study illustrate the importance of understanding the impact of the tissue niche on ASC phenotype and immunomodulatory function. In the context of an inflammatory disease such as MS, the skewed immunomodulatory function of ObASCs which promotes pro-inflammatory activation of innate immune cells may help explain the lack of therapeutic effect in previous studies. However, MS is only one of the numerous potential disease applications for ASCs, each of which are defined by unique pathogenic mechanisms. An ASC therapeutic ideally functions as a biological immunomodulator. One that enhances the pro-inflammatory function of macrophages or microglia may be beneficial for situations in which normal immune function is diminished or compromised. Successful translation of ASC therapeutics to the clinic will require the selection of ASCs that best fit the desired immunomodulatory response and produce the intended therapeutic outcome.

## LIST OF REFERENCES

1. Cagliani, R., D. Forni, A. Mozzi, and M. Sironi, *Evolution and Genetic Diversity of Primate Cytomegaloviruses*. Microorganisms, 2020. **8**(5).
2. Staras, S.A., S.C. Dollard, K.W. Radford, W.D. Flanders, R.F. Pass, and M.J. Cannon, *Seroprevalence of cytomegalovirus infection in the United States, 1988-1994*. Clin Infect Dis, 2006. **43**(9): p. 1143-51.
3. Mustakangas, P., S. Sarna, P. Ammala, M. Muttillainen, P. Koskela, and M. Koskiniemi, *Human cytomegalovirus seroprevalence in three socioeconomically different urban areas during the first trimester: a population-based cohort study*. Int J Epidemiol, 2000. **29**(3): p. 587-91.
4. Cannon, M.J., D.S. Schmid, and T.B. Hyde, *Review of cytomegalovirus seroprevalence and demographic characteristics associated with infection*. Rev Med Virol, 2010. **20**(4): p. 202-13.
5. Sinzger, C., M. Digel, and G. Jahn, *Cytomegalovirus cell tropism*. Curr Top Microbiol Immunol, 2008. **325**: p. 63-83.
6. Aiello, A.E., Y.L. Chiu, and D. Frasca, *How does cytomegalovirus factor into diseases of aging and vaccine responses, and by what mechanisms?* Geroscience, 2017. **39**(3): p. 261-271.
7. Dolan, A., C. Cunningham, R.D. Hector, A.F. Hassan-Walker, L. Lee, C. Addison, D.J. Dargan, D.J. McGeoch, D. Gatherer, V.C. Emery, P.D. Griffiths, C. Sinzger, B.P. McSharry, G.W.G. Wilkinson, and A.J. Davison, *Genetic content of wild-type human cytomegalovirus*. J Gen Virol, 2004. **85**(Pt 5): p. 1301-1312.
8. Murphy, E., I. Rigoutsos, T. Shibuya, and T.E. Shenk, *Reevaluation of human cytomegalovirus coding potential*. Proc Natl Acad Sci U S A, 2003. **100**(23): p. 13585-90.
9. Bhella, D., F.J. Rixon, and D.J. Dargan, *Cryomicroscopy of human cytomegalovirus virions reveals more densely packed genomic DNA than in herpes simplex virus type 1*. J Mol Biol, 2000. **295**(2): p. 155-61.
10. Gibson, W., *Structure and formation of the cytomegalovirus virion*. Curr Top Microbiol Immunol, 2008. **325**: p. 187-204.
11. Munger, J., B.D. Bennett, A. Parikh, X.J. Feng, J. McArdle, H.A. Rabitz, T. Shenk, and J.D. Rabinowitz, *Systems-level metabolic flux profiling identifies*

- fatty acid synthesis as a target for antiviral therapy*. Nat Biotechnol, 2008. **26**(10): p. 1179-86.
12. Yu, Y., A.J. Clippinger, F.J. Pierciey, Jr., and J.C. Alwine, *Viruses and metabolism: alterations of glucose and glutamine metabolism mediated by human cytomegalovirus*. Adv Virus Res, 2011. **80**: p. 49-67.
  13. Kaarbo, M., E. Ager-Wick, P.O. Osenbroch, A. Kilander, R. Skinnnes, F. Muller, and L. Eide, *Human cytomegalovirus infection increases mitochondrial biogenesis*. Mitochondrion, 2011. **11**(6): p. 935-45.
  14. Combs, J.A., E.B. Norton, Z.R. Saifudeen, K.H.Z. Bentrup, P.V. Katakam, C.A. Morris, L. Myers, A. Kaur, D.E. Sullivan, and K.J. Zwezdaryk, *Human Cytomegalovirus Alters Host Cell Mitochondrial Function during Acute Infection*. J Virol, 2020. **94**(2): p. 1-19.
  15. Kumari, P., I. Saha, A. Narayanan, S. Narayanan, A. Takaoka, N.S. Kumar, P. Tailor, and H. Kumar, *Essential role of HCMV deubiquitinase in promoting oncogenesis by targeting anti-viral innate immune signaling pathways*. Cell Death Dis, 2017. **8**(10): p. e3078.
  16. Siew, V.K., C.Y. Duh, and S.K. Wang, *Human cytomegalovirus UL76 induces chromosome aberrations*. J Biomed Sci, 2009. **16**: p. 107.
  17. Wagner, C.S., H.G. Ljunggren, and A. Achour, *Immune modulation by the human cytomegalovirus-encoded molecule UL18, a mystery yet to be solved*. J Immunol, 2008. **180**(1): p. 19-24.
  18. Yu, Y., T.G. Maguire, and J.C. Alwine, *Human cytomegalovirus activates glucose transporter 4 expression to increase glucose uptake during infection*. J Virol, 2011. **85**(4): p. 1573-80.
  19. Munger, J., S.U. Bajad, H.A. Collier, T. Shenk, and J.D. Rabinowitz, *Dynamics of the cellular metabolome during human cytomegalovirus infection*. PLoS Pathog, 2006. **2**(12): p. e132.
  20. Sharifi-Rad, M., N.V. Anil Kumar, P. Zucca, E.M. Varoni, L. Dini, E. Panzarini, J. Rajkovic, P.V. Tsouh Fokou, E. Azzini, I. Peluso, A. Prakash Mishra, M. Nigam, Y. El Rayess, M.E. Beyrouthy, L. Polito, M. Iriti, N. Martins, M. Martorell, A.O. Docea, W.N. Setzer, D. Calina, W.C. Cho, and J. Sharifi-Rad, *Lifestyle, Oxidative Stress, and Antioxidants: Back and Forth in the Pathophysiology of Chronic Diseases*. Front Physiol, 2020. **11**: p. 694.
  21. Magri, A., S. Reina, and V. De Pinto, *VDAC1 as Pharmacological Target in Cancer and Neurodegeneration: Focus on Its Role in Apoptosis*. Front Chem, 2018. **6**: p. 108.
  22. Hansen, K.G. and J.M. Herrmann, *Transport of Proteins into Mitochondria*. Protein J, 2019. **38**(3): p. 330-342.

23. Combs, J.A., C.H. Monk, M.A.A. Harrison, E.B. Norton, C.A. Morris, D.E. Sullivan, and K.J. Zvezdaryk, *Inhibiting cytomegalovirus replication through targeting the host electron transport chain*. Antiviral Res, 2021. **194**: p. 105159.
24. Sharon-Friling, R., J. Goodhouse, A.M. Colberg-Poley, and T. Shenk, *Human cytomegalovirus pUL37x1 induces the release of endoplasmic reticulum calcium stores*. Proc Natl Acad Sci U S A, 2006. **103**(50): p. 19117-22.
25. Goldmacher, V.S., *Cell death suppression by cytomegaloviruses*. Apoptosis, 2005. **10**(2): p. 251-65.
26. Hanahan, D. and R.A. Weinberg, *Hallmarks of cancer: the next generation*. Cell, 2011. **144**(5): p. 646-74.
27. Hanahan, D. and R.A. Weinberg, *The hallmarks of cancer*. Cell, 2000. **100**(1): p. 57-70.
28. Chang, Y., E. Cesarman, M.S. Pessin, F. Lee, J. Culpepper, D.M. Knowles, and P.S. Moore, *Identification of herpesvirus-like DNA sequences in AIDS-associated Kaposi's sarcoma*. Science, 1994. **266**(5192): p. 1865-9.
29. Epstein, M.A., B.G. Achong, and Y.M. Barr, *Virus Particles in Cultured Lymphoblasts from Burkitt's Lymphoma*. Lancet, 1964. **1**(7335): p. 702-3.
30. Taher, C., J. de Boniface, A.A. Mohammad, P. Religa, J. Hartman, K.C. Yaiw, J. Frisell, A. Rahbar, and C. Soderberg-Naucler, *High prevalence of human cytomegalovirus proteins and nucleic acids in primary breast cancer and metastatic sentinel lymph nodes*. PLoS One, 2013. **8**(2): p. e56795.
31. El Shazly, D.F., A.A. Bahnassey, O.S. Omar, E.T. Elsayed, A. Al-Hindawi, E. El-Desouky, H. Youssef, and A.N. Zekri, *Detection of Human Cytomegalovirus in Malignant and Benign Breast Tumors in Egyptian Women*. Clin Breast Cancer, 2018. **18**(4): p. e629-e642.
32. Cui, J., Q. Wang, H.B. Wang, B. Wang, and L. Li, *Protein and DNA evidences of HCMV infection in primary breast cancer tissues and metastatic sentinel lymph nodes*. Cancer Biomark, 2018. **21**(4): p. 769-780.
33. Harkins, L.E., L.A. Matlaf, L. Soroceanu, K. Klemm, W.J. Britt, W. Wang, K.I. Bland, and C.S. Cobbs, *Detection of human cytomegalovirus in normal and neoplastic breast epithelium*. Herpesviridae, 2010. **1**(1): p. 8.
34. Ohgaki, H. and P. Kleihues, *Epidemiology and etiology of gliomas*. Acta Neuropathol, 2005. **109**(1): p. 93-108.
35. Poon, M.T.C., C.L.M. Sudlow, J.D. Figueroa, and P.M. Brennan, *Longer-term (>= 2 years) survival in patients with glioblastoma in population-based studies pre- and post-2005: a systematic review and meta-analysis*. Sci Rep, 2020. **10**(1): p. 11622.

36. Fernandes, C., A. Costa, L. Osorio, R.C. Lago, P. Linhares, B. Carvalho, and C. Caeiro, *Current Standards of Care in Glioblastoma Therapy*, in *Glioblastoma*, S. De Vleeschouwer, Editor. 2017: Brisbane (AU). p. 197-241.
37. Cobbs, C.S., L. Harkins, M. Samanta, G.Y. Gillespie, S. Bharara, P.H. King, L.B. Nabors, C.G. Cobbs, and W.J. Britt, *Human cytomegalovirus infection and expression in human malignant glioma*. *Cancer Res*, 2002. **62**(12): p. 3347-50.
38. Maleki, F., Z.A. Sadigh, F. Sadeghi, A. Muhammadnejad, M. Farahmand, M. Parvin, and R. Shirkoohi, *Human cytomegalovirus infection in Iranian glioma patients correlates with aging and tumor aggressiveness*. *J Med Virol*, 2020. **92**(8): p. 1266-1276.
39. Mitchell, D.A., W. Xie, R. Schmittling, C. Learn, A. Friedman, R.E. McLendon, and J.H. Sampson, *Sensitive detection of human cytomegalovirus in tumors and peripheral blood of patients diagnosed with glioblastoma*. *Neuro Oncol*, 2008. **10**(1): p. 10-8.
40. Scheurer, M.E., M.L. Bondy, K.D. Aldape, T. Albrecht, and R. El-Zein, *Detection of human cytomegalovirus in different histological types of gliomas*. *Acta Neuropathol*, 2008. **116**(1): p. 79-86.
41. Rahbar, A., A. Orrego, I. Peredo, M. Dzabic, N. Wolmer-Solberg, K. Straat, G. Stragliotto, and C. Soderberg-Naucler, *Human cytomegalovirus infection levels in glioblastoma multiforme are of prognostic value for survival*. *J Clin Virol*, 2013. **57**(1): p. 36-42.
42. Libard, S., S.N. Popova, R.M. Amini, V. Karja, T. Pietilainen, K.M. Hamalainen, C. Sundstrom, G. Hesselager, M. Bergqvist, S. Ekman, M. Zetterling, A. Smits, P. Nilsson, S. Pfeifer, T.D. de Stahl, G. Enblad, F. Ponten, and I. Alafuzoff, *Human cytomegalovirus tegument protein pp65 is detected in all intra- and extra-axial brain tumours independent of the tumour type or grade*. *PLoS One*, 2014. **9**(9): p. e108861.
43. Bhattacharjee, B., N. Renzette, and T.F. Kowalik, *Genetic analysis of cytomegalovirus in malignant gliomas*. *J Virol*, 2012. **86**(12): p. 6815-24.
44. Ranganathan, P., P.A. Clark, J.S. Kuo, M.S. Salamat, and R.F. Kalejta, *Significant association of multiple human cytomegalovirus genomic Loci with glioblastoma multiforme samples*. *J Virol*, 2012. **86**(2): p. 854-64.
45. Lucas, K.G., L. Bao, R. Bruggeman, K. Dunham, and C. Specht, *The detection of CMV pp65 and IE1 in glioblastoma multiforme*. *J Neurooncol*, 2011. **103**(2): p. 231-8.
46. Lau, S.K., Y.Y. Chen, W.G. Chen, D.J. Diamond, A.N. Mamelak, J.A. Zaia, and L.M. Weiss, *Lack of association of cytomegalovirus with human brain tumors*. *Mod Pathol*, 2005. **18**(6): p. 838-43.

47. Baumgarten, P., M. Michaelis, F. Rothweiler, T. Starzetz, H.F. Rabenau, A. Berger, L. Jennewein, A.K. Braczynski, K. Franz, V. Seifert, J.P. Steinbach, R. Allwinn, M. Mittelbronn, and J. Cinatl, Jr., *Human cytomegalovirus infection in tumor cells of the nervous system is not detectable with standardized pathologico-virological diagnostics*. *Neuro Oncol*, 2014. **16**(11): p. 1469-77.
48. Foster, H., K. Piper, L. DePledge, H.F. Li, J. Scanlan, Y. Jae-Guen, M. Boeckh, and C. Cobbs, *Human cytomegalovirus seropositivity is associated with decreased survival in glioblastoma patients*. *Neurooncol Adv*, 2019. **1**(1): p. vdz020.
49. Stragliotto, G., M.R. Pantalone, A. Rahbar, J. Bartek, and C. Soderberg-Naucler, *Valganciclovir as Add-on to Standard Therapy in Glioblastoma Patients*. *Clin Cancer Res*, 2020. **26**(15): p. 4031-4039.
50. Stragliotto, G., A. Rahbar, N.W. Solberg, A. Lilja, C. Taher, A. Orrego, B. Bjurman, C. Tammik, P. Skarman, I. Peredo, and C. Soderberg-Naucler, *Effects of valganciclovir as an add-on therapy in patients with cytomegalovirus-positive glioblastoma: a randomized, double-blind, hypothesis-generating study*. *Int J Cancer*, 2013. **133**(5): p. 1204-13.
51. Batich, K.A., E.A. Reap, G.E. Archer, L. Sanchez-Perez, S.K. Nair, R.J. Schmittling, P. Norberg, W. Xie, J.E. Herndon, 2nd, P. Healy, R.E. McLendon, A.H. Friedman, H.S. Friedman, D. Bigner, G. Vlahovic, D.A. Mitchell, and J.H. Sampson, *Long-term Survival in Glioblastoma with Cytomegalovirus pp65-Targeted Vaccination*. *Clin Cancer Res*, 2017. **23**(8): p. 1898-1909.
52. Gomez Perdiguero, E., K. Klapproth, C. Schulz, K. Busch, E. Azzoni, L. Crozet, H. Garner, C. Trouillet, M.F. de Bruijn, F. Geissmann, and H.R. Rodewald, *Tissue-resident macrophages originate from yolk-sac-derived erythro-myeloid progenitors*. *Nature*, 2015. **518**(7540): p. 547-51.
53. Mc Carthy, D.J., M. Malhotra, A.M. O'Mahony, J.F. Cryan, and C.M. O'Driscoll, *Nanoparticles and the blood-brain barrier: advancing from in-vitro models towards therapeutic significance*. *Pharm Res*, 2015. **32**(4): p. 1161-85.
54. Sweeney, M.D., Z. Zhao, A. Montagne, A.R. Nelson, and B.V. Zlokovic, *Blood-Brain Barrier: From Physiology to Disease and Back*. *Physiol Rev*, 2019. **99**(1): p. 21-78.
55. Rochfort, K.D. and P.M. Cummins, *The blood-brain barrier endothelium: a target for pro-inflammatory cytokines*. *Biochem Soc Trans*, 2015. **43**(4): p. 702-6.
56. Liddelow, S.A., K.A. Guttenplan, L.E. Clarke, F.C. Bennett, C.J. Bohlen, L. Schirmer, M.L. Bennett, A.E. Munch, W.S. Chung, T.C. Peterson, D.K. Wilton, A. Frouin, B.A. Napier, N. Panicker, M. Kumar, M.S. Buckwalter,

- D.H. Rowitch, V.L. Dawson, T.M. Dawson, B. Stevens, and B.A. Barres, *Neurotoxic reactive astrocytes are induced by activated microglia*. *Nature*, 2017. **541**(7638): p. 481-487.
57. Park, H.J., J.Y. Shin, H.N. Kim, S.H. Oh, S.K. Song, and P.H. Lee, *Mesenchymal stem cells stabilize the blood-brain barrier through regulation of astrocytes*. *Stem Cell Res Ther*, 2015. **6**: p. 187.
  58. Yang, Y., E.Y. Estrada, J.F. Thompson, W. Liu, and G.A. Rosenberg, *Matrix metalloproteinase-mediated disruption of tight junction proteins in cerebral vessels is reversed by synthetic matrix metalloproteinase inhibitor in focal ischemia in rat*. *J Cereb Blood Flow Metab*, 2007. **27**(4): p. 697-709.
  59. Bohmwald, K., C.A. Andrade, N.M.S. Galvez, V.P. Mora, J.T. Munoz, and A.M. Kalergis, *The Causes and Long-Term Consequences of Viral Encephalitis*. *Front Cell Neurosci*, 2021. **15**: p. 755875.
  60. Liu, H., K. Qiu, Q. He, Q. Lei, and W. Lu, *Mechanisms of Blood-Brain Barrier Disruption in Herpes Simplex Encephalitis*. *J Neuroimmune Pharmacol*, 2019. **14**(2): p. 157-172.
  61. Atluri, V.S., M. Hidalgo, T. Samikkannu, K.R. Kurapati, R.D. Jayant, V. Sagar, and M.P. Nair, *Effect of human immunodeficiency virus on blood-brain barrier integrity and function: an update*. *Front Cell Neurosci*, 2015. **9**: p. 212.
  62. Reuter, J.D., D.L. Gomez, J.H. Wilson, and A.N. Van Den Pol, *Systemic immune deficiency necessary for cytomegalovirus invasion of the mature brain*. *J Virol*, 2004. **78**(3): p. 1473-87.
  63. Moir, R.D., R. Lathe, and R.E. Tanzi, *The antimicrobial protection hypothesis of Alzheimer's disease*. *Alzheimers Dement*, 2018. **14**(12): p. 1602-1614.
  64. Beason-Held, L.L., J.O. Goh, Y. An, M.A. Kraut, R.J. O'Brien, L. Ferrucci, and S.M. Resnick, *Changes in brain function occur years before the onset of cognitive impairment*. *J Neurosci*, 2013. **33**(46): p. 18008-14.
  65. Herbert, L., Weuve, J., Scherr, PA., Evans, DA., *Alzheimer disease in the United States (2010-2050) estimated using the 2010 census*. *Neurology*, 2013. **80**(19): p. 1778-1783.
  66. Sloane, P.D., S. Zimmerman, C. Suchindran, P. Reed, L. Wang, M. Boustani, and S. Sudha, *The public health impact of Alzheimer's disease, 2000-2050: potential implication of treatment advances*. *Annu Rev Public Health*, 2002. **23**: p. 213-31.
  67. Mehta, D., Jackson, R, Paul, G, Shi, J, Sabbagh, M, *Why do trials for Alzheimer's disease drugs keep failing? A discontinued drug perspective for 2010-2015*. *Expert Opin Investig Drugs*, 2017. **26**(6): p. 735-739.

68. Katan, M., Y.P. Moon, M.C. Paik, R.L. Sacco, C.B. Wright, and M.S. Elkind, *Infectious burden and cognitive function: the Northern Manhattan Study*. *Neurology*, 2013. **80**(13): p. 1209-15.
69. Lovheim, H., J. Olsson, B. Weidung, A. Johansson, S. Eriksson, G. Hallmans, and F. Elgh, *Interaction between Cytomegalovirus and Herpes Simplex Virus Type 1 Associated with the Risk of Alzheimer's Disease Development*. *J Alzheimers Dis*, 2018. **61**(3): p. 939-945.
70. Dickerson, F., C. Stallings, A. Origoni, E. Katsafanas, L.A. Schweinfurth, C.L. Savage, and R. Yolken, *Association between cytomegalovirus antibody levels and cognitive functioning in non-elderly adults*. *PLoS One*, 2014. **9**(5): p. e95510.
71. Warburg, O., *On respiratory impairment in cancer cells*. *Science*, 1956. **124**(3215): p. 269-70.
72. Warburg, O., F. Wind, and E. Negelein, *The Metabolism of Tumors in the Body*. *J Gen Physiol*, 1927. **8**(6): p. 519-30.
73. Pavlides, S., D. Whitaker-Menezes, R. Castello-Cros, N. Flomenberg, A.K. Witkiewicz, P.G. Frank, M.C. Casimiro, C. Wang, P. Fortina, S. Addya, R.G. Pestell, U.E. Martinez-Outschoorn, F. Sotgia, and M.P. Lisanti, *The reverse Warburg effect: aerobic glycolysis in cancer associated fibroblasts and the tumor stroma*. *Cell Cycle*, 2009. **8**(23): p. 3984-4001.
74. Chang, Y., P.S. Moore, and R.A. Weiss, *Human oncogenic viruses: nature and discovery*. *Philos Trans R Soc Lond B Biol Sci*, 2017. **372**(1732).
75. Kofman, A., L. Marcinkiewicz, E. Dupart, A. Lyshchev, B. Martynov, A. Ryndin, E. Kotelevskaya, J. Brown, D. Schiff, and R. Abounader, *The roles of viruses in brain tumor initiation and oncomodulation*. *J Neurooncol*, 2011. **105**(3): p. 451-66.
76. Saddawi-Konefka, R. and J.R. Crawford, *Chronic viral infection and primary central nervous system malignancy*. *J Neuroimmune Pharmacol*, 2010. **5**(3): p. 387-403.
77. Betsinger, C.N., C.S.R. Jankowski, W.A. Hofstadter, J.D. Federspiel, C.J. Otter, P.M. Jean Beltran, and I.M. Cristea, *The human cytomegalovirus protein pUL13 targets mitochondrial cristae architecture to increase cellular respiration during infection*. *Proc Natl Acad Sci U S A*, 2021. **118**(32): p. 1-12.
78. Britt, W.J., *Human cytomegalovirus: propagation, quantification, and storage*. *Curr Protoc Microbiol*, 2010. **Chapter 14**: p. Unit 14E3.1-3.17.
79. Krenzlin, H., P. Behera, V. Lorenz, C. Passaro, M. Zdioruk, M.O. Nowicki, K. Grauwet, H. Zhang, M. Skubal, H. Ito, R. Zane, M. Gutknecht, M.B. Griessl, F. Ricklefs, L. Ding, S. Peled, A. Rooj, C.D. James, C.S. Cobbs, C.H. Cook, E.A. Chiocca, and S.E. Lawler, *Cytomegalovirus promotes*

- murine glioblastoma growth via pericyte recruitment and angiogenesis.* J Clin Invest, 2019. **129**(4): p. 1671-1683.
80. Martin, K.R. and J.C. Barrett, *Reactive oxygen species as double-edged swords in cellular processes: low-dose cell signaling versus high-dose toxicity.* Hum Exp Toxicol, 2002. **21**(2): p. 71-5.
  81. Rodriguez-Sanchez, I., X.L. Schafer, M. Monaghan, and J. Munger, *The Human Cytomegalovirus UL38 protein drives mTOR-independent metabolic flux reprogramming by inhibiting TSC2.* PLoS Pathog, 2019. **15**(1): p. e1007569.
  82. Ezponda, T. and J.D. Licht, *Molecular pathways: deregulation of histone h3 lysine 27 methylation in cancer-different paths, same destination.* Clin Cancer Res, 2014. **20**(19): p. 5001-8.
  83. Ngollo, M., A. Lebert, M. Daures, G. Judes, K. Rifai, L. Dubois, J.L. Kemeny, F. Penault-Llorca, Y.J. Bignon, L. Guy, and D. Bernard-Gallon, *Global analysis of H3K27me3 as an epigenetic marker in prostate cancer progression.* BMC Cancer, 2017. **17**(1): p. 261.
  84. Fang, S., Y. Shen, B. Chen, Y. Wu, L. Jia, Y. Li, Y. Zhu, Y. Yan, M. Li, R. Chen, L. Guo, X. Chen, and Q. Chen, *H3K27me3 induces multidrug resistance in small cell lung cancer by affecting HOXA1 DNA methylation via regulation of the lncRNA HOTAIR.* Ann Transl Med, 2018. **6**(22): p. 440.
  85. Lin, B., H. Lee, J.G. Yoon, A. Madan, E. Wayner, S. Tonning, P. Hothi, B. Schroeder, I. Ulasov, G. Foltz, L. Hood, and C. Cobbs, *Global analysis of H3K4me3 and H3K27me3 profiles in glioblastoma stem cells and identification of SLC17A7 as a bivalent tumor suppressor gene.* Oncotarget, 2015. **6**(7): p. 5369-81.
  86. Lawler, S.E., *Cytomegalovirus and glioblastoma; controversies and opportunities.* J Neurooncol, 2015. **123**(3): p. 465-71.
  87. Stragliotto, G., M.R. Pantalone, A. Rahbar, and C. Soderberg-Naucler, *Valganciclovir as Add-On to Standard Therapy in Secondary Glioblastoma.* Microorganisms, 2020. **8**(10).
  88. Monk, C.H. and K.J. Zwezdaryk, *Host Mitochondrial Requirements of Cytomegalovirus Replication.* Curr Clin Microbiol Rep, 2020. **7**(4): p. 115-123.
  89. Xi, Y., S. Harwood, L.M. Wise, and J.G. Purdy, *Human Cytomegalovirus pUL37x1 Is Important for Remodeling of Host Lipid Metabolism.* J Virol, 2019. **93**(21): p. 1-19.
  90. Marin-Valencia, I., C. Yang, T. Mashimo, S. Cho, H. Baek, X.L. Yang, K.N. Rajagopalan, M. Maddie, V. Vemireddy, Z. Zhao, L. Cai, L. Good, B.P. Tu, K.J. Hatanpaa, B.E. Mickey, J.M. Mates, J.M. Pascual, E.A. Maher, C.R. Malloy, R.J. Deberardinis, and R.M. Bachoo, *Analysis of tumor metabolism*

- reveals mitochondrial glucose oxidation in genetically diverse human glioblastomas in the mouse brain in vivo.* Cell Metab, 2012. **15**(6): p. 827-37.
91. Maher, E.A., I. Marin-Valencia, R.M. Bachoo, T. Mashimo, J. Raisanen, K.J. Hatanpaa, A. Jindal, F.M. Jeffrey, C. Choi, C. Madden, D. Mathews, J.M. Pascual, B.E. Mickey, C.R. Malloy, and R.J. DeBerardinis, *Metabolism of [U-13 C]glucose in human brain tumors in vivo.* NMR Biomed, 2012. **25**(11): p. 1234-44.
  92. Sighel, D., M. Notarangelo, S. Aibara, A. Re, G. Ricci, M. Guida, A. Soldano, V. Adami, C. Ambrosini, F. Broso, E.F. Rosatti, S. Longhi, M. Buccarelli, Q.G. D'Alessandris, S. Giannetti, S. Pacioni, L. Ricci-Vitiani, J. Rorbach, R. Pallini, S. Roulland, A. Amunts, I. Mancini, A. Modelska, and A. Quattrone, *Inhibition of mitochondrial translation suppresses glioblastoma stem cell growth.* Cell Rep, 2021. **35**(4): p. 109024.
  93. Kumari, S., A.K. Badana, M.M. G, S. G, and R. Malla, *Reactive Oxygen Species: A Key Constituent in Cancer Survival.* Biomark Insights, 2018. **13**: p. 1-9.
  94. Liou, G.Y. and P. Storz, *Reactive oxygen species in cancer.* Free Radic Res, 2010. **44**(5): p. 479-96.
  95. Lee, S.R., K.S. Yang, J. Kwon, C. Lee, W. Jeong, and S.G. Rhee, *Reversible inactivation of the tumor suppressor PTEN by H<sub>2</sub>O<sub>2</sub>.* J Biol Chem, 2002. **277**(23): p. 20336-42.
  96. Sanzey, M., S.A. Abdul Rahim, A. Oudin, A. Dirkse, T. Kaoma, L. Vallar, C. Herold-Mende, R. Bjerkvig, A. Golebiewska, and S.P. Niclou, *Comprehensive analysis of glycolytic enzymes as therapeutic targets in the treatment of glioblastoma.* PLoS One, 2015. **10**(5): p. e0123544.
  97. de Wit, R.H., A. Mujic-Delic, J.R. van Senten, A. Fraile-Ramos, M. Siderius, and M.J. Smit, *Human cytomegalovirus encoded chemokine receptor US28 activates the HIF-1 $\alpha$ /PKM2 axis in glioblastoma cells.* Oncotarget, 2016. **7**(42): p. 67966-67985.
  98. Hjelmeland, A.B., Q. Wu, J.M. Heddleston, G.S. Choudhary, J. MacSwords, J.D. Lathia, R. McLendon, D. Lindner, A. Sloan, and J.N. Rich, *Acidic stress promotes a glioma stem cell phenotype.* Cell Death Differ, 2011. **18**(5): p. 829-40.
  99. Lai, S.W., H.J. Lin, Y.S. Liu, L.Y. Yang, and D.Y. Lu, *Monocarboxylate Transporter 4 Regulates Glioblastoma Motility and Monocyte Binding Ability.* Cancers (Basel), 2020. **12**(2).
  100. Cuyas, E., B. Corominas-Faja, and J.A. Menendez, *The nutritional phenome of EMT-induced cancer stem-like cells.* Oncotarget, 2014. **5**(12): p. 3970-82.

101. de la Cruz-Lopez, K.G., L.J. Castro-Munoz, D.O. Reyes-Hernandez, A. Garcia-Carranca, and J. Manzo-Merino, *Lactate in the Regulation of Tumor Microenvironment and Therapeutic Approaches*. Front Oncol, 2019. **9**: p. 1143.
102. Nakano, I., D. Garnier, M. Minata, and J. Rak, *Extracellular vesicles in the biology of brain tumour stem cells--Implications for inter-cellular communication, therapy and biomarker development*. Semin Cell Dev Biol, 2015. **40**: p. 17-26.
103. Seo, J.Y. and P. Cresswell, *Viperin regulates cellular lipid metabolism during human cytomegalovirus infection*. PLoS Pathog, 2013. **9**(8): p. e1003497.
104. Lin, H., S. Patel, V.S. Affleck, I. Wilson, D.M. Turnbull, A.R. Joshi, R. Maxwell, and E.A. Stoll, *Fatty acid oxidation is required for the respiration and proliferation of malignant glioma cells*. Neuro Oncol, 2017. **19**(1): p. 43-54.
105. Tardito, S., A. Oudin, S.U. Ahmed, F. Fack, O. Keunen, L. Zheng, H. Miletic, P.O. Sakariassen, A. Weinstock, A. Wagner, S.L. Lindsay, A.K. Hock, S.C. Barnett, E. Ruppin, S.H. Morkve, M. Lund-Johansen, A.J. Chalmers, R. Bjerkvig, S.P. Niclou, and E. Gottlieb, *Glutamine synthetase activity fuels nucleotide biosynthesis and supports growth of glutamine-restricted glioblastoma*. Nat Cell Biol, 2015. **17**(12): p. 1556-68.
106. Ullah, M.S., A.J. Davies, and A.P. Halestrap, *The plasma membrane lactate transporter MCT4, but not MCT1, is up-regulated by hypoxia through a HIF-1alpha-dependent mechanism*. J Biol Chem, 2006. **281**(14): p. 9030-7.
107. Liu, C., P.A. Clark, J.S. Kuo, and R.F. Kalejta, *Human Cytomegalovirus-Infected Glioblastoma Cells Display Stem Cell-Like Phenotypes*. mSphere, 2017. **2**(3).
108. Hou, Y., X. Dan, M. Babbar, Y. Wei, S.G. Hasselbalch, D.L. Croteau, and V.A. Bohr, *Ageing as a risk factor for neurodegenerative disease*. Nat Rev Neurol, 2019. **15**(10): p. 565-581.
109. Dubois, B., H. Hampel, H.H. Feldman, P. Scheltens, P. Aisen, S. Andrieu, H. Bakardjian, H. Benali, L. Bertram, K. Blennow, K. Broich, E. Cavedo, S. Crutch, J.F. Dartigues, C. Duyckaerts, S. Epelbaum, G.B. Frisoni, S. Gauthier, R. Genthon, A.A. Gouw, M.O. Habert, D.M. Holtzman, M. Kivipelto, S. Lista, J.L. Molinuevo, S.E. O'Bryant, G.D. Rabinovici, C. Rowe, S. Salloway, L.S. Schneider, R. Sperling, M. Teichmann, M.C. Carrillo, J. Cummings, C.R. Jack, Jr., G. Proceedings of the Meeting of the International Working, A.D. the American Alzheimer's Association on "The Preclinical State of, July, and U.S.A. Washington Dc, *Preclinical Alzheimer's disease: Definition, natural history, and diagnostic criteria*. Alzheimers Dement, 2016. **12**(3): p. 292-323.

110. Guzman-Velez, E., I. Diez, D. Schoemaker, E. Pardilla-Delgado, C. Vila-Castelar, J.T. Fox-Fuller, A. Baena, R.A. Sperling, K.A. Johnson, F. Lopera, J. Sepulcre, and Y.T. Quiroz, *Amyloid-beta and tau pathologies relate to distinctive brain dysconnectomics in preclinical autosomal-dominant Alzheimer's disease*. Proc Natl Acad Sci U S A, 2022. **119**(15): p. e2113641119.
111. Harris, S.A. and E.A. Harris, *Herpes Simplex Virus Type 1 and Other Pathogens are Key Causative Factors in Sporadic Alzheimer's Disease*. J Alzheimers Dis, 2015. **48**(2): p. 319-53.
112. Zhao, J., W. Bi, S. Xiao, X. Lan, X. Cheng, J. Zhang, D. Lu, W. Wei, Y. Wang, H. Li, Y. Fu, and L. Zhu, *Neuroinflammation induced by lipopolysaccharide causes cognitive impairment in mice*. Sci Rep, 2019. **9**(1): p. 5790.
113. Hritcu, L., A. Ciobica, M. Stefan, M. Mihasan, L. Palamiuc, and T. Nabeshima, *Spatial memory deficits and oxidative stress damage following exposure to lipopolysaccharide in a rodent model of Parkinson's disease*. Neurosci Res, 2011. **71**(1): p. 35-43.
114. Kahn, M.S., D. Kranjac, C.A. Alonzo, J.H. Haase, R.O. Cedillos, K.A. McLinden, G.W. Boehm, and M.J. Chumley, *Prolonged elevation in hippocampal Abeta and cognitive deficits following repeated endotoxin exposure in the mouse*. Behav Brain Res, 2012. **229**(1): p. 176-84.
115. Kranjac, D., K.A. McLinden, L.E. Deodati, M.R. Papini, M.J. Chumley, and G.W. Boehm, *Peripheral bacterial endotoxin administration triggers both memory consolidation and reconsolidation deficits in mice*. Brain Behav Immun, 2012. **26**(1): p. 109-21.
116. McLinden, K.A., D. Kranjac, L.E. Deodati, M. Kahn, M.J. Chumley, and G.W. Boehm, *Age exacerbates sickness behavior following exposure to a viral mimetic*. Physiol Behav, 2012. **105**(5): p. 1219-25.
117. Tarr, A.J., K.A. McLinden, D. Kranjac, R.A. Kohman, W. Amaral, and G.W. Boehm, *The effects of age on lipopolysaccharide-induced cognitive deficits and interleukin-1beta expression*. Behav Brain Res, 2011. **217**(2): p. 481-5.
118. Batista, C.R.A., G.F. Gomes, E. Candelario-Jalil, B.L. Fiebich, and A.C.P. de Oliveira, *Lipopolysaccharide-Induced Neuroinflammation as a Bridge to Understand Neurodegeneration*. Int J Mol Sci, 2019. **20**(9).
119. Lurain, N.S., B.A. Hanson, J. Martinson, S.E. Leurgans, A.L. Landay, D.A. Bennett, and J.A. Schneider, *Virological and immunological characteristics of human cytomegalovirus infection associated with Alzheimer disease*. J Infect Dis, 2013. **208**(4): p. 564-72.
120. Hoehl, S., A. Berger, S. Ciesek, and H.F. Rabenau, *Thirty years of CMV seroprevalence-a longitudinal analysis in a German university hospital*. Eur J Clin Microbiol Infect Dis, 2020. **39**(6): p. 1095-1102.

121. Holtappels, R., M.F. Pahl-Seibert, D. Thomas, and M.J. Reddehase, *Enrichment of immediate-early 1 (m123/pp89) peptide-specific CD8 T cells in a pulmonary CD62L(lo) memory-effector cell pool during latent murine cytomegalovirus infection of the lungs*. J Virol, 2000. **74**(24): p. 11495-503.
122. Bate, S.L., S.C. Dollard, and M.J. Cannon, *Cytomegalovirus seroprevalence in the United States: the national health and nutrition examination surveys, 1988-2004*. Clin Infect Dis, 2010. **50**(11): p. 1439-47.
123. Barnes, L.L., A.W. Capuano, A.E. Aiello, A.D. Turner, R.H. Yolken, E.F. Torrey, and D.A. Bennett, *Cytomegalovirus infection and risk of Alzheimer disease in older black and white individuals*. J Infect Dis, 2015. **211**(2): p. 230-7.
124. Lee, K.H., D.E. Kwon, K. Do Han, Y. La, and S.H. Han, *Association between cytomegalovirus end-organ diseases and moderate-to-severe dementia: a population-based cohort study*. BMC Neurol, 2020. **20**(1): p. 216.
125. Warren-Gash, C., H.J. Forbes, E. Williamson, J. Breuer, A.C. Hayward, A. Mavrodaris, B.H. Ridha, M.N. Rossor, S.L. Thomas, and L. Smeeth, *Human herpesvirus infections and dementia or mild cognitive impairment: a systematic review and meta-analysis*. Sci Rep, 2019. **9**(1): p. 4743.
126. Crowe, W.E., L.M. Maglova, P. Ponka, and J.M. Russell, *Human cytomegalovirus-induced host cell enlargement is iron dependent*. Am J Physiol Cell Physiol, 2004. **287**(4): p. C1023-30.
127. Taisne, C., M. Lussignol, E. Hernandez, A. Moris, L. Mouna, and A. Esclatine, *Human cytomegalovirus hijacks the autophagic machinery and LC3 homologs in order to optimize cytoplasmic envelopment of mature infectious particles*. Sci Rep, 2019. **9**(1): p. 4560.
128. Harrison, M.A.A., E.M. Hochreiner, B.P. Benjamin, S.E. Lawler, and K.J. Zwezdaryk, *Metabolic Reprogramming of Glioblastoma Cells during HCMV Infection Induces Secretome-Mediated Paracrine Effects in the Microenvironment*. Viruses, 2022. **14**(1).
129. Saffran, H.A., J.M. Pare, J.A. Corcoran, S.K. Weller, and J.R. Smiley, *Herpes simplex virus eliminates host mitochondrial DNA*. EMBO Rep, 2007. **8**(2): p. 188-93.
130. Vastag, L., E. Koyuncu, S.L. Grady, T.E. Shenk, and J.D. Rabinowitz, *Divergent effects of human cytomegalovirus and herpes simplex virus-1 on cellular metabolism*. PLoS Pathog, 2011. **7**(7): p. e1002124.
131. Cai, H., W.N. Cong, S. Ji, S. Rothman, S. Maudsley, and B. Martin, *Metabolic dysfunction in Alzheimer's disease and related neurodegenerative disorders*. Curr Alzheimer Res, 2012. **9**(1): p. 5-17.

132. Muddapu, V.R., S.A.P. Dharshini, V.S. Chakravarthy, and M.M. Gromiha, *Neurodegenerative Diseases - Is Metabolic Deficiency the Root Cause?* Front Neurosci, 2020. **14**: p. 213.
133. Kim, G.H., J.E. Kim, S.J. Rhie, and S. Yoon, *The Role of Oxidative Stress in Neurodegenerative Diseases*. Exp Neurobiol, 2015. **24**(4): p. 325-40.
134. Li, J., W. O. W. Li, Z.G. Jiang, and H.A. Ghanbari, *Oxidative stress and neurodegenerative disorders*. Int J Mol Sci, 2013. **14**(12): p. 24438-75.
135. Ashleigh, T., R.H. Swerdlow, and M.F. Beal, *The role of mitochondrial dysfunction in Alzheimer's disease pathogenesis*. Alzheimers Dement, 2022.
136. Wilkins, H.M., B.R. Troutwine, B.W. Menta, S.J. Manley, T.A. Strobe, C.R. Lysaker, and R.H. Swerdlow, *Mitochondrial Membrane Potential Influences Amyloid-beta Protein Precursor Localization and Amyloid-beta Secretion*. J Alzheimers Dis, 2022. **85**(1): p. 381-394.
137. Swerdlow, R.H., *The mitochondrial hypothesis: Dysfunction, bioenergetic defects, and the metabolic link to Alzheimer's disease*. Int Rev Neurobiol, 2020. **154**: p. 207-233.
138. Zurbach, K.A., T. Moghbeli, and C.M. Snyder, *Resolving the titer of murine cytomegalovirus by plaque assay using the M2-10B4 cell line and a low viscosity overlay*. Virol J, 2014. **11**: p. 71.
139. Brune, W., H. Hengel, and U.H. Koszinowski, *A mouse model for cytomegalovirus infection*. Curr Protoc Immunol, 2001. **Chapter 19**: p. Unit 19 7.
140. Swonger, A.K. and R.H. Rech, *Serotonergic and cholinergic involvement in habituation of activity and spontaneous alternation of rats in a Y maze*. J Comp Physiol Psychol, 1972. **81**(3): p. 509-22.
141. Jarvik, M.E. and R. Kopp, *An improved one-trial passive avoidance learning situation*. Psychol Rep, 1967. **21**(1): p. 221-4.
142. Woolfe, G. and A.D. Macdonald, *THE EVALUATION OF THE ANALGESIC ACTION OF PETHIDINE HYDROCHLORIDE (DEMEROL)*. Journal of Pharmacology and Experimental Therapeutics, 1944. **80**(3): p. 300.
143. Calvo, B., F. Rubio, M. Fernandez, and P. Tranque, *Dissociation of neonatal and adult mice brain for simultaneous analysis of microglia, astrocytes and infiltrating lymphocytes by flow cytometry*. IBRO Rep, 2020. **8**: p. 36-47.
144. Norton, E.B., D.L. Bauer, W.C. Weldon, M.S. Oberste, L.B. Lawson, and J.D. Clements, *The novel adjuvant dmLT promotes dose sparing, mucosal immunity and longevity of antibody responses to the inactivated polio vaccine in a murine model*. Vaccine, 2015. **33**(16): p. 1909-15.

145. Sakamuri, S.S., V.N. Sure, L. Kolli, W.R. Evans, J.A. Sperling, G.J. Bix, X. Wang, D.N. Atochin, W.L. Murfee, R. Mostany, and P.V. Katakam, *Aging related impairment of brain microvascular bioenergetics involves oxidative phosphorylation and glycolytic pathways*. *J Cereb Blood Flow Metab*, 2022. **42**(8): p. 1410-1424.
146. Kline, K.A. and D.M. Bowdish, *Infection in an aging population*. *Curr Opin Microbiol*, 2016. **29**: p. 63-7.
147. Campbell, A.E., V.J. Cavanaugh, and J.S. Slater, *The salivary glands as a privileged site of cytomegalovirus immune evasion and persistence*. *Med Microbiol Immunol*, 2008. **197**(2): p. 205-13.
148. Stacey, M.A., M. Marsden, E.C. Wang, G.W. Wilkinson, and I.R. Humphreys, *IL-10 restricts activation-induced death of NK cells during acute murine cytomegalovirus infection*. *J Immunol*, 2011. **187**(6): p. 2944-52.
149. Stacey, M.A., S. Clare, M. Clement, M. Marsden, J. Abdul-Karim, L. Kane, K. Harcourt, C. Brandt, C.A. Fielding, S.E. Smith, R.S. Wash, S.G. Brias, G. Stack, G. Notley, E.L. Cambridge, C. Isherwood, A.O. Speak, Z. Johnson, W. Ferlin, S.A. Jones, P. Kellam, and I.R. Humphreys, *The antiviral restriction factor IFN-induced transmembrane protein 3 prevents cytokine-driven CMV pathogenesis*. *J Clin Invest*, 2017. **127**(4): p. 1463-1474.
150. Wang, D., W. Bresnahan, and T. Shenk, *Human cytomegalovirus encodes a highly specific RANTES decoy receptor*. *Proc Natl Acad Sci U S A*, 2004. **101**(47): p. 16642-7.
151. Caldeira-Dantas, S., T. Furmanak, C. Smith, M. Quinn, L.Y. Teos, A. Ertel, D. Kurup, M. Tandon, I. Alevizos, and C.M. Snyder, *The Chemokine Receptor CXCR3 Promotes CD8(+) T Cell Accumulation in Uninfected Salivary Glands but Is Not Necessary after Murine Cytomegalovirus Infection*. *J Immunol*, 2018. **200**(3): p. 1133-1145.
152. Vom Berg, J., S. Prokop, K.R. Miller, J. Obst, R.E. Kalin, I. Lopategui-Cabezas, A. Wegner, F. Mair, C.G. Schipke, O. Peters, Y. Winter, B. Becher, and F.L. Heppner, *Inhibition of IL-12/IL-23 signaling reduces Alzheimer's disease-like pathology and cognitive decline*. *Nat Med*, 2012. **18**(12): p. 1812-9.
153. Vacinova, G., D. Vejrazkova, R. Rusina, I. Holmerova, H. Vankova, E. Jarolimova, J. Vcelak, B. Bendlova, and M. Vankova, *Regulated upon activation, normal T cell expressed and secreted (RANTES) levels in the peripheral blood of patients with Alzheimer's disease*. *Neural Regen Res*, 2021. **16**(4): p. 796-800.
154. Wilkins, H.M. and R.H. Swerdlow, *Mitochondrial links between brain aging and Alzheimer's disease*. *Transl Neurodegener*, 2021. **10**(1): p. 33.

155. Gao, F., B. Zuo, Y. Wang, S. Li, J. Yang, and D. Sun, *Protective function of exosomes from adipose tissue-derived mesenchymal stem cells in acute kidney injury through SIRT1 pathway*. *Life Sci*, 2020. **255**: p. 117719.
156. Mooradian, A.D., H.C. Chung, and G.N. Shah, *GLUT-1 expression in the cerebra of patients with Alzheimer's disease*. *Neurobiol Aging*, 1997. **18**(5): p. 469-74.
157. McDonald, C.J., Z.J. Blankenheim, and L.R. Drewes, *Brain Endothelial Cells: Metabolic Flux and Energy Metabolism*. *Handb Exp Pharmacol*, 2022. **273**: p. 59-79.
158. Zlokovic, B.V., *Neurovascular pathways to neurodegeneration in Alzheimer's disease and other disorders*. *Nat Rev Neurosci*, 2011. **12**(12): p. 723-38.
159. Herholz, K., E. Salmon, D. Perani, J.C. Baron, V. Holthoff, L. Frolich, P. Schonknecht, K. Ito, R. Mielke, E. Kalbe, G. Zundorf, X. Delbeuck, O. Pelati, D. Anchisi, F. Fazio, N. Kerrouche, B. Desgranges, F. Eustache, B. Beuthien-Baumann, C. Menzel, J. Schroder, T. Kato, Y. Arahata, M. Henze, and W.D. Heiss, *Discrimination between Alzheimer dementia and controls by automated analysis of multicenter FDG PET*. *Neuroimage*, 2002. **17**(1): p. 302-16.
160. Mosconi, L., V. Berti, L. Glodzik, A. Pupi, S. De Santi, and M.J. de Leon, *Pre-clinical detection of Alzheimer's disease using FDG-PET, with or without amyloid imaging*. *J Alzheimers Dis*, 2010. **20**(3): p. 843-54.
161. Marcus, C., E. Mena, and R.M. Subramaniam, *Brain PET in the diagnosis of Alzheimer's disease*. *Clin Nucl Med*, 2014. **39**(10): p. e413-22; quiz e423-6.
162. Andersen, J.V., A. Schousboe, and A. Verkhratsky, *Astrocyte energy and neurotransmitter metabolism in Alzheimer's disease: Integration of the glutamate/GABA-glutamine cycle*. *Prog Neurobiol*, 2022. **217**: p. 102331.
163. Brizic, I., B. Susak, M. Arapovic, P.C. Huszthy, L. Hirsil, D. Kvestak, V. Juranic Lisnic, M. Golemac, E. Pernjak Pugel, J. Tomac, A. Oxenius, W.J. Britt, J. Arapovic, A. Krmpotic, and S. Jonjic, *Brain-resident memory CD8(+) T cells induced by congenital CMV infection prevent brain pathology and virus reactivation*. *Eur J Immunol*, 2018. **48**(6): p. 950-964.
164. Esquivel, N., Y. Garcia, B. Lores, M. Gutierrez, and C. Rodriguez, *Characterization of aged male BALB/cenp mice as a model of dementia*. *Lab Anim Res*, 2020. **36**: p. 7.
165. Yang, C., K.E. Hawkins, S. Dore, and E. Candelario-Jalil, *Neuroinflammatory mechanisms of blood-brain barrier damage in ischemic stroke*. *Am J Physiol Cell Physiol*, 2019. **316**(2): p. C135-C153.

166. Tan, M.S., J.T. Yu, T. Jiang, X.C. Zhu, H.S. Guan, and L. Tan, *IL12/23 p40 inhibition ameliorates Alzheimer's disease-associated neuropathology and spatial memory in SAMP8 mice*. J Alzheimers Dis, 2014. **38**(3): p. 633-46.
167. Carr, J.A., J.A. Rogerson, M.J. Mulqueen, N.A. Roberts, and A.A. Nash, *The role of endogenous interleukin-12 in resistance to murine cytomegalovirus (MCMV) infection and a novel action for endogenous IL-12 p40*. J Interferon Cytokine Res, 1999. **19**(10): p. 1145-52.
168. Simon, C.O., C.K. Seckert, D. Dreis, M.J. Reddehase, and N.K. Grzimek, *Role for tumor necrosis factor alpha in murine cytomegalovirus transcriptional reactivation in latently infected lungs*. J Virol, 2005. **79**(1): p. 326-40.
169. Cook, C.H., J. Trgovcich, P.D. Zimmerman, Y. Zhang, and D.D. Sedmak, *Lipopolysaccharide, tumor necrosis factor alpha, or interleukin-1beta triggers reactivation of latent cytomegalovirus in immunocompetent mice*. J Virol, 2006. **80**(18): p. 9151-8.
170. Hemmersbach-Miller, M., B.D. Alexander, C.F. Pieper, and K.E. Schmader, *Age matters: older age as a risk factor for CMV reactivation in the CMV serostatus-positive kidney transplant recipient*. Eur J Clin Microbiol Infect Dis, 2020. **39**(3): p. 455-463.
171. Winkler, E.A., Y. Nishida, A.P. Sagare, S.V. Rege, R.D. Bell, D. Perlmutter, J.D. Sengillo, S. Hillman, P. Kong, A.R. Nelson, J.S. Sullivan, Z. Zhao, H.J. Meiselman, R.B. Wendy, J. Soto, E.D. Abel, J. Makshanoff, E. Zuniga, D.C. De Vivo, and B.V. Zlokovic, *GLUT1 reductions exacerbate Alzheimer's disease vasculo-neuronal dysfunction and degeneration*. Nat Neurosci, 2015. **18**(4): p. 521-530.
172. Pervaiz, I., F.T. Zahra, C.M. Mikelis, and A.J. Al-Ahmad, *An in vitro model of glucose transporter 1 deficiency syndrome at the blood-brain barrier using induced pluripotent stem cells*. J Neurochem, 2022. **162**(6): p. 483-500.
173. Wang, Q., X. Huang, Y. Su, G. Yin, S. Wang, B. Yu, H. Li, J. Qi, H. Chen, W. Zeng, K. Zhang, A. Verkhatsky, J. Niu, and C. Yi, *Activation of Wnt/beta-catenin pathway mitigates blood-brain barrier dysfunction in Alzheimer's disease*. Brain, 2022.
174. Angelova, M., K. Zvezdaryk, M. Ferris, B. Shan, C.A. Morris, and D.E. Sullivan, *Human cytomegalovirus infection dysregulates the canonical Wnt/beta-catenin signaling pathway*. PLoS Pathog, 2012. **8**(10): p. e1002959.
175. Zvezdaryk, K.J., J.A. Combs, C.A. Morris, and D.E. Sullivan, *Regulation of Wnt/beta-catenin signaling by herpesviruses*. World J Virol, 2016. **5**(4): p. 144-154.

176. Manczak, M. and P.H. Reddy, *Abnormal interaction of VDAC1 with amyloid beta and phosphorylated tau causes mitochondrial dysfunction in Alzheimer's disease*. Hum Mol Genet, 2012. **21**(23): p. 5131-46.
177. Cuadrado-Tejedor, M., M. Vilarino, F. Cabodevilla, J. Del Rio, D. Frechilla, and A. Perez-Mediavilla, *Enhanced expression of the voltage-dependent anion channel 1 (VDAC1) in Alzheimer's disease transgenic mice: an insight into the pathogenic effects of amyloid-beta*. J Alzheimers Dis, 2011. **23**(2): p. 195-206.
178. Smilansky, A., L. Dangoor, I. Nakdimon, D. Ben-Hail, D. Mizrahi, and V. Shoshan-Barmatz, *The Voltage-dependent Anion Channel 1 Mediates Amyloid beta Toxicity and Represents a Potential Target for Alzheimer Disease Therapy*. J Biol Chem, 2015. **290**(52): p. 30670-83.
179. Pastorino, J.G., J.B. Hoek, and N. Shulga, *Activation of glycogen synthase kinase 3beta disrupts the binding of hexokinase II to mitochondria by phosphorylating voltage-dependent anion channel and potentiates chemotherapy-induced cytotoxicity*. Cancer Res, 2005. **65**(22): p. 10545-54.
180. De Miranda, B.R., E.M. Rocha, S.L. Castro, and J.T. Greenamyre, *Protection from alpha-Synuclein induced dopaminergic neurodegeneration by overexpression of the mitochondrial import receptor TOM20*. NPJ Parkinsons Dis, 2020. **6**(1): p. 38.
181. Sakamuri, S., V.N. Sure, L. Kolli, N. Liu, W.R. Evans, J.A. Sperling, D.W. Busija, X. Wang, S.H. Lindsey, W.L. Murfee, R. Mostany, and P.V.G. Katakam, *Glycolytic and Oxidative Phosphorylation Defects Precede the Development of Senescence in Primary Human Brain Microvascular Endothelial Cells*. Geroscience, 2022. **44**(4): p. 1975-1994.
182. Divakaruni, A.S. and M.D. Brand, *The regulation and physiology of mitochondrial proton leak*. Physiology (Bethesda), 2011. **26**(3): p. 192-205.
183. Li, X., P. Fang, W.Y. Yang, K. Chan, M. Lavalley, K. Xu, T. Gao, H. Wang, and X. Yang, *Mitochondrial ROS, uncoupled from ATP synthesis, determine endothelial activation for both physiological recruitment of patrolling cells and pathological recruitment of inflammatory cells*. Can J Physiol Pharmacol, 2017. **95**(3): p. 247-252.
184. Valko, M., D. Leibfritz, J. Moncol, M.T. Cronin, M. Mazur, and J. Telser, *Free radicals and antioxidants in normal physiological functions and human disease*. Int J Biochem Cell Biol, 2007. **39**(1): p. 44-84.
185. Zhang, X.D., Y. Wang, J.C. Wu, F. Lin, R. Han, F. Han, K. Fukunaga, and Z.H. Qin, *Down-regulation of Bcl-2 enhances autophagy activation and cell death induced by mitochondrial dysfunction in rat striatum*. J Neurosci Res, 2009. **87**(16): p. 3600-10.

186. Combs, J.A., E.B. Norton, Z.R. Saifudeen, K. Honer Zu Bentrup, P.V. Katakam, C.A. Morris, L. Myers, A. Kaur, D.E. Sullivan, and K.J. Zwezdaryk, *Human Cytomegalovirus Alters Host Cell Mitochondrial Function During Acute Infection*. J Virol, 2019.
187. Yao, J., J.R. Rettberg, L.P. Klosinski, E. Cadenas, and R.D. Brinton, *Shift in brain metabolism in late onset Alzheimer's disease: implications for biomarkers and therapeutic interventions*. Mol Aspects Med, 2011. **32**(4-6): p. 247-57.
188. Descalzi, G., V. Gao, M.Q. Steinman, A. Suzuki, and C.M. Alberini, *Lactate from astrocytes fuels learning-induced mRNA translation in excitatory and inhibitory neurons*. Commun Biol, 2019. **2**: p. 247.
189. Shwetank, H.A. Abdelsamed, E.L. Frost, H.M. Schmitz, T.E. Mockus, B.A. Youngblood, and A.E. Lukacher, *Maintenance of PD-1 on brain-resident memory CD8 T cells is antigen independent*. Immunol Cell Biol, 2017. **95**(10): p. 953-959.
190. Wakim, L.M., A. Woodward-Davis, and M.J. Bevan, *Memory T cells persisting within the brain after local infection show functional adaptations to their tissue of residence*. Proc Natl Acad Sci U S A, 2010. **107**(42): p. 17872-9.
191. Puglisi-Allegra, S., S. Cabib, A. Ebel, J. Kempf, and C. Castellano, *Passive avoidance behavior in mice: interaction between age and genotype*. Exp Aging Res, 1986. **12**(2): p. 107-9.
192. Corbet, C., E. Bastien, N. Draoui, B. Doix, L. Mignon, B.F. Jordan, A. Marchand, J.C. Vanherck, P. Chaltin, O. Schakman, H.M. Becker, O. Riant, and O. Feron, *Interruption of lactate uptake by inhibiting mitochondrial pyruvate transport unravels direct antitumor and radiosensitizing effects*. Nat Commun, 2018. **9**(1): p. 1208.
193. Vohra, R., B.I. Aldana, H. Waagepetersen, L.H. Bergersen, and M. Kolko, *Dual Properties of Lactate in Muller Cells: The Effect of GPR81 Activation*. Invest Ophthalmol Vis Sci, 2019. **60**(4): p. 999-1008.
194. Lee, Y.J., K.J. Shin, S.A. Park, K.S. Park, S. Park, K. Heo, Y.K. Seo, D.Y. Noh, S.H. Ryu, and P.G. Suh, *G-protein-coupled receptor 81 promotes a malignant phenotype in breast cancer through angiogenic factor secretion*. Oncotarget, 2016. **7**(43): p. 70898-70911.
195. Pan, B.T. and R.M. Johnstone, *Fate of the transferrin receptor during maturation of sheep reticulocytes in vitro: selective externalization of the receptor*. Cell, 1983. **33**(3): p. 967-78.
196. Harding, C., J. Heuser, and P. Stahl, *Receptor-mediated endocytosis of transferrin and recycling of the transferrin receptor in rat reticulocytes*. J Cell Biol, 1983. **97**(2): p. 329-39.

197. Wortzel, I., S. Dror, C.M. Kenific, and D. Lyden, *Exosome-Mediated Metastasis: Communication from a Distance*. Dev Cell, 2019. **49**(3): p. 347-360.
198. Yoon, T., J. Okada, M.W. Jung, and J.J. Kim, *Prefrontal cortex and hippocampus subserve different components of working memory in rats*. Learn Mem, 2008. **15**(3): p. 97-105.
199. Szibor, M., P.K. Dhandapani, E. Dufour, K.M. Holmstrom, Y. Zhuang, I. Salwig, I. Wittig, J. Heidler, Z. Gizatullina, T. Gainutdinov, C. German Mouse Clinic, H. Fuchs, V. Gailus-Durner, M.H. de Angelis, J. Nandania, V. Velagapudi, A. Wietelmann, P. Rustin, F.N. Gellerich, H.T. Jacobs, and T. Braun, *Broad AOX expression in a genetically tractable mouse model does not disturb normal physiology*. Dis Model Mech, 2017. **10**(2): p. 163-171.
200. Zhang, H., K.J.A. Davies, and H.J. Forman, *Oxidative stress response and Nrf2 signaling in aging*. Free Radic Biol Med, 2015. **88**(Pt B): p. 314-336.
201. Zuk, P.A., M. Zhu, P. Ashjian, D.A. De Ugarte, J.I. Huang, H. Mizuno, Z.C. Alfonso, J.K. Fraser, P. Benhaim, and M.H. Hedrick, *Human adipose tissue is a source of multipotent stem cells*. Mol Biol Cell, 2002. **13**(12): p. 4279-95.
202. Yu, G., Z.E. Floyd, X. Wu, Y.D. Halvorsen, and J.M. Gimble, *Isolation of human adipose-derived stem cells from lipoaspirates*. Methods Mol Biol, 2011. **702**: p. 17-27.
203. Dominici, M., K. Le Blanc, I. Mueller, I. Slaper-Cortenbach, F. Marini, D. Krause, R. Deans, A. Keating, D. Prockop, and E. Horwitz, *Minimal criteria for defining multipotent mesenchymal stromal cells. The International Society for Cellular Therapy position statement*. Cytotherapy, 2006. **8**(4): p. 315-7.
204. Bourin, P., B.A. Bunnell, L. Casteilla, M. Dominici, A.J. Katz, K.L. March, H. Redl, J.P. Rubin, K. Yoshimura, and J.M. Gimble, *Stromal cells from the adipose tissue-derived stromal vascular fraction and culture expanded adipose tissue-derived stromal/stem cells: a joint statement of the International Federation for Adipose Therapeutics and Science (IFATS) and the International Society for Cellular Therapy (ISCT)*. Cytotherapy, 2013. **15**(6): p. 641.
205. Gimble, M.J., J.A. Katz, and A.B. Bunnell, *Adipose-Derived Stem Cells for Regenerative Medicine*. Circulation Research, 2007. **100**(9): p. 1249-1260.
206. Baer, P.C. and H. Geiger, *Adipose-Derived Mesenchymal Stromal/Stem Cells: Tissue Localization, Characterization, and Heterogeneity*. Stem Cells International, 2012. **2012**(2012).
207. Kar Wey, Y., P.-M. Belinda, X. Feng, A. Wan Abu Bakar Wan, C. Jane Ru, O. Siti Zawiah, A. Mat Adenan Noor, C. Kien Hui, and S. Wan Kamarul Zaman Wan, *Phenotypic and Functional Characterization of Long-Term*

- Cryopreserved Human Adipose-derived Stem Cells*. Scientific Reports, 2015. **5**(1).
208. Zanata, L.F., A.A. Bowles, M.T. Frazier, M.J. Curley, M.B. Bunnell, M.X. Wu, M.J. Wade, M.R. Devireddy, M.J. Gimble, and M.L. Ferreira, *Effect of Cryopreservation on Human Adipose Tissue and Isolated Stromal Vascular Fraction Cells: In Vitro and In Vivo Analyses*. Plastic and Reconstructive Surgery, 2018. **141**(2): p. 232e-243e.
209. Gruber, H., S. Somayaji, F. Riley, G. Hoelscher, H. Norton, J. Ingram, and E. Hanley, *Human adipose-derived mesenchymal stem cells: serial passaging, doubling time and cell senescence*. Biotechnic & Histochemistry, 2012. **87**(4): p. 303-311.
210. Debnath, T. and L.K. Chelluri, *Standardization and quality assessment for clinical grade mesenchymal stem cells from human adipose tissue*. Hematology, Transfusion and Cell Therapy, 2019. **41**(1): p. 7-16.
211. Truong, N.C., K.H.-T. Bui, and P. Van Pham, *Characterization of Senescence of Human Adipose-Derived Stem Cells After Long-Term Expansion*. Advances in experimental medicine and biology, 2019. **1084**: p. 109.
212. Dmitrieva, R.I., I.R. Minullina, A.A. Bilibina, O.V. Tarasova, S.V. Anisimov, and A.Y. Zaritskey, *Bone marrow- and subcutaneous adipose tissue-derived mesenchymal stem cells: Differences and similarities*. Cell Cycle, 2012. **11**(2): p. 377-383.
213. Lee, R.H., B. Kim, I. Choi, H. Kim, H.S. Choi, K. Suh, Y.C. Bae, and J.S. Jung, *Characterization and Expression Analysis of Mesenchymal Stem Cells from Human Bone Marrow and Adipose Tissue*. Cellular Physiology and Biochemistry, 2004. **14**(4-6): p. 311-324.
214. Wagner, W., F. Wein, A. Seckinger, M. Frankhauser, U. Wirkner, U. Krause, J. Blake, C. Schwager, V. Eckstein, W. Ansorge, and A.D. Ho, *Comparative characteristics of mesenchymal stem cells from human bone marrow, adipose tissue, and umbilical cord blood*. Experimental Hematology, 2005. **33**(11): p. 1402-1416.
215. Yanxia, Z., L. Tianqing, S. Kedong, F. Xiubo, M. Xuehu, and C. Zhanfeng, *Adipose-derived stem cell: A better stem cell than BMSC*. Cell Research, 2008. **18**(S1): p. S165.
216. Oedayrajsingh-Varma, M., S.M. van Ham, M. Knippenberg, M. Helder, J. Klein-Nulend, T. Schouten, M. Ritt, and F. van Milligen, *Adipose tissue-derived mesenchymal stem cell yield and growth characteristics are affected by the tissue-harvesting procedure*. Cytotherapy, 2006. **8**(2): p. 166-177.
217. Frazier, T.P., J.M. Gimble, J.W. Devay, H.A. Tucker, E.S. Chiu, and B.G. Rowan, *Body mass index affects proliferation and osteogenic differentiation*

- of human subcutaneous adipose tissue-derived stem cells.(Report)*. BMC Cell Biology, 2013. **14**(1).
218. Kolaparthi, L., S. Sanivarapu, S. Moogla, and R. Kutcham, *Adipose Tissue - Adequate, Accessible Regenerative Material*. Int J. Stem Cells, 2015. **8**(2): p. 121-127.
  219. Di Battista, J., W. Shebaby, O. Kizilay, E. Hamade, R. Abou Merhi, S. Mebarek, D. Abdallah, B. Badran, F. Saad, E. Abdalla, and W. Faour, *Proliferation and differentiation of human adipose-derived mesenchymal stem cells (ASCs) into osteoblastic lineage are passage dependent*. Official Journal of: The International Association of Inflammation Societies + The European Histamine Research Society, 2014. **63**(11): p. 907-917.
  220. Li, J., H. Huang, and X. Xu, *Biological and genetic characteristics of mesenchymal stem cells in vitro derived from human adipose, umbilical cord and placenta*. Int. J. Clin. Exp. Med., 2017. **10**(12): p. 16310-16318.
  221. Li, J., H. Huang, and X. Xu, *Biological characteristics and karyotyping of a new isolation method for human adipose mesenchymal stem cells in vitro*. Tissue and Cell, 2017. **49**(3): p. 376-382.
  222. Liu, G., H. Zhou, Y. Li, G. Li, L. Cui, W. Liu, and Y. Cao, *Evaluation of the viability and osteogenic differentiation of cryopreserved human adipose-derived stem cells*. Cryobiology, 2008. **57**(1): p. 18-24.
  223. Choudhery, M.S., M. Badowski, A. Muise, J. Pierce, and D.T. Harris, *Donor age negatively impacts adipose tissue-derived mesenchymal stem cell expansion and differentiation*. Journal of Translational Medicine, 2014. **12**(1).
  224. Badimon, L. and J. Cubedo, *Adipose tissue depots and inflammation: effects on plasticity and resident mesenchymal stem cell function*. Cardiovascular Research, 2017. **113**(9): p. 1064-1073.
  225. Gharibi, B. and F.J. Hughes, *Effects of medium supplements on proliferation, differentiation potential, and in vitro expansion of mesenchymal stem cells*. Stem Cells Transl Med, 2012. **1**(11): p. 771-82.
  226. Riis, S., F.M. Nielsen, C.P. Pennisi, V. Zachar, and T. Fink, *Comparative Analysis of Media and Supplements on Initiation and Expansion of Adipose-Derived Stem Cells*. STEM CELLS Translational Medicine, 2016. **5**(3): p. 314-324.
  227. Roxburgh, J., A. Metcalfe, and Y. Martin, *The effect of medium selection on adipose-derived stem cell expansion and differentiation: implications for application in regenerative medicine*. Incorporating Methods in Cell Science International Journal of Cell Culture and Biotechnology, 2016. **68**(4): p. 957-967.

228. Czaplá, J., S. Matuszczak, K. Kulik, E. WiAniewska, E. Pilny, M. Jarosz-Biej, R. Smolarczyk, T. Sirek, M.O. Zembala, M. Zembala, S. Szala, and T. CichoA, *The effect of culture media on large-scale expansion and characteristic of adipose tissue-derived mesenchymal stromal cells*. Stem Cell Research & Therapy, 2019. **10**(1).
229. Fraser, J.K., I. Wulur, Z. Alfonso, M. Zhu, and E.S. Wheeler, *Differences in stem and progenitor cell yield in different subcutaneous adipose tissue depots*. Cytotherapy, 2007. **9**(5): p. 459-467.
230. Jurgens, W., M. Oedayrajsingh-Varma, M. Helder, B. ZandiehDoulabi, T. Schouten, D. Kuik, M. Ritt, and F. Milligen, *Effect of tissue-harvesting site on yield of stem cells derived from adipose tissue: implications for cell-based therapies*. Cell and Tissue Research, 2008. **332**(3): p. 415-426.
231. Tucker, H.A. and B.A. Bunnell, *Characterization of human adipose-derived stem cells using flow cytometry*. Methods in molecular biology (Clifton, N.J.), 2011. **702**: p. 121.
232. Minteer, D., K.G. Marra, and J.P. Rubin, *Adipose-derived mesenchymal stem cells: biology and potential applications*. Advances in biochemical engineering/biotechnology, 2013. **129**: p. 59.
233. Baer, P.C., S. Kuci, M. Krause, Z. Kuci, S. Zielen, H. Geiger, P. Bader, and R. Schubert, *Comprehensive phenotypic characterization of human adipose-derived stromal/stem cells and their subsets by a high throughput technology.(Report)*. Stem Cells and Development, 2013. **22**(2): p. 330.
234. De Girolamo, L., D. Stanco, L. Salvatori, G. Coroniti, E. Arrigoni, G. Silecchia, M.A. Russo, S. Niada, E. Petrangeli, and A.T. Brini, *Stemness and Osteogenic and Adipogenic Potential are Differently Impaired in Subcutaneous and Visceral Adipose Derived Stem Cells (ASCs) Isolated from Obese Donors*. International Journal of Immunopathology and Pharmacology, 2013. **26**(1\_suppl): p. 11-21.
235. Bowles, A.C., A.L. Strong, R.M. Wise, R.C. Thomas, B.Y. Gerstein, M.F. Dutreil, R.S. Hunter, J.M. Gimble, and B.A. Bunnell, *Adipose Stromal Vascular Fraction-Mediated Improvements at Late-Stage Disease in a Murine Model of Multiple Sclerosis*. Stem Cells, 2017. **35**(2): p. 532-544.
236. Camilleri, E.T., M.P. Gustafson, A. Dudakovic, S.M. Riester, C.G. Garces, C.R. Paradise, H. Takai, M. Karperien, S. Cool, H.J. Sampen, A.N. Larson, W. Qu, J. Smith, A.B. Dietz, and A.J. van Wijnen, *Identification and validation of multiple cell surface markers of clinical-grade adipose-derived mesenchymal stromal cells as novel release criteria for good manufacturing practice-compliant production*. Stem Cell Res Ther, 2016. **7**(1): p. 107.
237. Poria Abdollah, L.Z., *Novel Negative Selection Marker CD54 Enhances Differentiation of Human Adipose-Derived Mesenchymal Stem Cells*. Journal of Clinical & Cellular Immunology, 2013.

238. Jiang, T., W. Liu, X. Lv, H. Sun, L. Zhang, Y. Liu, W.J. Zhang, Y. Cao, and G. Zhou, *Potent in vitro chondrogenesis of CD105 enriched human adipose-derived stem cells*. *Biomaterials*, 2010. **31**(13): p. 3564-3571.
239. Pham, L.H., N.B. Vu, and P. Van Pham, *The subpopulation of CD105 negative mesenchymal stem cells show strong immunomodulation capacity compared to CD105 positive mesenchymal stem cells*. *Biomedical Research and Therapy*, 2019. **6**(4): p. 3131-3140.
240. Suga, H., D. Matsumoto, H. Eto, K. Inoue, N. Aoi, H. Kato, J. Araki, and K. Yoshimura, *Functional implications of CD34 expression in human adipose-derived stem/progenitor cells.(ORIGINAL RESEARCH REPORT)(cluster of differentiation)(Report)*. *Stem Cells and Development*, 2009. **18**(8): p. 1201.
241. Choi, Y.S., G.J. Dusting, S. Stubbs, S. Arunothayaraj, X.L. Han, P. Collas, W.A. Morrison, and R.J. Dille, *Differentiation of human adipose-derived stem cells into beating cardiomyocytes*. *J Cell Mol Med*, 2010. **14**(4): p. 878-89.
242. Auxenfans, C., C. Lequeux, E. Perrusel, A. Mojallal, B. Kinikoglu, and O. Damour, *Adipose-derived stem cells (ASCs) as a source of endothelial cells in the reconstruction of endothelialized skin equivalents*. *J Tissue Eng Regen Med*, 2012. **6**(7): p. 512-8.
243. Jang, S., H.H. Cho, Y.B. Cho, J.S. Park, and H.S. Jeong, *Functional neural differentiation of human adipose tissue-derived stem cells using bFGF and forskolin*. *BMC Cell Biol*, 2010. **11**: p. 25.
244. Aurich, H., M. Sgodda, P. Kaltwasser, M. Vetter, A. Weise, T. Liehr, M. Brulport, J.G. Hengstler, M.M. Dollinger, W.E. Fleig, and B. Christ, *Hepatocyte differentiation of mesenchymal stem cells from human adipose tissue in vitro promotes hepatic integration in vivo*. *Gut*, 2009. **58**(4): p. 570-81.
245. Sakaguchi, Y., I. Sekiya, K. Yagishita, and T. Muneta, *Comparison of human stem cells derived from various mesenchymal tissues: Superiority of synovium as a cell source*. *Arthritis & Rheumatism*, 2005. **52**(8): p. 2521-2529.
246. Pachon-Pena, G., G. Yu, A. Tucker, X. Wu, J. Vendrell, B.A. Bunnell, and J. Gimble, *Stromal Stem Cells From Adipose Tissue and Bone Marrow of Age-Matched Female Donors Display Distinct Immunophenotypic Profiles*. *J. Cell. Physiol.*, 2011. **226**(3): p. 843-851.
247. De Ugarte, D.A., K. Morizono, A. Elbarbary, Z. Alfonso, P.A. Zuk, M. Zhu, J.L. Dragoo, P. Ashjian, B. Thomas, P. Benhaim, I. Chen, J. Fraser, and M.H. Hedrick, *Comparison of Multi-Lineage Cells from Human Adipose Tissue and Bone Marrow*. *Cells Tissues Organs*, 2003. **174**(3): p. 101-109.
248. Noël, D., D. Caton, S. Roche, C. Bony, S. Lehmann, L. Casteilla, C. Jorgensen, and B. Cousin, *Cell specific differences between human*

- adipose-derived and mesenchymal–stromal cells despite similar differentiation potentials*. *Experimental Cell Research*, 2008. **314**(7): p. 1575-1584.
249. Harmelen, V.V., T. Skurk, K. Röhrig, Y.M. Lee, M. Halbleib, I. Aprath-Husmann, and H. Hauner, *Effect of BMI and age on adipose tissue cellularity and differentiation capacity in women*. *International Journal of Obesity*, 2003. **27**(8): p. 889.
250. Cramer, C., E. Freisinger, R.K. Jones, D.P. Slakey, C.L. Dupin, E.R. Newsome, E.U. Alt, and R. Izadpanah, *Persistent high glucose concentrations alter the regenerative potential of mesenchymal stem cells.(Report)*. *Stem Cells and Development*, 2010. **19**(12): p. 1875.
251. Lopa, S., A. Colombini, D. Stanco, L. de Girolamo, V. Sansone, and M. Moretti, *DONOR- MATCHED MESENCHYMAL STEM CELLS FROM KNEE INFRAPATELLAR AND SUBCUTANEOUS ADIPOSE TISSUE OF OSTEOARTHRITIC DONORS DISPLAY DIFFERENTIAL CHONDROGENIC AND OSTEOGENIC COMMITMENT*. *Eur. Cells Mater.*, 2014. **27**: p. 298-311.
252. Kornicka, K., K. Marycz, K.A. Tomaszewski, M. Marędziak, and A. Śmieszek, *The Effect of Age on Osteogenic and Adipogenic Differentiation Potential of Human Adipose Derived Stromal Stem Cells ( hASCs) and the Impact of Stress Factors in the Course of the Differentiation Process*. *Oxidative Medicine and Cellular Longevity*, 2015. **2015**.
253. Siciliano, C., A. Bordin, M. Ibrahim, I. Chimenti, F. Cassiano, I. Gatto, G. Mangino, A. Coccia, S. Miglietta, D. Bastianelli, V. Petrozza, A. Calogero, G. Frati, and E. De Falco, *The adipose tissue of origin influences the biological potential of human adipose stromal cells isolated from mediastinal and subcutaneous fat depots*. *Stem Cell Research*, 2016. **17**(2): p. 342-351.
254. Prestwich, T.C. and O.A. Macdougald, *Wnt/ $\beta$ -catenin signaling in adipogenesis and metabolism*. *Current Opinion in Cell Biology*, 2007. **19**(6): p. 612-617.
255. Christodoulides, C., C. Lagathu, J.K. Sethi, and A. Vidal-Puig, *Adipogenesis and WNT signalling*. *Trends in Endocrinology & Metabolism*, 2009. **20**(1): p. 16-24.
256. Tsurutani, Y., M. Fujimoto, M. Takemoto, H. Irisuna, M. Koshizaka, S. Onishi, T. Ishikawa, M. Mezawa, P. He, S. Honjo, Y. Maezawa, Y. Saito, and K. Yokote, *The roles of transforming growth factor- $\beta$  and Smad3 signaling in adipocyte differentiation and obesity*. *Biochemical and Biophysical Research Communications*, 2011. **407**(1): p. 68-73.

257. Rana, K.G., A. Zoltan, S. Patrick, J.M. Rina, Y. Li, M.C. Heather, A.R. Yang, K. Heather, R.R. Randall, and M.S. Bruce, *Transcriptional control of preadipocyte determination by Zfp423*. *Nature*, 2010. **464**(7288): p. 619.
258. Cao, Z., R.M. Umek, and S. McKnight, *REGULATED EXPRESSION OF 3 C/EBP ISOFORMS DURING ADIPOSE CONVERSION OF 3T3-L1 CELLS*. *Genes Dev.*, 1991. **5**(9): p. 1538-1552.
259. Park, Byung o., R. Ahrends, and Mary n. Teruel, *Consecutive Positive Feedback Loops Create a Bistable Switch that Controls Preadipocyte-to-Adipocyte Conversion*. *Cell Reports*, 2012. **2**(4): p. 976-990.
260. Payne, V.A., W.-S. Au, C.E. Lowe, S.M. Rahman, J.E. Friedman, S. O'Rahilly, and J.J. Rochford, *C/EBP transcription factors regulate SREBP1c gene expression during adipogenesis*. *The Biochemical journal*, 2009. **425**(1): p. 215.
261. Wu, Z., Y. Xie, N.L. Bucher, and S.R. Farmer, *Conditional ectopic expression of C/EBP beta in NIH-3T3 cells induces PPAR gamma and stimulates adipogenesis*. *Genes & development*, 1995. **9**(19): p. 2350.
262. Wu, Z., N.L. Bucher, and S.R. Farmer, *Induction of peroxisome proliferator-activated receptor gamma during the conversion of 3T3 fibroblasts into adipocytes is mediated by C/EBPbeta, C/EBPdelta, and glucocorticoids*. *Molecular and Cellular Biology*, 1996. **16**(8): p. 4128.
263. Wu, Z., E.D. Rosen, R. Brun, S. Hauser, G. Adelmant, A.E. Troy, C. McKeon, G.J. Darlington, and B.M. Spiegelman, *Cross-Regulation of C/EBP $\alpha$  and PPAR $\gamma$  Controls the Transcriptional Pathway of Adipogenesis and Insulin Sensitivity*. *Molecular Cell*, 1999. **3**(2): p. 151-158.
264. Yun, S.-J., E.-K. Kim, D.F. Tucker, C.D. Kim, M.J. Birnbaum, and S.S. Bae, *Isoform-specific regulation of adipocyte differentiation by Akt/protein kinase B $\alpha$* . *Biochemical and Biophysical Research Communications*, 2008. **371**(1): p. 138-143.
265. Zhang, H.H., J. Huang, K. Düvel, B. Boback, S. Wu, R.M. Squillace, C.-L. Wu, and B.D. Manning, *Insulin Stimulates Adipogenesis through the Akt-TSC2-mTORC1 Pathway (TSC2-mTOR Control Adipogenesis)*. *PLoS ONE*, 2009. **4**(7): p. e6189.
266. Kim, J.E. and J. Chen, *Regulation of peroxisome proliferator-activated receptor-[gamma] activity by mammalian target of rapamycin and amino acids in adipogenesis.(Signal Transduction)*. *Diabetes*, 2004. **53**(11): p. 2748.
267. Nakae, J., T. Kitamura, Y. Kitamura, W. Biggs, K. Arden, and D. Accili, *The forkhead transcription factor Foxo1 regulates adipocyte differentiation*. *Developmental Cell*, 2003. **4**(1): p. 119.

268. Armoni, M., C. Harel, S. Karni, H. Chen, F. Bar-Yoseph, M.R. Ver, M.J. Quon, and E. Karnieli, *FOXO1 Represses Peroxisome Proliferator-activated Receptor- $\gamma$ 1 and - $\gamma$ 2 Gene Promoters in Primary Adipocytes: A NOVEL PARADIGM TO INCREASE INSULIN SENSITIVITY*. *FOXO1 Represses Peroxisome Proliferator-activated Receptor- $\gamma$ 1 and - $\gamma$ 2 Gene Promoters in Primary Adipocytes: A NOVEL PARADIGM TO INCREASE INSULIN SENSITIVITY*, 2006. **281**(29): p. 19881-19891.
269. Gimble, J.M. and F. Guilak, *Adipose- derived adult stem cells: isolation, characterization, and differentiation potential*. *Cytotherapy*, 2003, Vol.5(5), p.362-369, 2003. **5**(5): p. 362-369.
270. Bunnell, B.A., M. Flaat, C. Gagliardi, B. Patel, and C. Ripoll, *Adipose-derived stem cells: Isolation, expansion and differentiation*. *Methods*, 2008. **45**(2): p. 115-120.
271. Gimble, J.M. and B.A. Bunnell, *Adipose-derived stem cells methods and protocols*. 2011, New York : Humana Press: New York.
272. Vater, C., P. Kasten, and M. Stiehler, *Culture media for the differentiation of mesenchymal stromal cells*. *Acta Biomater*, 2011. **7**(2): p. 463-77.
273. Cawthorn, W.P., E. Scheller, and O. Macdougald, *Adipose tissue stem cells meet preadipocyte commitment: going back to the future*. *J. Lipid Res.*, 2012. **53**(2): p. 227-246.
274. Fam, T.K., A.S. Klymchenko, and M. Collot, *Recent Advances in Fluorescent Probes for Lipid Droplets*. *Materials (Basel)*, 2018. **11**(9).
275. Govender, T., L. Ramanna, I. Rawat, and F. Bux, *BODIPY staining, an alternative to the Nile Red fluorescence method for the evaluation of intracellular lipids in microalgae*. *Bioresource Technology*, 2012. **114**: p. 507-511.
276. Harris, L.-A.L.S., J.R. Skinner, and N.E. Wolins, *Imaging of Neutral Lipids and Neutral Lipid Associated Proteins*. 2013. p. 213-226.
277. Qiu, B. and M.C. Simon, *BODIPY 493/ 503 Staining of Neutral Lipid Droplets for Microscopy and Quantification by Flow Cytometry*. *Bio-protocol*, 2016. **6**(17).
278. Trujillo, M.E. and P. Scherer, *Adipose tissue-derived factors: Impact on health and disease*. *Endocr. Rev.*, 2006. **27**(7): p. 798-+.
279. Skalnikova, H., J. Motlik, S.J. Gadher, and H. Kovarova, *Mapping of the secretome of primary isolates of mammalian cells, stem cells and derived cell lines*. *Proteomics*, 2011. **11**(4): p. 691-708.
280. Abishek, I., P.F. David, B.P. Johannes, D.H. Bruce, and B. Lindsay, *Inflammatory lipid mediators in adipocyte function and obesity*. *Nature Reviews Endocrinology*, 2010. **6**(2): p. 71.

281. Zvonic, S., M. Lefevre, G. Kilroy, Z. Floyd, J.P. Delany, I. Kheterpal, A. Gravois, R. Dow, A. White, X. Wu, and J. Gimble, *Secretome of primary cultures of human adipose-derived stem cells - Modulation of serpins by adipogenesis*. Mol. Cell. Proteomics, 2007. **6**(1): p. 18-28.
282. Strong, A., J. Gimble, and B. Bunnell, *Analysis of the Pro- and Anti-Inflammatory Cytokines Secreted by Adult Stem Cells during Differentiation*. Stem Cells International, 2015. **2015**(2015).
283. Gesta, S., M. Bluher, Y. Yamamoto, A.W. Norris, J. Berndt, S. Kralisch, J. Boucher, C. Lewis, and C.R. Kahn, *Evidence for a role of developmental genes in the origin of obesity and body fat distribution.(Author abstract)*. Proceedings of the National Academy of Sciences of the United States, 2006. **103**(17): p. 6676.
284. Hocking, S.L., L.E. Wu, M. Guilhaus, D.J. Chisholm, and D.E. James, *Intrinsic depot-specific differences in the secretome of adipose tissue, preadipocytes, and adipose tissue-derived microvascular endothelial cells*. Diabetes, 2010. **59**(12): p. 3008.
285. Maury, E., K. Ehala-Aleksejev, Y. Guiot, R. Detry, A. Vandenhooft, and S.M. Brichard, *Adipokines oversecreted by omental adipose tissue in human obesity*. Am. J. Physiol.-Endocrinol. Metab., 2007. **293**(3): p. E656-E665.
286. Noriyuki, O., L.P. Jennifer, J.L. Jesse, and W. Kenneth, *Adipokines in inflammation and metabolic disease*. Nature Reviews Immunology, 2011. **11**(2): p. 85.
287. Im, G.I., Y.W. Shin, and K.B. Lee, *Do adipose tissue-derived mesenchymal stem cells have the same osteogenic and chondrogenic potential as bone marrow-derived cells? Osteoarthritis Cartilage*, 2005. **13**(10): p. 845-53.
288. Hayashi, O., Y. Katsube, M. Hirose, H. Ohgushi, and H. Ito, *Comparison of osteogenic ability of rat mesenchymal stem cells from bone marrow, periosteum, and adipose tissue*. Calcif Tissue Int, 2008. **82**(3): p. 238-47.
289. Niemeyer, P., K. Fechner, S. Milz, W. Richter, N.P. Suedkamp, A.T. Mehlhorn, S. Pearce, and P. Kasten, *Comparison of mesenchymal stem cells from bone marrow and adipose tissue for bone regeneration in a critical size defect of the sheep tibia and the influence of platelet-rich plasma*. Biomaterials, 2010. **31**(13): p. 3572-9.
290. Vishnubalaji, R., M. Al-Nbaheen, B. Kadalmani, A. Aldahmash, and T. Ramesh, *Comparative investigation of the differentiation capability of bone-marrow- and adipose-derived mesenchymal stem cells by qualitative and quantitative analysis*. Cell Tissue Res, 2012. **347**(2): p. 419-27.
291. Panetta, N.J., D.M. Gupta, and M.T. Longaker, *Bone regeneration and repair*. Curr Stem Cell Res Ther, 2010. **5**(2): p. 122-8.

292. Strong, A.L., R.S. Hunter, R.B. Jones, A.C. Bowles, M.F. Dutreil, D. Gaupp, D.J. Hayes, J.M. Gimble, B. Levi, M.A. McNulty, and B.A. Bunnell, *Obesity inhibits the osteogenic differentiation of human adipose-derived stem cells*. J Transl Med, 2016. **14**: p. 27.
293. Ding, D.C., H.L. Chou, W.T. Hung, H.W. Liu, and T.Y. Chu, *Human adipose-derived stem cells cultured in keratinocyte serum free medium: Donor's age does not affect the proliferation and differentiation capacities*. J Biomed Sci, 2013. **20**: p. 59.
294. Duan, W. and M.J. Lopez, *Effects of Cryopreservation on Canine Multipotent Stromal Cells from Subcutaneous and Infrapatellar Adipose Tissue*. Stem Cell Rev Rep, 2016. **12**(2): p. 257-68.
295. Kawagishi-Hotta, M., S. Hasegawa, T. Igarashi, T. Yamada, M. Takahashi, S. Numata, T. Kobayashi, Y. Iwata, M. Arima, N. Yamamoto, A. Yagami, S. Nakata, T. Uzawa, K. Matsunaga, K. Sugiura, and H. Akamatsu, *Enhancement of individual differences in proliferation and differentiation potentials of aged human adipose-derived stem cells*. Regen Ther, 2017. **6**: p. 29-40.
296. Grottkau, B.E. and Y. Lin, *Osteogenesis of Adipose-Derived Stem Cells*. Bone Res, 2013. **1**(2): p. 133-45.
297. Paduano, F., M. Marrelli, M. Amantea, C. Rengo, S. Rengo, M. Goldberg, G. Spagnuolo, and M. Tatullo, *Adipose Tissue as a Strategic Source of Mesenchymal Stem Cells in Bone Regeneration: A Topical Review on the Most Promising Craniomaxillofacial Applications*. Int J Mol Sci, 2017. **18**(10).
298. Shaik, S., E.C. Martin, D.J. Hayes, J.M. Gimble, and R.V. Devireddy, *Transcriptomic Profiling of Adipose Derived Stem Cells Undergoing Osteogenesis by RNA-Seq*. Sci Rep, 2019. **9**(1): p. 11800.
299. Liu, Q., L. Cen, H. Zhou, S. Yin, G. Liu, W. Liu, Y. Cao, and L. Cui, *The role of the extracellular signal-related kinase signaling pathway in osteogenic differentiation of human adipose-derived stem cells and in adipogenic transition initiated by dexamethasone*. Tissue Eng Part A, 2009. **15**(11): p. 3487-97.
300. Tsang, E.J., B. Wu, and P. Zuk, *MAPK signaling has stage-dependent osteogenic effects on human adipose-derived stem cells in vitro*. Connect Tissue Res, 2018. **59**(2): p. 129-146.
301. Lough, D.M., C. Chambers, G. Germann, R. Bueno, J. Reichensperger, E. Swanson, M. Dyer, L. Cox, C. Harrison, and M.W. Neumeister, *Regulation of ADSC Osteoinductive Potential Using Notch Pathway Inhibition and Gene Rescue: A Potential On/Off Switch for Clinical Applications in Bone Formation and Reconstructive Efforts*. Plast Reconstr Surg, 2016. **138**(4): p. 642e-52e.

302. Liu, Y., W.K. Zheng, W.S. Gao, Y. Shen, and W.Y. Ding, *Function of TGF-beta and p38 MAKP signaling pathway in osteoblast differentiation from rat adipose-derived stem cells*. Eur Rev Med Pharmacol Sci, 2013. **17**(12): p. 1611-9.
303. Fan, J., C.S. Im, M. Guo, Z.K. Cui, A. Fartash, S. Kim, N. Patel, O. Bezouglaia, B.M. Wu, C.Y. Wang, T.L. Aghaloo, and M. Lee, *Enhanced Osteogenesis of Adipose-Derived Stem Cells by Regulating Bone Morphogenetic Protein Signaling Antagonists and Agonists*. Stem Cells Transl Med, 2016. **5**(4): p. 539-51.
304. Dubey, N.K., V.K. Mishra, R. Dubey, Y.H. Deng, F.C. Tsai, and W.P. Deng, *Revisiting the Advances in Isolation, Characterization and Secretome of Adipose-Derived Stromal/Stem Cells*. Int J Mol Sci, 2018. **19**(8).
305. Guidotti, S., A. Facchini, D. Platano, E. Olivotto, M. Minguzzi, G. Trisolino, G. Filardo, S. Cetrullo, B. Tantini, E. Martucci, A. Facchini, F. Flamigni, and R.M. Borzi, *Enhanced osteoblastogenesis of adipose-derived stem cells on spermine delivery via beta-catenin activation*. Stem Cells Dev, 2013. **22**(10): p. 1588-601.
306. Wu, R., J. Ruan, Y. Sun, M. Liu, Z. Sha, C. Fan, and Q. Wu, *Long non-coding RNA HIF1A-AS2 facilitates adipose-derived stem cells (ASCs) osteogenic differentiation through miR-665/IL6 axis via PI3K/Akt signaling pathway*. Stem Cell Res Ther, 2018. **9**(1): p. 348.
307. Xie, J., D. Zhang, C. Zhou, Q. Yuan, L. Ye, and X. Zhou, *Substrate elasticity regulates adipose-derived stromal cell differentiation towards osteogenesis and adipogenesis through beta-catenin transduction*. Acta Biomater, 2018. **79**: p. 83-95.
308. Wang, Y., Y. Liu, M. Zhang, L. Lv, X. Zhang, P. Zhang, and Y. Zhou, *Inhibition of PTGS1 promotes osteogenic differentiation of adipose-derived stem cells by suppressing NF-kB signaling*. Stem Cell Res Ther, 2019. **10**(1): p. 57.
309. Cho, H.H., K.K. Shin, Y.J. Kim, J.S. Song, J.M. Kim, Y.C. Bae, C.D. Kim, and J.S. Jung, *NF-kappaB activation stimulates osteogenic differentiation of mesenchymal stem cells derived from human adipose tissue by increasing TAZ expression*. J Cell Physiol, 2010. **223**(1): p. 168-77.
310. Chang, J., F. Liu, M. Lee, B. Wu, K. Ting, J.N. Zara, C. Soo, K. Al Hezaimi, W. Zou, X. Chen, D.J. Mooney, and C.Y. Wang, *NF-kB inhibits osteogenic differentiation of mesenchymal stem cells by promoting beta-catenin degradation*. Proc Natl Acad Sci U S A, 2013. **110**(23): p. 9469-74.
311. Cao, X., W. Lin, C. Liang, D. Zhang, F. Yang, Y. Zhang, X. Zhang, J. Feng, and C. Chen, *Naringin rescued the TNF-alpha-induced inhibition of osteogenesis of bone marrow-derived mesenchymal stem cells by*

- depressing the activation of NF-small ka, CyrillicB signaling pathway. Immunol Res, 2015. 62(3): p. 357-67.*
312. Wang, Y.J., H.Q. Zhang, H.L. Han, Y.Y. Zou, Q.L. Gao, and G.T. Yang, *Taxifolin enhances osteogenic differentiation of human bone marrow mesenchymal stem cells partially via NF-kappaB pathway. Biochem Biophys Res Commun, 2017. 490(1): p. 36-43.*
  313. Chen, X., Y. Liu, W. Ding, J. Shi, S. Li, Y. Liu, M. Wu, and H. Wang, *Mechanical stretch-induced osteogenic differentiation of human jaw bone marrow mesenchymal stem cells (hJBMMSCs) via inhibition of the NF-kB pathway. Cell Death Dis, 2018. 9(2): p. 207.*
  314. Levi, B. and M.T. Longaker, *Concise review: adipose-derived stromal cells for skeletal regenerative medicine. Stem Cells, 2011. 29(4): p. 576-82.*
  315. Qureshi, A.T., C. Chen, F. Shah, C. Thomas-Porch, J.M. Gimble, and D.J. Hayes, *Human adipose-derived stromal/stem cell isolation, culture, and osteogenic differentiation. Methods Enzymol, 2014. 538: p. 67-88.*
  316. Zolocinska, A., *The expression of marker genes during the differentiation of mesenchymal stromal cells. Adv Clin Exp Med, 2018. 27(5): p. 717-723.*
  317. Kang, K.S., J.M. Hong, J.A. Kang, J.W. Rhie, Y.H. Jeong, and D.W. Cho, *Regulation of osteogenic differentiation of human adipose-derived stem cells by controlling electromagnetic field conditions. Exp Mol Med, 2013. 45(1): p. e6.*
  318. Grottkau, B.E., X. Yang, L. Zhang, L. Ye, and Y. Lin, *Comparison of Effects of Mechanical Stretching on Osteogenic Potential of ASCs and BMSCs. Bone Res, 2013. 1(3): p. 282-90.*
  319. Strong, A.L., J.F. Ohlstein, Q. Jiang, Q. Zhang, S. Zheng, S.M. Boue, S. Elliott, J.M. Gimble, M.E. Burow, G. Wang, and B.A. Bunnell, *Novel daidzein analogs enhance osteogenic activity of bone marrow-derived mesenchymal stem cells and adipose-derived stromal/stem cells through estrogen receptor dependent and independent mechanisms. Stem Cell Res Ther, 2014. 5(4): p. 105.*
  320. Marshall, C.D., E.A. Brett, A.L. Moore, D.C. Wan, and M.T. Longaker, *In Vitro and In Vivo Osteogenic Differentiation of Human Adipose-Derived Stromal Cells. Methods Mol Biol, 2019. 1891: p. 9-18.*
  321. Mohiuddin, O.A., B. Campbell, J.N. Poche, M. Ma, E. Rogers, D. Gaupp, M.A.A. Harrison, B.A. Bunnell, D.J. Hayes, and J.M. Gimble, *Decellularized Adipose Tissue Hydrogel Promotes Bone Regeneration in Critical-Sized Mouse Femoral Defect Model. Front Bioeng Biotechnol, 2019. 7: p. 211.*
  322. Hamidouche, Z., E. Hay, P. Vaudin, P. Charbord, R. Schule, P.J. Marie, and O. Fromigue, *FHL2 mediates dexamethasone-induced mesenchymal cell*

- differentiation into osteoblasts by activating Wnt/beta-catenin signaling-dependent Runx2 expression.* *Faseb j*, 2008. **22**(11): p. 3813-22.
323. Franceschi, R.T. and B.S. Iyer, *Relationship between collagen synthesis and expression of the osteoblast phenotype in MC3T3-E1 cells.* *J Bone Miner Res*, 1992. **7**(2): p. 235-46.
  324. Langenbach, F. and J. Handschel, *Effects of dexamethasone, ascorbic acid and beta-glycerophosphate on the osteogenic differentiation of stem cells in vitro.* *Stem Cell Res Ther*, 2013. **4**(5): p. 117.
  325. Liu, Q., L. Cen, S. Yin, L. Chen, G. Liu, J. Chang, and L. Cui, *A comparative study of proliferation and osteogenic differentiation of adipose-derived stem cells on akermanite and beta-TCP ceramics.* *Biomaterials*, 2008. **29**(36): p. 4792-9.
  326. Mussano, F., T. Genova, M. Corsalini, G. Schierano, F. Pettini, D. Di Venere, and S. Carossa, *Cytokine, Chemokine, and Growth Factor Profile Characterization of Undifferentiated and Osteoinduced Human Adipose-Derived Stem Cells.* *Stem Cells Int*, 2017. **2017**: p. 6202783.
  327. Bateman, M.E., A.L. Strong, R.S. Hunter, M.R. Bratton, R. Komati, J. Sridhar, K.E. Riley, G. Wang, D.J. Hayes, S.M. Boue, M.E. Burow, and B.A. Bunnell, *Osteoinductive effects of glyceollins on adult mesenchymal stromal/stem cells from adipose tissue and bone marrow.* *Phytomedicine*, 2017. **27**: p. 39-51.
  328. Zhao, X., M. Liang, X. Li, X. Qiu, and L. Cui, *Identification of key genes and pathways associated with osteogenic differentiation of adipose stem cells.* *J Cell Physiol*, 2018. **233**(12): p. 9777-9785.
  329. Cowper, M., T. Frazier, X. Wu, L. Curley, M.H. Ma, O.A. Mohuiddin, M. Dietrich, M. McCarthy, J. Bukowska, and J.M. Gimble, *Human Platelet Lysate as a Functional Substitute for Fetal Bovine Serum in the Culture of Human Adipose Derived Stromal/Stem Cells.* *Cells*, 2019. **8**(7).
  330. Mussano, F., T. Genova, S. Petrillo, I. Roato, R. Ferracini, and L. Munaron, *Osteogenic Differentiation Modulates the Cytokine, Chemokine, and Growth Factor Profile of ASCs and SHED.* *Int J Mol Sci*, 2018. **19**(5).
  331. Mohamed-Ahmed, S., I. Fristad, S.A. Lie, S. Suliman, K. Mustafa, H. Vindenes, and S.B. Idris, *Adipose-derived and bone marrow mesenchymal stem cells: a donor-matched comparison.* *Stem Cell Res Ther*, 2018. **9**(1): p. 168.
  332. Pagani, S., V. Borsari, F. Veronesi, A. Ferrari, S. Cepollaro, P. Torricelli, G. Filardo, and M. Fini, *Increased Chondrogenic Potential of Mesenchymal Cells From Adipose Tissue Versus Bone Marrow-Derived Cells in Osteoarthritic In Vitro Models.* *J Cell Physiol*, 2017. **232**(6): p. 1478-1488.

333. Xu, L., Y. Liu, Y. Sun, B. Wang, Y. Xiong, W. Lin, Q. Wei, H. Wang, W. He, B. Wang, and G. Li, *Tissue source determines the differentiation potentials of mesenchymal stem cells: a comparative study of human mesenchymal stem cells from bone marrow and adipose tissue*. *Stem Cell Res Ther*, 2017. **8**(1): p. 275.
334. Hill, T.P., D. Spater, M.M. Taketo, W. Birchmeier, and C. Hartmann, *Canonical Wnt/beta-catenin signaling prevents osteoblasts from differentiating into chondrocytes*. *Dev Cell*, 2005. **8**(5): p. 727-38.
335. Kim, H.J. and G.I. Im, *The effects of ERK1/2 inhibitor on the chondrogenesis of bone marrow- and adipose tissue-derived multipotent mesenchymal stromal cells*. *Tissue Eng Part A*, 2010. **16**(3): p. 851-60.
336. Bi, W., J.M. Deng, Z. Zhang, R.R. Behringer, and B. de Crombrughe, *Sox9 is required for cartilage formation*. *Nature Genetics*, 1999. **22**(1): p. 85-89.
337. Liu, T.M., X.M. Guo, H.S. Tan, J.H. Hui, B. Lim, and E.H. Lee, *Zinc-finger protein 145, acting as an upstream regulator of SOX9, improves the differentiation potential of human mesenchymal stem cells for cartilage regeneration and repair*. *Arthritis Rheum*, 2011. **63**(9): p. 2711-20.
338. Coricor, G. and R. Serra, *TGF-beta regulates phosphorylation and stabilization of Sox9 protein in chondrocytes through p38 and Smad dependent mechanisms*. *Sci Rep*, 2016. **6**: p. 38616.
339. Karystinou, A., A.J. Roelofs, A. Neve, F.P. Cantatore, H. Wackerhage, and C. De Bari, *Yes-associated protein (YAP) is a negative regulator of chondrogenesis in mesenchymal stem cells*. *Arthritis Res Ther*, 2015. **17**: p. 147.
340. Ying, J., P. Wang, S. Zhang, T. Xu, L. Zhang, R. Dong, S.B. Xu, P. Tong, C. Wu, and H. Jin, *Transforming growth factor-beta1 promotes articular cartilage repair through canonical Smad and Hippo pathways in bone mesenchymal stem cells*. *Life Sci.*, 2018. **192**: p. 84-90.
341. Mehlhorn, A.T., P. Niemeyer, K. Kaschte, L. Muller, G. Finkenzeller, D. Hartl, N.P. Sudkamp, and H. Schmal, *Differential effects of BMP-2 and TGF-beta1 on chondrogenic differentiation of adipose derived stem cells*. *Cell Prolif*, 2007. **40**(6): p. 809-23.
342. Kim, H.J. and G.I. Im, *Combination of transforming growth factor-beta2 and bone morphogenetic protein 7 enhances chondrogenesis from adipose tissue-derived mesenchymal stem cells*. *Tissue Eng Part A*, 2009. **15**(7): p. 1543-51.
343. Huang, L., L. Yi, C. Zhang, Y. He, L. Zhou, Y. Liu, L. Qian, S. Hou, and T. Weng, *Synergistic Effects of FGF-18 and TGF-beta3 on the Chondrogenesis of Human Adipose-Derived Mesenchymal Stem Cells in the Pellet Culture*. *Stem Cells Int*, 2018. **2018**: p. 7139485.

344. Johnstone, B., T.M. Hering, A.I. Caplan, V.M. Goldberg, and J.U. Yoo, *In vitro chondrogenesis of bone marrow-derived mesenchymal progenitor cells*. Exp Cell Res, 1998. **238**(1): p. 265-72.
345. Levick, J.R., *Microvascular architecture and exchange in synovial joints*. Microcirculation, 1995. **2**(3): p. 217-33.
346. Hirao, M., N. Tamai, N. Tsumaki, H. Yoshikawa, and A. Myoui, *Oxygen tension regulates chondrocyte differentiation and function during endochondral ossification*. J Biol Chem, 2006. **281**(41): p. 31079-92.
347. Amarilio, R., S.V. Viukov, A. Sharir, I. Eshkar-Oren, R.S. Johnson, and E. Zelzer, *HIF1alpha regulation of Sox9 is necessary to maintain differentiation of hypoxic prechondrogenic cells during early skeletogenesis*. Development, 2007. **134**(21): p. 3917-28.
348. Yang, L., K.Y. Tsang, H.C. Tang, D. Chan, and K.S. Cheah, *Hypertrophic chondrocytes can become osteoblasts and osteocytes in endochondral bone formation*. Proc Natl Acad Sci U S A, 2014. **111**(33): p. 12097-102.
349. Zhou, X., K. von der Mark, S. Henry, W. Norton, H. Adams, and B. de Crombrughe, *Chondrocytes transdifferentiate into osteoblasts in endochondral bone during development, postnatal growth and fracture healing in mice*. PLoS Genet, 2014. **10**(12): p. e1004820.
350. Zhou, G., Q. Zheng, F. Engin, E. Munivez, Y. Chen, E. Sebald, D. Krakow, and B. Lee, *Dominance of SOX9 function over RUNX2 during skeletogenesis*. Proc Natl Acad Sci U S A, 2006. **103**(50): p. 19004-9.
351. Ronziere, M.C., E. Perrier, F. Mallein-Gerin, and A.M. Freyria, *Chondrogenic potential of bone marrow- and adipose tissue-derived adult human mesenchymal stem cells*. Biomed Mater Eng, 2010. **20**(3): p. 145-58.
352. Kim, Y.J., H.J. Kim, and G.I. Im, *PTHrP promotes chondrogenesis and suppresses hypertrophy from both bone marrow-derived and adipose tissue-derived MSCs*. Biochem Biophys Res Commun, 2008. **373**(1): p. 104-8.
353. Dzobo, K., T. Turnley, A. Wishart, A. Rowe, K. Kallmeyer, F.A. van Vollenstee, N.E. Thomford, C. Dandara, D. Chopera, M.S. Pepper, and M.I. Parker, *Fibroblast-Derived Extracellular Matrix Induces Chondrogenic Differentiation in Human Adipose-Derived Mesenchymal Stromal/Stem Cells in Vitro*. Int J Mol Sci, 2016. **17**(8).
354. Sekiya, I., D.C. Colter, and D.J. Prockop, *BMP-6 enhances chondrogenesis in a subpopulation of human marrow stromal cells*. Biochem Biophys Res Commun, 2001. **284**(2): p. 411-8.
355. Ansboro, S., J.S. Hayes, V. Barron, S. Browne, L. Howard, U. Greiser, P. Lalor, F. Shannon, F.P. Barry, A. Pandit, and J.M. Murphy, A

- chondromimetic microsphere for in situ spatially controlled chondrogenic differentiation of human mesenchymal stem cells*. Journal of Controlled Release, 2014. **179**(1): p. 42-51.
356. Yoon, I.S., C.W. Chung, J.H. Sung, H.J. Cho, J.S. Kim, W.S. Shim, C.K. Shim, S.J. Chung, and D.D. Kim, *Proliferation and chondrogenic differentiation of human adipose-derived mesenchymal stem cells in porous hyaluronic acid scaffold*. J Biosci Bioeng, 2011. **112**(4): p. 402-8.
357. Calderon, L., E. Collin, D. Velasco-Bayon, M. Murphy, D. O'halloran, and A. Pandit, *Type II collagen- hyaluronan hydrogel – a step towards a scaffold for intervertebral disc tissue engineering*. European Cells & Materials, 2010. **20**: p. 134-148.
358. Gaudet, I. and D. Shreiber, *Characterization of Methacrylated Type- I Collagen as a Dynamic, Photoactive Hydrogel*. Journal for Biophysical Chemistry, 2012. **7**(1): p. 1-9.
359. Sridhar, B., E. Dailing, J. Brock, J. Stansbury, M. Randolph, and K. Anseth, *A Biosynthetic Scaffold that Facilitates Chondrocyte- Mediated Degradation and Promotes Articular Cartilage Extracellular Matrix Deposition*. Regenerative Engineering and Translational Medicine, 2015. **1**(1): p. 11-21.
360. Kabiri, A., E. Esfandiari, B. Hashemibeni, M. Kazemi, M. Mardani, and A. Esmaeili, *Effects of FGF-2 on human adipose tissue derived adult stem cells morphology and chondrogenesis enhancement in Transwell culture*. Biochem Biophys Res Commun, 2012. **424**(2): p. 234-8.
361. Grogan, S.P., A. Barbero, V. Winkelmann, F. Rieser, J.S. Fitzsimmons, S. O'Driscoll, I. Martin, and P. Mainil-Varlet, *Visual histological grading system for the evaluation of in vitro-generated neocartilage*. Tissue Eng, 2006. **12**(8): p. 2141-9.
362. Lattouf, R., R. Younes, D. Lutomski, N. Naaman, G. Godeau, K. Senni, and S. Changotade, *Picosirius red staining: a useful tool to appraise collagen networks in normal and pathological tissues*. J Histochem Cytochem, 2014. **62**(10): p. 751-8.
363. Cissell, D.D., J.M. Link, J.C. Hu, and K.A. Athanasiou, *A Modified Hydroxyproline Assay Based on Hydrochloric Acid in Ehrlich's Solution Accurately Measures Tissue Collagen Content*. Tissue Eng Part C Methods, 2017. **23**(4): p. 243-250.
364. Yi, S.W., H.J. Kim, H.J. Oh, H. Shin, J.S. Lee, J.S. Park, and K.H. Park, *Gene expression profiling of chondrogenic differentiation by dexamethasone-conjugated polyethyleneimine with SOX trio genes in stem cells*. Stem Cell Res Ther, 2018. **9**(1): p. 341.
365. Sekiya, I., K. Tsuji, P. Koopman, H. Watanabe, Y. Yamada, K. Shinomiya, A. Nifuji, and M. Noda, *SOX9 enhances aggrecan gene promoter/enhancer*

- activity and is up-regulated by retinoic acid in a cartilage-derived cell line, TC6. J Biol Chem, 2000. 275(15): p. 10738-44.*
366. Gao, L., P. Orth, M. Cucchiaroni, and H. Madry, *Effects of solid acellular type-I/III collagen biomaterials on in vitro and in vivo chondrogenesis of mesenchymal stem cells. Expert Rev Med Devices, 2017. 14(9): p. 717-732.*
367. Liu, T.M., M. Martina, D.W. Hutmacher, J.H. Hui, E.H. Lee, and B. Lim, *Identification of common pathways mediating differentiation of bone marrow- and adipose tissue-derived human mesenchymal stem cells into three mesenchymal lineages. Stem Cells, 2007. 25(3): p. 750-60.*
368. Bartholomew, A., C. Sturgeon, M. Siatskas, K. Ferrer, K. McIntosh, S. Patil, W. Hardy, S. Devine, D. Ucker, R. Deans, A. Moseley, and R. Hoffman, *Mesenchymal stem cells suppress lymphocyte proliferation in vitro and prolong skin graft survival in vivo. Exp Hematol, 2002. 30(1): p. 42-8.*
369. Waterman, R.S., S.L. Tomchuck, S.L. Henkle, and A.M. Betancourt, *A new mesenchymal stem cell (MSC) paradigm: polarization into a pro-inflammatory MSC1 or an Immunosuppressive MSC2 phenotype. PLoS One, 2010. 5(4): p. e10088.*
370. Liu, G.Y., Y. Liu, Y. Lu, Y.R. Qin, G.H. Di, Y.H. Lei, H.X. Liu, Y.Q. Li, C. Wu, X.W. Hu, and H.F. Duan, *Short-term memory of danger signals or environmental stimuli in mesenchymal stem cells: implications for therapeutic potential. Cell Mol Immunol, 2016. 13(3): p. 369-78.*
371. Ryan, J.M., F. Barry, J.M. Murphy, and B.P. Mahon, *Interferon-gamma does not break, but promotes the immunosuppressive capacity of adult human mesenchymal stem cells. Clin Exp Immunol, 2007. 149(2): p. 353-63.*
372. Martinez, V.G., I. Ontoria-Oviedo, C.P. Ricardo, S.E. Harding, R. Sacedon, A. Varas, A. Zapata, P. Sepulveda, and A. Vicente, *Overexpression of hypoxia-inducible factor 1 alpha improves immunomodulation by dental mesenchymal stem cells. Stem Cell Res Ther, 2017. 8(1): p. 208.*
373. Hoeffel, G. and F. Ginhoux, *Ontogeny of Tissue-Resident Macrophages. Front Immunol, 2015. 6: p. 486.*
374. Mosser, D.M. and J.P. Edwards, *Exploring the full spectrum of macrophage activation. Nat Rev Immunol, 2008. 8(12): p. 958-69.*
375. Daigneault, M., J.A. Preston, H.M. Marriott, M.K. Whyte, and D.H. Dockrell, *The identification of markers of macrophage differentiation in PMA-stimulated THP-1 cells and monocyte-derived macrophages. PLoS One, 2010. 5(1): p. e8668.*
376. Rybalko, V., P.L. Hsieh, L.M. Ricles, E. Chung, R.P. Farrar, and L.J. Suggs, *Therapeutic potential of adipose-derived stem cells and macrophages for ischemic skeletal muscle repair. Regen Med, 2017. 12(2): p. 153-167.*

377. Adutler-Lieber, S., T. Ben-Mordechai, N. Naftali-Shani, E. Asher, D. Loberman, E. Raanani, and J. Leor, *Human macrophage regulation via interaction with cardiac adipose tissue-derived mesenchymal stromal cells*. J Cardiovasc Pharmacol Ther, 2013. **18**(1): p. 78-86.
378. Manferdini, C., F. Paoella, E. Gabusi, L. Gambari, A. Piacentini, G. Filardo, S. Fleury-Cappellesso, A. Barbero, M. Murphy, and G. Lisignoli, *Adipose stromal cells mediated switching of the pro-inflammatory profile of M1-like macrophages is facilitated by PGE2: in vitro evaluation*. Osteoarthritis Cartilage, 2017. **25**(7): p. 1161-1171.
379. Park, H.J., J. Kim, F.T. Saima, K.J. Rhee, S. Hwang, M.Y. Kim, S.K. Baik, Y.W. Eom, and H.S. Kim, *Adipose-derived stem cells ameliorate colitis by suppression of inflammasome formation and regulation of M1-macrophage population through prostaglandin E2*. Biochem Biophys Res Commun, 2018. **498**(4): p. 988-995.
380. Domenis, R., A. Cifu, S. Quaglia, C. Pistis, M. Moretti, A. Vicario, P.C. Parodi, M. Fabris, K.R. Niazi, P. Soon-Shiong, and F. Curcio, *Pro inflammatory stimuli enhance the immunosuppressive functions of adipose mesenchymal stem cells-derived exosomes*. Sci Rep, 2018. **8**(1): p. 13325.
381. Li, C., M.M. Xu, K. Wang, A.J. Adler, A.T. Vella, and B. Zhou, *Macrophage polarization and meta-inflammation*. Transl Res, 2018. **191**: p. 29-44.
382. Roberts, C.A., A.K. Dickinson, and L.S. Taams, *The Interplay Between Monocytes/Macrophages and CD4(+) T Cell Subsets in Rheumatoid Arthritis*. Front Immunol, 2015. **6**: p. 571.
383. Li, Z., F. Liu, X. He, X. Yang, F. Shan, and J. Feng, *Exosomes derived from mesenchymal stem cells attenuate inflammation and demyelination of the central nervous system in EAE rats by regulating the polarization of microglia*. Int Immunopharmacol, 2019. **67**: p. 268-280.
384. Guillen, M.I., J. Platas, M.D. Perez Del Caz, V. Mirabet, and M.J. Alcaraz, *Paracrine Anti-inflammatory Effects of Adipose Tissue-Derived Mesenchymal Stem Cells in Human Monocytes*. Front Physiol, 2018. **9**: p. 661.
385. Sun, M., L. Sun, C. Huang, B.C. Chen, and Z. Zhou, *Induction of Macrophage M2b/c Polarization by Adipose Tissue-Derived Mesenchymal Stem Cells*. J Immunol Res, 2019. **2019**: p. 7059680.
386. Anderson, P., L. Souza-Moreira, M. Morell, M. Caro, F. O'Valle, E. Gonzalez-Rey, and M. Delgado, *Adipose-derived mesenchymal stromal cells induce immunomodulatory macrophages which protect from experimental colitis and sepsis*. Gut, 2013. **62**(8): p. 1131-41.
387. Stojanovic, S. and S. Najman, *The Effect of Conditioned Media of Stem Cells Derived from Lipoma and Adipose Tissue on Macrophages' Response*

- and Wound Healing in Indirect Co-culture System In Vitro*. Int J Mol Sci, 2019. **20**(7).
388. Song, W.J., Q. Li, M.O. Ryu, J.O. Ahn, D. Ha Bhang, Y. Chan Jung, and H.Y. Youn, *TSG-6 Secreted by Human Adipose Tissue-derived Mesenchymal Stem Cells Ameliorates DSS-induced colitis by Inducing M2 Macrophage Polarization in Mice*. Sci Rep, 2017. **7**(1): p. 5187.
389. Furuhashi, K., N. Tsuboi, A. Shimizu, T. Katsuno, H. Kim, Y. Saka, T. Ozaki, Y. Sado, E. Imai, S. Matsuo, and S. Maruyama, *Serum-starved adipose-derived stromal cells ameliorate crescentic GN by promoting immunoregulatory macrophages*. J Am Soc Nephrol, 2013. **24**(4): p. 587-603.
390. Hattori, H. and M. Ishihara, *Altered protein secretions during interactions between adipose tissue- or bone marrow-derived stromal cells and inflammatory cells*. Stem Cell Res Ther, 2015. **6**: p. 70.
391. Kornicka, K., A. Smieszek, A.S. Wegrzyn, M. Rocken, and K. Marycz, *Immunomodulatory Properties of Adipose-Derived Stem Cells Treated with 5-Azacytidine and Resveratrol on Peripheral Blood Mononuclear Cells and Macrophages in Metabolic Syndrome Animals*. J Clin Med, 2018. **7**(11).
392. Li, J.Z., T.H. Cao, J.C. Han, H. Qu, S.Q. Jiang, B.D. Xie, X.L. Yan, H. Wu, X.L. Liu, F. Zhang, X.P. Leng, K. Kang, and S.L. Jiang, *Comparison of adipose and bone marrow-derived stem cells in protecting against oxLDL-induced inflammation in M1 macrophage-derived foam cells*. Mol Med Rep, 2019. **19**(4): p. 2660-2670.
393. Alvarez, D., E.H. Vollmann, and U.H. von Andrian, *Mechanisms and consequences of dendritic cell migration*. Immunity, 2008. **29**(3): p. 325-42.
394. Castell-Rodríguez, A., G. Piñón-Zárate, M. Herrera-Enríquez, K. Jarquín-Yáñez, and I. Medina-Solares, *Dendritic Cells: Location, Function, and Clinical Implications*, in *Biology of Myelomonocytic Cells*. 2017.
395. Kadowaki, N., *The divergence and interplay between pDC and mDC in humans*. Front Biosci (Landmark Ed), 2009. **14**: p. 808-17.
396. Yanez, R., A. Oviedo, M. Aldea, J.A. Bueren, and M.L. Lamana, *Prostaglandin E2 plays a key role in the immunosuppressive properties of adipose and bone marrow tissue-derived mesenchymal stromal cells*. Exp Cell Res, 2010. **316**(19): p. 3109-23.
397. Zhou, L.J. and T.F. Tedder, *CD14(+) blood monocytes can differentiate into functionally mature CD83(+) dendritic cells*. Proceedings of the National Academy of Sciences of the United States of America, 1996. **93**(6): p. 2588-2592.

398. Kim, M.K. and J. Kim, *Properties of immature and mature dendritic cells: phenotype, morphology, phagocytosis, and migration*. Rsc Advances, 2019. **9**(20): p. 11230-11238.
399. Blanco, P., A.K. Palucka, V. Pascual, and J. Banchereau, *Dendritic cells and cytokines in human inflammatory and autoimmune diseases*. Cytokine Growth Factor Rev, 2008. **19**(1): p. 41-52.
400. Ivanova-Todorova, E., I. Bochev, M. Mourdjeva, R. Dimitrov, D. Bukarev, S. Kyurkchiev, P. Tivchev, I. Altunkova, and D.S. Kyurkchiev, *Adipose tissue-derived mesenchymal stem cells are more potent suppressors of dendritic cells differentiation compared to bone marrow-derived mesenchymal stem cells*. Immunol Lett, 2009. **126**(1-2): p. 37-42.
401. Valencia, J., B. Blanco, R. Yanez, M. Vazquez, C. Herrero Sanchez, M. Fernandez-Garcia, C. Rodriguez Serrano, D. Pescador, J.F. Blanco, M. Hernando-Rodriguez, F. Sanchez-Guijo, M.L. Lamana, J.C. Segovia, A. Vicente, C. Del Canizo, and A.G. Zapata, *Comparative analysis of the immunomodulatory capacities of human bone marrow- and adipose tissue-derived mesenchymal stromal cells from the same donor*. Cytotherapy, 2016. **18**(10): p. 1297-311.
402. Melief, S.M., J.J. Zwaginga, W.E. Fibbe, and H. Roelofs, *Adipose tissue-derived multipotent stromal cells have a higher immunomodulatory capacity than their bone marrow-derived counterparts*. Stem Cells Transl Med, 2013. **2**(6): p. 455-63.
403. Wang, Y.C., R.F. Chen, G. Brandacher, W.P.A. Lee, and Y.R. Kuo, *The suppression effect of dendritic cells maturation by adipose-derived stem cells through TGF-beta1 related pathway*. Exp Cell Res, 2018. **370**(2): p. 708-717.
404. Pegram, H.J., D.M. Andrews, M.J. Smyth, P.K. Darcy, and M.H. Kershaw, *Activating and inhibitory receptors of natural killer cells*. Immunol Cell Biol, 2011. **89**(2): p. 216-24.
405. Glimcher, L.H., M.J. Townsend, B.M. Sullivan, and G.M. Lord, *Recent developments in the transcriptional regulation of cytolytic effector cells*. Nat Rev Immunol, 2004. **4**(11): p. 900-11.
406. Wang, G., G. Yu, D. Wang, S. Guo, and F. Shan, *Comparison of the purity and vitality of natural killer cells with different isolation kits*. Exp Ther Med, 2017. **13**(5): p. 1875-1883.
407. Alter, G., J.M. Malenfant, and M. Altfeld, *CD107a as a functional marker for the identification of natural killer cell activity*. J Immunol Methods, 2004. **294**(1-2): p. 15-22.
408. DelaRosa, O., B. Sanchez-Correa, S. Morgado, C. Ramirez, B. del Rio, R. Menta, E. Lombardo, R. Tarazona, and J.G. Casado, *Human adipose-derived stem cells impair natural killer cell function and exhibit low*

- susceptibility to natural killer-mediated lysis*. *Stem Cells Dev*, 2012. **21**(8): p. 1333-43.
409. Spaggiari, G.M., A. Capobianco, H. Abdelrazik, F. Becchetti, M.C. Mingari, and L. Moretta, *Mesenchymal stem cells inhibit natural killer-cell proliferation, cytotoxicity, and cytokine production: role of indoleamine 2,3-dioxygenase and prostaglandin E2*. *Blood*, 2008. **111**(3): p. 1327-33.
  410. Ribeiro, A., P. Laranjeira, S. Mendes, I. Velada, C. Leite, P. Andrade, F. Santos, A. Henriques, M. Graos, C.M. Cardoso, A. Martinho, M. Pais, C.L. da Silva, J. Cabral, H. Trindade, and A. Paiva, *Mesenchymal stem cells from umbilical cord matrix, adipose tissue and bone marrow exhibit different capability to suppress peripheral blood B, natural killer and T cells*. *Stem Cell Res Ther*, 2013. **4**(5): p. 125.
  411. Blanco, B., M.D. Herrero-Sanchez, C. Rodriguez-Serrano, M.L. Garcia-Martinez, J.F. Blanco, S. Muntion, M. Garcia-Arranz, F. Sanchez-Guijo, and C. Del Canizo, *Immunomodulatory effects of bone marrow versus adipose tissue-derived mesenchymal stromal cells on NK cells: implications in the transplantation setting*. *Eur J Haematol*, 2016. **97**(6): p. 528-537.
  412. Bonilla, F.A. and H.C. Oettgen, *Adaptive immunity*. *The Journal of Allergy and Clinical Immunology*, 2010. **125**(2): p. S33-S40.
  413. Wherry, E.J. and D. Masopust, *Chapter 5 - Adaptive Immunity: Neutralizing, Eliminating, and Remembering for the Next Time*. 2016: Elsevier Ltd. 57-69.
  414. Puissant, B., C. Barreau, P. Bourin, C. Clavel, J. Corre, C. Bousquet, C. Taureau, B. Cousin, M. Abbal, P. Laharrague, L. Penicaud, L. Casteilla, and A. Blancher, *Immunomodulatory effect of human adipose tissue-derived adult stem cells: comparison with bone marrow mesenchymal stem cells*. *British Journal of Haematology*, 2005. **129**(1): p. 118-129.
  415. Wolbank, S., A. Peterbauer, M. Fahrner, S. Hennerbichler, M. van Griensven, G. Stadler, H. Redl, and C. Gabriel, *Dose-dependent immunomodulatory effect of human stem cells from amniotic membrane: a comparison with human mesenchymal stem cells from adipose tissue*. *Tissue engineering*, 2007. **13**(6): p. 1173.
  416. Hasbold, J., G. Av, R. Js, E. Deenick, D. Avery, J. Jun, and H. Pd, *Quantitative analysis of lymphocyte differentiation and proliferation in vitro using carboxyfluorescein diacetate succinimidyl ester*. *Immunology and Cell Biology*, 1999. **77**(6): p. 516.
  417. Borgulya, P., H. Kishi, U. Muller, J. Kirberg, and H. Vonboehmer, *DEVELOPMENT OF THE CD4 AND CD8 LINEAGE OF T-CELLS - INSTRUCTION VERSUS SELECTION*. *Embo J.*, 1991. **10**(4): p. 913-918.

418. Whitmire, J.K. and R. Ahmed, *Costimulation in antiviral immunity: differential requirements for CD4 + and CD8 + T cell responses*. 2000. p. 448-455.
419. Lanzavecchia, A. and F. Sallusto, *Understanding the generation and function of memory T cell subsets*. *Current Opinion in Immunology*, 2005. **17**(3): p. 326-332.
420. Kronsteiner, B., S. Wolbank, A. Peterbauer, C. Hackl, H. Redl, M. van Griensven, and C. Gabriel, *Human mesenchymal stem cells from adipose tissue and amnion influence T-cells depending on stimulation method and presence of other immune cells*. *Stem cells and development*, 2011. **20**(12): p. 2115.
421. Menard, C., L. Pacelli, G. Bassi, J. Dulong, F. Bifari, I. Bezier, J. Zanoncello, M. Ricciardi, M. Latour, P. Bourin, H. Schrezenmeier, L. Sensebe, K. Tarte, and M. Krampera, *Clinical-grade mesenchymal stromal cells produced under various good manufacturing practice processes differ in their immunomodulatory properties: standardization of immune quality controls.(Report)*. *Stem Cells and Development*, 2013. **22**(12): p. 1789.
422. Najjar, M., G. Raicevic, H.I. Boufker, H.F. Kazan, C.D. Bruyn, N. Meuleman, D. Bron, M. Toungouz, and L. Lagneaux, *Mesenchymal stromal cells use PGE2 to modulate activation and proliferation of lymphocyte subsets: Combined comparison of adipose tissue, Wharton's Jelly and bone marrow sources*. *Cellular Immunology*, 2010. **264**(2): p. 171-179.
423. Chien, C.-M., Y.-W. Chen, C.-C. Chen, Y.-C. Wu, S.-H. Huang, S.-S. Lee, C.-S. Lai, S.-D. Lin, C.-J. Wang, and Y.-R. Kuo, *Adipose-Derived Stem Cell Modulation of T-Cell Regulation Correlates with Heme Oxygenase-1 Pathway Changes*. *Plastic and Reconstructive Surgery*, 2016. **138**(5): p. 1015-1023.
424. Kizilay Mancini, O., D. Shum-Tim, U. Stochaj, J.A. Correa, and I. Colmegna, *Age, atherosclerosis and type 2 diabetes reduce human mesenchymal stromal cell-mediated T-cell suppression*. *Stem Cell Research & Therapy*, 2015. **6**(1).
425. Wu, L.W., Y.-L. Wang, J.M. Christensen, S. Khalifian, S. Schneeberger, G. Raimondi, D.S. Cooney, W.P.A. Lee, and G. Brandacher, *Donor age negatively affects the immunoregulatory properties of both adipose and bone marrow derived mesenchymal stem cells*. *Transplant Immunology*, 2014. **30**(4): p. 122-127.
426. Chen, W., *Conversion of peripheral CD4+CD25- naive T cells to CD4+CD25+ regulatory T cells by TGF-beta induction of transcription factor Foxp3*. *Journal of Experimental Medicine*, 2003. **198**(12): p. 1875-1887.
427. Ivanova-Todorova, E., I. Bochev, R. Dimitrov, K. Belezmezova, M. Mourdjeva, S. Kyurkchiev, P. Kinov, I. Altankova, and D. Kyurkchiev,

- Conditioned Medium from Adipose Tissue-Derived Mesenchymal Stem Cells Induces CD4+FOXP3+ Cells and Increases IL-10 Secretion.* Journal of Biomedicine and Biotechnology, 2012. **2012**.
428. Lopez, J.A., O. Susanto, M.R. Jenkins, N. Lukoyanova, V.R. Sutton, R.H. Law, A. Johnston, C.H. Bird, P.I. Bird, J.C. Whisstock, J.A. Trapani, H.R. Saibil, and I. Voskoboinik, *Perforin forms transient pores on the target cell plasma membrane to facilitate rapid access of granzymes during killer cell attack.* Blood, 2013. **121**(14): p. 2659-68.
429. Hassin, D., O.G. Garber, A. Meiraz, Y.S. Schiffenbauer, and G. Berke, *Cytotoxic T lymphocyte perforin and Fas ligand working in concert even when Fas ligand lytic action is still not detectable.* Immunology, 2011. **133**(2): p. 190-6.
430. Hof-Nahor, I., L. Leshansky, S. Shivtiel, L. Eldor, D. Aberdam, J. Itskovitz-Eldor, and S. Berrih-Aknin, *Human mesenchymal stem cells shift CD8+ T cells towards a suppressive phenotype by inducing tolerogenic monocytes.* Journal of cell science, 2012. **125**(19): p. 4640.
431. Ollila, J. and M. Vihinen, *B cells.* International Journal of Biochemistry and Cell Biology, 2005. **37**(3): p. 518-523.
432. Barrio, L., V.D. Cuevas, R. Menta, P. Mancheño-Corvo, O. Delarosa, W. Dalemans, E. Lombardo, and Y.R. Carrasco, *Human adipose tissue-derived mesenchymal stromal cells promote B-cell motility and chemoattraction.* Cytotherapy, 2014. **16**(12): p. 1692-1699.
433. Samoylovich, M., A. Pinevich, O. Shashkova, N. Vartanian, L. Kiseleva, and V. Klimovich, *The influence of mesenchymal stromal cells on B-cell line growth and immunoglobulin synthesis.* Cell and Tissue Biology, 2013. **7**(3): p. 227-234.
434. Bochev, I., G. Elmadjian, D. Kyurkchiev, L. Tzvetanov, I. Altankova, P. Tivchev, and S. Kyurkchiev, *Mesenchymal stem cells from human bone marrow or adipose tissue differently modulate mitogen-stimulated B-cell immunoglobulin production in vitro.* Cell Biology International, 2008. **32**(4): p. 384-393.
435. Ceccarelli, S., P. Pontecorvi, E. Anastasiadou, C. Napoli, and C. Marchese, *Immunomodulatory Effect of Adipose-Derived Stem Cells: The Cutting Edge of Clinical Application.* Front Cell Dev Biol, 2020. **8**: p. 236.
436. Andras, I.E., A. Leda, M.G. Contreras, L. Bertrand, M. Park, M. Skowronska, and M. Toborek, *Extracellular vesicles of the blood-brain barrier: Role in the HIV-1 associated amyloid beta pathology.* Mol Cell Neurosci, 2017. **79**: p. 12-22.
437. Semon, J.A., C. Maness, X. Zhang, S.A. Sharkey, M.M. Beuttler, F.S. Shah, A.C. Pandey, J.M. Gimble, S. Zhang, B.A. Scruggs, A.L. Strong, T.A. Strong, and B.A. Bunnell, *Comparison of human adult stem cells from*

- adipose tissue and bone marrow in the treatment of experimental autoimmune encephalomyelitis*. Stem Cell Res Ther, 2014. **5**(1): p. 2.
438. Zhao, P.T., L.J. Zhang, H. Shao, L.L. Bai, B. Yu, C. Su, L.J. Dong, X. Liu, X.R. Li, and X.M. Zhang, *Therapeutic effects of mesenchymal stem cells administered at later phase of recurrent experimental autoimmune uveitis*. Int J Ophthalmol, 2016. **9**(10): p. 1381-1389.
439. Bai, L., H. Shao, H. Wang, Z. Zhang, C. Su, L. Dong, B. Yu, X. Chen, X. Li, and X. Zhang, *Effects of Mesenchymal Stem Cell-Derived Exosomes on Experimental Autoimmune Uveitis*. Sci Rep, 2017. **7**(1): p. 4323.
440. Burgos-Silva, M., P. Semedo-Kuriki, C. Donizetti-Oliveira, P.B. Costa, M.A. Cenedeze, M.I. Hiyane, A. Pacheco-Silva, and N.O. Camara, *Adipose Tissue-Derived Stem Cells Reduce Acute and Chronic Kidney Damage in Mice*. PLoS One, 2015. **10**(11): p. e0142183.
441. Gonzalez, M.A., E. Gonzalez-Rey, L. Rico, D. Buscher, and M. Delgado, *Adipose-derived mesenchymal stem cells alleviate experimental colitis by inhibiting inflammatory and autoimmune responses*. Gastroenterology, 2009. **136**(3): p. 978-89.
442. Jung, W.Y., J.H. Kang, K.G. Kim, H.S. Kim, B.I. Jang, Y.H. Park, and I.H. Song, *Human adipose-derived stem cells attenuate inflammatory bowel disease in IL-10 knockout mice*. Tissue Cell, 2015. **47**(1): p. 86-93.
443. Kawata, Y., A. Tsuchiya, S. Seino, Y. Watanabe, Y. Kojima, S. Ikarashi, K. Tominaga, J. Yokoyama, S. Yamagiwa, and S. Terai, *Early injection of human adipose tissue-derived mesenchymal stem cell after inflammation ameliorates dextran sulfate sodium-induced colitis in mice through the induction of M2 macrophages and regulatory T cells*. Cell Tissue Res, 2019. **376**(2): p. 257-271.
444. Ma, T., B. Fu, X. Yang, Y. Xiao, and M. Pan, *Adipose mesenchymal stem cell-derived exosomes promote cell proliferation, migration, and inhibit cell apoptosis via Wnt/beta-catenin signaling in cutaneous wound healing*. J Cell Biochem, 2019. **120**(6): p. 10847-10854.
445. Sun, Y., L. Song, Y. Zhang, H. Wang, and X. Dong, *Adipose stem cells from type 2 diabetic mice exhibit therapeutic potential in wound healing*. Stem Cell Res Ther, 2020. **11**(1): p. 298.
446. Skubis-Sikora, A., B. Sikora, A. Witkowska, U. Mazurek, and J. Gola, *Osteogenesis of adipose-derived stem cells from patients with glucose metabolism disorders*. Mol Med, 2020. **26**(1): p. 67.
447. Payr, S., T. Schuseil, M. Unger, C. Seeliger, T. Tiefenboeck, E.R. Balmayor, and M.V. Griensven, *Effect of donor age and 3D-cultivation on osteogenic differentiation capacity of adipose-derived mesenchymal stem cells*. Sci Rep, 2020. **10**(1): p. 10408.

448. Huang, X., H. Zhang, X. Liang, Y. Hong, M. Mao, Q. Han, H. He, W. Tao, G. Jiang, Y. Zhang, and X. Li, *Adipose-Derived Mesenchymal Stem Cells Isolated from Patients with Abdominal Aortic Aneurysm Exhibit Senescence Phenomena*. *Oxid Med Cell Longev*, 2019. **2019**: p. 1305049.
449. Wang, L., L. Zhang, X. Liang, J. Zou, N. Liu, T. Liu, G. Wang, X. Ding, Y. Liu, B. Zhang, R. Liang, and S. Wang, *Adipose Tissue-Derived Stem Cells from Type 2 Diabetics Reveal Conservative Alterations in Multidimensional Characteristics*. *Int J Stem Cells*, 2020. **13**(2): p. 268-278.
450. Jung, J.S., C. Volk, C. Marga, A. Navarrete Santos, M. Jung, D. Rujescu, and A. Navarrete Santos, *Adipose-Derived Stem/Stromal Cells Recapitulate Aging Biomarkers and Show Reduced Stem Cell Plasticity Affecting Their Adipogenic Differentiation Capacity*. *Cell Reprogram*, 2019. **21**(4): p. 187-199.
451. Scruggs, B.A., J.A. Semon, X. Zhang, S. Zhang, A.C. Bowles, A.C. Pandey, K.M. Imhof, A.V. Kalueff, J.M. Gimble, and B.A. Bunnell, *Age of the donor reduces the ability of human adipose-derived stem cells to alleviate symptoms in the experimental autoimmune encephalomyelitis mouse model*. *Stem Cells Transl Med*, 2013. **2**(10): p. 797-807.
452. Strong, A.L., A.C. Bowles, R.M. Wise, J.P. Morand, M.F. Dutreil, J.M. Gimble, and B.A. Bunnell, *Human Adipose Stromal/Stem Cells from Obese Donors Show Reduced Efficacy in Halting Disease Progression in the Experimental Autoimmune Encephalomyelitis Model of Multiple Sclerosis*. *Stem Cells*, 2016. **34**(3): p. 614-26.
453. Zhang, X., A.C. Bowles, J.A. Semon, B.A. Scruggs, S. Zhang, A.L. Strong, J.M. Gimble, and B.A. Bunnell, *Transplantation of autologous adipose stem cells lacks therapeutic efficacy in the experimental autoimmune encephalomyelitis model*. *PLoS One*, 2014. **9**(1): p. e85007.
454. Widholz, B., S. Tsitlakidis, B. Reible, A. Moghaddam, and F. Westhauser, *Pooling of Patient-Derived Mesenchymal Stromal Cells Reduces Inter-Individual Confounder-Associated Variation without Negative Impact on Cell Viability, Proliferation and Osteogenic Differentiation*. *Cells*, 2019. **8**(6).
455. Jo, J., O. Gavrilova, S. Pack, W. Jou, S. Mullen, A.E. Sumner, S.W. Cushman, and V. Perival, *Hypertrophy and/or Hyperplasia: Dynamics of Adipose Tissue Growth*. *PLoS Comput Biol*, 2009. **5**(3): p. e1000324.
456. Reilly, S.M. and A.R. Saltiel, *Adapting to obesity with adipose tissue inflammation*. *Nat Rev Endocrinol*, 2017. **13**(11): p. 633-643.
457. Lee, Y.S., J.W. Kim, O. Osborne, D.Y. Oh, R. Sasik, S. Schenk, A. Chen, H. Chung, A. Murphy, S.M. Watkins, O. Quehenberger, R.S. Johnson, and J.M. Olefsky, *Increased adipocyte O<sub>2</sub> consumption triggers HIF-1 $\alpha$ , causing inflammation and insulin resistance in obesity*. *Cell*, 2014. **157**(6): p. 1339-1352.

458. Zatterale, F., M. Longo, J. Naderi, G.A. Raciti, A. Desiderio, C. Miele, and F. Beguinot, *Chronic Adipose Tissue Inflammation Linking Obesity to Insulin Resistance and Type 2 Diabetes*. *Front Physiol*, 2019. **10**: p. 1607.
459. Silva, K.R., S. Liechocki, J.R. Carneiro, C. Claudio-da-Silva, C.M. Maya-Monteiro, R. Borojevic, and L.S. Baptista, *Stromal-vascular fraction content and adipose stem cell behavior are altered in morbid obese and post bariatric surgery ex-obese women*. *Stem Cell Res Ther*, 2015. **6**: p. 72.
460. Onate, B., G. Vilahur, S. Camino-Lopez, A. Diez-Caballero, C. Ballesta-Lopez, J. Ybarra, F. Moscatiello, J. Herrero, and L. Badimon, *Stem cells isolated from adipose tissue of obese patients show changes in their transcriptomic profile that indicate loss in stemcellness and increased commitment to an adipocyte-like phenotype*. *BMC Genomics*, 2013. **14**: p. 625.
461. Patel, R.S., G. Carter, G. El Bassit, A.A. Patel, D.R. Cooper, M. Murr, and N.A. Patel, *Adipose-derived stem cells from lean and obese humans show depot specific differences in their stem cell markers, exosome contents and senescence: role of protein kinase C delta (PKCdelta) in adipose stem cell niche*. *Stem Cell Investig*, 2016. **3**: p. 2.
462. Serena, C., N. Keiran, V. Ceperuelo-Mallafre, M. Ejarque, R. Fradera, K. Roche, C. Nunez-Roa, J. Vendrell, and S. Fernandez-Veledo, *Obesity and Type 2 Diabetes Alters the Immune Properties of Human Adipose Derived Stem Cells*. *Stem Cells*, 2016. **34**(10): p. 2559-2573.
463. Martinez, F.O. and S. Gordon, *The M1 and M2 paradigm of macrophage activation: time for reassessment*. *F1000Prime Rep*, 2014. **6**: p. 13.
464. Funes, S.C., M. Rios, J. Escobar-Vera, and A.M. Kalergis, *Implications of macrophage polarization in autoimmunity*. *Immunology*, 2018. **154**(2): p. 186-195.
465. Martinez, F.O., A. Sica, A. Mantovani, and M. Locati, *Macrophage activation and polarization*. *Front Biosci*, 2008. **13**: p. 453-61.
466. Sabol, R.A., A. Beighley, P. Giacomelli, R.M. Wise, M.A.A. Harrison, B.A. O'Donnell, B.N. Sullivan, J.D. Lampenfeld, M.D. Matossian, M.R. Bratton, G. Wang, B.M. Collins-Burow, M.E. Burow, and B.A. Bunnell, *Obesity-Altered Adipose Stem Cells Promote ER(+) Breast Cancer Metastasis through Estrogen Independent Pathways*. *Int J Mol Sci*, 2019. **20**(6).
467. Sabol, R.A., V.A. Villela, A. Denys, B.T. Freeman, A.B. Hartono, R.M. Wise, M.A.A. Harrison, M.B. Sandler, F. Hossain, L. Miele, and B.A. Bunnell, *Obesity-Altered Adipose Stem Cells Promote Radiation Resistance of Estrogen Receptor Positive Breast Cancer through Paracrine Signaling*. *Int J Mol Sci*, 2020. **21**(8).
468. Cheon, S.Y., E.J. Kim, J.M. Kim, E.H. Kam, B.W. Ko, and B.N. Koo, *Regulation of Microglia and Macrophage Polarization via Apoptosis Signal-*

- Regulating Kinase 1 Silencing after Ischemic/Hypoxic Injury*. Front Mol Neurosci, 2017. **10**: p. 261.
469. Ning, K., W.W. Liu, J.L. Huang, H.T. Lu, and X.J. Sun, *Effects of hydrogen on polarization of macrophages and microglia in a stroke model*. Med Gas Res, 2018. **8**(4): p. 154-159.
470. Bureta, C., T. Setoguchi, Y. Saitoh, H. Tominaga, S. Maeda, S. Nagano, S. Komiya, T. Yamamoto, and N. Taniguchi, *TGF-beta Promotes the Proliferation of Microglia In Vitro*. Brain Sci, 2019. **10**(1).
471. Nagamoto-Combs, K., J. Kulas, and C.K. Combs, *A novel cell line from spontaneously immortalized murine microglia*. J Neurosci Methods, 2014. **233**: p. 187-98.
472. Mohiuddin, O.A., B.T. O'Donnell, J.N. Poche, R. Iftikhar, R.M. Wise, J.M. Motherwell, B. Campbell, S.D. Savkovic, B.A. Bunnell, D.J. Hayes, and J.M. Gimble, *Human Adipose-Derived Hydrogel Characterization Based on In Vitro ASC Biocompatibility and Differentiation*. Stem Cells Int, 2019. **2019**: p. 9276398.
473. Yin, Y., R.X. Wu, X.T. He, X.Y. Xu, J. Wang, and F.M. Chen, *Influences of age-related changes in mesenchymal stem cells on macrophages during in-vitro culture*. Stem Cell Res Ther, 2017. **8**(1): p. 153.
474. Yu, H., X. Wang, F. Kang, Z. Chen, Y. Meng, and M. Dai, *Propofol attenuates inflammatory damage on neurons following cerebral infarction by inhibiting excessive activation of microglia*. Int J Mol Med, 2019. **43**(1): p. 452-460.
475. Kidd, S., E. Spaeth, J.L. Dembinski, M. Dietrich, K. Watson, A. Klopp, V.L. Battula, M. Weil, M. Andreeff, and F.C. Marini, *Direct evidence of mesenchymal stem cell tropism for tumor and wounding microenvironments using in vivo bioluminescent imaging*. Stem Cells, 2009. **27**(10): p. 2614-23.
476. Cho, K.S., H.K. Park, H.Y. Park, J.S. Jung, S.G. Jeon, Y.K. Kim, and H.J. Roh, *IFATS collection: Immunomodulatory effects of adipose tissue-derived stem cells in an allergic rhinitis mouse model*. Stem Cells, 2009. **27**(1): p. 259-65.
477. Chen, L., E.E. Tredget, P.Y. Wu, and Y. Wu, *Paracrine factors of mesenchymal stem cells recruit macrophages and endothelial lineage cells and enhance wound healing*. PLoS One, 2008. **3**(4): p. e1886.
478. van Harmelen, V., T. Skurk, K. Rohrig, Y.M. Lee, M. Halbleib, I. Aprath-Husmann, and H. Hauner, *Effect of BMI and age on adipose tissue cellularity and differentiation capacity in women*. Int J Obes Relat Metab Disord, 2003. **27**(8): p. 889-95.
479. Pachon-Pena, G., C. Serena, M. Ejarque, J. Petriz, X. Duran, W. Oliva-Olivera, R. Simo, F.J. Tinahones, S. Fernandez-Veledo, and J. Vendrell,

- Obesity Determines the Immunophenotypic Profile and Functional Characteristics of Human Mesenchymal Stem Cells From Adipose Tissue.* Stem Cells Transl Med, 2016. **5**(4): p. 464-75.
480. Roldan, M., M. Macias-Gonzalez, R. Garcia, F.J. Tinahones, and M. Martin, *Obesity short-circuits stemness gene network in human adipose multipotent stem cells.* FASEB J, 2011. **25**(12): p. 4111-26.
481. Atri, C., F.Z. Guerfali, and D. Laouini, *Role of Human Macrophage Polarization in Inflammation during Infectious Diseases.* Int J Mol Sci, 2018. **19**(6).
482. Cui, K., C.L. Ardell, N.P. Podolnikova, and V.P. Yakubenko, *Distinct Migratory Properties of M1, M2, and Resident Macrophages Are Regulated by alphaDbeta2 and alphaMbeta2 Integrin-Mediated Adhesion.* Front Immunol, 2018. **9**: p. 2650.
483. Vogel, D.Y., P.D. Heijnen, M. Breur, H.E. de Vries, A.T. Tool, S. Amor, and C.D. Dijkstra, *Macrophages migrate in an activation-dependent manner to chemokines involved in neuroinflammation.* J Neuroinflammation, 2014. **11**: p. 23.
484. Lively, S. and L.C. Schlichter, *The microglial activation state regulates migration and roles of matrix-dissolving enzymes for invasion.* J Neuroinflammation, 2013. **10**: p. 75.
485. Frausto-Del-Rio, D., I. Soto-Cruz, C. Garay-Canales, X. Ambriz, G. Soldevila, J. Carretero-Ortega, J. Vazquez-Prado, and E. Ortega, *Interferon gamma induces actin polymerization, Rac1 activation and down regulates phagocytosis in human monocytic cells.* Cytokine, 2012. **57**(1): p. 158-68.
486. Tarique, A.A., J. Logan, E. Thomas, P.G. Holt, P.D. Sly, and E. Fantino, *Phenotypic, functional, and plasticity features of classical and alternatively activated human macrophages.* Am J Respir Cell Mol Biol, 2015. **53**(5): p. 676-88.

## BIOGRAPHY

Mark Alexander Awtrey Harrison was born on December 24<sup>th</sup>, 1983, the only child of Dr. Colin and Lynn Harrison. He was raised in Brookfield, CT and his youth was spent traveling, playing numerous sports (poorly) and being a voracious reader. Mark discovered a passion for science in high school and graduated from Boston College with a degree in Biology. Subsequently, Mark began working as a research associate at Cell Signaling Technologies where he excelled and assumed leadership of product validation for immunofluorescence. He also attended classes at Salem State U completing another BS in Psychology. After 8 years in industry, Mark embraced his inner YOLO and decided to pursue an advanced degree to broaden his career opportunities. At Tulane, Mark completed his MS in Neuroscience and joined the PhD program working in the lab of Dr. Bruce Bunnell on multiple sclerosis. Amid a flurry of life changes and a global pandemic, Mark joined the lab of Dr. Kevin Zwezdaryk and began researching metabolic reprogramming that occurs following infection with cytomegalovirus. His research defined a mechanistic link between pathogen exposure and accelerated cognitive decline in a mouse model. Throughout his grad school career he made a concerted effort to mentor the numerous undergrad and early graduate students he has been fortunate enough to work with. Moving forward, Mark intends to travel and regroup. He'll eventually find employment in a small biotech company hopefully in the mountains so his dogs Edie and Bismark can enjoy the wilderness.